Unravelling the regulatory network controlling lateral root hydropatterning

Jason Pascal Banda, MSc

Thesis submitted to the University of Nottingham
for the degree of Doctor of Philosophy

February 2021

Acknowledgements

First and foremost, I would like to thank my supervisor Malcolm Bennett for his continued support over all these years, since I began working in the group as a Master student almost 6 years ago. Thank you for always believing in me. I'm very thankful that we can continue to work together in the coming years.

I would also like to thank my co-supervisor Tony Bishopp for always offering up his time to help me. Your insights and comments made a real difference to this thesis.

I've been lucky enough to have an extra co-supervisor in Durham to enlighten me on the ways of SUMO. Thank you Ari Sadanandom, for opening my eyes to the world of post-translational modification. I'm thrilled to work with you on the next chapter of unravelling the SUMO code.

Next I'd like to thank the many friends I've made over the years in the lab. Of course, firstly the hydropatterning team: Nicky, Emily and Daniel. Thanks for all the great laughs we had in the lab, I learned so much from all of you and I hope to see you all soon! Thank you to John, Ute, Priya, George, Jon, Al, Matt, Tom and Veronika, when I got here you made me feel right at home so thanks for becoming my surrogate family. I've been lucky to work surrounded by friends, and so to Johanna, Martina, Mickey, Alex, Cameron, Marie, Cindy, Carlos, Mimi, Lorna, Jayne, Daniella, Bipin, Ricci, Elina, Dylan and many more: thank you all for making going to work so enjoyable.

I'm also very grateful to have such good friends in the Netherlands. Joey, Stanley, Chris and Gerard (The Magic Boys)- thanks for all the banter over the years, I couldn't have kept my sanity without you guys. Thanks as well to my Utrecht Uni group of friends: Sjon, Sarah, Rutger, Jesse and Mo, for all the fun times we have together.

Most importantly I want to thank my family. Thank you to my parents who have supported me always, even when I moved to a different country to pursue science. I couldn't have done any of this without your support in good and bad times! Thanks to my lovely sisters, for always being a phone call away and sending me lots of packages filled with Dutch food and drink. I miss you all and hope to see you soon. It has been too long.

Most of all I want to thank Jordan for always being by my side through thick and thin. Your support means the world to me and I couldn't have gotten through these past four years if it wasn't for you. You make me a better man and I can't wait to see what adventures are waiting for us in the future.

TABLE OF CONTENTS

Acknowledgements 2

Abstract 7

Publications arising from this thesis 8

1 Introduction 9

1.1 Roots for sustainable plant growth 9

1.2 Root system architecture 11

1.3 Auxin signalling 13

1.3.1 Auxin signalling pathway 13

1.3.2 Auxin Response factors 17

1.3 Auxin controls multiple facets of lateral root formation 20

1.3.1 Lateral root morphogenesis in *Arabidopsis* 20

1.3.2 Pre-branch site oscillations 22

1.3.3 The birth of lateral root founder cells 24

1.3.4 Primordia morphogenesis 26

1.3.5 Patterning under pressure 28

1.3.6 Lateral root meristem activation 32

1.4 Lateral root adaptive responses to water availability 32

1.4.1 Xerobranching: root branching inhibition during absence of water 32

1.4.2 Hydropatterning: root branching towards external water 34

1.5 Water transport and movement 37

1.5.1 Soil water uptake 37

1.5.2 Symplastic transport through plasmodesmata 38

1.5.3 Transcellular water transport through aquaporins 42

1.6 Sensing water availability at a cellular scale 44

1.7 Could SUMOylation provide a water stress sensing mechanism? 47

1.7.1 The SUMOylation cycle 47

1.7.2 Environmental stress induced SUMOylation 50

1.8 Aims 52

2 Materials & Methods 54

2.1 Plant lines and growth conditions 54

2.1.1 Arabidopsis material 54

2.1.2 Arabidopsis growth 54

2.2 Plant phenotyping analysis 55

2.2.1 LR hydropatterning phenotyping bioassay 55

2.2.2 Bending assay 55

2.2.3 Plant growth on salt media 55
2.2.4 Plant growth on auxin media 55
2.2.2 Lateral root staging 56
2.3 DNA extraction and genotyping 56
2.3.1 DNA extraction 56
2.3.2 PCR set-up 56
2.3.3 Gel electrophoresis 56
2.3.4 PCR purification 57
2.3.5 DNA gel extraction 57
2.3.6 DNA sequencing 57
2.4 Gene cloning and construct design 57
2.4.1 Multisite Gateway cloning 57
2.4.2 GreenGate cloning 58
2.4.3 Plasmid DNA isolation 59
2.4.4 Floral dipping protocol 59
2.4.5 Construct data storage 59
2.5 Confocal microscopy 60
2.5.1 Lateral root deviation angle measurements 60
2.5.2 Multi-view imaging employing Light Sheet Fluorescent Microscopy for investigating lateral root hydropatterning 60
2.5.3 Confocal microscopy using the Leica SP5 and SP8 61
2.5.4 Relative fluorescence measurements. 61
2.6 Gene expression analysis 61
2.6.1 Plant growth and harvest 61
2.6.2 RNA extraction and RT qPCR 61
2.7 Hormone treatments 62
2.7.1 General hormone treatment 62
2.7.2 Relative fluorescence measurements 63
2.8 Phylogeny reconstruction 63
2.9 Statistical analysis 64
3 Early developmental plasticity of lateral roots in response to asymmetric water availability 65
3.1 Introduction 65
3.2 Results 69
3.2.1 Light Sheet Fluorescence Microscopy as a tool to visualize LRP emergence angle. 69
3.2.2 Lateral root initiation and emergence angle is influenced by the availability of water 71
3.2.3 Lateral root primordium emergence angle is flexible at all primordium developmental stages 74

3.2.4 *LBD16* over-expression reduces lateral root primordium deviation angle 77
3.3 Discussion 79
3.3.1 The external hydrological landscape influences LR primordia positioning 79
3.3.2 External hydrological landscape determines primordium emergence angle 83
4 Lateral root hydropatterning depends on ARF7 SUMOylation 87
4.1 Introduction 87
4.2 Results 91
4.2.1 Hydropatterning is regulated by an ARF7 and LBD16 dependent pathway 91
4.2.2 Employing light sheet fluorescent microscopy to study lateral root hydropatterning 94
4.2.3 The asymmetrical localisation of gLBD16-GFP in root elongation zone is dependent on ARF7 97
4.2.5 Early gLBD16-GFP signal in vascular procambium cells. 103
4.2.6 SUMO site K151 and K282 on ARF7 are evolutionary highly conserved 105
4.3 Discussion 109
4.3.1 Lateral root hydropatterning is regulated by an ARF7-LBD16 dependent pathway 109
4.3.2 SUMOylation regulates ARF7 activity during lateral root hydropatterning 113
4.3.3 Asymmetric LBD16 expression is key to lateral root hydropatterning 116
4.3.4 Evolutionary conservation of ARF SUMOylation 119
5. SUMO protease OTS1 regulates hydropatterning 123
5.1 Introduction 123
5.2 Results 126
5.2.1 Mutants in *OTS1* and *OTS2* exhibit a hydropatterning defect 126
5.2.2 Lateral root initiation is dependent on OTS1 133
5.2.3 *ots1-2gk* is a gain of function mutation causing OTS1 overexpression 137
5.2.4 OTS1 OE and *ots1-2gk* lines exhibit increased salt tolerance 139
5.2.5 *OTS1* is expressed in meristem, elongation zone and lateral root primordia 142
5.2.7 Auxin induced lateral root formation in *ots2-1* mutants 152
5.2.8 OTS1 exhibits differential stability to selected hormone signals 158
5.3 Discussion 162
5.3.1 Lateral root hydropatterning is dependent on OTS1 162
5.3.2 A gradient of OTS1 activity rather than stability appears to regulate hydropatterning 164
5.3.3 OTS1 promotes early initiation of lateral root primordia 165
5.3.4 Could other SUMO proteases affect lateral root hydropatterning? 167
6. General Discussion 175
6.1 Hydropatterning regulates lateral root initiation and emergence 175
6.2 SUMOylation regulates ARF7 activity during lateral root hydropatterning 180
6.3 SUMO protease OTS1 regulates LR hydropatterning 184

6.4 Future Directions and Wider implications of the thesis findings 188
Bibliography 191
Appendices 218
PIPS reflective statement 218
Publications arising from this thesis 220

Abstract

The 3-dimensional shape of a root system is of crucial importance to its ability to take up nutrients and water. As these resources are heterogeneously distributed in the soil, plants need to adapt their root growth to aid foraging. One such adaptive response is termed lateral root (LR) hydropatterning where roots branch towards areas with higher water availability.

The main aim of this thesis is to investigate how plant roots sense water distribution and which regulatory pathways control lateral root branching towards available water using the model plant *Arabidopsis thaliana*. We observed that the choice of lateral root founder cells (LRFC) in the pericycle cell layer they originate from is influenced by external water availability. This allows lateral roots to angle towards water from the very first round of formative cell divisions. Additionally, the emerging lateral root primordium grows towards water availability through asymmetric rounds of cell division in its primordium flanks.

LR hydropatterning is genetically regulated through a major regulator of LR initiation AUXIN RESPONSE FACTOR7 (ARF7). Knock-out mutants lose the ability to branch towards water and do not asymmetrically express the key transcription factor LBD16-GFP, a direct target for ARF7. This mechanism is regulated through post-translational regulation of ARF7. The ARF7 sequence contains four sites that can be SUMOylated. Transgenic lines expressing ARF7 with mutations in each of these four SUMO sites cannot rescue *arf7-1* LR hydropatterning, revealing a key role for SUMOylation controlling water sensing by roots.

ARF7 SUMO status appears to be controlled by SUMO protease OVERLY TOLERANT TO SALT1 (OTS1). Double knock-out mutants in *OTS1* and its close homolog *OTS2* have severely delayed root development and a LR hydropatterning defect. Additionally, *ots1 ots2* mutants display reduced LR initiation and emergence defects that can be restored to Wild-Type levels by expressing an *OTS1-Venus* transgene. OTS1-Venus can be detected from the late elongation zone onwards in root pericycle cells and is stably

expressed in the primordia. However, no asymmetrical localisation of OTS1-Venus is observed after a hydropatterning cue suggesting that SUMO protease activity, rather than stability, controls LR hydropatterning. This thesis highlights the early response of lateral roots to asymmetrical water distribution and role the deSUMOylation machinery plays in its molecular regulation.

Publications arising from this thesis

Orosa-Puente, B., Leftley, N., von Wangenheim, D., **Banda, J.,** Srivastava, A.K., Hill, K., Truskina, J., Bhosale, R., Morris, E., Srivastava, M., Kümpers, B., Goh, T., Fukaki, H., Vermeer, J.E.M., Vernoux, T., Dinneny, J.R., French, A.P., Bishopp, A., Sadanandom, A., Bennett, M.J., 2018. Root branching toward water involves posttranslational modification of transcription factor ARF7. ***Science*** 362, 1407–1410.

Banda, J., Bellande, K., von Wangenheim, D., Goh, T., Guyomarc'h, S., Laplaze, L., Bennett, M.J., 2019. Lateral Root Formation in Arabidopsis: A Well-Ordered LRexit. ***Trends in Plant Science*** 24, 826–839.

von Wangenheim, D., **Banda, J**., Schmitz, A., Boland, J., Bishopp, A., Maizel, A., Stelzer, E.H.K., Bennett, M., 2020. Early developmental plasticity of lateral roots in response to asymmetric water availability. ***Nature Plants*** 6, 73–77.

<u>Accepted for publication:</u>

Leftley, N., **Banda, J**., Pandey, B., Bennett, M.J., Voss, U. Uncovering how auxin optimises root systems architecture in response to environmental stresses., 2021***.*** ***Auxin Signaling, second edition.*** CSHL Perspectives.

1 INTRODUCTION

Parts of this introduction were published in: **Banda, J.,** Bellande, K., von Wangenheim, D., Goh, T., Guyomarc'h, S., Laplaze, L., Bennett, M.J., 2019. Lateral Root Formation in Arabidopsis: A Well-Ordered LRexit. ***Trends in Plant Science*** 24, 826–839.

1.1 Roots for sustainable plant growth

A growing demand for food, a limited amount of fertilizers and an increased frequency of extreme weather events, these are some of the most important challenges we face for crop production world-wide (Godfray et al. 2010; Wheeler and von Braun 2013; Lobell et al. 2011). In the recent past, agricultural productivity has significantly increased thanks to the success of the First Green Revolution (Borlaug and Dowswell 2003). During this Revolution the focus was on the introduction of semi-dwarf varieties in combination with high fertilisation to make a huge impact on crop yield in developed countries (Borlaug and Dowswell 2003; Godfray et al. 2010). However, this approach often did not reach farmers in developing countries, who do not have access to a stable supply of fertilisers and often farmed nutrient poor and eroded soils (Lynch 2007). Additionally, the varieties were bred for high input agriculture and dwarf shoot phenotypes, thereby indirectly selecting against root traits which are instrumental for growth in low input environments (Lynch 2007; White et al. 2013). In order to address this challenge, we need a second, sustainable Green Revolution, also termed 'Evergreen Revolution', in which the focus lies on decreasing inputs whilst maintaining crop productivity (White et al. 2013).

Improved uptake of nutrients and water by the root system is necessary to optimise resource capture and reduce the use of fertilisers. Soil exploration plays a crucial part in resource capture as it allows the plant root to access new areas with untapped resources. Many root architectural traits aid in soil foraging and are vital for resource acquisition such as primary root length, root hair density and lateral branching (Lynch 2007). Other traits such as aerenchyma formation and secondary development are important for reducing the metabolic costs of soil exploration (Lynch 2007). Next to

resource capture, a well-developed root system can go a long way in combatting extreme weather events such as drought. The FAO global drought map (1984-2017) in Fig. 1.1 shows the frequency of drought events that affected 30% of the cropland in that region. Regions such as southern Africa, India and Australia, experience severe drought on an almost yearly basis. Global climate change is expected to make droughts even more severe, by changes to rain fall pattern and increased temperatures (Wheeler and von Braun 2013; Lobell et al. 2011). In addition, fresh water sources, used for irrigation, are depleted in an alarmingly fast rate (Cotterman et al. 2017). Without fresh water sources, drought will have an even greater impact on crop survival and yield. To combat drought damage to crops, the world requires more drought tolerant crops. Therefore, the soil exploration by a root is an essential trait for crop breeders as it defines the amount of water that can be captured. However, to make a real impact we have to first need to understand the underlying mechanisms for how roots sense and respond to soil resource availability. Only by understanding these mechanisms can gene directed breeding make a major improvement in soil exploration to optimize water and nutrient acquisition.

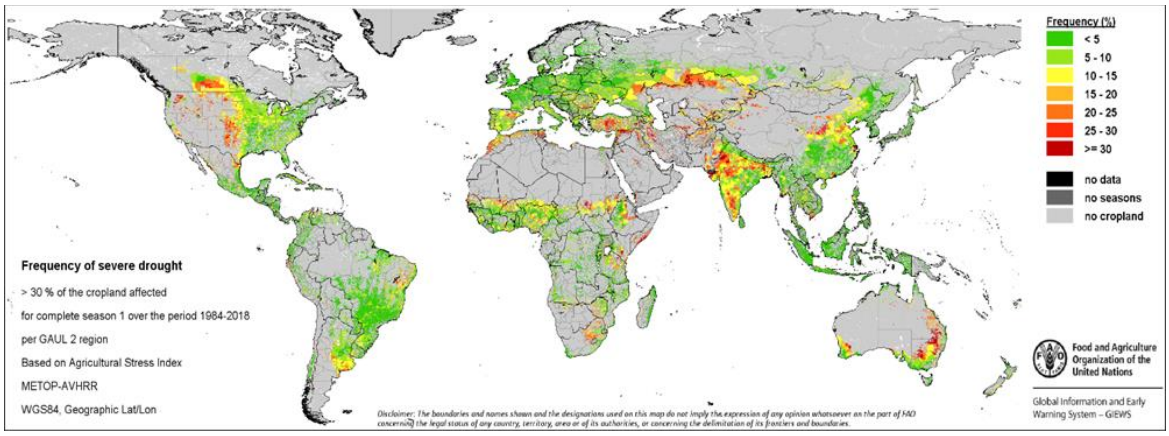

Source: http://www.fao.org/giews/earthobservation/asis/index_1.jsp?lang=en#uvhi

Figure 1-1 Data from FAO showing areas in the world where >30% of the cropland has been affected by severe drought for a complete season over the period 1984 till 2018.

1.2 Root system architecture

Roots forage the heterogenous soil to acquire valuable resources like nutrients and water. It is therefore no surprise that these invaluable resources also drive the 3D root architecture by controlling how and where roots grow and branch (Morris et al., 2017). The heterogenous soil structure is driven by processes such as type of soil and tillage practice (Mangalassery et al. 2014), which determine the size and connectivity of pores. These pores are crucial for roots as they provide a channel to grow through and supply the growing root with water, gas, and nutrients to absorb. The patchiness of nutrients can be driven by decomposition of organic materials, which are spread out through the soil (Hodge 2004). Nutrients also differ in their mobility. Nitrate is highly soluble in water and will quickly leak to lower depths, whilst phosphate forms insoluble complexes and stays near the topsoil (Hodge 2004). Water distribution is also highly varied in soil. The topsoil layer will dry quickly due to evaporation, whilst deeper layers of the soil are spared from this (Tracy et al. 2015). Additionally, soil pore size affects the ability to retain water. Micropores (<30mm) will hold less water more readily, yet macropores (>1,000 mm) will allow for efficient drainage of water from the topsoil (Luxmoore 1981). Responding to the complex mix of environmental signals ensures optimal resource capture by the root system, resulting in an infinite number of root architectures reflecting the infinite number of different soil environments that can be found worldwide.

Increased exploration of soil can have a big impact on a plant's efficiency to take up water and mobile nutrients such as nitrate (Trachsel et al. 2013). A root's architecture is mostly determined by four shape parameters: growth, branching, surface area and angle. These parameters are all under environmental and genetic regulation to underpin resource capture from their surroundings. The surrounding soil consists of air and water filled pores, localised patches of nutrients and varying soil texture, making the environment a real maze for a root to navigate. To optimize resource uptake some species have adapted their rooting system to their environment. Pearl millet is one of these species, which has evolved a steep root architecture to increase water uptake from the deeper soil (Passot et al. 2016). In *A. thaliana,* a similar adaptation was seen

in which the gravitropic set point angle of lateral roots was increased under water deficiency (Rellán-Álvarez et al. 2015). This novel adaptive trait, termed xerotropism, allows plants to explore deeper soil levels for potential water sources. Additionally, the primary root can grow towards available water using hydrotropism (Dietrich et al. 2017). This abscisic acid (ABA) mediated response assures the optimal capture of water as the location of water in the soil can vary due to weather, seasons and human interference (Atkinson et al. 2009). The plasticity of a root system to change its growth and branching is therefore of crucial importance to survive in these challenging and changing soil conditions.

Root systems attributes can vary between plants species. The eudicot model *A. thaliana* exhibits a simple primary and lateral root system architecture. In this model species the embryo derived primary root stays active throughout the plant life cycle. The primary root consists of four growth zones: (I) the root apical meristem where cells divide; (II) basal meristem where root cells finish dividing and start elongating; (III) elongation zone where cells rapidly expand; and (IV) differentiation zone where cell elongation ceases and root hairs form (Verbelen et al. 2006). Lateral roots are primed in the basal meristem and eventually emerge from the differentiation zone, where they serve to increase root surface area and volume of soil being explored. In contrast, adventitious roots originate from the hypocotyl post-embryonically and are often formed during prolonged plant stress (Steffens and Rasmussen 2016). Legume and monocot species form additional classes of root organs such as seminal and crown roots that aid exploration of topsoil, especially for immobile nutrients like phosphate (Lynch 2011). These latter classes of roots also help stabilize plants in soil to counteract lodging (Rogers and Benfey 2015).

In this thesis I will mainly focus on the relatively simple root architecture of *A. thaliana*. Its simple root system will help me to delve into the relationship between root branching and water availability. A response that seems very logical from a resource acquisition point of view but is poorly understood from a genetic and mechanistic perspective.

1.3 Auxin signalling

1.3.1 Auxin signalling pathway

Many root developmental processes are regulated by the phytohormone auxin. The nuclear auxin response pathway has been studied in great detail and is dependent on three classes of proteins. Firstly, this consists of the Aux/IAAs as repressors of the auxin response pathway. Secondly, the DNA binding transcription factors Auxin Response Factors (ARFs). Lastly, to abolish the repression of the ARFs by Aux/IAAs the system uses the SCF (TIR1/AFB) ubiquitin ligases. These auxin receptors increase their affinity for Aux/IAA proteins when bound to auxin, leading to 26S proteasomal degradation of Aux/IAAs (Gray et al. 2001; Zenser et al. 2001). Degradation of the suppressors leads to activation of ARF gene transcription and thereby the nuclear auxin induced response output (Fig. 1.2).

Although the nuclear auxin response pathway might be simple given its composed of only three classes, the outputs of the system can greatly vary as indicated by the wide variety of developmental responses controlled by auxin (Vanneste and Friml 2009). This is partially explained by the number of family members in each of these three classes of components, with the ARF gene family containing 23 members in flowering plants such as *A. thaliana*, 29 Aux/IAA members and six AFB members (Mutte et al. 2018). The diversity of spatial expression pattern and the cell specific stability of different components has a major impact on local auxin response (Rademacher et al. 2011, 2012). Another difference in auxin response can be generated by the biochemical properties of the different components. Binding assays using purified TIR1 and Aux/IAA proteins revealed different complex combinations have distinct affinities for auxin (Calderón Villalobos et al. 2012). This difference could partially be explained by the DII sequence of the Aux/IAA proteins, which is crucial for auxin binding with TIR1/AFB co-receptors (Calderón Villalobos et al. 2012). The many different components and variations within the protein sequences in these families forms the basis for explaining the complexity of the auxin signalling pathway and its differential response outputs.

The TIR1/AFB proteins are part of four-subunit ubiquitin ligase $SCF^{TIR1/AFB}$ that resides in the nucleus (Gray et al. 1999, 2002). The TIR1/AFB part of this complex is crucial for the binding of auxin through its N-terminal located leucine-rich-repeat region (Dharmasiri et al. 2005a). Mutants in the TIR1/AFB family display different levels of auxin resistance in accordance with their role in auxin perception (Dharmasiri et al. 2005b; Parry et al. 2009). The $SCF^{TIR1/AFB}$ complex consists of other components whose mutants cause a similar auxin resistant phenotype by stabilizing Aux/IAAs such as ARABIDOPSIS SKP1 HOMOLOGUE (ASK1), CULLIN 1 (CUL1) and RING-BOX 1 (RBX1) (Gray et al. 1999, 2002)(Fig. 1.2). These components are necessary for the binding of E2 ubiquitin conjugation enzymes that control the ubiquitination of Aux/IAAs after auxin binding, leading to their degradation. By solving the crystal structure of the TIR1-ASK1 complex, researchers could demonstrate the importance of the leucine-rich-repeat region as auxin binding pocket and the C-terminal located F-box domain as the binding region for ASK1 (Tan et al. 2007). The leucine-rich-repeat region is also in contact with Aux/IAA proteins, which might be necessary for stabilizing the interaction between auxin, TIR1/AFB and Aux/IAA.

Members of the Aux/IAA family interact with ARFs to supress gene transcription. Aux/IAA and ARF bind through their highly similar C-terminal domain named Phox and Bem1 (PB1). The PB1 domain mediates homo- and heterodimerization between family members of ARFs and Aux/IAAs (Han et al. 2014a). Repression is thought to be dependent on the multimerization of Aux/IAAs when bound to ARFs PB1 domain (Korasick et al. 2014). The significance of this oligomerization is still unknown, yet it could determine the speed or affinity with which the Aux/IAA binds the $SCF^{TIR1/AFB}$ complex. Over-expressing a stabilized Aux/IAA16 led to stunted growth in *A. thaliana*. The researchers modified the Aux/IAA in such a way that it could only bind one other PB1 domain. This led to a new form of Aux/IAA that could bind ARF yet not form any multimers with other Aux/IAAs. Transforming this mutated version into *A. thaliana* did not lead to stunted growth, indicating the necessity of multimerization in Aux/IAA repression of ARFs (Korasick et al. 2014).

Repression of Aux/IAAs is also dependent on the recruitment of corepressors to form a complex. The two N-terminal located ETHYLENE- RESPONSIVE ELEMENT BINDING FACTOR–ASSOCIATED REPRESSOR (EAR) domains (also called degron or DI and DII) are required for binding with several partners (Ke et al. 2015). The EAR motif 1 (DI) binds to co-suppressors such as the Tup1/Groucho/TLE family proteins called TOPLESS (TPL) or TOPLESS RELATED (TPR) (Szemenyei et al. 2008; Causier et al. 2012; Ke et al. 2015). TPL represses auxin induced gene expression by recruiting histone deacetylases (HDACs) such as HDA19 (Long et al. 2006)(Fig 1.2). These HDAC proteins remove acetyl groups from lysines on histones, which leads to condensed chromatins and reduced binding of a multitude of transcription factors to induce gene expression (Eberharter and Becker 2002). Knock-out mutants in *hda19* could partially restore the phenotype of Aux/IAA *gain-of-function* mutations, suggesting a role downstream of AUX/IAA (Long et al. 2006). Furthermore, both TPL and HDA19 are bound to ARFs especially during low auxin conditions (Szemenyei et al. 2008; Wu et al. 2015). When auxin concentration in the cells rise, Aux/IAA proteins will be degraded and TPL and HDA19 dissociate from the chromatin (Wu et al. 2015).

The second EAR domain (DII) is important for AUX/IAA protein stability as this region is involved in auxin-dependent binding with the auxin co-receptor TIR1/AFB (Tan et al. 2007). Mutations in this domain results in strong or complete auxin insensitive phenotypes (Tian and Reed 1999; Rogg et al. 2001). Some variation in this domain exists within the different Aux/IAA family members, which leads to a variation in auxin sensitivity (Dreher et al. 2006). Next to the DII region, also other regions regulate auxin sensitivity such as the conserved pair of lysine (K) and arginine (R) between EAR domain 1 and 2, and the polar amino acids downstream of the DII (Dreher et al. 2006; Moss et al. 2015). When mutated or absent these two regions can significantly alter the auxin sensitivity and lead to gain-of-function phenotypes.

Conservation of the different motifs on Aux/IAA is crucial for its functioning. There is a big difference between the half-lives of different Aux/IAA ranging from minutes to hours, which translates into different auxin binding affinities for TIR1/AFB (Zenser et al. 2001; Dreher et al. 2006). Binding of TIR1 and IAA7 DII domain was weaker than the

binding of TIR1 with full IAA7 protein (Calderón Villalobos et al. 2012). This data suggests that other domains on Aux/IAA mediate some parts of the binding with the receptor and partially mediate the stability of Aux/IAAs.

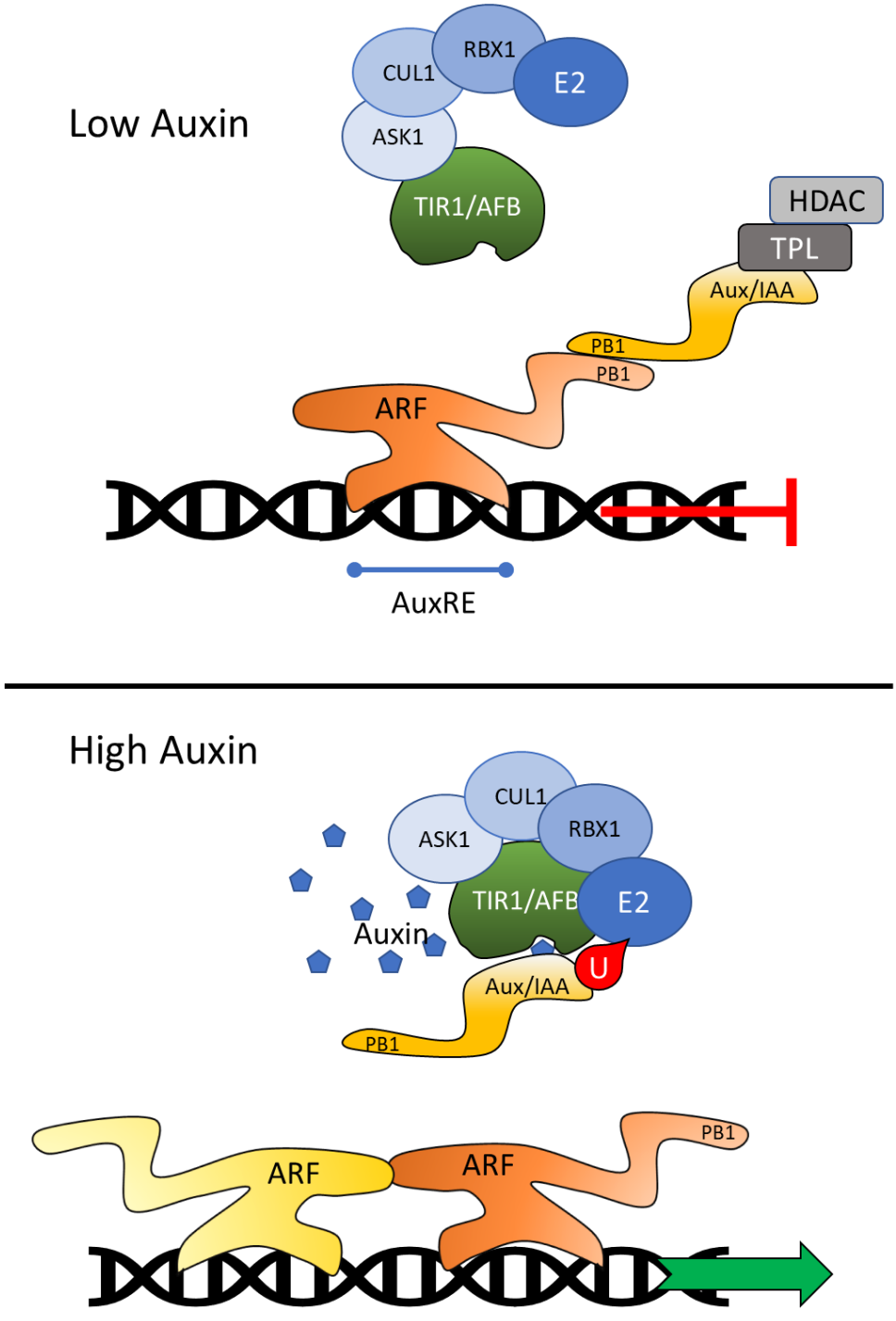

Figure 1.2 – The main auxin signalling components. When auxin levels are low, Aux/IAA proteins bind through their shared PB1 to ARF proteins. This prevents the induction of ARFs downstream genes through co-repressors such as TPL and binding of HDAC proteins that close the access through chromatin condensation. When auxin levels in the cell are high, auxin enables the binding of Aux/IAA

and TIR1/AFB receptor of the SCFTIR1/AFB complex. This binding leads to the ubiquitination of Aux/IAA and its subsequent degradation. This releases the repression of ARFs and increased transcription of downstream genes. ARFs can also dimerize with other ARFS through their Dimerization Domain to mediate transcriptional activity.

1.3.2 Auxin Response factors

Auxin transcriptional activity is regulated by 23 ARF genes that make up this family in *A. thaliana* (Okushima et al. 2005). These 23 genes fall into three classes, termed A, B and C of which only class A (ARF5, 6, 7, 8, 19) consist of transcriptional activators (Tiwari et al. 2003). Mutations in these class A-ARFs can lead to severe phenotypes in both shoot and root tissues. Research on promoter swaps between the ARFs together with analysis of knock-out mutants has demonstrated that these are not interchangeable and, although these ARFs are very similar in domains structure, they all play distinct roles in auxin signalling (Rademacher et al. 2011, 2012). Furthermore, the open chromatin configuration of the class A-ARFs implies that these can actively be transcribed during multiple developmental stages and tissues (Truskina et al. 2020). Class A-ARFs are mostly regulated by a set of transcriptional repressors, which supports a model where transcriptional repressors inhibit transcription by binding to the open chromatin of these ARFs, thereby repressing transcription (Truskina et al. 2020).

In turn, ARFs can also regulate the chromatin state. In one such case ARF5 controls histone modification through interaction with SWI/SNF chromatin remodellers BRHAMA (BRM) and SPLAYED (SYD) (Wu et al. 2015). These SWI/SNF remodellers compete for binding on ARF5 with Aux/IAA (Wu et al. 2015). High auxin levels lead to breakdown of Aux/IAAs and binding of SWI-SNF to ARF5 which actively opens up the chromatin around ARF5 DNA binding sites enabling transcription of ARF5 downstream targets (Wu et al. 2015). On the contrary, chromatin remodelling can also negatively affect ARF signalling as is seen in the regulation of ARF7 and ARF19 by IAA14 and PICKLE (PKL) (Fukaki et al. 2006). *slr-1 gain-of-function* mutants are well known for the absence of lateral root formation (Fukaki et al. 2002). However, through use of a suppressor screen researchers found a gene that could restore lateral roots in *slr-1*. This gene termed *PKL*, is a homologue of an animal chromatin-remodelling factor. The restoration

of LRs in double mutants indicates PKL represses transcription by ARF7 and ARF19 (Fukaki et al. 2006).

All class A-ARFs consists of three domains; the N-terminal DNA-binding domain (DBD), the middle region (MR) and the C-terminal located PB1 domain that was discussed earlier (Boer et al. 2014). The N-terminal DBD domain is highly conserved between all the ARFs (Boer et al. 2014). The crystal structures of the DBD of two of these ARFs, ARF1 and ARF5, showed the existence of three sub-domains on the DBD (Boer et al. 2014). Firstly, the B3 subdomain controls binding of ARF onto DNA. Secondly, the dimerization domain (DD) allows homo- and hetero-dimerization of ARFs. Thirdly, a Tudor-like ancillary domain which function is unknown, but might be involved in dimerization together with the DD. As transcription factors, ARFs main function is to activate gene expression by binding to auxin-responsive elements (AuxRE) in the promoter of auxin inducible genes (Ballas et al. 1993; Li et al. 1994; Ulmasov et al. 1997a). Further work highlighted the importance of the DNA-binding motif TGTCTC as interactor with the ARF DBD (Boer et al. 2014; Ulmasov et al. 1997a). However, this motif did not have the highest affinity for ARF binding. Additional work demonstrated higher affinity for TCTCGG motif (Boer et al. 2014; Franco-Zorrilla et al. 2014). Another high affinitive motif, TGTCGG, was picked up when analysing *in vitro* binding of ARF2 and ARF5 (O'Malley et al. 2016). There is some evidence to suggest a correlation between the AuxRE motif and its function in specific developmental processes to steer a particular auxin response pathway (Zemlyanskaya et al. 2016). However, not only the motif sequence plays a role in the binding affinity. Another important part is the space between two AuxREs. ARF1 and ARF5 had different binding affinities depending on the space between two motifs (Boer et al. 2014). This introduced the idea of co-operative binding of two AuxRE elements by ARFs forming homo- or hetero-dimers. The binding of the first ARF could increase the affinity for a second ARF to bind through dimerization and thus strengthen the ARF gene expression response. Even the orientation of the repeat motifs and the number of repeats can affect ARF binding specificity and affinity (Berendzen et al. 2012; O'Malley et al. 2016).

The middle region (MR) of the ARFs is much less conserved than its DBD. However, it does seem to be important for the classification of the ARFs into activating and repressing types. The activating class A-ARFs contain a MR that is enriched in glutamines, contrasting with the enrichment of serines, prolines and threonines in class B- and C-ARFs. However, the exact mechanism how the difference in sequence relates to its activating or supressing role is still unknown. Interestingly, the MR in activating ARFs consists of long stretches of intrinsic disorder (ID) (Roosjen et al. 2018). These regions of high ID permit the fast 3-dimensional change in protein conformation, necessary to rapidly response to changing conditions (Liu et al. 2006). Most known proteins that contain IDs are related to processes such as cell cycle, DNA metabolism, RNA splicing and signalling (Pietrosemoli et al. 2013), indicating that these regions still serve a crucial function. Another function of this ID regions could be to form the basis for post-translational modification (Xie et al. 2007). These modifications could lead to changes in 3D protein shape that enhance or diminish the activity of ARFs.

The third domain structure, PB1, is the C-terminal domain that interacts with the PB1 domain on Aux/IAA (Ulmasov et al. 1997b). The affinity to form heterodimer ARF-Aux/IAA complexes is 10 to 100 times greater than to form ARF-ARF homodimers, suggesting a strong trend towards heterodimerization (Han 2014). Previous studies using yeast two-hybrid (Y2H) have determined that many combinations are possible between the family members of ARFs and Aux/IAA proteins (Vernoux et al. 2011; Piya et al. 2014). Surprisingly, not many class B- and C- ARFs showed interaction with Aux/IAAs indicating limited regulation of the repressor ARFs by auxin signalling. Potentially, these repressing ARFs function by competing for binding sites of the activating ARFs, thereby limiting auxin induced gene expression? Or is this the result of an artefact of Y2H and do these ARFs bind *in planta* by use of co-factors? More research needs to focus on the interplay between B- and C-class ARFs with Aux/IAA to further clarify their relationship. Surprisingly, a truncated ARF5 lacking a PB1 domain showed reduced binding to DNA in vitro, suggesting a role for the PB1 domain in more than just repression (Ulmasov et al. 1997a).

1.3 Auxin controls multiple facets of lateral root formation

1.3.1 Lateral root morphogenesis in *Arabidopsis thaliana*

Lateral roots originate primarily from the pericycle tissue in angiosperm species (Casimiro et al., 2003; Torres-Martínez et al., 2019). The pericycle consists of a single cell layer surrounding the vascular tissues, which is overlain by endodermal, cortex and epidermal tissues (Fig. 1.3A). In *A. thaliana,* lateral roots are derived from pairs of pericycle cells overlaying the xylem pole (Casero et al. 1993; Laskowski et al. 1995; Von Wangenheim et al. 2016). Phloem-pole pericycle (PPP) cells are reported to be mitotically dormant, whilst xylem-pole-pericycle (XPP) cells retain stem cell activity after leaving the primary root meristem and can consequently form LRs (Parizot et al. 2008). The meristematic abilities of XPP cells are hypothesized to be dependent on the adjacent vasculature cells, since the Rm1007 and J0121 enhancer trap lines are specifically expressed in xylem-pole associated pericycle cells (Parizot et al. 2008). Further proof of concept comes from research on AHP6, a negative regulator of cytokinin signalling, which is involved in protoxylem formation (Mähönen et al. 2006). *AHP6* is expressed in protoxylem and adjacent pericycle cells from the very first pericycle initials, suggesting that the regulation of XPP cell identity is made in a very early stage.

A. thaliana lateral root development can be divided in five main steps: (1) pre-branch site formation which takes place in the basal meristem/elongation zone (De Smet et al. 2007; Moreno-Risueno et al. 2010); (2) LR initiation which features pericycle nuclear migration to a common cell wall between pairs of lateral root founder cells (LRFCs) followed by an asymmetric cell division in the differentiation zone (Casimiro et al., 2001; Goh et al., 2012); (3) LR morphogenesis in which the LRFCs divide further to form a lateral root primordium (LRP) that eventually acquires a root meristem organization (Goh et al., 2016; Malamy and Benfey, 1997); (4) concomitant LR emergence where the new organ grows through overlaying tissue layers to emerge from the parent root in the differentiation zone (Du and Scheres 2017) and finally (5) LR meristem activation corresponding to the initiation of cell divisions in the newly emerged lateral root meristem (Celenza et al., 1995; Fig 1.3A). Recent advancement in microscopy and image

analysis now allows us to visualize these five key steps in LR development in more detail (Fig 1.3B). This can help distinguish the spatial and temporal changes that LRs undergo during these five main development steps and how these changes are affected by the roots local environment (Goh 2019; Ovečka et al. 2018).

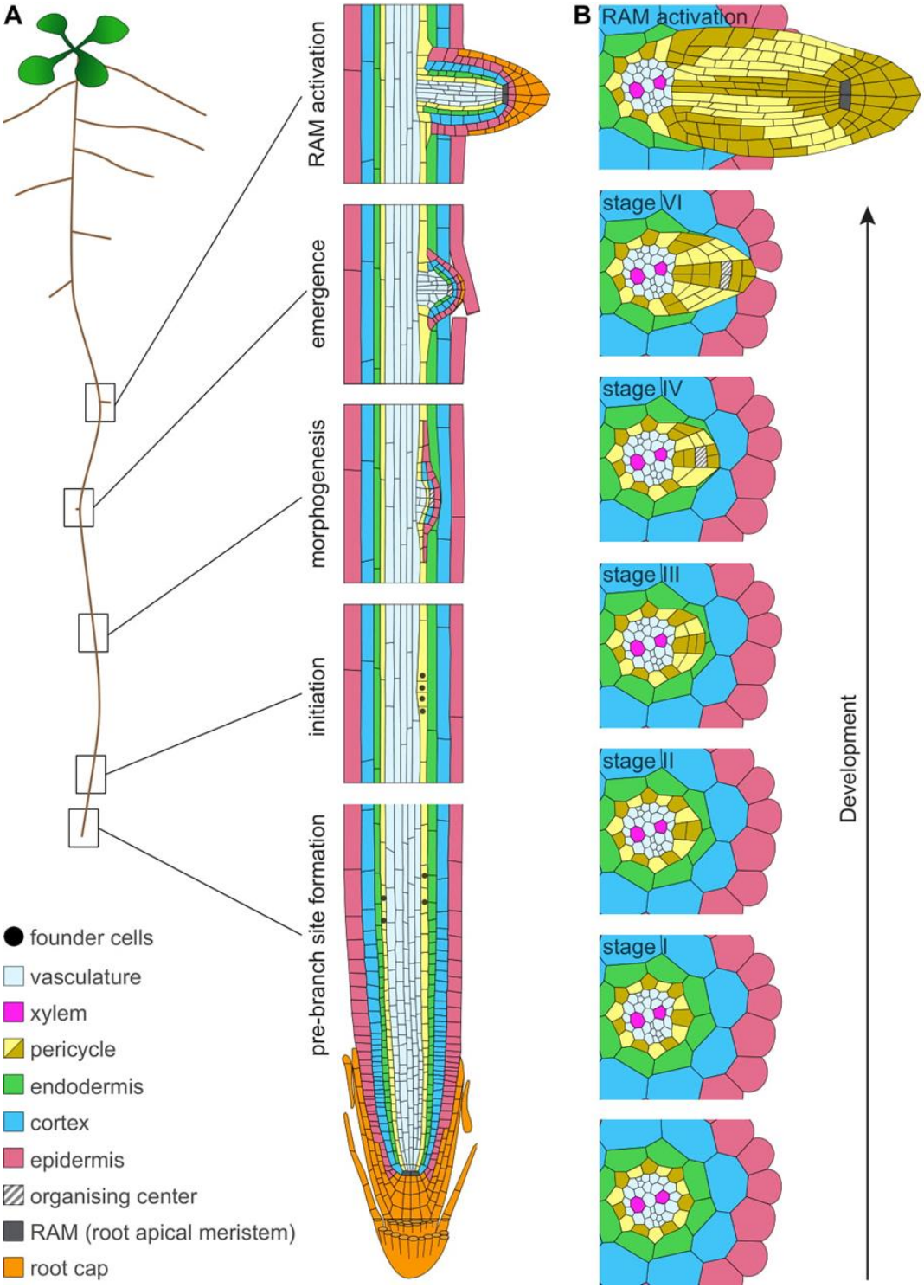

Figure 1.3 – The birth of a new lateral root primordia. The longitudinal section of the root showcases the five main steps of LR formation (A). This process begins with the formation of a pre-branch site in

the basal meristem and elongation zone. Followed by the selection of the LR founder cells and the first anticlinal division in the differentiation zone. These rounds of cell division continue laterally and radially during LR morphogenesis to form a LRP. The growing LRP then has to emerge through the overlying tissue layers of the endodermis, cortex and epidermis, before emerging and gaining an active meristem. These 5 steps are also visualized radially to show the contribution of the multiple pericycle cells to the 3-dimensional shape of the LRP (B). Note that adjacent pericycle cells are in two distinct colour to highlight the difference in contribution of each cell file to the growing LRP (Banda et al., 2019).s

1.3.2 Pre-branch site oscillations

The first phase of lateral root formation starts in the basal meristem where pre-branch sites are formed. The first evidence of this process comes from the recurring expression of DR5 (DIRECT REPEAT5) auxin-responsive GUS reporter (De Smet et al. 2007). The DR5 signal can be observed every 15 hr in protoxylem cells starting from the basal meristem and correlates with subsequent formation of primordia. How the formation of an auxin response in protoxylem develops into initiation of a primordium in the adjacent pericycle cells is still unknown. A similar oscillation pattern was observed by fusion of DR5 promoter to a luciferase (LUC) reporter (Moreno-Risueno et al. 2010). This DR5-LUC oscillatory behaviour was observed from the basal meristem up to the elongation zone and termed the oscillatory region. DR5 oscillatory peaks in this zone were termed pre-branch sites and have the potential to develop into LRP (Fig. 1.4). Although this work focusses on auxin response, exogenous applied auxin could not increase the number of pre-branch sites (Moreno-Risueno et al. 2010), suggesting that auxin responsiveness is dependent on more than just cellular auxin levels. Several important lateral root developmental transcription factors were shown to oscillate, such as AUXIN RESPONSIVE FACTOR7 (ARF7) and LATERAL ORGAN BOUNDARIES DOMAIN16 (LBD16) (Okushima et al. 2007; Moreno-Risueno et al. 2010). Knock-out mutant in ARF7 demonstrated irregular formation of pre-branch sites, indicating the crucial role for this transcription factor in oscillatory gene expression (Moreno-Risueno et al. 2010). Recently new evidence emerged that ARF7 regulates DR5 oscillations through heterodimerization with IAA18/POTENT (Perianez-rodriguez et al. 2021). Expression of a mutated IAA18, which increased protein stability, caused an increased in the

formation of LRFCs and a reduction in spacing of pre-branch sites. Likely, ARF7 is regulated both by IAA28, which controls oscillation amplitude and intensity, and by IAA18, which controls the oscillations periodicity. Without degradation of IAA18 by auxin influx in the basal meristem, the pre-branch site spacing gets distorted leading to increased LRFC formation (Perianez-rodriguez et al. 2021). The influx of auxin into this regulatory loop could be distorted by external stimuli, which in turn can control pre-branch site spacing and LR formation.

Auxin distribution in the root tip is thought to be instrumental in formation of the DR5 expressing pre-branch sites. Blocking polar auxin transport by application of NPA reduced or completely abolished LR initiation due to reduced transport from root tip to basal tissues (Casimiro et al. 2001). Key to this transport is the auxin influx carrier AUX1, which drives the epidermal auxin flux from tip to basal meristem (Bennett et al. 1996; Swarup et al. 2005). Mutations in *AUX1* severely decrease LR density and positioning, and also diminished DR5 expression and oscillation (De Smet et al. 2007). The disruption in LR patterning could be restored by solely expressing AUX1 in the epidermal and Lateral Root Cap (LRC) cells. These results suggest that AUX1 expression in the pericycle is not crucial for loading basal meristem cells with auxin necessary for establishing pre-branch sites and directing LR spacing (Laskowski et al. 2008; De Smet et al. 2007).

Another vital component of the oscillating pre-branch site formation is the conversion of IBA-to-IAA in the root cap. This enzymatic step was first revealed important in LR patterning by a small-molecule screen (De Rybel et al. 2012). This screen identified naxillin as stimulator of LR formation by promotion of the conversion of auxin precursor IBA into the active auxin IAA in the root cap (De Rybel et al. 2012). Naxilin specifically induced DR5-GUS activity in the basal meristem and induced a subset of specific auxin responsive genes (De Rybel et al. 2012). Mutations in genes involved in IBA-to-IAA conversion, the *IBA-RESPONSE* (*IBR*) genes, caused a decrease in DR5-LUC frequency and amplitude, suggesting this conversion directly affects pre-branch site oscillation (Xuan et al. 2015). By tissue specific expression of *IBR3* in the outer cells of the LRC, the IBA-derived IAA transport towards the oscillation zone could be restored which led to the restoration of LR formation (Xuan et al. 2015). The timing of IBA-derived IAA

transport correlates with recurrent program cell death in the LRC cells (Xuan et al. 2016). Programmed cell death of these LRC cells is thought to release pulses of auxin into the adjacent peridermal cells, establishing the oscillation signal for pre-branch site formation. How this auxin is subsequently transported radially into protoxylem or xylem pole pericycle cells remains elusive, but likely this is due to a combination of carrier-dependent and plasmodesmatal-mediated transport of auxin (Xuan et al. 2016; Mellor et al. 2020).

1.3.3 The birth of lateral root founder cells

When a pre-branch sites receives more activating than inhibitor signals it enters the next stage of development, the initiation of LRFC (Fig 1.4). Not all pre-branch sites will further develop into a LRFC. This is thought to be dependent on secondary signals that are linked to a root's direct environment. This assures an extra regulatory step before resources are wasted in creating a new root organ. In this scenario pre-branch sites are continuously made in the oscillation zone but are only activated for further development in late elongation or differentiation zone.

One candidate for the specification of LRFCs is the transcription factor GATA23. Its patchy expression pattern in a subset of XPP cells indicates strong oscillatory regulation (De Rybel et al. 2010). GATA23 acts in an auxin dependent signalling cascade together with AUX/IAA28 and class A (activating) ARFs (ARF5, 6, 7, 8, and 19). Analysis of *pGATA23-GUS* revealed expression just behind the basal meristem in the early elongation zone. Both *GATA23* knock-out and *gain-of-function* mutations led to alterations in numbers and spacing of LRP (De Rybel et al. 2010). Its oscillatory expression, localisation, and role in LR numbers makes it a strong candidate for coordination of the transition from pre-branch site to LRFC.

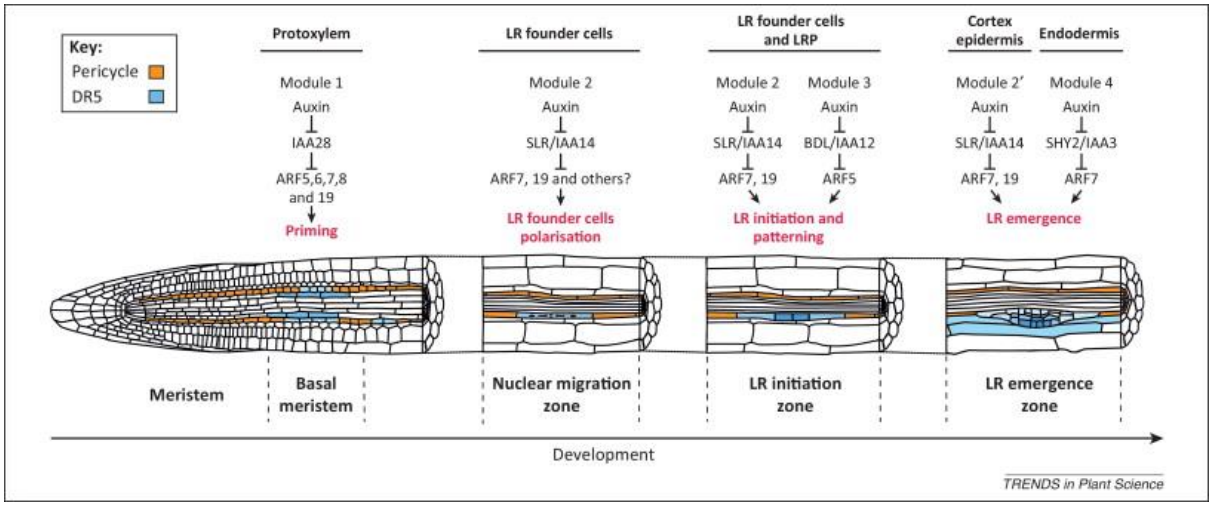

Figure 1.4 – Auxin signalling modules are key in all steps of lateral root formation. LR pre-branch sites are formed in the basal meristem or oscillation zone, where cells are primed by slightly increased auxin response through IAA28- ARF5,6,7,8,19 module. In the older root tissue, LR initiation start by the selection of xylem-pole pericycle cells that will become LR founder cells (LRFCs). These cells are specified by auxin accumulation and controlled by IAA14/SLR and ARF7,19 module. The auxin accumulation drives the migration of LR founder cell nuclei to a common cell wall. LR initiation is then modulated by two auxin modules, the IAA14/SLR– ARF7,19 and the IAA12/BDL–ARF5 modules. This starts as the LRFCs undergo the first round of asymmetric divisions. These two modules also regulate the development of the LR primordium. When the LRP starts to push against the overlaying tissue layers, auxin modules induce localized cell shrinking and cell wall remodelling in the endodermis through IAA3/SHY2 –ARF7 module. Whereas in the cortex and epidermis cell wall remodelling enzymes are mostly activated through IAA14/SLR- ARF7,19 module, which induces different gene targets than in LRP development (Lavenus et al., 2013).

Another candidate for regulating this pre-branch site transition is MEMBRANE-ASSOCIATED KINASE REGULATOR4 (MAKR4). MAKR4 is a downstream component important for the conversion of IBA to IAA (Xuan et al. 2015). This gene is lowly expressed in the oscillation zone, but strongly induced in the newly formed pre-branch sites, which corresponds with the oscillation time of DR5 in the oscillation zone. MAKR4 is localized on the plasma membrane of pericycle cells prior to nuclear migration. MAKR4 amiRNAi knock-down lines, displayed a normal number of pre-branch sites, but a reduction in LRP (Xuan et al. 2015). The opposite was true for over-expression lines of MAKR4 that showed increased LR formation. This indicates a promising role for MAKR4 in the specification and activation of LRFC.

1.3.4 Primordia morphogenesis

After a pre-branch site is activated, the next phase starts with nuclear migration towards a common cell wall and the swelling of the nuclei into a sphere shape. This developmental process coincides with swelling of the two LRFCs prior to division (Vermeer et al. 2014). The phase ends after the first asymmetrical division in the pericycle generates two short and two longer daughter cells (De Smet et al. 2006). New research suggests that LRP initiate from a single LRFC, which recruits neighbouring XPP cells to become FCs, both longitudinally and radially (Torres-Martinez et al., 2020). These cells then recruit their neighbouring cells within a couple of hours through auxin signalling and transport (Torres-Martínez et al. 2020). In the end even the PPP cells are recruited, potentially to form part of the vasculature system of the new LR (Torres-Martínez et al. 2020). Auxin levels in LRFC are increased by synthesis and transport. Transcription factors FUSCA3 (FUS3) and LEAFY COTYLEDON (LEC2) induce transcription of *YUCCA4*, an auxin biosynthesis gene, in LRFCs (Tang et al. 2017). In parallel, auxin transport directs the flow of auxin towards LRFCs. A major component of this auxin movement is induction of PIN3 in overlying endodermal cells during nuclear migration (Marhavý et al. 2013). The *pin3* mutant exhibits a delay in very early stages of LR initiation (Marhavý et al. 2013). PIN3 directs the flow of auxin from endodermis to LRFC as is observed by the localisation of PIN3 on the inner membrane adjacent to the LRFC (Marhavý et al. 2013). Likely this is to boost the influx of auxin into the LRFC to induce rounds of cell division.

Auxin signalling in overlying tissues also regulates LR initiation (Fig 1.4). The major regulator of the endodermal auxin response is SHOOT HYPOCOTYL2 (SHY2)/IAA3. By using the strong endodermal promoter of *CASP1* to drive the expression of the gain of function mutation *shy2-2*, Vermeer et al., observed strong inhibition of LR initiation (Vermeer et al. 2014). The authors observed that endodermal cells overlaying LRP did not shrink, blocking anticlinal LRFC division (Vermeer et al. 2014). Hence, SHY2 degradation in endodermal cells induces the volume loss necessary to allow cell division in the initiating LRP. Related research from Marhavy et al., (2016) showed a similar role for the endodermis. Ablation of the overlying endodermis cell triggers mitoses in the underlying XPP cells (Marhavy 2016). However, this ablation does not lead to formation

of a functioning LRP, for that auxin co-treatment is necessary. This experimental approach neatly demonstrated the importance of a reduction in size of the overlaying endodermal layer coupled with functional enhanced auxin signalling as a prerequisite for lateral root organogenesis (Marhavy 2016). Both results demonstrate the importance of pericycle and endodermal feedback that allows for the initiation of primordia.

The activation of anticlinal division is dependent on a second auxin module involving SLR/IAA14, ARF7 and ARF19, and its downstream targets such as *LBD16* and *LBD29* (Fukaki et al., 2005, 2002; Okushima et al., 2007; Fig 1.4). Mutants in *SLR* and *ARF7 ARF19* lack lateral roots, indicating their importance in this process. De-repression of ARFs, by auxin induced breakdown of AUX/IAA, triggers transcriptional activation of *LBD16* specifically in LRFCs adjacent to the XPP (Goh et al. 2012a). LBD16 is vital for nuclear migration to a common cell wall which precedes the first asymmetrical cell division as this is blocked in LBD16-SRDX dominant repressor lines (Goh et al. 2012a). In addition, several other LBD family members are involved in breaking of cell asymmetry. LBD18 and LBD33 proteins function as dimers to bind the promoter of cell cycle transcriptional activator *E2Fa*, which also regulates the first asymmetric cell division (Berckmans et al. 2011). Overexpression of LBD18 could even promote LR formation in *arf7 arf19* mutants (Lee et al. 2009). Interestingly, LBD16 and LBD18 might work in tandem as the double *lbd16 lbd18* mutant has a stronger reduction in LR emergence than either of the single mutants (Lee et al. 2009).

Evidence is emerging that next to auxin also several signalling peptides are involved in LR initiation (Fernandez et al. 2013). One well studied peptide is GLV6. This member of the GROWTH FACTOR/CLE-like (GLV/RGF/CLEL) family is expressed before the first asymmetric division in LRFCs and controls the patterning of the first pericycle divisions (Fernandez et al. 2015). *Loss-of-function* mutants in *GLV6* and its close homologue *GLV10* increases asymmetric cell divisions during lateral root initiation (Fernandez et al. 2020). *glv6 glv10* double mutants showed increased initiation events in the pericycle, indicating these GLV's function as inhibitors of cell division. The authors hypothesize this inhibitory effect might be a way to block adjacent pericycle cells from initiating cell

division, thereby creating a central LRFC and delimiting cell divisions in the pericycle layer (Fernandez et al. 2020).

In addition, cell wall remodelling enzymes from the EXPANSIN (EXPA) family modulate the mechanical properties of the pericycle cell wall during LR initiation. Mutants in *expa1* displayed defects in the positioning of the first anticlinal divisions as well as swelling of the LRFCs (Ramakrishna 2019). In *expa1* mutants LRFCs swell across the whole cell length, instead of locally near the common cell wall. This in turn affects where the first anticlinal division takes place. Hence, localized radial expansion is required for the right positioning of the first anticlinal division plane during LR initiation. Furthermore, EXPA14 and EXPA17 play a role in later LR developmental stages and are LBD18 inducible (Lee HW 2013a;Lee HW 2013b). Knocking down levels of *EXPA17* by using RNAi demonstrated the importance of this gene in stage 2 and 3 of LRP development, where there is a delay in organ emergence (lee 2013). Contrastingly, overexpressing *EXPA14* and *EXPA*17 results in an increase in LR density, demonstrating that the enzymatic modification of the cell wall is of crucial importance to the speed of LR emergence, potentially through modulating cell swelling.

1.3.5 Patterning under pressure

After the LR initiation stage and the first asymmetric division within the pericycle cells, the newly formed LRP has to grow through overlying endodermal, cortical and epidermal tissues before emerging (Swarup et al. 2008). This involves complex biomechanical interactions between the overlying tissues and primordium that impact organ initiation and morphogenesis (Kumpf et al. 2013; Lucas et al. 2013; Péret et al. 2012; Vermeer et al. 2014). This involves the adaptation and remodelling of both the expanding dome-shaped LRP as well as the overlying endodermal tissue, which is the first tissue layer encountered by the growing primordia (Lucas 2013). The endodermal layer also contains the hydrophobic impermeable barrier, the Casparian strip (Naseer et al. 2012; Lee et al. 2013b). Simultaneously, the overlaying cells have to shrink and degrade the Casparian strip. To progress through this diffusional barrier it has to be

locally degraded at the tip of the LRP (Vermeer et al. 2014). This allows passage of the growing LRP yet protects the vasculature.

The shrinkage of the endodermal cells is possibly facilitated through transport of water via plasmodesmata or aquaporins (discussed in more detail in subchapter 1.5). During development the primordium becomes increasingly more isolated from the overlaying layer through callose deposition, blocking cell-to-cell transport via plasmodesmata (Benitez-Alfonso 2013). This development might block the diffusion of water back into the shrinking endodermal cells. Furthermore, aquaporins passively move water across the cell membrane following the direction of the osmotic pressure. Some classes of aquaporins are excluded from the developing primordium possibly to retain water and block water from flowing back to the shrinking overlying endodermal cells. Mutating several aquaporins localised to the tonoplast and plasma membrane severely delay LR emergence, indicating a prime role for aquaporins in LRP outgrowth (Peret 2012; Reinhardt 2016).

Emerging LRP have to pass through the overlying endodermal, cortex and epidermal tissues which are tightly linked together by cell walls. To break these strong bonds, specialised cell wall enzymes are needed which are induced through a signalling network involving peptides. One of these is the signal peptide INFLORESCENCE DEFICIENT IN ABSCISSION (IDA) and its leucine rich repeat receptor-like kinases HAESA (HAE) and HAESA-LIKE2 (HSL2) (Kumpf et al. 2013). Mutations in these three genes impairs LRP emergence especially through the cortex and epidermis (Kumpf et al. 2013). The IDA peptide is induced by auxin flow originating from the growing primordia and facilitated by the LIKE-AUXIN3 (LAX3) transporter in first cortex and subsequently epidermis cells overlying the LRP. This causes breakdown of Aux/IAAs repressors and de-repression of ARF7 and, in turn, induction of IDA. The IDA receptors HAE and HSL2 regulate the expression of several polygalacturonases which hydrolyze pectins (González-Carranza et al. 2007; Kumpf et al. 2013). The simultaneous increase of several other cell wall degrading enzymes such as pectate lyase (Laskowski et al. 2006; Swarup et al. 2008) and xyloglucan endotransglucosylase/hydrolase (Swarup et al. 2008) loosen cell-cell connections, enabling cell separation in advance of the emerging LRP.

Interestingly, these enzymes do not affect the LRP itself. This might be explained by the difference in cell wall composition in which the cell walls in the LRP are mostly methylated, while the overlying cells have become demethylated through action of the pectin methyl esterases (Laskowski et al. 2006). Another possibility is that suberin lamellae, deposited on the primordium when developing through the endodermis, protects it from the action of cell wall degrading enzymes (Martinka et al. 2012). This restricts cell wall enzymes action specifically to the overlying cortex and epidermis tissues.

Recent work has highlighted a potential role for cell death in cells overlaying the LRP. The expression of several marker genes for developmental cell death were detected in a subset of cells overlaying the LRP (Escamez et al. 2020). Stains and live-imaging were used to confirm dead of overlying LRP cells. Cell death of the overlaying endodermis was in some cases observed before the developing LRP had crossed this layer. When cell death was distorted by a mutation in ORESARA1/ ANAC092 (ORE1), a transcription factor contributing to activation of downstream cell death related genes, LRP emergence was delayed (Escamez et al. 2020). This delay could be restored by laser ablation of the overlaying endodermis or expression of a cell-death promoting factor, indicating an important role for induced cell death in emergence of the LRP. This data is in conflict with what was earlier demonstrated by Vermeer et al., (2014) in which the endodermal cells seemed to shrink to allow the emerging LRP through. Likely, both processes occur in a seedling during LRP development. This might be influenced by the overlaying endodermis. Potentially if the LRP is overlain by one endodermis, shrinking of this one cell will not be enough to allow emergence of the LRP and the build-up of mechanical forces by the growing LRP can induce cell death when reaching a certain threshold. However, if the primordium is overlain by two endodermal cells, shrinkage might be enough to allow passage through without cell death being induced. Therefore, LRP emergence is a highly plastic process, which can impact the overlaying tissue layers in several ways.

LAX3 is a crucial driver of auxin influx from the primordium apex into the overlying tissues (Swarup et al. 2008). *LAX3* is induced in cortex and endodermal cells overlying

LRP to selectively promote auxin influx (Swarup et al. 2008). An ARF7 and LBD29 signal transduction pathway underlies the induction of LAX3 in these tissues (Porco et al. 2016). *LAX3* expression is often restricted to two cortex and epidermal cells files to ensure local cell wall separation (Peret et al. 2013). The LAX3 auxin influx is induced with the auxin efflux carrier PIN3 to create a reflux loop between overlaying tissues and developing LRP (Peret et al. 2013). The auxin that moves from the XPP cells to the overlaying cell files activates PIN3 in the cortex that then causes signal efflux into the epidermis (Peret et al. 2013). The two cortex cells overlaying the LRP accumulate the most auxin which slowly induces *LAX3* and facilitates greater auxin accumulation. This then triggers cell wall remodelling enzymes induction that cause localised cell separation.

Another source of a signalling molecule that has been proposed to function during LR emergence is ROS. The addition of ROS to media increased LR density and can restore the formation of LRs in *aux1 lax3* mutants (Orman-Ligeza et al. 2016). These results indicate a role for ROS in inducing cell wall remodelling and cell separation. ROS was detected in the middle lamellae of cells overlying LRPs (Orman-Ligeza et al. 2016). Mutation of ROS producer RESPIRATORY BURST OXIDASE HOMOLOGS (RBOH) led to the deceleration of LRP emergence. Hence, RBOH-mediated ROS production mediates cell wall remodelling of overlying tissues. However, the direct target or receptor of this signal is still unknown. In turn, ROS levels are balanced through control of RBOHs and ROS scavengers such as peroxides (Manzano et al. 2014). Several peroxidases have been shown to be induced in developing LRP (Manzano et al. 2014). A subset of these peroxidases are controlled by the transcription factor *MYB36*, which is expressed in cells surrounding the LRP (Fernández-Marcos et al. 2017). Mutants in *MYB36* display deformed LRPs and a delay in their emergence (Fernández-Marcos et al. 2017). Interestingly, LR emergence could be restored to Col-0 levels by reducing the levels of hydrogen peroxide, indicating a role for MYB36 in balancing ROS levels to define the LRP boundary (Fernández-Marcos et al. 2017). However, has to be noted that *MYB36* mutants display increased levels of lignification similar to other mutants in Casparian strip formation such as: *esb1-1* and *casp1-1/casp3-1* (Lucas et al. 2013). The LR emergence delay might therefore be a result of increased lignification of the

endodermis overlaying the LRP, which first has to be degraded before the LRP can penetrate this layer.

1.3.6 Lateral root meristem activation

The final step in LR formation involves activation of the LR meristem. A large number of genes that regulate the root apical meristem (RAM) also controls this process in LRP. This includes members of the transcription factor family of AP2/ERF PLETHORA (PLT) (Scheres and Krizek 2018). These genes are expressed in LRP, where they control spacing and emergence (Hofhuis et al. 2013). In this family, PLT3, PLT5 and PLT7 regulate expression of other members (PLT1, PLT2 and PLT4) in LRP development (Hofhuis et al. 2013). Creation of the triple null *plt3 plt5 plt7* mutant resulted in defects in the very first anticlinal division of LRFC (Du and Scheres 2017). Furthermore, these LRP were deformed and did not have a defined meristem. This phenotype could be restored by expression of any of these three PLTs (Du and Scheres 2017). This result demonstrates that these PLTs act redundantly to organize LR initiation and LRP meristem activation.

Another established regulator of meristem activation is the GRAS-family member SCARECROW (SCR). Disruption of this gene alters periclinal divisions in LRP and obstructs quiescence centre (QC) formation (Goh et al. 2016). *SCR* expression is especially important for patterning in the outer layer of stage II LRP (Goh et al. 2016). This is the start of early QC morphogenesis until stage V LRP where positioning of QC is defined, and meristem formation phase begins. Both the role of SHR and PLT shows the high degree of similarity between meristem organisation in the root apex and the activation of a new LRP QC.

1.4 Lateral root adaptive responses to water availability

1.4.1 Xerobranching: root branching inhibition during absence of water

Soil consists of heterogeneously available water and other nutrients that roots need to acquire. Roots have developed adaptive mechanisms to locate and respond to local water availability. In soil, water is bound by pores or adheres to soil particles (Luxmoore

1981). During drought pores will slowly release water and increase the proportion of gas filled pores. It is crucial for a root to access water rich pores, so plants have developed several adaptive mechanisms designed to guide root growth and branch towards available water. For example, barley and maize roots growing through air filled macropores exhibit a complete inhibition of branching (Orman-Ligeza et al. 2018). This adaptive response, termed xerobranching, was first observed in aeroponically grown maize and barley roots exposed to a transient water deficient (Babe et al. 2012). This root response conserves water and resources necessary for the development of LRs in more favourable areas (Fig. 1.5A). Intriguingly, LR initiation in water deficient barley was blocked at the very first stage of asymmetrical cell division (Babe et al. 2012). This indicated that LR repression acts upon a very early developmental stage sensed near the root tip (Babe et al. 2012). LR inhibition could be partially restored by treatment with auxin analogue, IBA (Babe et al. 2012). This demonstrated that root cells in this developmental zone did not lose their competency to form LRs, but might experience reduced auxin accumulation necessary to promote asymmetric cell division. A similar lack of LR initiation was observed when barley roots were treated with ABA using aeroponics (Orman-Ligeza et al. 2018). Phytohormone measurement in root tissues exposed to water deficit revealed a significant increase in ABA levels compared to well-watered plants (Orman-Ligeza et al. 2018). The ABA response is regulated by PYR/PYL/RCAR family of ABA receptors (Gonzalez-Guzman et al. 2012). Higher-order *A. thaliana* mutants in *PYR/PYL* exhibited a loss of the LR suppression when treated with ABA (Orman-Ligeza et al. 2018). Interestingly, the plasma-membrane permeable NAA could fully restore LR initiation yet treatment with actively transported IAA could only partially restore LR number. Active auxin transport might therefore be crucial for ABA mediated LR suppression. Additionally, profiling auxin precursors and conjugates in the competent zone revealed a decrease in free IAA levels and an increase in auxin conjugates (Orman-Ligeza et al. 2018). Auxin response was monitored using the DR5-Luciferase reporter, which showed decreased pre-branch site formation. These results led the authors to speculate that ABA accumulation in the water deficit zone supresses the formation of pre-branch sites by impairing either auxin response or accumulation.

1.4.2 Hydropatterning: root branching towards external water

When a primary root is exposed to asymmetric water availability across its circumferential axis, lateral roots emerge on the side the water source is located (Fig. 1.5A). This adaptive response has been observed in *A. thaliana* and several monocots and termed lateral root hydropatterning (Bao et al. 2014). This assures branching in areas of available water. For the LR hydropatterning response to sense water location it requires external water influx. Hydropatterning was supressed when primary root growth was blocked by chemical inhibitors, suggesting that the rate of water influx is crucial for water sensing. Mathematical modelling of water uptake and distribution in maize demonstrated that local water availability drives a change in internal water hydraulics controlling the hydropatterning response (Robbins and Dinneny 2018). This ability of roots was termed the "sense-by-growth" mechanism in which external water influx in the zone of elongation perceives localisation of water availability (Fig. 1.5B). This mechanism proposes that the elongation zone is the site where water is perceived, as also recently proposed for the hydrotropism response (Dietrich et al. 2017). Focussing in on this zone could help unravel the molecular mechanisms that lead to perception of the hydropatterning stimuli and the origin of the signalling cascade which leads to LR emergence on the side of roots exposed to water.

The genetic mechanism explaining how plant roots respond to a hydropatterning stimuli is still being elucidated. In contrast to xerobranching, where *pyr/pyl* ABA receptor mutants exhibited a xerobranching defect (Orman-Ligeza et al. 2018), no suppression of LR hydropatterning response was observed (Bao et al. 2014), indicating these responses are distinct. Instead hydropatterning is controlled by attenuating auxin signalling. Mutants in auxin biosynthesis (*wei8-1*) and auxin transport (*pin2/3/7*) increased the proportion of laterals emerged towards the air versus agar, suggesting this hormone regulates root hydropatterning (Bao et al. 2014). Recent research validated the importance of auxin during hydropatterning, demonstrating that AUXIN RESPONSE FACTOR 7 (ARF7) knock-out mutants could no longer orientate their lateral roots towards agar (Orosa-Puente et al. 2018). This thesis will expand on this finding and explore how ARF7 regulates LR hydropatterning.

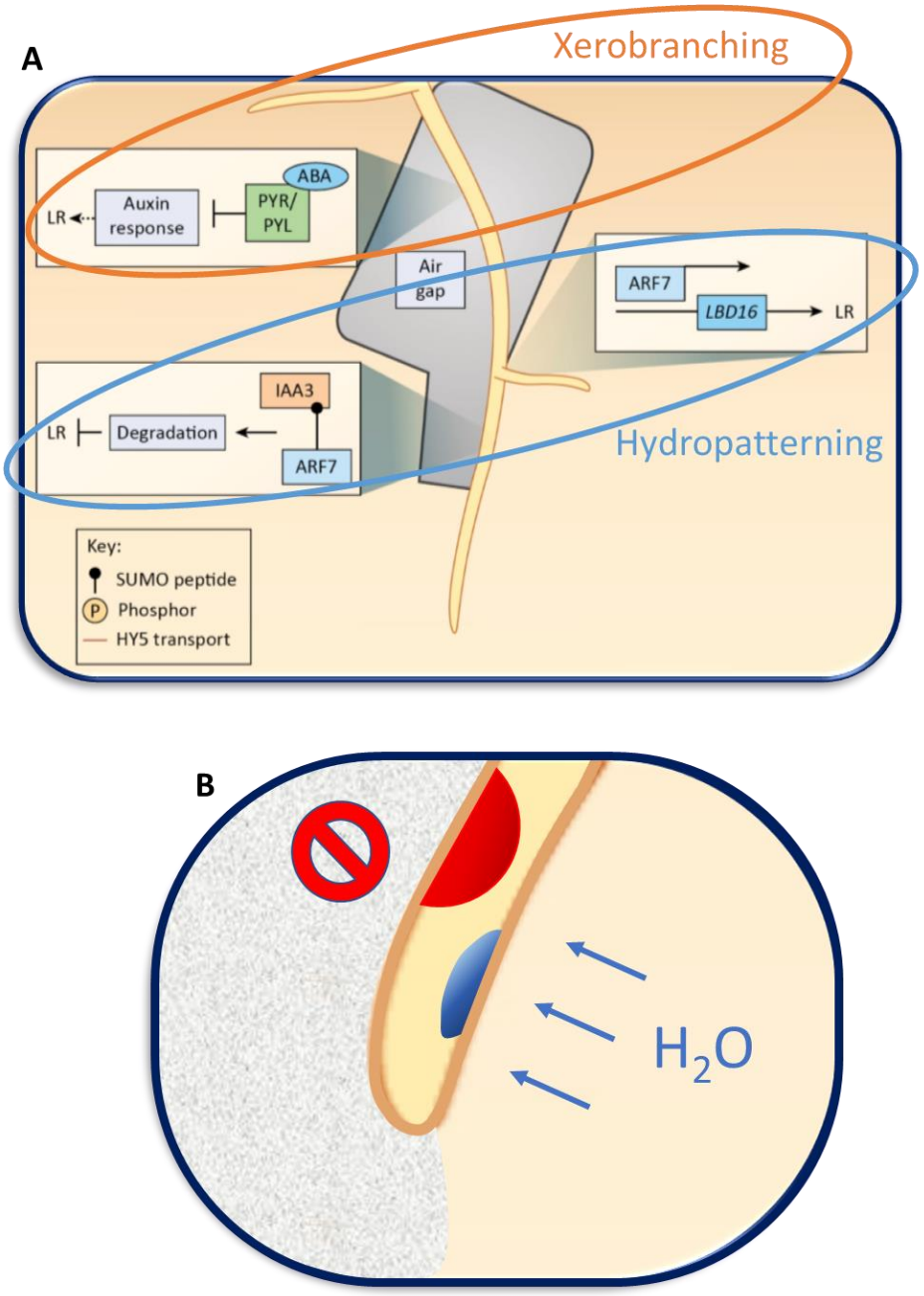

Figure 1.5 – Lateral root adaptive responses in soil regulated through water availability. Xerobranching is the adaptive response in which lateral root initiation is blocked when a root grows through an air gap (A). This response is regulated through accumulation of ABA, which binds to its receptor the family of PYR/PYL proteins. This binding indirectly leads to the conjugation of auxin and therefore the inhibition of the auxin response. The lateral root hydropatterning response directs root branching towards soil containing available water (A). SUMOylated ARF7 on the root side exposed to air causes binding to IAA3 repressor proteins that lead to ubiquitination and degradation of ARF7. However, on the side exposed to water deSUMOylated ARF7 is active and transcribes downstream targets to induce LR formation. Water is thought to be perceived in the fast growing elongation zone where a root acquires the signal to initiate or inhibit lateral root formation (B)(Banda et al., 2019).

1.5 Water transport and movement

1.5.1 Soil water uptake

Water uptake and shootwards transport is driven by leaf transpiration and xylem hydraulic conductance. Hydraulic conductivity describes the ease with which water flows through the xylem by means of high capillary force and surface tension of water molecules. This can be directly affected by radial expansion of the vasculature. Water moves through the xylem from high to low water potential. Shoot transpiration creates a negative water potential in the shoot and forces water in via the root, where it is transported via the vasculature xylem towards the shoot (Kramer and Boyer 1995). In natural conditions, water potential is modulated by changing atmospheric humidity and soil water content. In the plant, water potential varies per organ and is dependent on local tissue pressure, osmotic, gravimetric, air pressure and matric potentials. Roots need a water potential that is lower than that of the surrounding soil to take up water, but not too low as to limit transport to shoot tissue. Internal changes in long distance water potential can be mediated by regulation of hydraulic (Cochard et al. 2007), stomatal conductance (Tardieu and Davies 1993), and osmotic adjustment through build-up of solutes. Between different plant tissues the water potential is often kept in equilibrium. However, the local soil environment can directly influence tissue water potentials. During hydropatterning, when one side of the root is in contact with water, the water potential across the root circumference is strongly variable (Robbins and Dinneny 2018). This change in water potential observed during hydropatterning could be part of the sensory mechanism, which controls this adaptive response.

Other than internal adaptations to optimize water uptake, plants also display morphological responses. The three-dimensional shape of the root system dictates the availability of external water, yet not all classes of roots take up the same rate of water. Research using neutron radiography revealed in lupin and maize roots water is mostly taken up by the proximal zone compared to the distal zone (Zarebanadkouki et al. 2013; Ahmed et al. 2016). In these experiments water uptake was tracked using D_2O (heavy water), as a proxy for water, and imaged using neutron radiography. Water uptake by lateral roots was much higher than seminal roots in two week old maize plants.

However, in five-week old maize plants most water was take up by crown roots and only a minor fraction by laterals (Ahmed et al. 2018). There results indicate that in maize laterals are crucial for water uptake in early plant life, but this is taken over by other classes of roots when more mature.

1.5.2 Symplastic transport through plasmodesmata

There are multiple routes for water to travel through root tissues; the apoplastic and the symplastic pathway (Fig. 1.6A). In the apoplastic pathway water never enters the cells but travels through the apoplastic space between membrane and cell wall. In the symplastic pathway water moves from cell-to-cell through water channels termed plasmodesmata (PD). PD are channels spanning cell walls and directly connecting two cell's cytosol with each other (Fig. 1.6B). Primary PDs are formed during cell division and consist of part of the endoplasmic reticulum (ER) which gets stuck between the newly formed cell wall. PDs formed after cell division between existing cell walls are called secondary PDs (Ehlers and Kollmann 2001). PD allow cytosolic molecules to move freely between two neighbouring cells through diffusion as long as molecules are small enough. Research has shown that this size is roughly between 60 - 70 kD, but this can be influenced by age, tissue and environmental conditions (Kim et al. 2005; Paultre et al. 2016). Molecules that can move across PD include transcription factors (TFs) (Rim et al. 2011), RNAs (Furuta et al. 2012) and phytohormones (Rutschow et al. 2011).

In *A. thaliana* the phytohormone auxin, with a size of ~200 Da, can be symplastically transported through PD (Rutschow et al. 2011). This flux is under fast control of internal signals such as hydrogen peroxide (Rutschow et al. 2011). Auxin can also directly regulate its own transport through PD by affecting callose deposition (Han et al. 2014b). The quantity of callose (β-1,3-glucan) deposition on the PD controls the size of the molecules that can freely flow through. Higher callose deposition excludes larger molecules from diffusional flow through the PD (Iglesias and Meins 2000; Vatén et al. 2011). Through callose deposition PD flow can be finely regulated spatially and temporally.

Auxin regulates callose deposition through GLUCAN SYNTHASE-LIKE 8 (GSL8), a callose synthase, which was shown to control the uneven distribution of auxin after phototropic bending. (Han et al. 2014b). Knocking down *GSL8* levels disrupted the ability to create an asymmetrical concentration gradient which is necessary for tropic bending. The observed asymmetrical gradient was not regulated by active polar auxin transport (PAT), since blocking PAT did not disturb it. Since earlier studies have shown that PIN3 mediated auxin transport was also involved in phototropic bending (Friml et al. 2002), tight regulation of PAT and symplastic auxin diffusion must exist.

Many other proteins regulate levels of callose on PD. β-(1,3)-glucanases break down the callose and increased intracellular connectivity (Levy et al. 2007). Two of these enzymes, Plasmodesmata β-(1,3)-glucanase 1 (PdBG1) and PdBG2, are localized at PD and expressed in the root (Benitez-Alfonso et al. 2013). *pdbg1,2* double mutants exhibited increased callose deposition, resulting in decreased PD dependent transport. These mutants displayed increased LR density and distorted primordia patterning. Decreased symplastic flow of auxin due to increased callose formation could contribute to local auxin accumulation, essential for lateral root initiation. Following the first asymmetric cell division LRP become increasingly isolated from overlying cells due to callose accumulation on PD, which was visualized using the carboxyfluorescein diacetate (CFDA) dye. In Wild-Type *A. thaliana* the dye was blocked between developing primordium and overlying tissue. However, in *PdBG1* over-expressors the dye was clearly visible in the LRP, indicating that PdBG1 lessens callose formation, thereby disrupting PD isolation between LRP and overlaying cells. Symplastic transport is likely to be crucial for regulating movement of mobile TF's or peptides that can inhibit LR formation in adjacent XPP cells, thereby controlling LR spacing and DR5 oscillation (Moreno-Risueno et al., 2010).

Members of the plasmodesmata-localized protein (PDLP) family induce the formation of callose on PD. PDLPs are located to the PD by a single transmembrane domain (Lee et al. 2011; Thomas et al. 2008). Lines overexpressing *PDLP1* and *PDLP5* limit symplastic protein trafficking and induce the formation of callose on PD (Lee et al. 2011; Caillaud et al. 2014). During LRP development, auxin induced PDLP5 is expressed in cells

overlaying the LRP (Sager et al. 2020). PDLP5 localizes to the plasmodesmata where it controls callose deposition and negatively regulates LRP emergence. The authors suggest that the symplastic isolation of LRP at early stages in development might be necessary to build up turgor pressure in the swelling LRP cells.

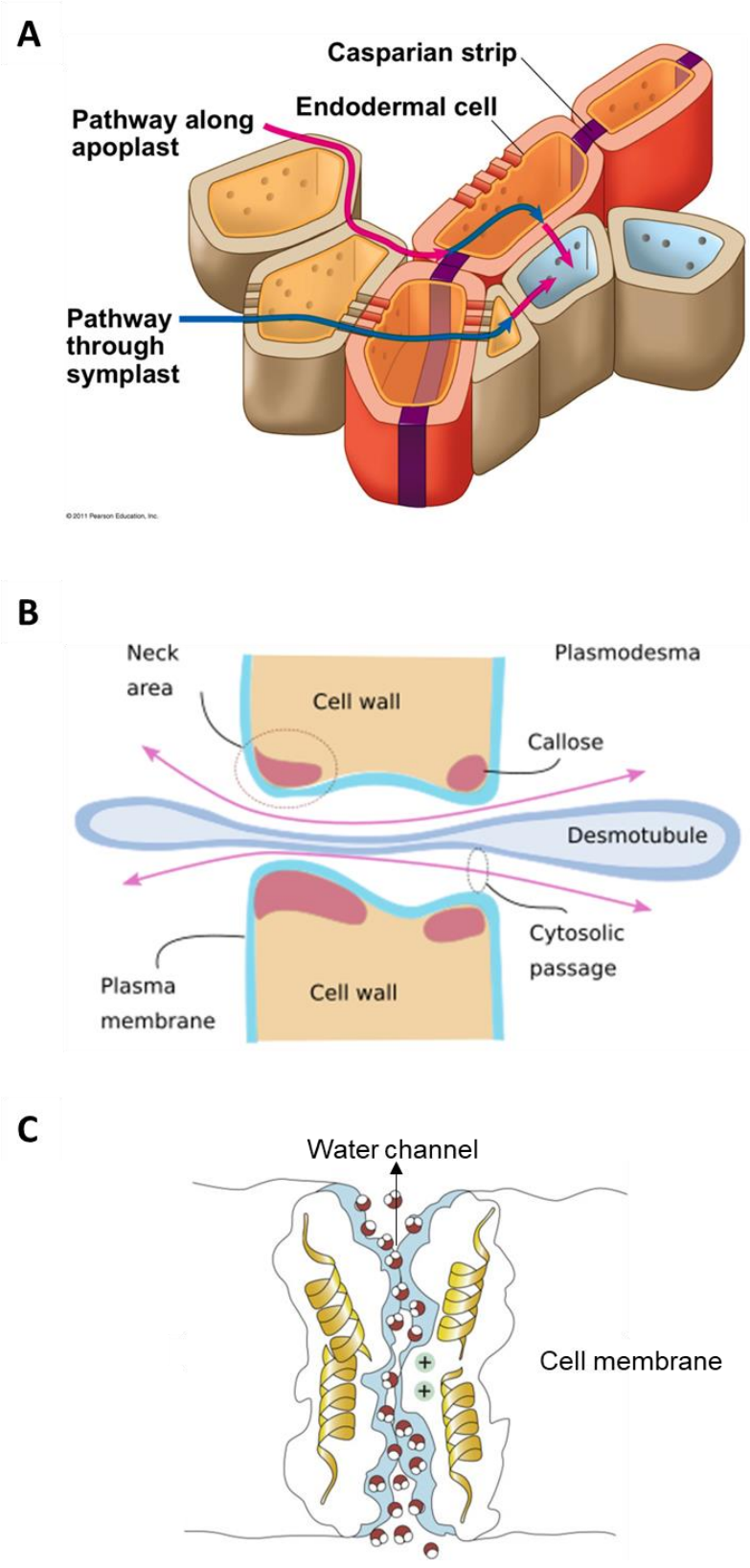

Figure 1.6 – The symplastic water flow in plants is controlled by plasmodesmata and aquaporins. Water in plants can follow two pathways, the apoplastic and symplastic pathway (Pearson Education 2001). In the apoplastic pathway water flows in the extracellular space between cell wall and membrane (A). This pathway is blocked by the lignified endodermis border termed the Casparian strip, blocking water

flow from cortex to pericycle. In the symplastic pathway water flows from cell-to-cell using plasmodesmata and aquaporins driven by osmotic pressure. Plasmodesmata are channels that directly connects the cytosol of two neighbouring cells Plasmodesmata (Atlas of plant and animal histology; https://mmegias.webs.uvigo.es/02-english/5-celulas/ampliaciones/3-plasmodesmos.php). The size of this opening can be adjusted by the level of callose deposition on the neck area (B). Reduced size can exclude bigger molecules from crossing the plasmodesmata. Aquaporins are part of a big family of channel proteins that form pores in the membrane to accommodate water flux (Litwack 2020)(C). The six transmembrane helices of this protein form a major part of this membrane channel.

1.5.3 Transcellular water transport through aquaporins

Another form of cell-to-cell water transport is established through water channels in the cell membrane termed aquaporins (Agre et al., 1993; Maurel, 1997; Fig. 1.6C). Aquaporins belong to the superfamily of Major Intrinsic Proteins (MIPs) consisting of four subfamilies conserved across plant species: plasma membrane intrinsic proteins (PIPs), tonoplast intrinsic proteins (TIPs), nodulin 26 like intrinsic proteins (NIPs), small basic intrinsic proteins (SIPs). However, some plant species evolved a new class of aquaporins termed X intrinsic proteins (XIPs), which are uncharacterized and distantly related to PIPs (Gustavsson et al. 2005). Aquaporins consist of six transmembrane helices with the protein N- and C-terminal on the cytoplasmic side of the membrane (Gomes et al. 2009). Four monomers dimerize together through hydrogen bonds to form a tetrameric complex. Each monomer can function as a single channel. The major subgroups of aquaporins are located at the plasma membrane and tonoplast. In addition to water transport these channels can also transport several small molecules, such as glycerol and H_2O_2, and small neutral solutes and ions (Gomes et al. 2009; Dynowski et al. 2008). Due to their localisation, aquaporins are believed to control cell expansion and water homeostasis.

Aquaporins expression and regulation are mechanisms to cope with environmental stresses. Waterlogging stress in the root of *Sorghum* led to differential expression *of PIP2-6, PIP2-7, TIP2-2, TIP4-4*, and *TIP5-1* in tolerant compared to sensitive genotypes (Kadam et al. 2017). This data suggests that aquaporins can react to changing water levels and this could be associated with the degree of waterlogging tolerance. However, the transcript level of aquaporin might not be an accurate measurement of water transport capability as recent observation showed that higher expression of PIPs does

not always lead to higher water uptake rate (Xu et al. 2017). This is due to multiple regulatory processes that control aquaporin functioning, such as phosphorylation and dephosphorylation (Maurel et al. 1995), ROS levels (Kapilan et al. 2018), cytosolic pH (Tournaire-Roux et al. 2003), vesicle trafficking (Vera-Estrella et al. 2004) and methylation (Santoni et al. 2006). These processes control localisation as well as opening and closing of the channels, increasing the complexity of the flux regulation by aquaporins.

During drought stress, *A. thaliana* overexpressing *PIP1;4* or *PIP2;5* displayed accelerated water loss, which reduced growth and survival rate (Jang et al. 2007). Overexpressing of these PIPs led to differential expression of other PIPs, suggesting a feedback mechanism that helps to regulate PIP levels during stress. Overexpressing the same two genes, AtPIP1;4 or AtPIP2;5, in Tobacco could increase plant growth rate, transpiration rate and photosynthetic efficiency under favourable conditions, whilst negatively affecting growth under drought stress (Aharon et al. 2003). These results suggest a tight control by aquaporins in controlling water homeostasis that is crucial for plant responses to drought.

Not only do aquaporins manage plant stress response, but they are also involved in local development of new organs. *pip2;1* mutants and overexpressing of *PIP2;1* disrupted the dome shape of LRP leading to a delay in emergence (Péret et al., 2012). Auxin caused a repression in the expression of multiple PIPs, which is under regulation of ARF7 as *arf7* mutants exhibited increased *PIP2;1* transcript and protein levels (Péret et al. 2012). As the LRP is increasingly symplastically isolated during development, it is likely that aquaporin transport is blocked within primordium cells, where auxin response is high, and increased in surrounding cells. This in order to stimulate water transport to the growing LRP and away from the overlying tissue layer. In addition to PIP also TIPs play a significant role in LRP emergence (Reinhardt et al. 2016). The *tip1;1,tip1;2,tip2;1* triple mutant displayed a delay in LR emergence, which could be rescued by complementation with TIP2;1. *TIP2;1* showed expression in the base of the LRP and might be mediating turgor pressure increase in early stages of LRP development (Reinhardt et al. 2016). PIPs

and TIPS thus work together to regulate turgor pressure in the developing primordium and overlying endodermis to facilitate emergence.

1.6 Sensing water availability at a cellular scale

Water is crucial for plant growth and development, yet not much is known on how it is perceived by plants. Most of the cell water resides within the vacuole accounting for nearly 80% of the cells volume (Haswell and Verslues 2015). The vacuole is one of the main drivers of turgor pressure in which the elastic plasma membrane, and all it encapsulates, pushes against the rigid cell wall. Turgor pressure is sustained by external water uptake and internal osmotic difference that is the results of solutes. The term osmo-sensing thus refers to the perception of the external or internal osmotic environment that drives water fluxes. As water is so freely available in cells it cannot alone be sensed by a simple receptor-based sensing mechanism. Multiple models for water or osmo-sensing have been described in literature and will be discussed below.

One of the most discussed water sensors are the membrane-bound mechano-sensitive (MS) ion channels (Fig. 1.7A). These can directly translate changes in hydraulic stimuli into chemical signals (Christmann et al. 2013; Hamilton et al. 2015). Tension changes in the membrane caused by the change in cellular turgor pressure could open MS ion channels. In plants multiple families of MS channels have been identified. One of the more well studied ion channels is the OSCA/TMEM63 family. The first plant identified member of this family, REDUCED HYPEROSMOLALITY-INDUCED $[Ca2+]_i$ INCREASE1 (OSCA1), encodes a calcium channel that is osmo-sensitive (Yuan et al. 2014). Mutants in *osca1* displayed reduced root growth and stomatal closure after osmotic stress resulting from impaired Ca^{2+} signalling. *OSCA1* is part of a family containing 15 homologs, one other member, *OSCA1.2*, also displayed osmotic stress induced Ca^{2+} influx (Hou et al. 2014). Further research concluded that this MS channel can be regulated through pressure, linking both mechanical regulation with a role as fast Ca^{2+} signalling component (Murthy et al. 2018). The recently revealed crystal structure of OSCA1.2 might give a better understanding of how the channel opening could be regulated (Liu et al. 2018).

Another MS Ca^{2+} channel candidate are the Mid1-complementing activity (MCA) proteins. In yeast studies MCA1 was shown to be located to the plasma membrane and function in Ca^{2+} influx (Nakagawa et al. 2007). Overexpressing this gene led to a failure to penetrate hard agar mediums, indicating a possible MS angle to MCA1. Overexpression of this gene's ortholog in rice, *OsMCA1*, led to activation of NADPH oxidases through binding to their EF-hand region. This binding led to the generation of ROS and could be the beginning of a signalling cascade on the osmo-status of the cell (Kurusu et al. 2012).

A second way of sensing osmotic changes is through detecting changes in cell wall composition as observed in yeast (Monshausen and Haswell, 2013; Fig. 1.7B). Receptor-Like Kinases (RLK) represent promising targets to fulfil this role. In general, RLKs are involved in early signal transductions and are located at the plasma membrane. Two of these RLK families are the WAK-Associated Kinases (WAK) family and *Catharanthus roseus* RLK family (crRLK). The WAK family contains an extracellular domain that is capable of binding pectin in the cell wall (Kohorn and Kohorn 2012). Pectin is an important structural component of the cell wall and therefore any change in composition could function as a signal for stress. Furthermore, *wak1* and *wak2* mutants exhibit reduced cell size and root growth on low osmotic media (Lally et al. 2001; Kohorn et al. 2006). These proteins seem important for cell wall expansion, but more research needs to elaborate if they sense changes in osmotic potential through their binding with pectin.

Another candidate for this type of cell wall integrity sensor is the crRLK FERONIA (FER). Mutations in this gene lead to defects in root growth, root hair development and penetrating hard agar (Guo et al. 2009; Duan et al. 2010; Haruta et al. 2014). Furthermore, *fer* mutants have a reduction of Ca^{2+} induction after touch or bending response (Shih et al. 2014). FER was also shown to be involved in sensing salt stress through monitoring the damage done to pectin cross-linking in the cell wall by high salinity (Feng et al. 2018). Pectin composition is sensed by the extracellular domain of FER that directly interacts with pectin (Feng et al. 2018). Damage to the cell wall is thought to be transmitted to the nucleus through interaction of FER with a calcium

channel, explaining the reduction in Ca^{2+} induction in mutants. Other members of this family such as THESUS, ANXUR1 and ANXUR2 have an extracellular maltose binding domain that might monitor similar changes in cell wall composition (Hématy et al. 2007; Boisson-Dernier et al. 2009; Miyazaki et al. 2009).

Other potential mechanisms of water sensing have also been proposed. A recent study showed proteins with high levels of intrinsic disorder (ID) are restructured during water deficient conditions (Cuevas-Velazquez et al., 2016; Fig. 1.7C). In this study the late embryogenesis abundant (LEA) proteins, which contain regions of ID, were shown to change from unstructured to structured depending on the level of water deficiency (Cuevas-Velazquez et al. 2016). This could be a direct way of changing protein activity or localisation due to a direct change in conformation.

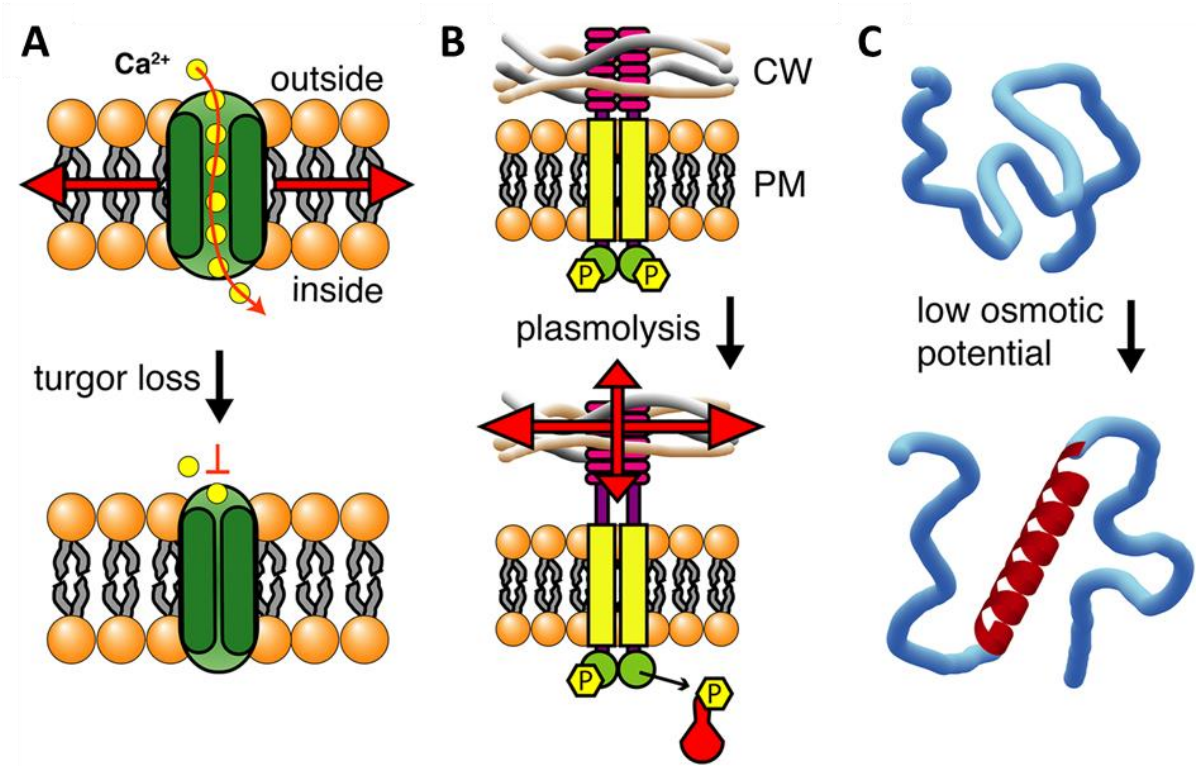

Figure 1.7 – Potential osmo-sensor models to detect changes in cellular water levels in plants. Mechano-sensitive (MS) ion channels are affected by a change in turgor pressure levels that affects cell membrane tension causing the opening and closing of these channels (A). Receptor-Like Kinases (RLKs) contain an extracellular domain that binds cell wall components such as maltose or pectin. Changes in the cell wall composition can signal drought and subsequently lead to phosphorylation and further signal transduction (B) Intrinsic-disorder (ID) domains can change their 3-dimensional shape due to changes in water potential and attain new functions (C). (Scharwies and Dinneny 2019).

Finally, instead of measuring plasma membrane and cell wall components, could the cell measure a change in water flux? Water itself would not be the ideal component to measure as it is so ubiquitously present. However, could water flux be measured through the movement of a signal molecule dissolved in water? One such water proxy could be Reactive Oxygen Species (ROS). These formerly known toxic by-products have recently been linked to a role as abiotic signalling molecules (reviewed in Baxter et al. 2014; Gilroy et al. 2014). ROS can easily move from cell-to-cell through plasmodesmata and can even control the flux by affecting callose accumulation (Benitez-Alfonso and Jackson 2009). Additionally, ROS and class III peroxidases are localized near the plasmodesmata, indicating some sort of ROS regulation of these water channels (Ehlers and van Bel 2010). Furthermore, ROS can also be transported from cell-to-cell via certain members of the TIPS and PIPs protein family, adding a secondary layer of fine-tuning ROS fluxes (Bienert et al. 2007; Hooijmaijers et al. 2012). A possible receptor to measure this flux is yet unknown. Likely candidates for this role are Cysteine-rich Receptor Kinases (CRKs). This family appears to be involved in detecting and transducing extracellular ROS signals (Idänheimo et al. 2014; Bourdais et al. 2015). Multiple other Leucine-Rich Repeat (LRR) RLKs have been implied to function in a similar manner and provide the plant with a valuable set of receptors to sense stress (Hua et al. 2012; Bourdais et al. 2015).

1.7 Could SUMOylation provide a water stress sensing mechanism?

1.7.1 The SUMOylation cycle

SUMO, or Small Ubiquitin-like Modifier, is a small polypeptide of approximately 11 kDa, found in both plant and eukaryotic cells. SUMO is bound to its substrate via a lysine residue in a process called SUMOylation, which enables plants to quickly respond to biotic and abiotic stress. In *A. thaliana* >1000 proteins are targets for SUMOylation, many of which are nuclear localised (Rytz et al. 2018). These proteins include transcription factors, coactivators, repressors and chromatin modifying proteins (Rytz et al. 2018). SUMOylation of a protein can cause a variety of responses including: (I) new protein-protein interaction, (II) a change in subcellular localisation, (III) a change in protein structure and activity, (IV) a blockage of protein-protein interaction, (V) SUMO-

targeted ubiquitin ligases (STuBLs) protein mediated ubiquitination and protein degradation, (VI) or a blockage of a ubiquitination site thereby inhibiting ubiquitination (Morrell and Sadanandom 2019). New protein interactions can be formed through non-covalent SUMO bonds with SIM sites (SUMO-interacting motif), thereby presenting the SUMOylated protein with a new range of interaction partners (Johnson 2004). Alternatively, SUMOylation can also prevent interaction by binding in a protein-protein interaction domain. The outcome of SUMOylation is not only dependent on the location of the SUMO binding site, but also on the number of SUMOs bound to a protein and the formation of poly-SUMO chains. This leads to a high variety of developmental responses all catalysed by the binding of one more SUMO peptides to a protein.

The SUMO cycle is highly dynamic with many parallels to the ubiquitination pathway, consisting of activation, conjugation, and ligation (Fig. 1.8). It starts with the transcription and translation of inactive preSUMO that becomes activated through cleavage by SUMO proteases, exposing a glycine residue (Kurepa et al. 2003). The *A. thaliana* genomes encodes eight SUMO isoforms of which only four appear to be expressed (*SUMO1, SUMO2, SUMO3* and *SUMO5*). Of these four, the highly similar *SUMO1* and *SUMO2* are dominant as they are both highly expressed and highly efficiently conjugated (Castaño-Miquel et al. 2011). The active SUMO can be bound by the E1 activation enzyme, which consists of a heterodimer of SAE1 and SAE2. Both SAE1a and SAE1b can be used to create the E1 complex, which needs ATP to form a high energy thioester bond between SUMO and SAE2. Activated SUMO is then transferred from E1 activation enzyme to the cysteine residue in the E2 conjugation enzyme, SCE1 which catalyses SUMOylation onto lysines (K) of target protein/substrates. This conjugation enzyme recognizes the SUMO site by its motif: ψKXE/D, in which ψ denotes a large hydrophobic residue, K the acceptor lysine, X any amino acid, and E (glutamate) or D (aspartate).

SIZ1 and HPY2 E3 ligase enzymes, interact with SCE1 to assist in the transfer of SUMO to substrates. However, SUMOylation can occur without E3 ligases, which begs the question of what the exact function of these E3 ligases is? Additionally, SUMO proteins can form poly-SUMO chains, leading to specific interactions with regulatory proteins

containing multiple SIM motifs (Aguilar-Martinez et al. 2015). This step is catalysed by E4 ligases of which two were identified in the *A. thaliana* genome, *PIAL1* and PIAL*2* (Tomanov et al. 2014). These polySUMO chains are direct targets for STUbL binding, a new class of ubiquitin E4 ligases (Elrouby et al. 2013). Binding of STUbLs to poly-SUMOylated substrate leads to ubiquitination and degradation of the substrate (Elrouby et al. 2013). At the end of the SUMO cycle, SUMO can be cleaved off of a substrate by deSUMOylating enzymes (isopeptidase activity). This refills the pool of free SUMO, as well as reverting the substrate into its prior non-SUMOylated state. These deSUMOylating enzymes are also crucial for maturing preSUMO at the start of the cycle by cleaving of the c-terminal peptide (peptidase activity).

In plants deSUMOylation is believed to be the key process in response to sensing stress. This is due to three main reasons. First, levels of free SUMO in the cell are low, therefor most SUMO in the cell is believed to be conjugated to a substrate (Johnson 2004). Second, a limited number of SUMO E1 activators and E2 conjugators are found in the *A. thaliana* genome and they showed no specificity for the various SUMO proteins, thus these do not discriminate during conjugation reactions (Chosed et al., 2006). Third, in contrast to E2 and E3 enzymes, 14 SUMO proteases have been characterized in the *A. thaliana* genome. These SUMO proteases have diverse levels of isopeptidase and peptidase activity (Chosed et al. 2006). Additionally, the proteases cannot cleave the same SUMO's, indicating possible diverse functions for some of these genes (Chosed et al. 2006). It is therefore proposed that in plants deSUMOylation provides the specificity to the SUMO system and plays a key role in regulation of stress responses.

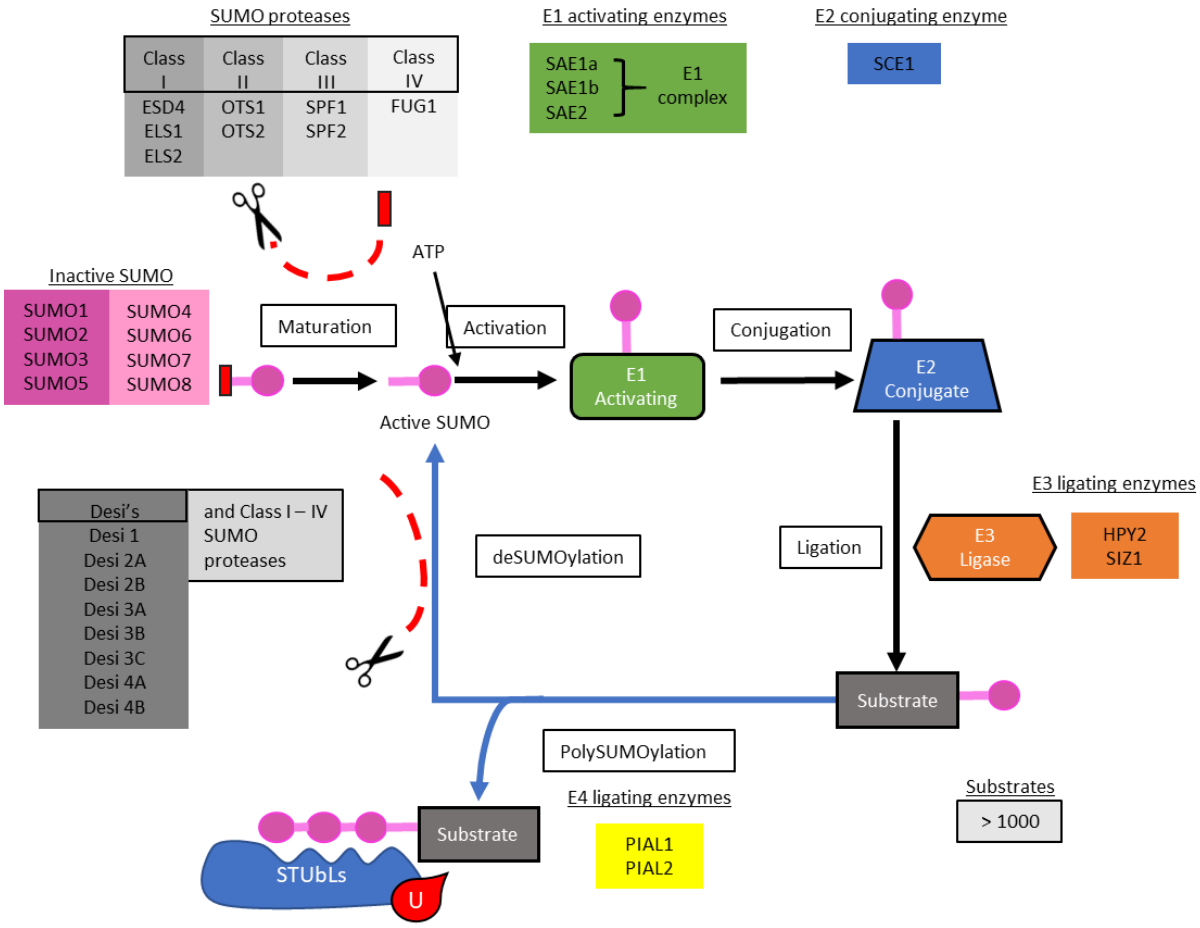

Figure 1.8 – A schematic representation of the SUMOylation pathway with the correlating gene names in plants. This pathway starts with an inactive pre-SUMO, which is activated by SUMO proteases. Free SUMO is then bound, at the expenditure of one ATP molecule, by the E1 activating enzyme complex. The E1 activating enzyme transfers the SUMO peptide to the E2 conjugating enzyme (SCE1) which binds target substrate, of which there are over a 200, and needs the help of the E3 ligase to form the covalent bond between substrate and SUMO. The substrate can be SUMOylated multiple times with the help E4 ligating enzymes, thereby forming a polySUMO chain. These polySUMO chains are targeted by ubiquitin E4 ligases termed STUbLs, which leads to substrate ubiquitination and degradation of the SUMOylated substrate. Lastly these SUMO bonds can be cleaved by SUMO proteases, after which the SUMO can be recycled.

1.7.2 Environmental stress controls SUMO protease stability

SUMOylation has been shown to be involved in development and responses to multiple stresses. Studies addressing the core SUMO machinery established that mutations in *SAE1*, *SAE2*, and *SCE1* single mutants, and *SUMO1 SUMO 2* and *SIZ1 HPY2 (MMS21)* double mutants were embryo lethal, indicating how essential SUMOylation is for plant developmental (Saracco et al. 2007; Ishida et al. 2012). However, single mutants for

some of this components and mutants in deSUMOylation genes have aided our understanding of how SUMO mediates stress responses, such as heat and cold stress, drought and salt stress, nutrient imbalance (Castro et al. 2012).

During stress responses the level of SUMO conjugates rises rapidly, as observed first during heat and oxidative stress (Augustine et al. 2016). Putting plants back to normal temperature allowed for the slow reduction in SUMO conjugates, which illustrates the reversibility of this process. Genetically increasing the pool of available SUMO could increase level of SUMO conjugates levels (Kurepa et al. 2003). This provides evidence that the amount of SUMO is often the limited factor during a stress response. Proteomics studies revealed that under stress conditions the abundance of existing SUMO conjugates is often increased instead of SUMOylation of new targets (Miller et al. 2013). This might suggest the forming of SUMO chains is more important during stress.

During drought stress the level of SUMO conjugates rapidly increase (Catala et al. 2007). This increase is partially dependent on the E3 ligase enzyme SIZ1 as level of SUMO conjugates are lowered in the *siz1-3* knock-out mutant (Catala et al. 2007). Levels of crucial genes induced by drought stress were reduced in *siz1-3*, suggesting that SUMOylation affects the expression levels of these gene potentially by SUMOylation and activation of transcription factors (Catala et al. 2007). Additionally, *siz1-2 and siz1-3* showed increased drought resistance, potentially through negatively regulating stomatal aperture (Miura et al. 2013; Kim 2017). However, two independent publications showed decreased tolerance to drought after reducing SUMO conjugation, indicating that this is dependent on experimental conditions (Catala et al. 2007; Castaño-Miquel et al. 2017). Interestingly, under drought stress SIZ1 is SUMOylated potentially as a feedback mechanism to control E3 ligase activity (Kim et al., 2017).
Another class of proteins that have been studied under drought stress are the OTS SUMO proteases. Knocking out OTS1/2 in rice exhibited drought tolerance, whilst overexpression led to drought sensitive plants and ABA accumulation (Srivastava et al. 2017). The authors showed that OsOTS1 interacts with the OsBZIP23 transcription factor that regulated ABA and drought responses. In the *OsOTS1* RNAi lines higher levels

of SUMOylated OsBZIP23 were found, resulting in more stable protein and increased expression of drought tolerant genes. OsOTS1 was degraded after drought stress and ABA treatment, suggesting that ABA accumulation leads to OTS1 degradation, which allows for the accumulation of SUMOylated OSBZIP23 and drought induced gene transcription (Srivastava et al. 2017).

1.8 Aims

The main aim of this thesis is to investigate how plant roots sense water distribution and which genetic pathways regulate lateral root branching towards available water, ie. the lateral root hydropatterning response.

In **Chapter 2** I will give an overview of all the techniques and materials used for this study.

In **Chapter 3** I first characterize the cellular and tissue scale processes that control LR hydropatterning, demonstrating that both LR initiation and primordium emergence are controlled by external water availability.

To elucidate the role of ARF7 SUMOylation on lateral root hydropatterning transgenic *ARF7* constructs with mutated SUMO sites were constructed. In **Chapter 4** I demonstrated that SUMOylation of ARF7 is crucial for the asymmetrical expression of its direct downstream target *LBD16*. In addition, I demonstrated that LBD16 is expressed in cells underneath the pericycle, the xylem-procambium cells.

After demonstrating that ARF7 SUMOylation is crucial for LR hydropatterning, I investigated which genes regulate the ARF7 SUMO status. The results in **Chapter 5** demonstrate a role for the SUMO protease OVERLY TOLERANT TO SALT 1 (OTS1) in regulating ARF7 deSUMOylation (Fig. 1.9). I characterize the role of OTS1 as a putative water sensor by examining its expression and protein localisation. I observed that OTS1 is expressed in the pericycle, but does not exhibited an asymmetrical localisation akin

to LBD16. Instead, I propose that OTS1 controls ARF7 SUMO status and LR hydropatterning by an activity gradient.

In **Chapter 6** I review the regulatory pathway controlling LR hydropatterning that has been elucidated in this thesis and discuss the impact of my observations and the future direction of this research.

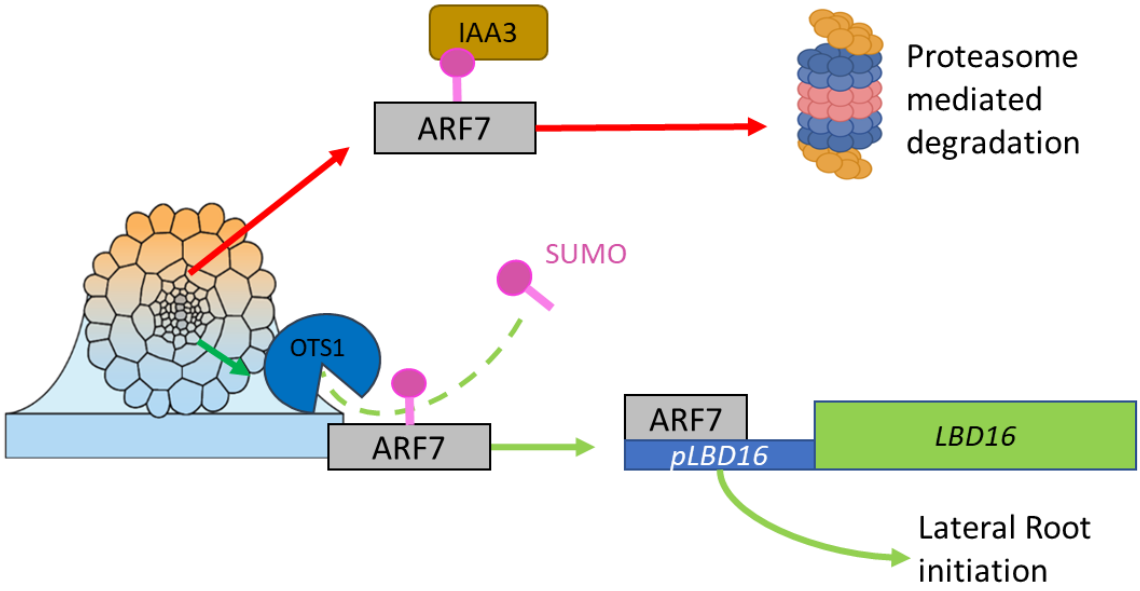

Figure 1.9 – The hypothesizes role of SUMO protease OTS1 in the lateral root hydropatterning signalling pathway. On the root side exposed to air ARF7 is SUMOylated, which causes recruitment of IAA3 repressor proteins through SUMO and SIM interaction. This leads to ubiquitination of ARF7 and subsequent degradation by the proteasome. On the root side exposed to water ARF7 is deSUMOylated through activity of OTS1 causing ARF7 to actively transcribe target genes such as LBD16 to drive LR initiation.

2 MATERIALS & METHODS

2.1 Plant lines and growth conditions

2.1.1 Arabidopsis thaliana material

Arabidopsis thaliana, ecotype Columbia (Col-0), was used as the control for all experiments. The following mutant alleles were used in these experiments:

Table 1 - Mutants and primers used in this thesis

Mutants	Insert ID	FW genotyping primer	RV genotyping primer
arf7-1	SALK_040394	AGCACATCACCATTTAGGTGC	CAGCTAGATCGTTCGAAATGG
lbd16-1	SALK_095791	TTTCTTCCTTTTTGCTTTGCC	CAATGGCCAGTGACTTAAAGC
lbd18-1	SALK_038125		
lbd29-1	SALK_071133		
ots1-1	SALK_022798	GATGATGCAAGGAGGCTAGTG	GTAGGATCAGCGAAGCTGTTG
ots1-2gk	GK-207D11-014550	GTGCAAAGCAGTTTGATTCTGG	CACAAACGGACCACAATCAA
ots2-1	SALK_001579	GCTTCTTCCGGTTTAAACCAC	TTTTTCTTCTGGCGACTCATG
siz1-3	SALK_034008	ATCCTTGAGTGGAGGTGACG	AATGACGCAAACAGAAAAGACA

The *OTS* and *siz1-3* mutants were kindly provided by Prof. Ari Sadanandom (The University of Durham). The *ots1-2gk* was supplied by the Nottingham Arabidopsis Stock Centre (NASC). p*LBD16::gLBD16:GFP* and *35S::gLBD16* (LBD16 OE) was donated by Tatsuaki Goh (Goh et al., 2012).

2.1.2 A. thaliana growth

A. thaliana seeds were sterilized using 30 % (v/v) bleach for 4 minutes and afterwards washed with 0.0001 % Triton followed by five washes with sterile water and then plated out on agar. The plates were sealed with micropore tap and stratified at 4 °C for 24 hours in the dark. Seeds were germinated on media containing ½ MS (2.2 g/L) (Murashige and Skoog media, Sigma), 0.5 g/L MES, 0.5 % sucrose and 1 % Bacto agar at pH 5.8. Seedlings were grown in Conviron growth cabinets in a continuous temperature of 23 °C with a 16 h photoperiod (120 µmol m^{-2} s^{-1}).

2.2 Plant phenotyping analysis

2.2.1 LR hydropatterning phenotyping bioassay

In order to quantify the orientation of the lateral root emergence in respect to the agar surface on the plate, the LR hydropatterning phenotyping bioassay was used described in Bao et al., (2014) and Orosa-Puente et al., 2018. In short, a light microscope (8x magnification) was used to determine emergence orientation of lateral roots from twelve day old seedlings. Images of whole plates were taken using a Canon digital camera. Primary root length was measured using the NeuronJ plugin in ImageJ. LR number was counted manually and LR density was calculated in Excel.

2.2.2 Bending assay

Plates containing 5 day old seedlings were turned 90°. Seedlings were transferred after 18 hours and 48 hours into labelled petri dishes containing acidified methanol (0.24 M HCL in 20 % MeOH) and placed into a 55 °C incubator for 15 min. The solution was replaced with a 7 % NaOH solution containing 60 % EtOH for another 15 mins. The roots were then further rehydrated in a series of EtOH solutions (40 %, 20 % and 10 %) for 10 mins each. They were then put in 50% glycerol solution and stored in 4 °C in the dark. Seedlings were transferred to a microscope slide and LRP stage development analysed on a brightfield microscope (Zeiss) with 40x magnification.

2.2.3 Plant growth on salt media

Seeds were germinated on ½ MS media. 5 dpg seedlings were transferred to mock (½ MS media) plates or plates containing ½ MS media and 100 mM NaCl (added before autoclaving). After transfer to fresh plates, the primary root growth was marked to be able to distinguish growth after transfer from growth before transfer. 7 days after transfer images were taken and root parameters (i.e. primary too growth, LR number and density) measured using Fiji software.

2.2.4 Plant growth on auxin media

Seeds were germinated on ½ MS media. 5 dpg seedlings were transferred to mock (½ MS media plus 0.01% EtOH) plates or plates containing ½ M media and 50 nM NAA (dissolved in 100% EtOH, final concentration 0.01%) or 200nM NAA (added after autoclaving). After transfer to fresh plates, the primary root growth was marked to be

able to distinguish growth after transfer from growth before transfer. 7 days after transfer images were taken and root parameters (i.e. primary too growth, LR number and density) measured using Fiji software.

2.2.2 Lateral root staging

Seedlings were grown and transferred similarly as in section 2.2.4 on ½ MS media plus 0.01% EtOH and 50nM NAA plus 0.01% EtOH. Primary roots were cut off from the section just above the first fully emerged lateral root. This root sections was then cleared following the same protocol as in section 2.2.2. Roots were then transferred to a microscope slide and LRP stage development analysed on a brightfield microscope (Zeiss) with 40x magnification.

2.3 DNA extraction and genotyping

2.3.1 DNA extraction

Leaves of three week old *A. thaliana* seedlings were harvested in Eppendorf tubes containing 200 µl DNA extraction buffer. This buffer consists of 200 mM Tris-HCl (pH 7.5), 250 mM NaCl, 25 mM EDTA, and 0.5% SDS diluted ten times with 10 mM Tris-HCl (pH 8) and 1 mM EDTA buffer. The leave tissue is then crushed against the tube walls by use of a P1000 pipette tip. Plant residues are removed by centrifugation at 14,000 rpm for 5 min. Afterwards the supernatant containing the DNA can be transferred to a clean tube. 1µl of extracted DNA solution can be used in 20 µl PCR reactions.

2.3.2 PCR set-up

PCR reaction mixtures contained 2 µl of 10X PCR reaction buffer (Sigma), 0.4 µl dNTPS (Sigma), 1 µl of each primer, 0.4 µl JumpStart taq polymerase, 1 µl sample DNA solution and 14.2 µl of deionized water. PCR strips were placed into PCR machine running the following program: 2 min on 94 °C then 35 cycles of 30 s on 94 °C, 30 s on primer specific temperature and flexible time, depending on product size, on 72 °C. These cycles were followed by an extra DNA extension time of 10 min on 72°C and finished on a temperature of 4 °C at which point it can be taken out.

2.3.3 Gel electrophoresis

To run the PCR product a 1% agarose (Sigma) gel was made using 1X TBE buffer solution. The solution was heated up until all agarose particles were dissolved and cooled down

before adding 0.01% Ethidium Bromide and pouring it into a mould. The gel was then placed inside of the gel electrophoresis tank. Before loading of the PCR product, 6 µl of loading buffer was added to the sample and mixed in. 10 µl of the resulting sample was loaded and run on 100 V for 40 min. Next, the gel was imaged using a UV light box (trans-illuminator).

2.3.4 PCR purification

5 µl of PCR product was run on a gel to check product size and specific primer binding. The remaining 15 µl of PCR product was purified using PCR purification kit (GeneJET, Thermo Scientific). Purified product was diluted in elution buffer and stored at -20°C.

2.3.5 DNA gel extraction

The DNA was briefly visualized using a UV light box and excised. Excised DNA was then purified using a gel extraction kit (GeneJET, Thermo Scientific). Purified DNA was eluted in elution buffer provided with the kit.

2.3.6 DNA sequencing

Plasmid DNA and PCR products were prepared for sequencing in accordance with Source Bioscience guidelines (www.sourcebioscience.com/services/genomics/sanger-sequencing-service/).

2.4 Gene cloning and construct design

2.4.1 Multisite Gateway cloning

pOTS1::3xVenus was made using Multisite Gateway. pOTS1 was amplified using *A. thaliana* DNA, whilst OTS1 CDS was amplified using *A. thaliana* cDNA. PCR fragments were cloned into Gateway compatible pENTRY vectors. Recombination with Gateway recombinant cloning technology) assembled the multiple DNA fragments into the pk7m34gw0_rc destination vector.

Table 2 - Gateway vectors used

Gene/construct name	Box	FW primer	RV primer
pOTS1	Box1	GGGGACAACTTTGTATAGAAAAGTTGCTAGTAGTGAATTGCTTTGGAGTC	GGGGACTGCTTTTTTGTACAAACTTGCCACCTTAGAACTTCTGTCCACCTCCTG
pENTR_3xVENUS_N7	Box2	Multisite Gateway kit	
OTS1 (CDS)	Box2	GGGGACAAGTTTGTACAAAAAAGCAGGCTATGACGAAGAGGAAGAAGGAAGTAATAGATG	GGGGACCACTTTGTACAAGAAAGCTGGGTcCTCTGTCTGGTCACTGACACGG
nosT (Terminator)	Box3	Multisite Gateway kit	
OTS1 (CDS)	Box3	aacaggtctcgaacaATGACGAAGAGGAAGAAGGAA	aacaggtctctagccCTCTGTCTGGTCACTGACACG
VENUS_N7	Box3	Multisite Gateway kit	

2.4.2 GreenGate cloning

pOTS1::OTS1:mVenus, pOTS1::gOTS1:GFP and pOTS1::gOTS1:mCherry were made using GreenGate cloning. pOTS1 and gOTS1 were cloned into GreenGate compatible pENTRY vectors. Recombination using GreenGate technology was used to assemble final constructs in pGGZ003 or pGGZ003-RMM destination vectors. The Greengate pENTRY vectors were supplied by Lampropoulos *et al* (2013) via Addgene.

Table 3 - GreenGate vectors used

Gene/construct name	Module	FW primer	RV primer
pOTS1	A	AACAGGTCTCGACCTctagtagtgaattgctttggag	ACCAGGTCTCGTGTTttccgagagagaacgaagg
B-dummy	B	GreenGate cloning kit	
mVenus (N-tag)	B	GreenGate cloning kit	
gOTS1	C	ACCAGGTCTCGGGCTTTATGACGAAGAGGAAGAAGGA	AACAGGTCTCTCTGACTCTGTCTGGTCACTGACA
mCherry	D	GreenGate cloning kit	
GFP	D	GreenGate cloning kit	
mVenus (C-tag)	D	GreenGate cloning kit	
D-dummy	D	GreenGate cloning kit	
RBCS Terminator	E	GreenGate cloning kit	
Hygromycin	F	GreenGate cloning kit	

2.4.3 Plasmid DNA isolation

Liquid cultures of colonies containing construct were incubated in a 37 °C shaker overnight. Plasmid was extracted using the plasmid mini-prep kit (GeneJET, Thermo Scientific). Extracted plasmid was eluted in elution buffer provided with the kit and stored at -20°C

2.4.4 Floral dipping protocol

The resulting plasmid was transformed into Agrobacterium tumefaciens GV3101 strain by electroporation and transformed into *A. thaliana* plants by the floral dip method described in (Clough and Bent 1998). T1 seedlings were selected through plating on media containing ½ MS, 1% bacto-agar and the appropriate concentration of antibiotic.

2.4.5 Construct data storage

DNA sequences, primers, sequence alignments and plasmid maps were stored on Benchling.com.

2.5 Confocal microscopy

2.5.1 Lateral root deviation angle measurements

A. thaliana seedlings were carefully (without moving them) glued on the media plate using 1% agarose. Root segments (2 cm in length from the root tip) were cut out (including the gel) and transferred to a sample holder as previously described. The entire volume of the root was captured, including the gel substrate, using a 405-nm laser (laser intensity in ZEN set to 35%). Autofluorescence was filtered between 505 and 545 nm. The angles of the xylem pole axis and of the lateral root relative to the surface of the medium were measured in a cross-section using ImageJ/Fiji (ImageJ). Agar was visualized by a difference in contrast between water and agar. The image was then rotated to position the agar at the bottom of the image in parallel with the horizon. The angle between agar and xylem pole initiation site could then be measured using the angle tool on Fiji software by drawing one line between both xylem poles, which are characterized by a high level of auto-fluorescence resulting in two bright dots. Another line was drawn from the agar with a straight bend (90°) up to the xylem pole furthest from the LRP. The angle between these lines is termed the initiation site angle since it points towards the xylem pole wherefrom a LRP initiates. A third line was drawn between initiation site near the xylem pole and the centre of the LRP (yellow line in Fig. 3.1C). The angle between this line and the xylem pole axis line results in the LRP deviation angle, as it measures the deviation between xylem pole axis and LRP emergence. The LRP deviation angle are presented as follows: orientations towards the gel have positive values and those away from the gel have negative values.

2.5.2 Multi-view imaging employing Light Sheet Fluorescent Microscopy for investigating lateral root hydropatterning

A. thaliana seedlings expressing *pOTS1::OTS1-mVenus*, *pOTS1::mVenus-OTS1* and *pLBD16::gLBD16:GFP* were grown on the surface of media plates. Roots were covered with 1% agarose containing fluorescent beads (PS-Speck, fluorescent beads, ThermoFisher, Catalog number: P7220). two cm root segments from the root tip were cut out, including the media and transferred to a sample holder similar to the protocol previously described. Roots were imaged with a Zeiss Light Sheet Fluorescent Microscope Z1. Images were captured using the W Plan-Apochromat 20x/1.0 and the

PCO.edge camera module (CMOS, 1920x1920 pixel). Excitation wavelengths: 488 nm for GFP and 514 nm for YFP. Emission filter: Bandpass 505-545 nm for GFP and Bandpass 525-545 nm for YFP. Multi-view images were set up using the Quick-Setup option in the ZEN software. Single views were fused using the bead-based registration using the Fiji plugin Multiview Reconstruction (Preibisch et al. 2010, 2014).

2.5.3 Confocal microscopy using the Leica SP5 and SP8

A. thaliana seedlings were grown on the surface of media for 5 days. Seedlings were carefully transferred to a microscope slide and covered by a cover slip. For cell wall staining propidium iodide solution (15 µg ml^{-1}) was used before the addition of a cover slip. Confocal microscopy was performed using a Leica SP5 or SP8 confocal laser scanning microscope (Leica Microsystems). Roots were imaged from the root tip to the shoot using the argon 488 nm laser (GFP) or 514 laser (Venus). Emission was detected at 505 – 550 nm for GFP, 525 – 560 nm for mVenus and 600 – 650 nm for pi.

2.5.4 Relative fluorescence measurements.

Relative fluorescence, or intensity, was measured using ImageJ software. In the case of LBD16-GFP and OTS1-Venus asymmetry study, the relative fluorescence of 10 nuclei on either side were analysed and averaged using the max projection images. The mean fluorescence and standard error were then plotted in box plots. In case of the LBD16-GFP vasculature vs pericycle data, the relative fluorescence of two vasculature and two pericycle nuclei were measured in each dataset and averaged.

2.6 Gene expression analysis

2.6.1 Plant growth and harvest

Total RNA was extracted from five day-old seedlings grown on ½ MS media. The roots were cut two cm up from the tip and pooled together with a total of 12 roots per sample tube and three samples per independent line.

2.6.2 RNA extraction and RT qPCR

RNA was extracted by snap-freezing roots in liquid nitrogen and grinding before treatment with Trizol and chloroform followed by use of the column from the Qiagen RNeasy kit and a DNAse treatment. RNA levels were measured using a NanoDropTM 1000 Spectrophotometer (Thermo Scientific) and stored at -80 °C. Total RNA

concentration per sample was then normalized before cDNA synthesis using the SuperScript™ II Reverse transcriptase kit (Invitrogen) and oligo dT primers (Invitrogen). The cDNA was stored for a month in -20°C. RT-qPCR was performed using the Roche Lightcycler 480 system and software. Reactions contained 5 µl cDNA, 6 µl 2x SYBR Green Mastermix (Roche), 0.1 µl of forward and reverse primer (100 µM) and 0.8 µl RNA-free water. The following default PCR program (40 cycles) was run: 95 °C for 10 min (first denaturation), 95 °C for 10 s, 60 °C for 30 s (amplification), 95 °C for 1 min, 60 °C for 30 s and 95 °C continuous (dissociation curve). Average CT values were derived from 3 technical replicates. Relative transcript abundance was calculated using the comparative CT method (Livak and Schmittgen 2001). Expression was normalised by comparing with ACTIN7 (At5g09810) expression. Gene expression in plots are relative to corresponding gene expression in Col-0.

Primers shown here were designed using Roche universal probe library online software (https://lifescience.roche.com/en_gb/brands/universal-probe-library.html#assay-design-center).

Table 4 - RT qPCR primers used

Gene	FW primer	RV primer
ACT	CCGCTCTTTCTTTCCAAG	CCGGTACCATTGTCA
ARF7	tagctgtcaacgatgctgga	agcctcgtttttgcacctt
LBD16	AGCCGCCGGAGATCTAAGACA	CACTAGTTTGTTGCCACGTCATAAAC
OTS1.1	CGTAGAGTTTTAGAAGGCTCGAA	GCGGTAAAACATCTGAACCTG
OTS1.2	TCAGCGAAGCTGTTGTTCAG	CACAAACGGACCACAATCAA
OTS2	tcccaatatgatcaacgaagc	aaacgtcttatgaagaagagcagaa

2.7 Hormone treatments

2.7.1 General hormone treatment

5-day old *A. thaliana* seedlings containing *pOTS1::OTS1-mVENUS*; *pOTS1::mVENUS-OTS1* and *pOTS1::3xmVenus* were treated with a drop of mock (0.1% DMSO), 1µM 1-Naphthaleneacetic acid (NAA, auxin), 10 µM abscisic acid (ABA), 10 µM 6-Benzylaminopurine (BA, cytokinin), 10 µM salicylic acid (SA) and 10 µM 1-Aminocyclopropane-1-carboxylic acid (ACC, ethylene) on the root tip (1cm). These hormones were all dissolved in DMSO and had a final concentration of DMSO of ≤ 0.1%. Roots were scanned after 4 hours of treatment. Root meristems of OTS1-Venus lines

were scanned on the SP8, root meristems of *pOTS1::3xmVenus* were scanned on the SP5. Within experiments the same laser power, pinhole and digital gain were used.

2.7.2 Relative fluorescence measurements

The relative fluorescence after hormonal treatment of *pOTS1::OTS1-mVenus* and *pOTS1::mVenus-OTS1* lines was measured by measuring fluorescence per area. The integrated density of a square on the epidermis was measured and divided by the total area of the measured square to gain the fluorescence per area of the OTS1 expression nuclei in the epidermis layer.

In the case of *pOTS1::3xmVenus*, a square was measured incorporating the quiescent centre and columella cells. Integrated density and area were then used to calculate relative fluorescence per area.

2.8 Phylogeny reconstruction

Full-length ARF protein sequences were downloaded from multiple online databases (table 5). These sequences were aligned using MUSCLE alignment (Edgar 2004) and data viewed with Mview (Brown et al. 1998).

Table 5 - Species, gene codes and databases used for ARF phylogeny

Species	Gene code	Database
Mesotaenium caldariorum	Mcaldo2048527 (proto-ARF A/B)	1000 plants (1KP) project
Marcantia polymorpha	Mapoly0019s0045.1 (MpARF1)	Phytozome
Physcomitrella patens	Pp3c1_14480 (PpARFa1) Pp3c2_25890 (PpARFa3) Pp3c13_4720 (PpARFa4)	Phytozome
Selaginella moellendorffii	Selmo117217 (SmARFa1) Selmo424114 (SmARFa2) Selmo181406 (SmARFa3)	Phytozome
Picea abies	Pabies00020544 (ARF-AI) Pabies00012050 (ARF-AII) Pabies00010949 (ARF-AIII)	PLAZA
Arabidopsis thaliana	AT5G20730.1 (ARF7) AT1G19220.1 (ARF19) AT1G19850.1 (ARF5) AT1G30330.2 (ARF6) AT5G37020.1 (ARF8)	Phytozome

The same approach was used to align LBD16 (AT2G42430), LBD17 (AT2G42440), LBD18 (AT2G45420), LBD29 (AT3G58190) and LBD33 (AT5G06080). Bootstrap values were generated in MEGA-X software.

2.9 Statistical analysis

Data was plotted using GraphPad PRISM v8. The statistical tests were performed using IBM SPSS v24 software. Data was analysed using student T-test when two groups were compared or one-way Analyses of Variances (ANOVA) followed by Tukey's honestly significant difference (HSD) post hoc test ($p \leq 0.05$; 95% confidence interval) when more than two groups were compared. Statistically similar groups are indicated by similar letters. Bivariate Pearson correlation was used to test the linear relationship in Chapter 3.

3 EARLY DEVELOPMENTAL PLASTICITY OF LATERAL ROOTS IN RESPONSE TO ASYMMETRIC WATER AVAILABILITY

Jason Banda and Daniel von Wangenheim

Parts of this chapter have been published as: von Wangenheim, D., **Banda, J.,** Schmitz, A., Boland, J., Bishopp, A., Maizel, A., Stelzer, E.H.K., Bennett, M., 2020. Early developmental plasticity of lateral roots in response to asymmetric water availability. ***Nature Plants*** 6, 73–77.

3.1 Introduction

Root branching is influenced by its local soil environment and displays a high level of plasticity. The heterogenous soil and distribution of its resources makes it crucial for a plant to branch specifically in locations containing nutrients and water. Plants have adapted multiple mechanisms to find resources and branch towards them, for example branching is induced in nutrient rich patches (Drew 1975) and reduced in water limiting areas (Babe et al. 2012; Orman-Ligeza et al. 2018). When water is asymmetrically available on one side of the root, the branching is specifically directed to the water exposed root side, termed lateral root (LR) hydropatterning (Bao et al. 2014). This response is regulated through auxin response and mediated through a ARF7-LBD16 dependent pathway (Orosa-Puente et al. 2018). The authors visualized that 70-80% of the emerged lateral roots are orientated towards the agar. However, it remains unclear whether the bias in water availability directs LR initiation or emergence.

A. thaliana roots are built up of a diarch system containing two xylem and two phloem poles (Casero et al. 1993). LRs primarily stem from one of three Xylem-Pole Pericycle (XPP) cells on top of one of these xylem poles (Blakely et al. 1982; Casero et al. 1993). These XPP cells retain their meristematic abilities and can re-enter the cell cycle (Parizot et al. 2008). This idea is based on the characterization of small vacuoles, dense cytoplasm and ribosomes in XPP cells and ability to remain longer in the G2 phase of the cell cycle (Beeckman et al. 2001; Himanen et al. 2004; Parizot et al. 2008). In contrast, Phloem-Pole Pericylce (PPP) cells, overlaying the phloem poles, retain no

meristematic ability (Parizot et al. 2008). A set of two longitudinally adjacent XPP cells in the differentiation zone, termed lateral root founder cells (LRFCs) undergo anticlinal division to start the initiation of a new LRP (Malamy and Benfey 1997; Van Norman et al. 2013). The first division is anticlinal (along the shoot-root axis), afterwards the LRFCs divide periclinal (along the radial axis) to form a dome-shaped primordium. Although new research on this topic demonstrated that possibly only one FC starts to divide and forms the stage 0 of LRP development (Torres-Martínez et al. 2020). After which the immediate neighbours, both longitudinal and radial, are recruited. These pericycle cells will be the ground layer for an entire LRP that can consist out of five to eight radially orientated pericycle cell files (Casero et al. 1993; Laskowski et al. 1995; Von Wangenheim et al. 2016). There is some variation in number of cell files that make up the LRP and how these contribute to the complete LRP and its development. However, data suggests that LRP morphogenesis is based on an extensive set of rules that determine cell growth and division orientation (Von Wangenheim et al. 2016). There is a great level of plasticity in the regulation of cell growth and division needed to explain the LRP growth dynamics after the first anticlinal division. How this plasticity in growth and division of LRP is regulated remains unknown.

After the LRFC initiation stage, LRP emerge through overlying tissue layers; namely the endodermis, cortex and epidermis (Malamy and Benfey 1997). The endodermis is the first layer that the developing LRP must cross. The overlaying endodermis cells receives signals from swelling LRFC's to promote cells volume loss, change shape and locally degrade the Casparian strip in the overlying endodermal cells. These developmental steps allow the LRP to grow through the first barrier (Vermeer et al. 2014). In turn, the endodermis signals back to the LRFCs for them to start swelling and enter cell division. This cellular cross talk is under tight regulation of the phytohormone auxin. After LRFC specification, a PIN3 driven auxin reflux from the overlying endodermis is required to progress the LRFC to the next initiation phase (Marhavý et al. 2013). Key to this it the polar re-localisation of PIN3 towards the plasma membrane facing the LRFC, to drive efflux of endodermal auxin towards the LRFCs. Additionally, auxin originating from the initiating LRFC's can induce cell wall modification and cell separation in the overlaying tissue (Swarup et al. 2008). The sequentially induction of PIN3 auxin efflux carrier

followed by the influx carrier LAX3, was shown to select two cortex cells for separation to allow emergence growth (Peret et al. 2013). Thus, auxin signalling between the overlying cells is of high importance for the outgrowth direction of the developing LRP.

Auxin signalling in the overlying endodermal cells can directly affect LR initiation in the XPP cells. Vermeer et al., (2014) demonstrated this by over-expressing a *shy2*-2 *gain-of-function* mutant, IAA3, in the elongating endodermal cells specifically using the *CASP1* promoter. *shy2-2 gain-of-function* mutants have a missense mutation in domain II, which causes it to become less degradable (Tian et al. 2002). Without auxin-mediated degradation of SHY2/IAA3, ARF transcription factors will stay inactive and the plant becomes unable to activate auxin responses resulting in a number of phenotypes, including a reduction in the number of LRs. By expressing the *shy2-2* allele solely in the endodermis, the auxin-IAA3 response is specifically blocked in endodermal tissue (Vermeer et al. 2014). Experiments with this line revealed that a functional de-repression of auxin response, through auxin mediated degradation of SHY2, is necessary to allow for the loss of volume and cell shape change needed for LRP emergence through the endodermis (Vermeer et al. 2014). Without functional auxin signalling in the endodermis and feedback from this to the LRFCs in the XPP cells, the LRFC will not enter the cell cycle nor start swelling. This result revealed a strong signalling feedback from two neighbouring tissue types in initiation of LRs.

The volume changes seen in the LRP development are likely caused by the intercellular connectivity between these cells and neighbouring cells under control of auxin. Coordination of aquaporin expression and plasmodesmata opening and closing due to callose deposition are instrumental in building up turgor pressure in the LRP, whilst reducing the volume in the overlaying endodermis (Péret et al. 2012; Benitez-Alfonso et al. 2013). Exogenous auxin treatment represses the expression of almost every aquaporin, whilst the expression of the aquaporin *PIP2;1* is solely maintained at the base and underlying vasculature. This might be increasingly important as developing LRP slowly become symplastically isolated through closure of plasmodesmata (Benitez-Alfonso et al. 2013). LRP reach complete symplastic isolation at stage 4 of LRP development. Overlying LRP cells are also targets for plasmodesmatal modification. Auxin in these cells controls the spatiotemporal distribution of PLASMODESMATA-

LOCATED PROTEIN5 (PDLP5). *pdlp5* knock-out mutants displayed increased callose deposition on the plasmodesmata, whilst overexpression has the opposite effect (Lee et al. 2011). In the overlying cells, PDLP5 moves to the plasma membrane to restrict cell-to-cell movement of water in an auxin mediated way (Sager et al. 2020). Symplastic isolation of the LRP and overlying cells would increase the importance of water transport during the swelling of the LRP through aquaporins. Based on mathematical modelling and experimental validation, Péret et al., (2012) constructed a model in which water uptake of the overlying cells is reduced and transport is promoted towards the swelling primordium (Péret et al. 2012). However, it remains unclear which proteins contribute to this change in waterflow and how water flow from the external environment can impact LRP emergence direction.

In this chapter Light Sheet Fluorescence Microscopy (LSFM) is applied to understand which stage of LRP development is affected by the non-uniform distribution of water. This demonstrated a strong regulation of LR emergence towards the water containing agar when the initiation site was close to the air exposed side. The observed LR deviation angle is driven by growth and division of lateral root flanking cells that steer the LR quiescent centre into the direction of water. Additionally, use of *LBD16pro::gLBD16-GFP* showed a high level of flexibility in positioning of the LRFC initiation site. This creates early development angle towards agar even in the case when the initiation site is distal to the agar. Results suggest that both initiation site positioning in XPP cells and LRP angling during emergence are steered by external water availability.

3.2 Results

3.2.1 Light Sheet Fluorescence Microscopy as a tool to visualize LRP emergence angle.

To visualize the LRP initiation site and emergence angle when grown on agar, we deployed a LSFM approach. *A. thaliana* roots were first glued onto the agar using 1% low-melting agarose. Primary root and agar sections were cut from the early differentiation zone, where the LRP are in early stages of development, through to the full emergence of the youngest lateral root (Fig. 3.1A). In this way we can focus solely on non-emerged LRP. The root and agar section were then placed upon a LSFM holder and put into the Light Sheet chamber filled with water (Fig. 3.1B). The entire root volume was captured using the 405-nm laser (laser intensity 35%). Autofluorescence was filtered from 505 till 545-nm. Agar was visualized by a difference in contrast between water and agar. The image was then rotated to position the agar at the bottom of the image in parallel with the horizon. The angle between agar and xylem pole initiation site could then be measured using the angle tool in Fiji software by drawing one line between both xylem poles (white dotted line in Fig. 3.1C), which are characterized by a high level of auto-fluorescence resulting in two bright dots. Another line was drawn from the agar with a straight bend (90°) up to the xylem pole furthest from the LRP (purple dotted line in Fig. 3.1C). The angle between these lines is termed the initiation site angle since it points towards the xylem pole from where a LRP initiates. A third line was drawn between initiation site near the xylem pole and the centre of the LRP (yellow line in Fig. 3.1C). The angle between this line and the xylem pole axis line results in the LRP deviation angle, as it measures the deviation between xylem pole axis and LRP emergence. LRP that grew towards the agar were given a positive value, whilst LRP emerging away from the agar a negative value, indicating if a LRP angles towards or away from the water source.

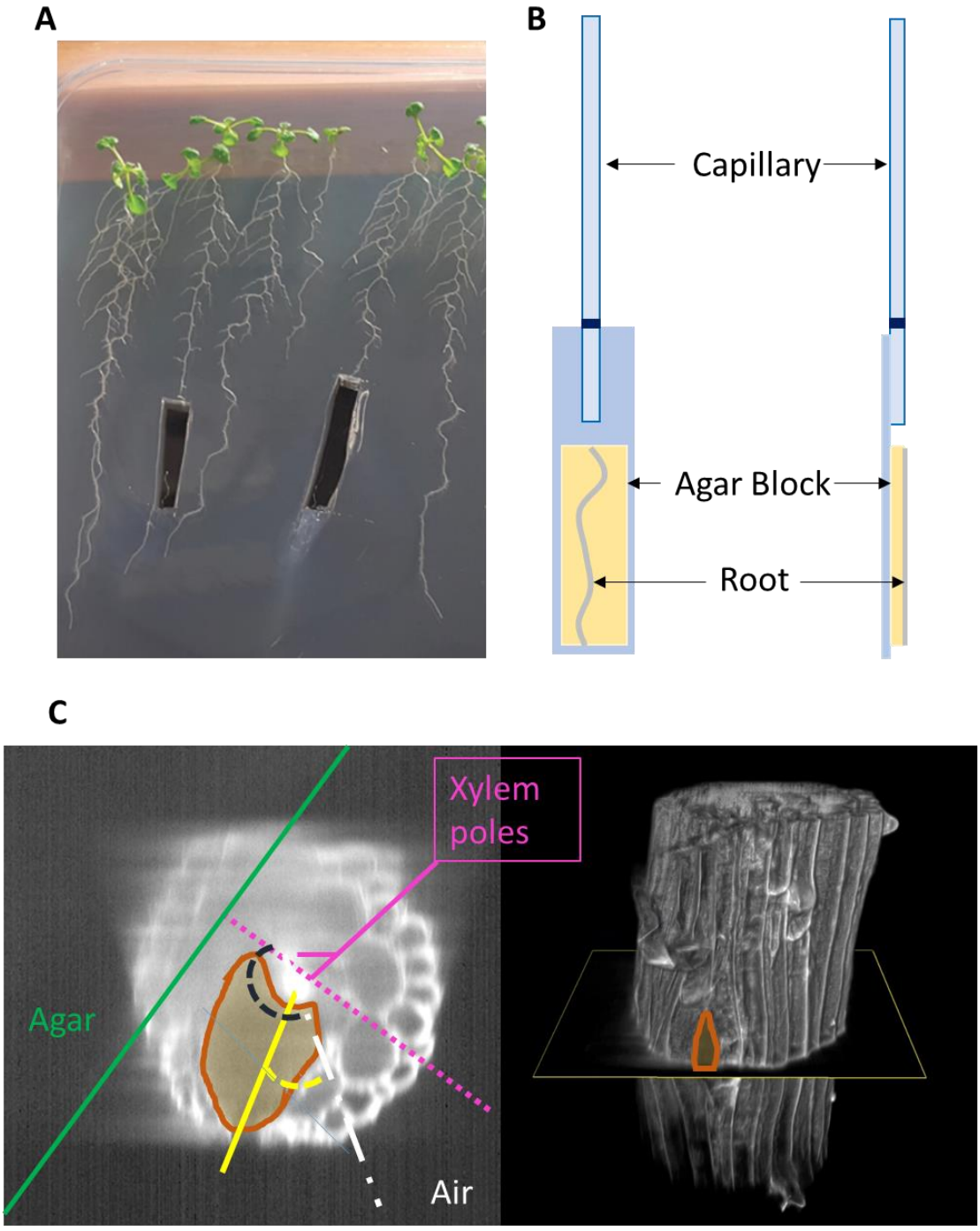

Figure 3.1 – Light Sheet Fluorescence Microscopy (LSFM) set-up for imaging lateral root deviation angles. Root and agar sections were cut from A. thaliana plants grown for 12 days (A). These sections were placed on a holder and glued on with low melting agarose (B). The holder and sample were placed into the Light Sheet chamber and z-stacks scanned with the 405 laser (C). We were then able to visualize the agar (left of the green line), xylem pole axis (white dotted line) and lateral root primordium (orange field and yellow line) by the difference in contrast. These were then used to measure the angle between agar and xylem pole initiation site (black dotted angle) and the angle between xylem pole axis and lateral root primordium (yellow dotted line).

3.2.2 Lateral root initiation and emergence angle is influenced by the availability of water

The three-dimensional (3D) image stacks were used to investigate xylem pole axis and LRP emergence angles relative to agar. This demonstrated that the orientation of the xylem pole axis in comparison with the agar was completely random and not influenced by the position of the agar (Fig. 3.2A). Likewise, the initiation site of LRP, where the yellow line meets the purple line, was not affected by the availability of water. 54% of the LRP initiations sites were nearer to the agar vs 46% towards the air exposed root side (Fig. 3.1B). In contrast, 79% of the LRP angle towards the agar when considering initiation site and LRP angle (end of the yellow line in Fig. 3.2A). The schematic of LRP outgrowth suggests that when LRP initiate on the air side, they bend towards the agar to secure optimal water uptake by the new organ. Furthermore, when a root initiates on the agar side, the lateral root bends away from the agar. To further assess this bending behaviour the angle of the LRP relative to the xylem pole axis was measured and termed the LRP deviation angle. In case of no deviation angle (0°), the LRP would initiate and emerge in a straight line from the xylem pole axis (Fig. 3.2C). When the LRP would emerge in a strong, almost 90°, angle away from the xylem pole axis we termed this as a strong deviation angle (Fig. 3.2C). To classify all the possible initiation sites and LRP deviation angles, we plotted these out against each other. Four classifications were made depending on the position on the graph: (I) initiation site on the xylem pole closest to agar and LRP deviation away from agar (bottom left), (II) initiation site away from agar and deviation away from agar (top left), (III) initiation site away from agar and LRP deviation towards agar (top right), and lastly (IV) initiation site near agar and LRP deviation towards agar (bottom right) (Fig. 3.2D). There was a clear trend visible in which most initiation sites near the agar have LRP deviation angles away from the agar towards the agar surface. In contrast, when a primordium initiates on the xylem pole distant from the agar it tends to bend towards the agar. This positive correlation was tested by Pearson correlation coefficient and found to be robust, with $r = 0.6901$ ($P = <0.0001$; two-tailed test). These results indicate a highly plastic organ emergence steered by the position of agar.

To investigate if LRP initiation and emergence angle is truly controlled by the availability of water, the initiation sites and LRP deviation angle were measured when roots were grown in water (hydroponics) or through agar. This set-up would provide the root with a uniform mechanical and aqueous environment. Results revealed an unbiased initiation in relation to the agar when roots are fully surrounded by water or agar (Fig. 3.2E, F). Furthermore, lateral root primordia emergence showed an unbiased angle of LRP emergence (Fig. 3.2F). This is in contrast with what was earlier observed in Col-0 growing on agar, where LRP developed towards agar through a deviation in the LRP angle. Part of this reduction could be explained by the significant reduction in LRP deviation angle when grown in water or agar (Fig. 3.2G). This data suggests that when water is uniformly available along the radial root axis, lateral root outgrowth is more in line with the xylem pole axis.

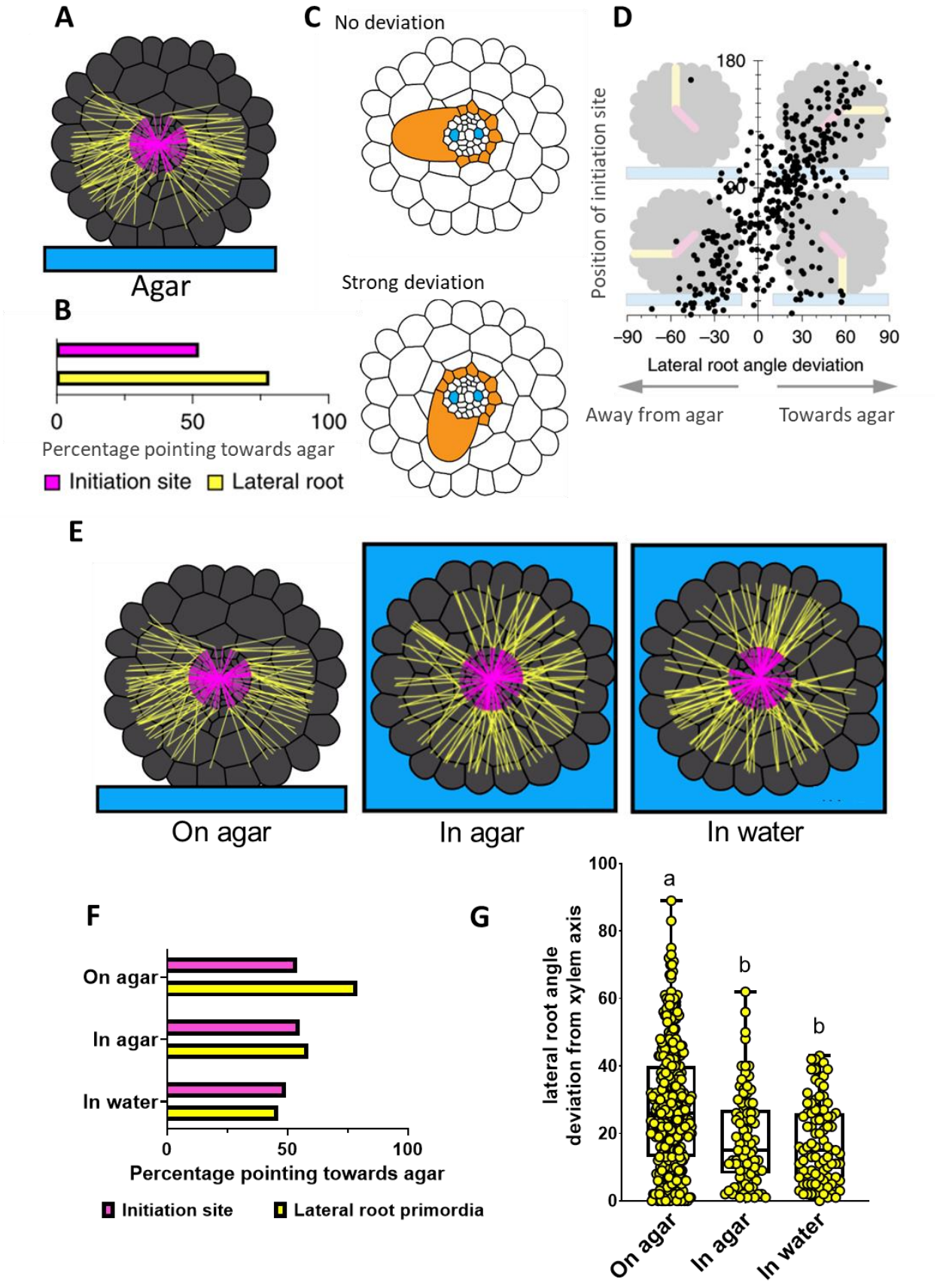
A
Agar
B
0
50
100
Percentage pointing towards agar
Initiation site
Lateral root
C
No deviation
Strong deviation
D
180
90
Position of initiation site
−90 −60 −30 0 30 60 90
Lateral root angle deviation
Away from agar
Towards agar
E
On agar
In agar
In water
F
On agar
In agar
In water
0
50
100
Percentage pointing towards agar
Initiation site
Lateral root primordia
G
lateral root angle deviation from xylem axis
100
80
60
40
20
0
a
b
b
On agar
In agar
In water

Figure 3.2 – A. thaliana lateral root emergence is influenced by water availability. A schematic representation of xylem pole axis (purple line) and lateral root primordium (yellow line) positioning in accordance with the position of the agar in 87 lateral root primordia in Col-0 (A). The percentage of initiation sites (purple bar) and lateral root primordia (yellow bar) pointing towards the agar/gel, indicating no bias towards water during initiation but a strong bias of lateral root emergence towards the agar (B). Schematic example of a lateral root primordium without deviation angle and one with a strong deviation angle (C). Lateral root deviation angle plotted against the position of the initiation site (D). Lateral root primordia orientate towards the agar when initiation occurs on the airside (upper right) and away from the agar when initiation faces the contact side (lower left). No lateral root primordia are orientated towards the air when initiation occurs on the airside (upper left) and only few lateral root primordia emerge towards the agar when initiated towards the agar. In total, 352 primordia from 42 plants were analysed. The plants used for this experiment came from were grown in 5 different batches in the same growth chamber. Bivariate Pearson correlation was used to test the linear relationship between the position of the xylem pole and the lateral root outgrowth angle. A strong positive correlation was found, with r = 0.6901(P = <0.0001; two-tailed test). Lateral root primordia initiating and emerging in complete agar or water (in hydroponics) showed a more distributed initiation and emergence of lateral root primordia compared to a root grown on agar (E). The bias towards LRP emergence towards agar is absent when roots were grown in hydroponics (in water) or in agar (F). The lateral root deviation angles of the three treatments are depicted in the boxplot and showed a significant reduction in angle deviation when grown in agar or water compared to grown on agar (G). Data points are plotted as yellow circles. Statistical differences were analysed using one-way analysis of variance and Tukey's Honestly Significant Difference test (P < 0.0001; 95% confidence interval). Statistically similar groups are indicated by the same letters. Data collected and analysed by D. von Wangenheim and J. Banda

3.2.3 Lateral root primordium emergence angle is flexible at all primordium developmental stages

Former LRP growth datasets were re-analysed to understand at what developmental stage the angling of the LRP is regulated (Von Wangenheim et al. 2016). The role of the different cell files making up a primordium and how these cell files contribute to the emergence angle was examined. The contribution of each cell files was assessed by tracking cell contours in a transversal cross-section of LRP near emergence stage in two independent experiments. This revealed contribution of all cell files to the dome shape of the primordium, but increased contribution of the flanking cell files during emergence growth (Fig. 3.3A). These flanking cells demonstrated a high variety in the number of cells and volume compared to the central cell file, containing the LRP

quiescent centre. These results highlight the importance the flanking cells and not the central cell file in steering the direction of primordium emergence (Fig. 3.3B).

To address if the difference in flanking cell file volume growth is due to cell division or growth, the radial division pattern was closely examined in five LRP dataset (Von Wangenheim et al. 2016). In these datasets the radial and anticlinal divisions in the LRP varied greatly. Especially in datasets 121211 and 130607 (shown in Fig 3.3C), radial divisions occurred preferentially on one side of the primordium, which resulted in a bend in LRP emergence. Although it must be specified that these samples were submerged as they were grown in a light sheet chamber. LRs of plant roots grown in uniform aqueous environment exhibited decreased deviation angle in previous experiments and the number of radial cell divisions therefore might be more extreme in roots grown on agar. Taken together this data indicates that the direction of LRP outgrowth is strongly affected by radial division in the flanking cell files.

An early lateral root marker, *pLBD16::gLBD16-GFP* (Goh et al. 2012a), was used to investigate if external water availability can affect the early stages of LR development. The expression of the gLBD16-GFP and the autofluorescence of the root were captured during different stages of LRP development (Fig. 3.3D-G). These two illumination channels were combined to give a clear image of lateral root initiation relative to the xylem pole axis. The datasets consisted of 39 LRP of which 13 primordia showed gLBD16-GFP expression not on top of the xylem pole. Already during the very first stage of lateral root initiation, the first anticlinal cell divisions, a significant deviation from the xylem pole was observed (Fig. 3.3E). The deviation of initiation site positioning also seemed to affect the direction of the gLBD16-GFP signal and thus LRP growth in later stages (Fig. 3.3F,G). These findings reveal that developmental plasticity already exists in very early stages of LRP development and that selection of pericycle initiation sites deviate much more than earlier thought (Casimiro et al. 2001).

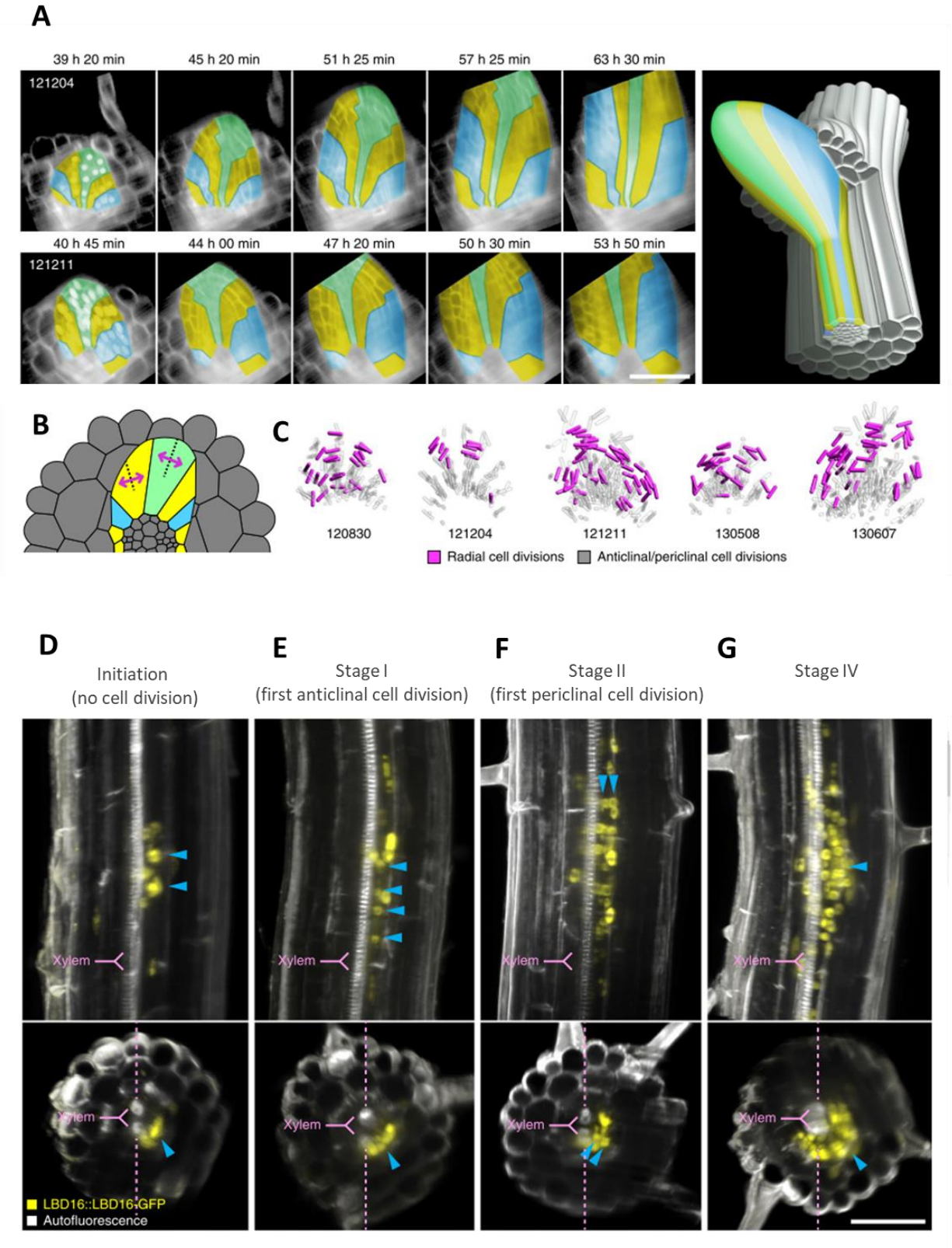

Figure 3.3 – Lateral root primordium development is flexible at all stages of development. Cell file tracking from 3D LSFM time-course datasets (121204 and 121211)12 of two biologically independent experiments (A). The colour of the cell file indicates which group of cells are derived from the same mother cell. Here, the green cells represent the central cell file. They derive from the cell that

undergoes the first periclinal division on its way to becoming a lateral root primordium. This figure illustrates that the contribution of flanking cell files (yellow and blue cell files) increases over time and pushes the central cell file out of the primary root. Four individual roots show the expression pattern of *LBD16pro::gLBD16-GFP* during the first stages of lateral root development (B-E) That is, indicated by blue arrowheads, the migration of nuclei before the first cell division (d), the first anticlinal cell division (e), the first periclinal division (f) and a stage IV primordium (g). The central file is not strictly above the xylem pole. The dashed pink lines indicate the xylem pole axis. The upper panels show a longitudinal section of a 50-µm thick central section of the root (maximum intensity projection); the lower panels show a transversal cross section spanning a 100-µm long segment of the root (maximum intensity projection). A total of 39 primordia were scanned in three independent experiments. For these experiments, the number of times that the central file was not in line with the xylem pole axis was 14. Scale bars, 50 µm. Note, panel A-C contains data produced and analysed by D. von Wangenheim.

3.2.4 *LBD16* over-expression reduces lateral root primordium deviation angle

LBD16 encodes a transcription factor that regulates early stages of lateral root initiation (Goh et al. 2012a). We tested the role of this regulator during hydropatterning by examining whether *LBD16* knock-out and over-expression lines were affected in lateral root outgrowth towards available water. *lbd16-1* showed a very similar linear trend as Col-0 in which xylem pole axis appears random, whilst LRP angle towards the horizontal plane (Fig. 3.4A). This is observed in more detail when plotting lateral root deviation angle against position of the xylem pole initiation site (Fig. 3.4B). A similar positive correlation was observed in *lbd16-1,* r=0.3965 (P=0.0014 ; two-tailed test), as with Col-0. When the initiation site was parallel to the agar (90°) the deviation angle was near zero, whilst initiation site near the agar or opposite the agar leads to strong deviation angles. In contrast, the *LBD16* over-expression (OE) line showed a more uniform distribution of LRP emergence angle, with some LRP emerging straight into the air (Fig. 3.4C). The positive linear correlation between position of xylem pole and lateral root deviation angle is perturbed in this OE line r=0.1437 (P=0.2387 ; two-tailed test) (Fig. 3.4D). Further investigation revealed that the initiation site was not affected in both *lbd16-1* and LBD16 OE and was still similar to Col-0 (Fig. 3.4E). However, the strong LRP angling towards the agar detected in Col-0 was diminished in *lbd16-1* and more strongly in *LBD16* OE lines (Fig. 3.4E). In the case of *LBD16* OE this was caused by a significant reduction in LRP deviation angle (Fig. 3.4F). In the *LBD16* OE line LRP initiating on the

side opposite the agar cannot achieve the same level of angling as Col-0 to emerge towards the agar. This reveals radial expression of *LBD16* plays a key role regulating the deviation angle towards available water.

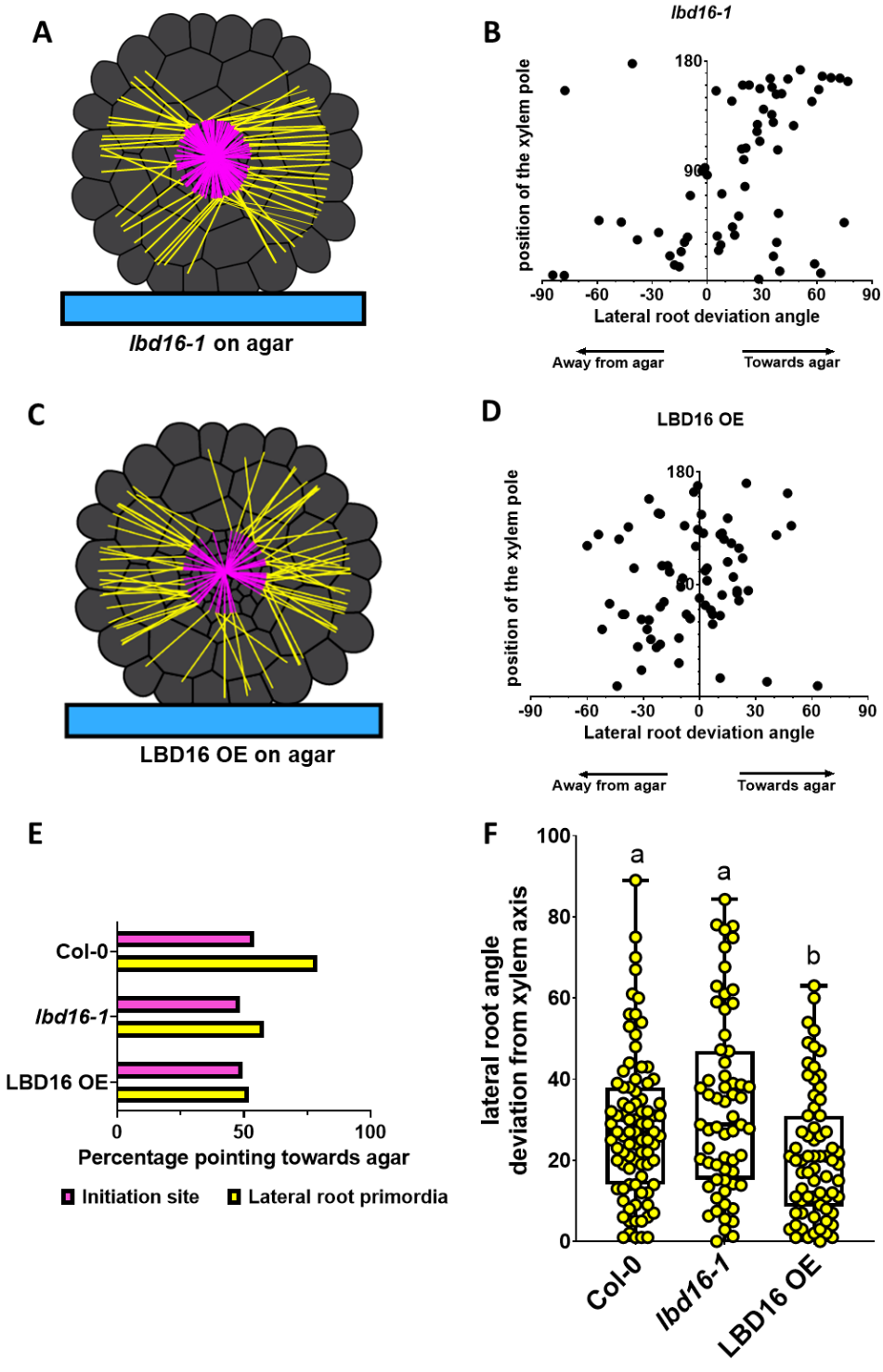

Figure 3.4 – *LBD16* over-expression causes a defect in lateral root angling towards available water. Cross-sections root schematics show the initiation site (where purple line meets yellow line) and emergence angle of growing LRP (yellow line). Distribution of lateral root primordia initiation site and

LRP angle is not affected in *lbd16-1* mutants (A). A significant linear correlation was present between LR deviation angle and position of the xylem pole initiation site r=0.3965 (P=0.0014 ; two-tailed test; B) However, in *LBD16* over-expression (OE) lines more laterals emerge away from the agar, into the air and a linear correlation was absent r=0.1437 (P=0.2387 ; two-tailed test) (C,D). This is more clearly visible in the graph comparing percentage of initiation sites and lateral root primordia angling towards agar (E). Col-0 data from Fig. 3.2 was combined with data from *lbd16-1* and *LBD16* OE lines to demonstrate the lack of difference in initiation site angle, but the strong LRP angle defect in LBD16 OE and a mild defect in *lbd16-1*. The LR deviation angle is significantly lower in LBD16 OE lines compared to Col-0 and *lbd16-1.* Deviation data points are plotted as yellow circles. Statistical differences were analysed using one-way analysis of variance and Tukey's Honestly Significant Difference test (P < 0.05; 95% confidence interval). Statistically similar groups are indicated by the same letters.

3.3 Discussion

3.3.1 The external hydrological landscape influences LR primordia positioning

Water availability can have a striking effect on root system architecture (Morris et al. 2017). Water availability drives root growth direction via hydrotopism (Dietrich et al. 2017). Additionally, air-filled gaps in soil can abolish lateral root primordium (LRP) development via xerobranching (Orman-Ligeza et al. 2018). Hydropatterning represents another adaptive root response enabling plant roots to increase water uptake by promoting lateral root emergence towards soil water availability (Bao et al. 2014; Orosa-Puente et al. 2018). Previous studies have focussed on identifying the hydropatterning response in maize and *A. thaliana* and characterising its underlying molecular basis. This thesis chapter revealed that hydropatterning is also regulated by cell and tissues scale mechanisms designed to steer new LRs in the direction of external water sources.

Previous research on hydropatterning reported preferential LR emergence towards agar, but these experiments only considered emerged lateral roots (Bao et al. 2014; Orosa-Puente et al. 2018). In this chapter, experiments focussed on the positioning of initiation sites and LRP outgrowth angle relative to agar and xylem pole axis. Light Sheet Fluorescent Microscopy (LSFM) proved an ideal technique to distinguish new branches initiating on agar versus air side of roots and enabled us to analyse LRP before emergence. Primordia originate from xylem-pole pericycle (XPP) cells overlaying one of two xylem poles in *A. thaliana* roots. The orientation of the xylem pole axis was

completely random when grown on an agar surface. LRP were observed to initiate on either side of the xylem pole, unbiased by the availability of agar or water. This alternation in LRP position is under regulation of an oscillating transcriptional mechanism that operates as the driving force behind alternating left-right LR patterning (De Smet et al. 2007; Moreno-Risueno et al. 2010). This oscillation mechanism causes the spacing of pre-branch sites and was followed by monitoring *DR5* reporters. The oscillation of DR5 reporter occurs from basal meristem until elongation zone, which is termed the oscillation zone (OZ). The use of *DR5:GUS* reporters revealed tissue specific DR5 expression in both the protoxylem cells during oscillations (De Smet et al. 2007). Cells with high DR5 expression were termed pre-branch sites and can obtain LRFC identity. However, not all these pre-branch sites become LRFCs, suggesting another step of regulation is necessary potentially through environmental cues or additional auxin signalling components. Experimental data in this chapter demonstrate that the left-right alternation of LRFCs is not altered by the external availability of water, but the selection of which XPP cell files become LRFCs is.

Results reported in this chapter revealed that the selection of XPP cell files that gain lateral root founder cell (LRFC) identity are influenced by external water availability. Reporter analysis employing the early LRP marker, *pLBD16::gLBD16-GFP*, revealed a great level of flexibility in positioning of new LRP. Although, a strong deviation angle (90°), where the LRFC initiates on top of the phloem pole pericycle cells, is never observed, indicating a strong role for the pluripotent xylem-pole pericycle cells in LRFC initiation position. Additionally, *LBD16* over-expression (OE) lines displayed distorted LR patterning and diminished LRP deviation angles. These results demonstrated that the positioning of LRFC can deviate from the xylem pole axis and that process is partly regulated through cell specific expression of *LBD16*. It has to be noted that the lateral root deviation angle is a combination of angling during the selection of LRFCs and the emergence angle. These cannot yet be separated with our experimental approach as the Light Sheet imaging chamber is under water and long term tracking with a biased water cue is therefore impossible. What can be deduced from data in this chapter is that both selection of XPP cell files and the radial divisions in flanking cell files of the primordium create the observed LRP angling (Fig. 3.3A-G). LDB16 is involved in polar

nuclear migration before the first round of asymmetrical cell division (Goh et al. 2012a). It is likely that over-expressing *LBD16* leads to non-specific selection of XPP cells to undergo cell division, diminishing the effect of local water availability on this process. Interestingly, *lbd16-1* mutants exhibited no alteration in LRP deviation angle, but did show reduced outgrow towards the agar (Fig. 3.4E,F). This mild phenotype might be explained by genetic redundancy amongst *LBD* family members in *A. thaliana* (Goh et al. 2012a). Together these results reveal an important role for spatial regulation of *LBD16* expression in controlling LRP deviation towards external water.

The flexibility in XPP cell selection provides the plant with a rapid way of responding to local water availability during early stages of LR formation. External water appears to be sensed by the root in the elongation zone, where it possibly connected to LRFC positioning in the pericycle (Bao et al, 2014; Orosa-Puente et al, 2018; Robbins & Dinneny, 2018). The localisation of LRFCs is established in the early differentiation zone, where DR5 reporter in the XPP indicates a high auxin response in pre-branch sites (Dubrovsky et al. 2008). DR5 induction at first in protoxylem cells followed by XPP cells suggests there might be interconnectivity between these cell types, possibly through exchange of mobile signals via plasmodesmata. Intriguingly, disruption of plasmodesmata transport by mutating callose degradation in *plasmodesmal- localized β-1,3-glucanase1 (pdbg1) pdbg2* double-mutants severely impacts longitudinal LRFC patterning (Benitez-Alfonso et al. 2013). However, it is currently unclear if plasmodesmata mutants affect radial positioning of LRFCs after a hydropatterning stimulus. Another option for movement between protoxylem and XPP cells is the movement of auxin through transport mediated by PIN efflux carriers (Benkova et al. 2003). PIN directed transport could cause a flux of auxin towards LRFCs to select them for initiation. Furthermore, PIN auxin transport is crucial for the spacing of LRP by driving auxin in a small group of XPP cells, thereby promoting local cell division and inhibiting adjacent cells from undergoing LR initiation (Laskowski et al. 2008). The role of these PIN proteins in hydropatterning has to be further elucidated.

Future research should also focus on auxin signalling components that regulate LRFC identity, such as *GATA23*. This gene is part of the AUX/IAA28 and ARFs signalling module that coordinates the transition from pre-branch site into LRFC and acts prior to LBD16

(De Rybel et al. 2010). Another interesting candidate gene is *MAKR4* which regulates the conversion of IBA to IAA (Xuan et al. 2015). MAKR4 is involved in the specification of LRFC cells from pre-branch sites as *MAKR4* amiRNAi lines have normal levels of pre-branch sites, but a reduced number of LRPs. Analysing mutants in these genes would confirm if the deviation angle is regulated through LRFC specification via cell specific expression of *GATA23* or *MAKR4* in XPP cells of the elongation zone. This hypothesis fits well with modelling studies which indicated that the elongation zone is crucial for water sensing and LR hydropatterning (Robbins and Dinneny 2018).

The overlying endodermal tissue could influence the expression of *GATA23* and *MAKR4* during XPP LRFC specification. Laser ablation of endodermal cells induced pericycle cell division, yet these symmetric (as opposed to asymmetric, formative) divisions did not result in LRP formation (Marhavý et al. 2016). However, exogenous addition of auxin after endodermal cell laser ablation could trigger LRFC specification and LRP formative cell divisions (Marhavý et al. 2016). Conversely, expressing a non-degradable variant of AUX/IAA3 termed *shy2-2* solely in the overlying endodermal cells could block the first anticlinal division (Vermeer et al. 2014). These results indicate the importance of early auxin signalling between pericycle and endodermis in specifying LRFCs. IAA3 and ARF mediated responses in the endodermis might be crucial for early expression of LRFC markers such as *GATA23* during lateral root hydropatterning.

How could external water availability impact the signalling pathway that regulates LRFC specification? One theory is that external radial water inflow through plasmodesmata (symplastic transport) promotes co-transport of signalling molecules as water moves from outer epidermal to inner xylem pole cells. Such signalling molecules could comprise of hormones like auxin which is predicted to accumulate in elongating epidermal cells and able to be transported through plasmodesmata (Band et al. 2014; Mellor et al. 2020). Alternatively, ions such as calcium might play a role in a comparable way as during physical bending of the root, which increases levels of Ca^{2+} on the root convex side, but not on the concave side (Richter et al. 2009). Additionally, blockage of calcium channel by LA^{3+} treatment, could abolish bend-induced Ca^{2+} rise and inhibit LR development, indicating a direct effect of calcium influx and LR formation. Contrastingly, water flow on the ‘air’ side of the root will be reduced, which might

increase the build-up of inhibitory signalling molecules that affect LRFC induction such as ABA (Orman et al, 2018). Such water transported signalling molecules (which can be termed Hydrosignals) might therefore play a promising role in defining radial positioning of LRFCs in response to external water availability.

3.3.2 External hydrological landscape determines primordium emergence angle

Results presented in this chapter revealed that LRP which initiated near the air side exhibited a strong emergence deviation towards the agar (Fig 3.2A). This results in the high percentage of LR emergence on the agar side of the root as reported in previous research (Bao et al. 2014; Orosa-Puente et al. 2018). In contrast, LRP initiated at the xylem pole opposite the agar side exhibited strong deviation towards the air side. This suggests that either the osmotic potential or mechanical constraint of the agar might prove to be a barrier for LR emergence. The osmotic potential difference in a radial cross section of a root varies between agar and air side. Mathematical modelling approaches suggest a water potential difference of 1 MPA in the LR competent zone in Maize root models with a 1 mm cylindrical diameter (Robbins and Dinneny 2018). Highest water potential was visualized when in direct contact with the agar, whilst near the air side of the root the water potential dropped. This would drive water transport from the agar (high water potential) into adjacent root tissue (lower water potential) and through root tissue towards the air side of the root (lowest water potential), causing a water potential gradient across the root circumference. In *A. thaliana* root absorption of water from the meniscus would play an increasingly important role compared to the thicker maize root. However, the exact size of the meniscus has not yet been confirmed for growing *A. thaliana* roots. It is hypothesized to extend to near half the roots diameter, severely increasing the circumferential water uptake area of *A. thaliana* roots. Combining meniscus contribution and water potential root modelling data, suggests that the root might take up more water from the meniscus contact area where the water potential difference is greatest. This would be in accordance with our results which showed a strong trend towards LRs emergence parallel to the agar surface.

How are new LRP able to deviate their angle of emergence? Our results suggest this is a consequence of the variability of anticlinal and radial divisions observed during emergence. The primordia originate from between five to eight adjacent pericycle cell

files (Von Wangenheim et al. 2016). The central cell file undergoes the very first anticlinal division and later forms the LR quiescent centre once a four layered primordia is formed (Goh et al. 2016). The central cell file contributes most of the volume when LRP reaches emergence, however the adjacent flanking cell files contribute the most mass at the base of the primordia (Fig. 3.3A). Cell file contour tracking of LRP development over time demonstrated preferential radial divisions on one side of the primordium, causing an asymmetry increased in LRP width. Although these datasets were grown submerged in a light sheet microscope chamber, it does reveal how the plasticity we observed in lateral root deviation angle can be generated by an asymmetry in radial divisions. The division and expansion of cells on one side of the primordium bends it towards the opposing side. These results identify that the asymmetry in radial divisions in central and flanking cell files control the LRP outgrowth angle.

How is the division pattern in the LRP controlled? The first asymmetrical division of LRFCs is tightly regulated, but the following round of division follow no pre-determined pattern (Von Wangenheim et al. 2016). Further rounds of cell division are dependent on proliferation of the central cell file and changes in volume of the overlying endodermal cells (Lucas et al. 2013). These round of cell divisions are instrumental in creating the dome shape of a primordium. Possibly feedback from the overlying tissue has a directing role in LRP deviation angle. Symplastic transport between endodermis and pericycle is reduced after stage 2 and 3 of primordium development (Benitez-Alfonso et al. 2013). This is partly due to increased levels of callose deposition, which reaches a maximum at stage 4 and 5 (Benitez-Alfonso et al. 2013). This blocks passive diffusion between developing LRP and endodermis, however active transport is still possible. In very early LRP stages active auxin transport via PIN3 directs auxin from endodermis into LRFCs (Marhavý et al. 2013). This induces rounds of cell division and could be important for early changes in LRP outgrowth direction. In later stages auxin from the growing primordium gets transported into overlying endodermal and cortex cells through a PIN3 and LAX3 reflux loop to coordinate expression of cell wall remodelling enzymes (Peret et al. 2013). This creates a path for the LRP to emerge through. These two auxin carriers might be controlled by water availability to steer primordium emergence. Mutant analysis of *PIN3* and *LAX3* lines using our light sheet

set-up can identify if these mutants have a defect in forming LRP deviation angles. Furthermore, fluorescent reporters of these genes could help identify the radial expression pattern in endodermal and cortex cells and if this is affected by water availability.

Another driver of the LR deviation angle could be a mechanical sensing mechanism. We observed a strong LRP deviation angle when the initiation side was near the agar. Additionally, roots grown in agar, showed a similar uniform LRP emergence pattern and deviation angle as roots grown in water. These results indicate a possible role for mechano-sensing in hydropatterning. The agar side of the root is in direct contact with moisture, this might result in increased turgor pressure. In contrast, the turgor pressure on the air side might be lower as it has no direct water source. This could be investigated by use of vacuole and tonoplast markers employing our LSFM approach. The reduction in turgor pressure can cause the activation of mechanosensitive channels that act upon dissociation of plasma membrane from the cell wall or RLK's that monitor changes in cell wall integrity (Feng et al. 2016). Mechanosensitive channels function by opening or closing after changes in membrane tension, whilst mechanosensitive RLKs monitor cell wall integrity (Hamant and Haswell 2017). Cell wall integrity is based on structural components such as pectin, maltose and cellulose microfibrils (Marín-Rodríguez et al. 2002; Hamant et al. 2008). The mechanical properties of the cell wall and plasma membrane are directly influenced by changes in environmental osmotic potential. The mechanosensitive calcium channel OSCA1 is affected by stress and regulated through pressure sensing (Yuan et al. 2014; Murthy et al. 2018). The RLK FERIONA is reported to sense osmotic changes via changes in pectin content in the cell wall (Guo et al. 2009; Duan et al. 2010; Haruta et al. 2014). Future research using mutants in these mechano-sensitive components should reveal the contribution of mechano-sensing during a hydropatterning stimuli.

The non-stereotypical growth after the first LRFC asymmetrical division suggests possible influence of environmental factors that determine LRP outgrowth angle. This corresponds with what is shown in this chapter and could be controlled by external water availability. This is supported by further studies of LRP emergence when faced with a uniform distribution of mechanical constraints and aqueous environment, by

growing roots in hydroponics and in agar. Roots grown in agar and water showed a uniform radial distribution of LRP emergence and a significant decrease in LRP deviation angle (Fig. 3.2E,F). The deviation angle is thus dependent on the distribution of water in the environment and can steer the organs emergence towards water. In conclusion, results in this chapter reveal that the positioning of first asymmetrical division in the XPP cells and subsequent radial divisions in the LRP are controlled by, and subsequently steer emergence towards, external water availability.

4 LATERAL ROOT HYDROPATTERNING DEPENDS ON ARF7 SUMOYLATION

Jason Banda, Nicky Leftley, Daniel von Wangenheim and Beatriz Orosa-Puente

Parts of this chapter have been published as: Orosa-Puente, B., Leftley, N., von Wangenheim, D., **Banda, J.**, Srivastava, A.K., Hill, K., Truskina, J., Bhosale, R., Morris, E., Srivastava, M., Kümpers, B., Goh, T., Fukaki, H., Vermeer, J.E.M., Vernoux, T., Dinneny, J.R., French, A.P., Bishopp, A., Sadanandom, A., Bennett, M.J., 2018. Root branching toward water involves posttranslational modification of transcription factor ARF7. ***Science*** 362, 1407–1410.

4.1 Introduction

Root system architecture is crucial for exploration of soil and foraging for heterogeneously distributed resources such as water (Hodge 2004; Morris et al. 2017). To help acquire water, roots need to increase their surface area when in direct contact. Roots do this by branching in the direction of the water source. This adaptive response is called lateral root hydropatterning and enables plants to regulate branching at a local scale (Bao et al. 2014; Robbins and Dinneny 2018). However, the molecular mechanism plants employ to control their branching towards water is still unknown. Similarly, what stage of lateral root initiation or development is affected by local availability of water in the surrounding root environment is also unclear.

A role for the hormone auxin has been reported during LR hydropatterning (Bao et al. 2014). Rice seedlings expressing the auxin response reporter *ProDR5:GUS* showed preferential reporter activity in root cells in contact with agar (versus those oriented towards the air). Mutants in the auxin transcription factor AUXIN RESPONSE FACTOR7 (ARF7) have been reported to disrupt roots ability to preferentially orient a high percentage of their LRs towards water (Orosa-Puente et al. 2018). Mutant alleles defective for 3 of the other 4 activating ARF's were also tested, but exhibited no defect, indicating that the LR hydropatterning response is ARF7 dependent. These experiments were executed on agar plates, with agar representing the primary water source for these plants. In the case of Col-0, approximately 80% of emerged lateral roots grew

towards the agar, while 20% emerged into the air yet often bend towards the agar after emergence. However, *arf7 loss-of-function* mutant alleles disrupt the ability to hydropattern, as they exhibit a 60/40 distribution of water/air directional lateral root emergence. Multiple studies have linked ARF7 with lateral root development, as the ARF7 –ARF19 auxin signalling module is crucial for lateral root organogenesis (Fukaki et al. 2002; Okushima et al. 2005, 2007; Wilmoth et al. 2005; Goh et al. 2012b).

Interestingly, over-expressing *ARF7* in *arf7-1* can restore a Col-0 hydropatterning phenotype (Orosa-Puente 2018). This result revealed two key points. First, the ARF7 protein is crucial for LR hydropatterning. Second, the *ARF7* gene does not need to be expressed under its own promoter to rescue the Col-0 LR hydropatterning phenotype. Hence, in the case of LR hydropatterning we can hypothesize that regulation of ARF7 protein activity, rather than transcription, is most critical. Still, it remains unknown how ARF7 activity is controlled by water distribution in its local environment.

This chapter aims to analyse ARF7 activity by focussing on its downstream genes. Gene regulatory network inference using time series transcriptomics analysed using an mathematical algorithm (termed TDCor) has identified downstream genes controlled by ARF7 during lateral root development (Lavenus et al. 2015). *LBD16*, *LBD29*, IAA19 and *ARF19* were identified and confirmed as primary targets of ARF7, validated by chromatin immunoprecipitation-quantitative PCR (ChIP-qPCR). LATERAL ORGAN BOUNDARY DOMAIN 16 (LBD16) / ASYMMETRIC LEAVES2-LIKE18 (ASL18) and LBD29 are both auxin inducible members of the AS2/LATERAL ORGAN BOUNDARY (LOB) family of transcription factors. This family of proteins, from here on called LBD, consists of 42 members and are involved in many aspects of plant development, including embryo, root, leaf, pollen, photomorphogenesis, secondary growth, plant defence, plant regeneration, and inflorescence development (Iwakawa et al. 2002; Xu et al. 2016). Members of this family have a conserved LOB domain at the N terminus. This LOB domain, entailing 100 base pairs, comprises a 'C-block' containing four cysteine required for DNA-binding activity, a Gly-Ala-Ser (GAS) block and a leucine zipper-like coiled-coil motif crucial for LBD protein dimerization and biological function (Shuai et al. 2002; Lee et al. 2017). The C-terminal domain of LBD18 contains a transcriptional activation domain (TAD) that can induce expression of downstream targets. One of the

biological functions of this protein family is regulation of lateral root initiation and development by auxin inducible family members *LBD16, LBD17, LBD18, LBD29 and LBD33* (Okushima et al. 2007; Lee et al. 2009; Majer & Hochholdinger 2011). All are expressed in the lateral root primordia, although levels of expression greatly vary (Lee et al. 2009; Goh et al. 2012a).

An extensive amount of work has focussed on the role of LBD16 in lateral root development as a transcriptional activator and direct target of ARF7 (Lavenus et al. 2015). Less is known about a parallel pathway that induces LR formation through LBD16 and WUSCHEL-RELATED HOMEOBOX11 (WOX11) (Sheng et al. 2017). WOX11 directly binds the *LBD16* promoter to activate transcription. Interestingly, WOX11 did not seem important for LR induction on *A. thaliana* seedlings grown on plates but might play a role in soil grown seedlings. WOX11-SDRX, dominant repressors, grown in soil showed reduced formation of LRs (Sheng et al. 2017). Furthermore, increased expression of WOX11-GUS was observed in roots grown in soil (Sheng et al. 2017). These results suggest there is more than one pathway to induce LBD16-mediated LR formation. Potentially environmental factors decide which pathway is initiated in the root increasing the roots plasticity.

When re-engineered to become a transcriptional repressor (termed LBD16-SRDX), Goh et al., observed transgenic roots underwent normal lateral root founder cell establishment, but repressed nuclear migration and asymmetric cell division (Goh et al., 2012). This elegantly demonstrated LBD16 is required in xylem pole pericycle cells to regulate polar nuclear migration and asymmetric cell division during lateral root initiation. Homodimerization of LBD16 (like LBD18) is crucial for its function (Lee et al. 2017). Mutation of the Leucine, Valine, or Isoleucine residues of the coiled-coil motif into Proline eliminates homodimerization and limits restoration of lateral root initiation in *lbd16* and *lbd18* mutants (Lee et al. 2017). LBD16 controls genes such as *PUCHI*, *MAKR4*, TARGET OF LBD SIXTEEN 2 (*TOLS2)* and *GATA23* which play key roles later in the lateral root developmental programme (Goh et al. 2012a; Toyokura et al. 2019; Goh et al. 2019).

LBD29 represents another LBD member playing a major role in lateral root development. A SALK insertion in the *AuxRE* motif nearest to the transcription start site

on the *LBD29* promoter reduced numbers of lateral root primordia (Liu et al. 2010; Feng et al. 2012). Whilst this T-DNA insert did not affect the coding sequence of the gene, it blocked *LBD29* auxin-inducibility, significantly lowering transcript levels (Porco et al. 2016). *LBD29* expression was correlated with cell cycle-related gene expression, which potentially controls the mitotic potential of the pericycle during lateral root primordia initiation and development (Feng et al. 2012). Furthermore, LBD29 can bind the *LAX3* promoter, which triggers the auxin-dependent induction of this auxin influx carrier in cells overlying LRP (Porco et al. 2016). *LAX3* can in turn switch on genes that degrade pectin to aid cell wall remodelling in cells overlying LRP (Swarup et al. 2008). Through this network of sequential gene induction, *LBD29* can promote LRP emergence.

LBD18 and LBD33 work cooperatively to regulate lateral root initiation. These two LBD genes dimerize and induce *E2Fa* expression (Berckmans et al. 2011). The transcription factor E2Fa promotes cell cycle activation and asymmetric division in the pericycle cells and expression of E2Fa under the *LBD18* promoter can restore the impaired number of lateral roots in *lbd18-1* mutants (Berckmans et al. 2011). Additionally, LBD18 was shown to induce expression of *LAX3* and the cell wall remodelling genes, *EXP14* and *EXP17* (Lee et al. 2013a; Lee and Kim 2013). All these five LBD's thus have their own specific niche in regulating LR initiation and/or development, although all are directly or indirectly controlled by ARF7 and ARF19.

The role of LBD17 in LR development remains unclear. Although expressed in lateral root primordia levels of *LBD17* are quickly repressed after LR initiation, suggesting a possible role for LBD17 in LR initiation, but a limited role in LRP emergence (Goh et al. 2012a; Lavenus et al. 2015). Additionally, no known *loss-of-function* allele is available for this gene.

This chapter aims to characterise (1) if LBD16 is required for hydropatterning, (2) if LBD16 is expressed asymmetrically during hydropatterning and (3) to test how post-translational modification of the ARF7 transcription factor controls its ability to bind target genes like LBD16 and regulate LR hydropatterning.

4.2 Results

4.2.1 Hydropatterning is regulated by an ARF7 and LBD16 dependent pathway

To investigate the role of *ARF7* regulated genes during LR hydropatterning, we characterised this adaptive response in multiple mutants from the LBD family involved in LR formation and targets for ARF7 transcriptional activity (Lavenus et al. 2015). To assess the role of these LBD's on LR hydropatterning a bioassay in which plants grew vertically on agar was employed (Fig. 4.1A). After 12 days, the length of the primary root and the number of lateral roots emerging towards the agar and dry sides were quantified. Using this bioassay, the hydropatterning response of the *loss-of-function* allele *lbd16-1*, the LBD16 translational reporter line LBD16pro::*gLBD16-GFP lbd16-1* (Goh et al. 2012) and two independent *LBD16* over-expresser lines (*LBD16* OX 72 and 73) was characterized. Knocking out *LBD16* expression resulted in a reduction of primary root length, whilst in *arf7-1* primary root growth is similar to Col-0 (Fig. 4.1.B). However, this reduction in *lbd16-1* primary root growth was not consistently shown in repeats of this experiments and might have been the results of plate conditions. Lateral root number and density was reduced in both *lbd16-1* and *arf7-1* mutants, indicating they both perform important functions during lateral root development (Fig. 4.1C,D). Like *arf7-1,* lateral root hydropatterning was also significantly impaired in *lbd16-1* (Fig. 4.1E). Complementation of *lbd16-1* with the genomic LBD16 construct tagged with GFP (gLBD16-GFP), can rescue primary root length to Col-0 levels and lateral root density and number to significantly higher numbers (Fig. 4.1B-D). Additionally, the LR hydropatterning response can be rescued to Col-0 levels in this complementation line (Fig. 4.1E).

Overexpressing *LBD16* using the 35S promoter had a severe effect on root system architecture (Fig. 4.1A-E). Primary root length was strongly reduced and lateral root number and density were significantly lower than Col-0. Surprisingly, hydropatterning was more strongly affected in the *lbd16-1* mutant, with LR emergence of approximately 50% towards the agar. This revealed *LBD16* over-expressing lines exhibited no bias towards water or air, highlighting how important its spatial regulation by ARF7 is during hydropatterning.

Mutants in *LBD18* and *LBD29* showed no hydropatterning defect, indicating that hydropatterning is not dependent on these two LBD family members (Supp. Fig. S4.1A, B).

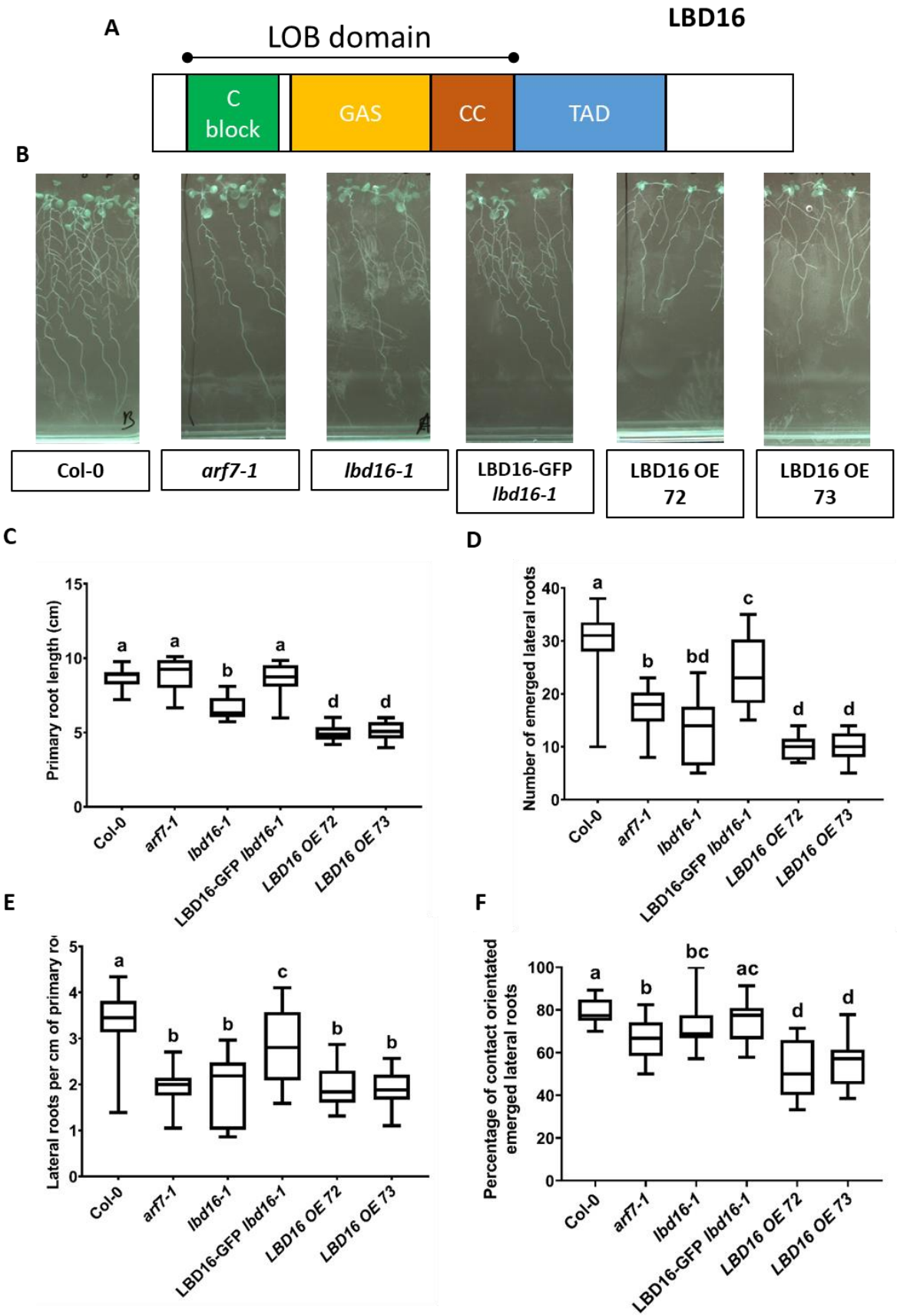
A
LOB domain
LBD16
C block
GAS
CC
TAD
B
Col-0
arf7-1
lbd16-1
LBD16-GFP lbd16-1
LBD16 OE 72
LBD16 OE 73
C
Primary root length (cm)
D
Number of emerged lateral roots
E
Lateral roots per cm of primary ro
F
Percentage of contact orientated emerged lateral roots

Figure 4.1 – *LBD16* knock-out and two independent LBD16 over-expression (OE) lines have a hydropatterning defect. The LBD16 protein sequence contains multiple domains of which the LOB domain is present in all LBD family members (A). This LOB domain consists of a :C-block' containing four cysteine required for DNA-binding activity, a Gly-Ala-Ser (GAS) block and a leucine zipper-like coiled-coil motif (CC) crucial for LBD protein dimerization and biological function. This domain is followed by a transcriptional activation domain (TAD) on the C-terminal. Both the *lbd16-1* knock-out and *LBD16* OE lines have impaired primary root length (A, B), reduced number of emerged lateral roots (C) as well as a reduced lateral root density (D). The LBD16-GFP translational fusion in *lbd16-1* background can rescue most of these developmental defects, proving its functionality. Knock-out and OE lines also display a significant defect in their lateral root hydropatterning response (E). In the independent *LBD16* OE lines 72 and 73 this is most severe. Box plots show data distribution. Different letters indicate a significant different (p≤0.05, one-way ANOVA, Tukey's HSD test) n=10-15 seedlings.

4.2.2 Employing light sheet fluorescent microscopy to study lateral root hydropatterning

To test if the spatial availability of water impacts expression of early lateral root primordia (LRP) genes like *LBD16*, we imaged the gLBD16-GFP reporter exposed to a hydropatterning stimulus (Goh et al. 2012a).

The first challenge was how to 3D image the root in such a way that we could identify the root side facing the agar and the side facing air. This was addressed by distinguishing between root cells in contact with agar versus air by employing fluorescent beads to demark the side of the root facing the air (Fig. 4.2. A-I). By adding these fluorescent beads to 1% low melting agarose mix and pipetting them on top of the primary root, we were able to distinguish air side (with fluorescent beads) from agar side (no beads). These beads fluoresce at the same wavelength as GFP, aiding co-imaging. The elongation and early differentiation zones of the primary root were excised and placed inside a 1 mm glass capillary. This capillary was then filled with fluorescent bead containing agarose to hold the sample, plus a plunger to position each sample in place and then push the sample out into the LSFM imaging chamber before imaging.

The second challenge was to develop a way to image cells through the entire radius of an *A. thaliana* root. Regular confocal microscope imaging of root tissues suffers from light scattering, reducing image quality for several reasons. For example, light scattering causes the side furthest away from the laser source to experience lower excitation of GFP molecules and thus emit lower fluorescence. The effect of light scattering was

countered by using the Multi-View Imaging software on the Zeiss Z1 Light Sheet Fluorescence Microscope. This involves rotating the sample six times in six equal angles around the primary root. These six z-stacks were then fused together based on the location of the beads in every angle stack using ImageJ Multi-View reconstruction software (Preibisch et al. 2010, 2014)(Fig. 4.2H,I). This resulted in a crisp radial image across root elongation zone tissues and eliminated the light scattering effect (Fig. 4.2).

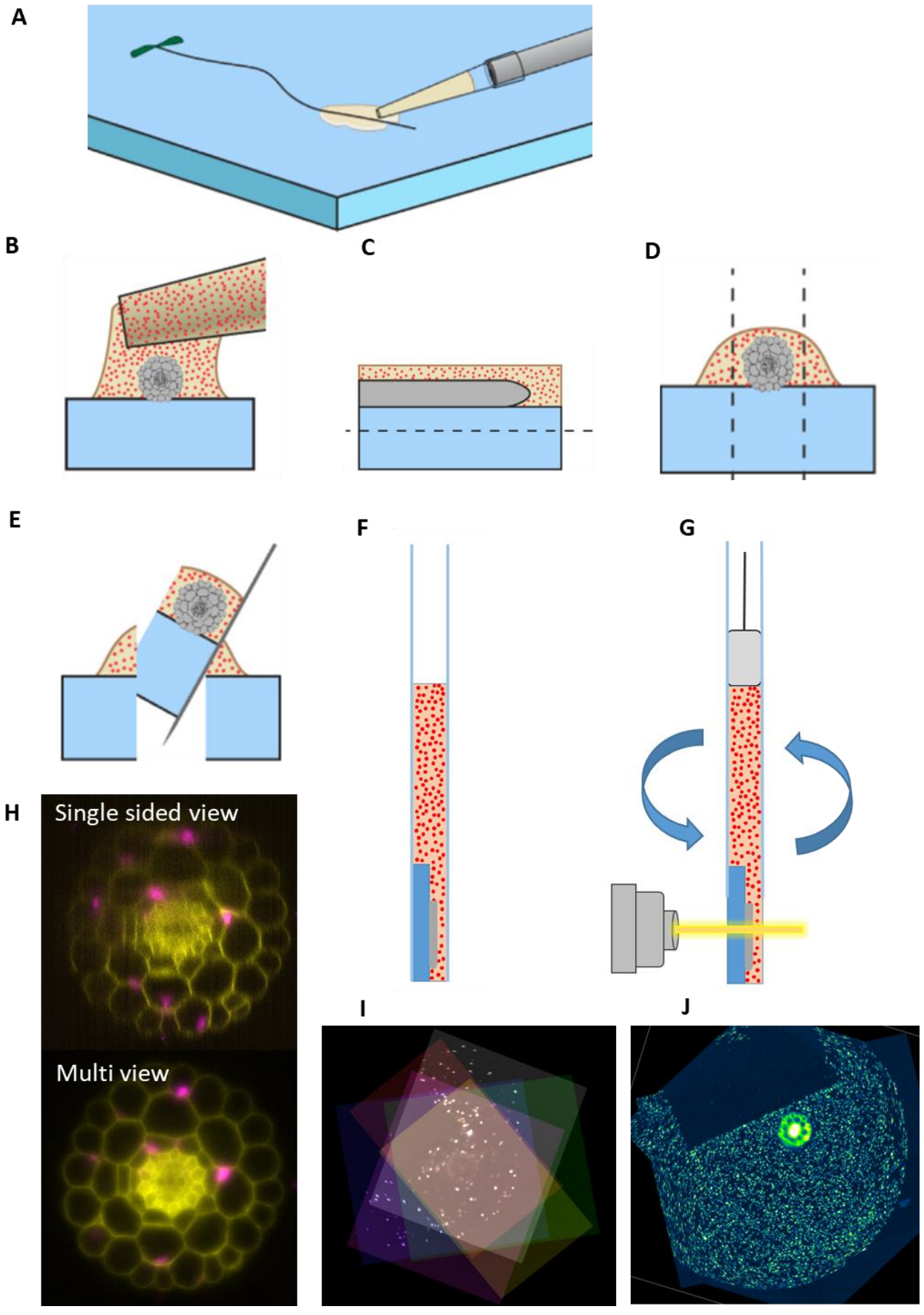
A
B
C
D
E
F
G
H
Single sided view
Multi view
I
J

Figure 4.2 – Light Sheet Fluorescence Microscopy (LSFM) protocol used in imaging LR hydropatterning using gLBD16-GFP. Plant roots were overlain with low melting agarose containing fluorescent beads (A, B). The root was then cut above the elongation zone together with the surrounding agar in a rectangular shape (C). To fit the capillary the section of root and agar have to be cut even thinner (D). The cut section will then be picked up with a blade and placed into the 1 mm glass capillary (E, F). A plunger will be inserted at the top to create a vacuum and keep the sample stable (G). When the sample is inserted into the LSFM chamber, the plunger is pushed down to push the agar and root sample out into the water filled chamber. We then used Multi view imaging to image the sample from six different angles creating a high resolution radial image relative to single sided illumination (H). The six z-stacks from different angles are shown here in different colours (I), before they are fuses together using the Multiview Reconstruction tool from ImageJ (J).

4.2.3 The asymmetrical localisation of gLBD16-GFP in root elongation zone is dependent on ARF7

The LSFM hydropatterning protocol was employed to address if gLBD16-GFP is either: (1) expressed more strongly on the side in contact with agar or (2) switched on earlier on the agar side compared to the air side.

gLBD16-GFP expression was first observed in the late root elongation (Fig. 4.3A). The fused images acquired from this zone were then radially cross sectioned and the maximum intensity projection was rendered to separate *the gLBD16-GFP* signal originating from the xylem pole near the agar and the distant xylem pole (Fig. 4.3B-D). The spatial difference between the onset of the fluorescent signal on the agar xylem pole and air xylem pole was measured and termed as the index of asymmetry (Fig. 4.3C). Measuring this index for the gLBD16-GFP reporter revealed a high level of signal asymmetry (Fig 4.3D,F). However, the level of fluorescence between gLBD16-GFP fluorescence on the air and on the agar side was very similar (Fig 4.3D,G). This result suggests that gLBD16-GFP might initiate or stabilize on one side first, but that both sides will eventually reach the same signal level.

To assess if ARF7 was necessary to generate this asymmetrical localisation of gLBD16-GFP, a cross was made with the *arf7-1 loss-of-function* knock-out mutant. This gLBD16-GFP *lbd16-1 arf7-1* line was scanned using the LSFM hydropatterning protocol. This line exhibited a low level of gLBD16-GFP signal asymmetry (Fig 4.3E,F). Additionally, the level of fluorescence in gLBD16-GFP was significantly lower in the *arf7-1 lbd16-1* background

compared to *lbd16-1.* However, no difference between the intensity of gLBD16-GFP on agar and air side was observed (Fig 4.3E,G). Hence, gLBD16-GFP asymmetry in the root elongation zone appears to be dependent on ARF7.

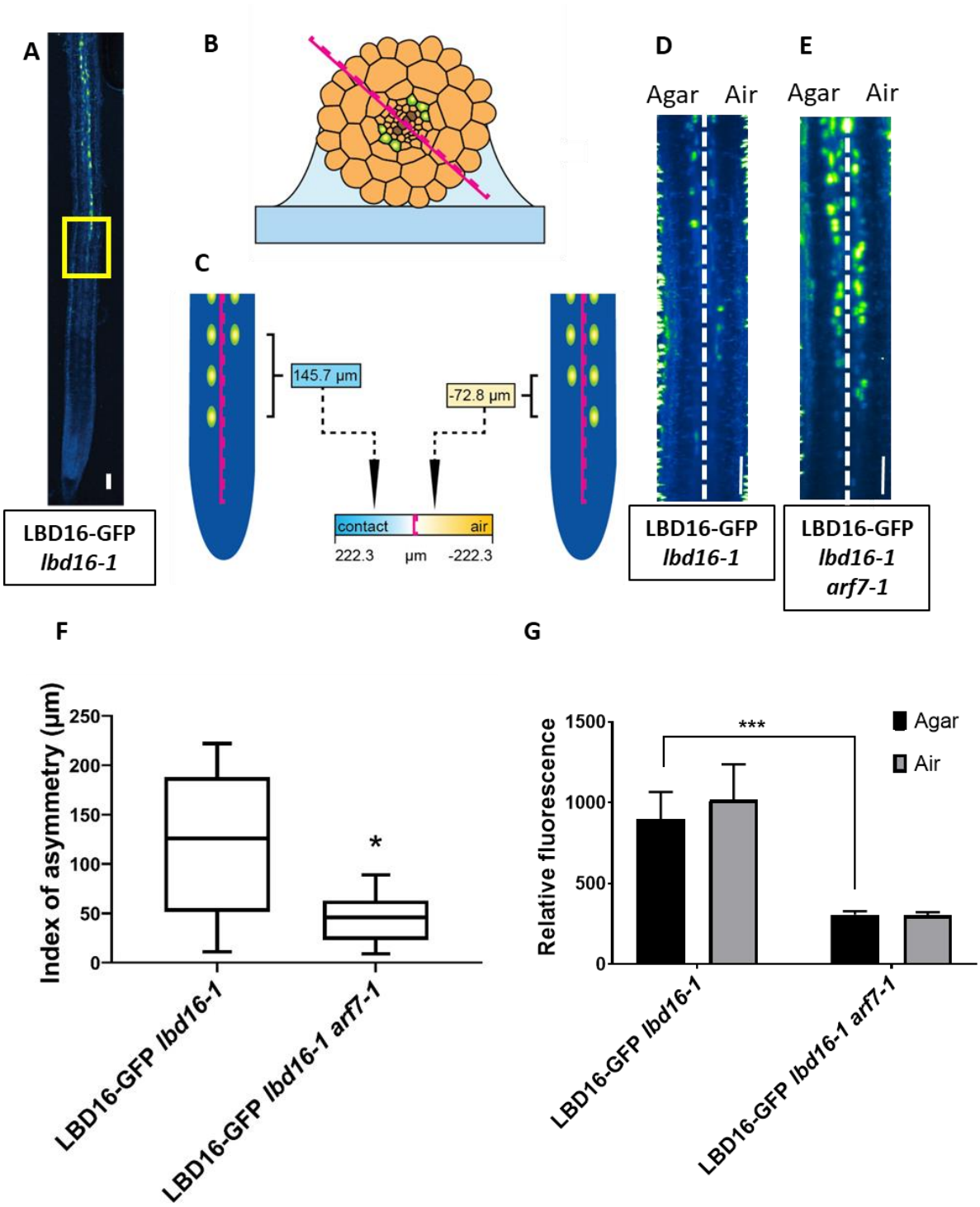

Figure 4.3 – ARF7 SUMOylation is crucial for lateral root hydropatterning by triggering the asymmetric localisation of LBD16. Confocal image showing the onset of LBD16-GFP fluorescence in the late root elongation zone (A). In order to distinguish the onset of the nuclear LBD16-GFP signal on the agar

(contact) and air side we split the root in half (pink line), separating the two xylem poles according to which one is closest to the agar (B). Creating an agar side of the root, left from the pink dashed line, and an air side of the root, on the right side of the pink dashed line. Distance between the onset (first visible nucleus) was then measured in µm and displayed as the index of asymmetry (C). Maximal intensity projections from radial reslices taken using the LSFM of LBD16-GFP in *lbd16-1* (D) and *lbd16-1 arf7-1* (E) background, were used to unravel the localisation of LBD16-GFP on the agar and air side of the primary root. The index of asymmetry indicates the level of asymmetry between first nuclear LBD16-GFP signal on the agar compared to the air side (H). The intensity of these nuclei on agar and air side were also measured and compared (I). Asterisk indicates significant differences ($p<0.05$) with LBD16-GFP lbd16-1 using one-way ANOVA (F) or two-sided Student T-test (G) n=8. Scale bar represents 50 µm.

4.2.4 Asymmetric gLBD16-GFP expression is dependent on ARF7 SUMOylation

Next, we addressed how the asymmetric pattern of gLBD16-GFP expression was regulated by ARF7. Significantly, 35S driven ARF7 could restore LR hydropatterning in *arf7-1*, indicating a possible role for ARF7 post-translational (rather than transcriptional) regulation. Additionally, no asymmetry was detected in roots when using an gARF7-Venus translational reporter when exposed to a hydropatterning stimulus (Orosa-Puente et al. 2018), further supporting the likelihood of a post-translational modification (PTM) regulating ARF7 activity during LR hydropatterning. In collaboration with Ari Sadanandom's team (University of Durham) it was directly established that ARF7 is a PTM target for Small Ubiquitin-like MOdifier (SUMO). SUMO site prediction software identified 4 SUMO sites on the ARF7 protein sequence including one located in the DNA binding domain (Fig 4.4A). These four SUMO sites are numbered after the lysine amino acid position in ARF7, namely K104, K151, K283 and K890. By mutating the lysine (K) into an arginine (R) in the SUMO site (which disrupts formation of the isopeptide bond between this lysine and the SUMO carboxyl terminal glycine), SUMOylation of these ARF7 residues is blocked. This was shown by transiently co-expressing SUMO-HA and either ARF7 WT-YFP (ARF7-WT refers to ARF7 gene from Col-0 ecotype) or ARF7 4KR (with the 4 lysines mutated to an arginine) (Orosa-Puente et al. 2018). ARF7 SUMOylation was abolished when all 4 lysines were mutated. When the *ARF7*^{4KR} transgene, driven under its own promoter, was transformed into *arf7-1*, the resulting line was unable to rescue the mutant's lateral root hydropatterning defect. In contrast, complementation with the *ARF7*^{WT} transgene could rescue LR hydropatterning

to Col-0 levels (Orosa-Puente et al. 2018). These results suggest that ARF7 SUMOylation controls LR hydropatterning.

To verify this model, we tested if SUMOylation of ARF7 also regulates the asymmetrical expression of gLBD16-GFP during LR hydropatterning. A cross between gLBD16-GFP *lbd16-1 arf7-1* and either *ARF7^{WT}* or *ARF7^{4KR}* was made. To confirm homozygosity of the *ARF7* transgene in the F3 we genotyped six lines of both *ARF74KR* and *ARF7^{WT}* with a primer pair spanning the *arf7-1* SALK insertion, to avoid amplifying the genomic *ARF7*. This confirmed that all plants were homozygous for the insert (Fig. 4.4C). From these amplicons the four SUMO sites were sequenced and confirmed (Fig. 4.4B). gLBD16-GFP homozygosity of lines was confirmed by confocal microscopy analysis of multiple seedlings from individual lines, and in there was no segregation of individual plants without GFP.

The hydropatterning response of these new crosses was first tested to confirm the same phenotypic response was present in both LBD16-GFP ARF7^{4KR} and LBD16-GFP ARF7^{WT} lines as earlier recorded. The cross with ARF7^{WT} could fully restore LR hydropatterning, while the cross with ARF7^{4KR} could not (Fig. 4.5A), which aligns with the published data (Orosa-Puente et al. 2018). Next, we addressed if ARF7 SUMOylation could regulate asymmetrical localisation of gLBD16-GFP during LR hydropatterning. Lines complementing gLBD16-GFP *lbd16-1 arf7-1* with *ARF7^{WT}* revealed a strong recovery in *gLBD16-GFP* asymmetry, whilst *ARF7^{4KR}* complementation lines had, on average, a low level of asymmetry (Fig. 4.5B-D). This indicates that the ARF7^{4KR} line is unable to direct a bias in response to a hydropatterning stimulus. Hence, ARF7 SUMOylation appears to regulate asymmetrical localisation of gLBD16-GFP during LR hydropatterning.

Comparing the average relative fluorescence of *gLBD16-GFP* in the nuclei of these two lines with gLBD16-GFP in *lbd16-1* and *lbd16-1 arf7-1* backgrounds, revealed that only ARF7^{4KR} could restore Col-0 relative fluorescence levels in the nuclei. In contrast, both gLBD16-GFP *arf7-1* and gLBD16-GFP *arf7-1* ARF7 ^{WT} had a lower relative fluorescence in the root elongation zone (Fig 4.5E). Comparing the level of gLBD16-GFP fluorescence between agar and dry sides of the root in all these lines resulted in no measurable difference. These results suggest that the non-SUMOylatable version of ARF7 is more active in inducing expression of *LBD16* in the root elongation zone.

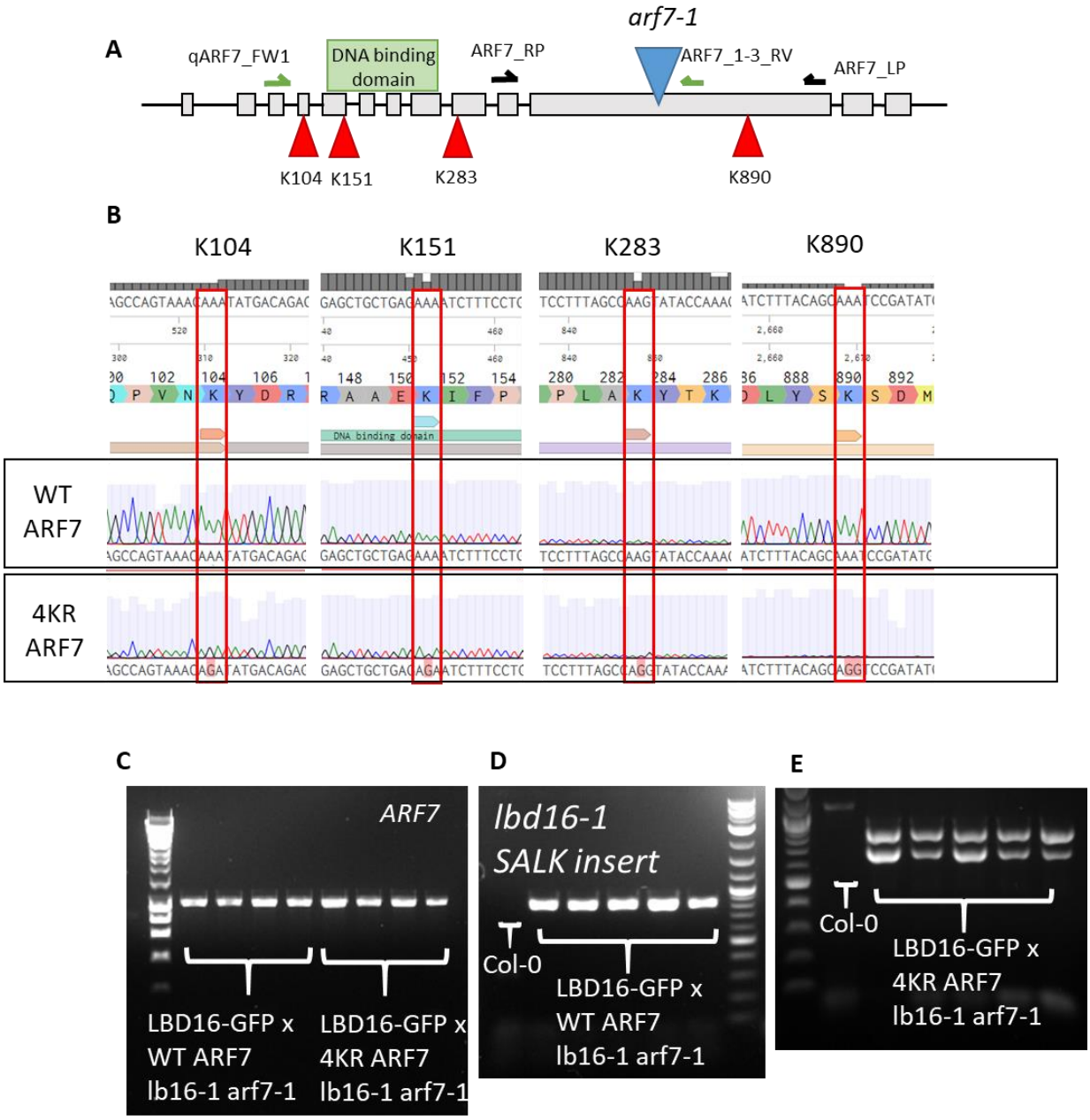

Figure 4.4 – Location and mutation of the four SUMO sites on ARF7. Bioinformatics work in Durham on the ARF7 gene resulted in the identification of four SUMO sites, named after the lysine and amino acid number they are on: K104, K151, K283 and K830 (A). The gene map also shows localisation of the arf7-1 SALK insertion and primer pairs used to sequence SUMO sites and identify the mutations in the ARF7 4KR line. LBD16-GFP *lbd16-1 arf7-1* crosses with WT ARF7 *arf7-1* and 4KR ARF7 *arf7-1* mutation sites were checked using the earlier mentioned primers (B). Genotype confirmation of ARF7 transgene using ARF7 LP and RP primer pair spanning the SALK insertion site to avoid amplifying genomic ARF7 (C). The homozygosity of the lbd16-1 SALK insert was also verified in WT ARF7 (D) and 4KR ARF7 (E). Note that in WT ARF7 a two primer approach is used to visualize the lbd16-1 SALK insert, whilst in 4KR genotyping this was a three primer approach.

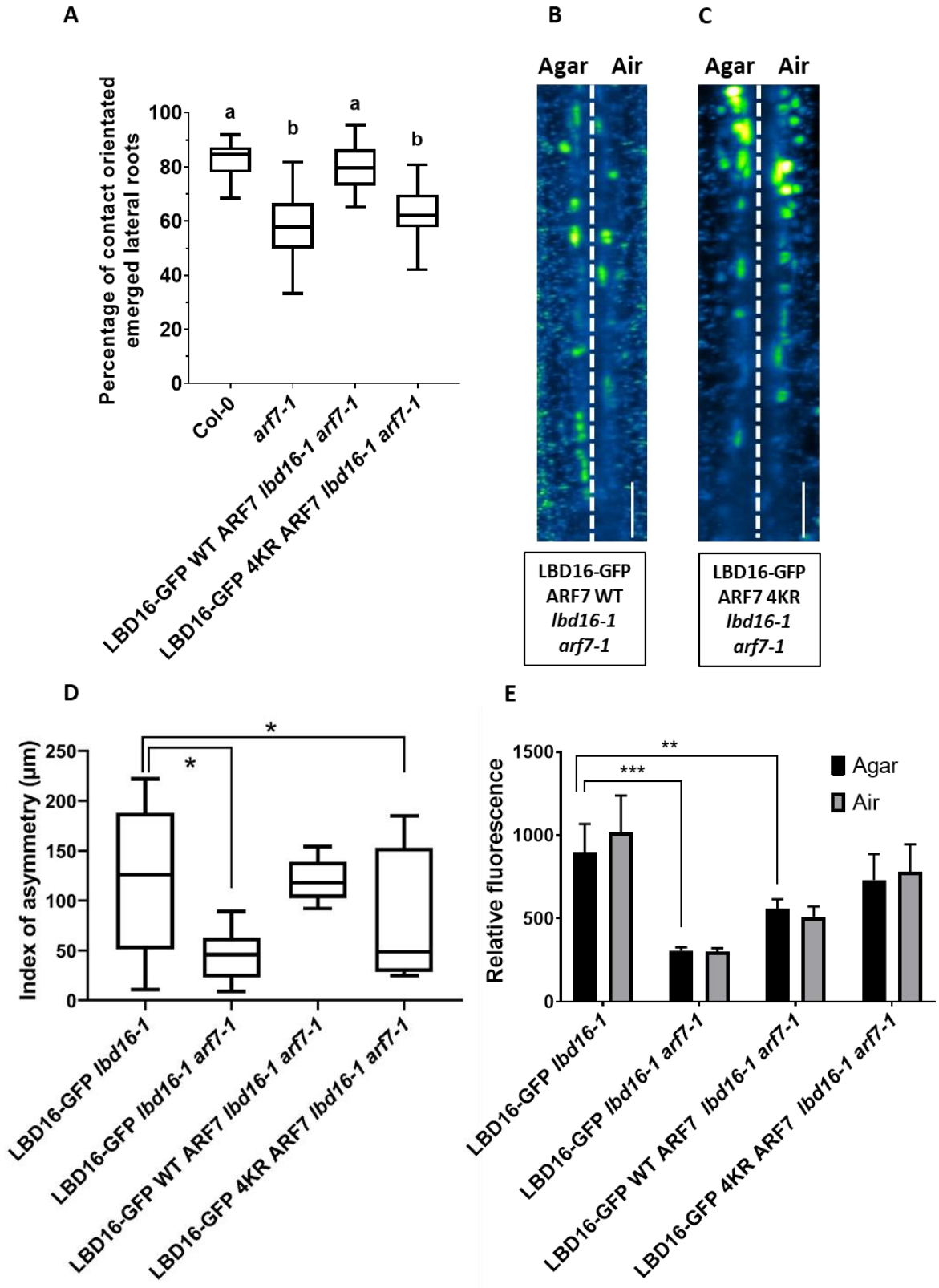

Figure 4.5 – LBD16 asymmetric localisation is dependent on ARF7 SUMOylation status. LBD16-GFP *arf7-1 lbd16-1* 4KR lines exhibit a defect LR hydropatterning response, while the WT ARF7 transgene can fully restore the hydropatterning response to Col-0 level (A). Restoring WT ARF7 gene in *arf7-1 lbd16-1* background can restore asymmetrical distribution of LBD16-GFP (B, D). Restoring ARF7 with

mutated SUMO sites, 4KR ARF7, cannot rescue Col-0 level of LBD16-GFP asymmetry (C-D). Nuclei relative fluorescence was measured in all these lines on agar and air side and compared. Asterisk indicates significant differences (p<0.05, 95% confidence interval) with LBD16-GFP *lbd16-1* measurements using one-way ANOVA (D) n=8. Scale bar represents 50 µm.

4.2.5 Early gLBD16-GFP signal in vascular procambium cells.

Previous research characterising gLBD16-GFP expression reported reporter localisation in the pericycle and LRP during lateral root development (Goh et al. 2012a). However, closer examination of early gLBD16-GFP expression using LSFM gave us a new insight into the radial localisation of LBD16. Analysing radial images of gLBD16-GFP in the root elongation zone revealed an earlier weak expression pattern. Propidium iodide was used to stain cell walls and gain a tissue specific localisation pattern of LBD16. Cross sections suggested that the earliest gLBD16-GFP fluorescent signal could be observed in cells underlying the xylem pole pericycle, termed xylem-procambium cells (Fig. 4.6A, B). Fluorescence could be detected in three or four xylem-procambium cells, but often not in the same 2D cross section, which is why a z-projection was made to visualize the expression pattern. The longitudinal difference in gLBD16-GFP localisation might reflect a difference in nuclear subcellular localisation or difference in cell elongation between these cells. This very early expression was significantly lower than the fluorescence in XPP cells and therefore might have been missed in earlier experiments (Fig. 4.7C). It is unknown if the gLBD16-GFP fluorescent signal, originating from these xylem-procambium cells, has a direct link to the expression seen in overlying XPP cells.

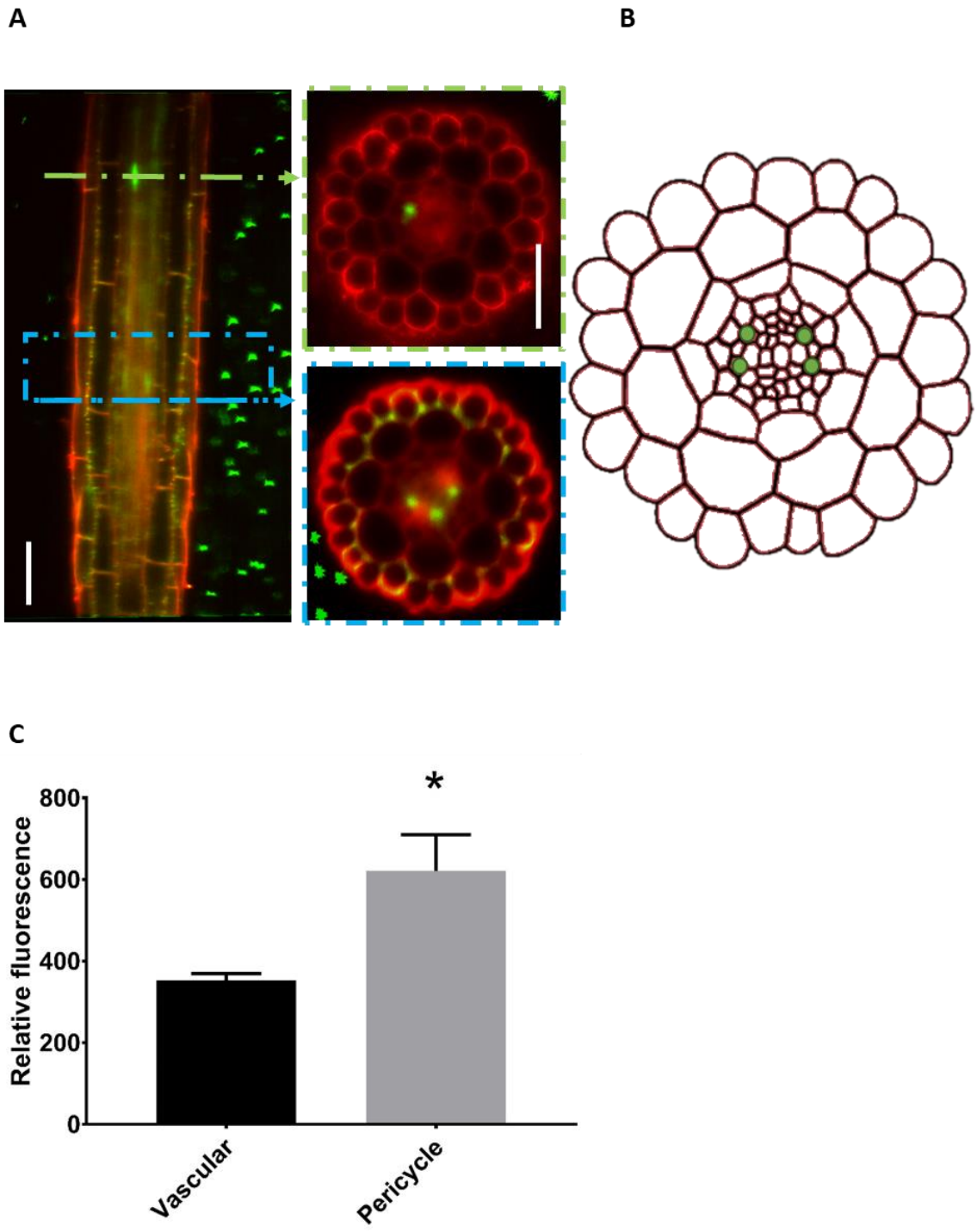

Figure 4.6 – *LBD16* is early expressed in the xylem-procambium cells. Longitudinal root section taken on the LSFM showed strong LBD16-GFP signal (green nuclei) located in pericycle cell of the elongation zone. Weak expression was visible earlier in the elongation zone in three xylem-procambium cells visible in this z-projection of a 100 radial sections (A). Propidium iodide (red) was used to stain cell walls. Schematic representation of a root cross section demonstrates the nuclear LBD16-GFP expression in xylem-procambium cells (green highlighted area). This early signal is significantly weaker

than previously observed signal in the pericycle (C). The asterisk demonstrates a significant difference between the intensity measurements tested using Student T-test ($p<0.05$). Scale bar represents 50 µm.

4.2.6 SUMO site K151 and K282 on ARF7 are evolutionary highly conserved

To identify which of the four SUMOylation sites performs a key function in auxin signalling, the evolutionary conservation of these four sites was studied. Firstly, the domain structure of ARF7 was identified, to visualize which domains are influenced by SUMOylation (Guilfoyle 2015; Fig. 4.6A). SUMO site, K104, sits on the flanking region of Dimerization domain 1 (DD1), important for hetero- and homodimerization with other ARFs. K151 sits on the B3 DNA-interaction Domain (B3 DBD) and K282 sits on the Ancillary Domain (AD), both are highly conserved domains across the ARF family members in *A. thaliana*. The last SUMO site, K890, sits on the 3' end of the middle region, near the PB1 domain. Secondly, we checked the alignment of ARF7 like proteins in multiple sequence alignments based on taxa from divergent plant lineages. A recent paper of Mutte et al, (2018) was used as the blueprint for the evolution of A-class ARFs, of which ARF7 is a member, as are ARF5, ARF6, ARF8 and ARF19 (Mutte et al. 2018). Focus lay on extracting Class A-ARF protein sequences from available proteomic data in several evolutionary clades. The ARF protein sequence in multiple evolutionary lineages were used in this alignment analysis. The following species were used in this sequence analysis: *Arabidopsis thaliana* (to represent angiosperms), *Picea abies* (to represent gymnosperms), *Selaginella moellendorffii* (to represent Lycophytes), *Physcomitrella patens* (to represent Mosses), *Marchantia polymorpha* (to represent Liverworts) and *Mesotaenium caldariorum* (to represent Charophytes). Protein sequences of ARFs were obtained from Phytozome (Goodstein et al. 2012), PLAZA (Van Bel et al. 2018) and *M. caldariorum* from 1000 plants (1KP) project (Matasci et al. 2014). Proteins were chosen for further alignment on the basis of blast score and Expectation value (E value) relative to the *A. thaliana* ARF7 protein sequence. The blast score relates to the highest alignment without gaps that is possible between input sequence and query, where higher scores indicates better alignments. The E-value relates to the chance of getting an alignment with the same or a better alignment score than the query, the lower the E-value, the higher the significance. The subset of chosen proteins of each lineage with the highest scores (up to three proteins with the exception of *A. thaliana*) were then aligned using MUSCLE alignment (Edgar 2004) and results displayed using MView

(Brown et al. 1998). ARF proteins of *S. moellendorffii* and *M. polymorpha* were named as in Lavy et al. (2016). The focus of this alignment was on the conservation of the lysine as the core residue in a SUMO site. Alignment results showed highest conservation of K151 and K282 (Fig. 4.6B, C). These two lysine residues are present up till the Marchantia polymorpha (liverworts), indicating a possible functional importance of the SUMOylation of these lysine residues through land plant evolution. The lysine K282 was also conserved in the proto-ARF of *M. caldariorum*. However, the flanking residues are completely different, which indicates that this would likely not function as a SUMO site. K890 showed a similar degree of lysine conservation but more variability of residues in the flanking sites, which will likely impact SUMOylation of this site (Fig. 4.6D). In contrast, SUMO sites K104 showed no conservation of the lysine residue within the different evolutionary clades (Fig. 4.6B).

In contrast to *A. thaliana*, *M. polymorpha* genome contains only three ARFs, one class A, one class B and a class C. Our earlier results showed that the class A ARF in *M. polymorpha* contained a high degree of conservation of SUMO sites K151 and K282 and some conservation of K890 when aligned with *A. thaliana* ARF7. We further studied if this conservation was present when aligning all three classes of ARFs from *M. polymorpha* (Fig. 4.6E, F). Class B contained the lysine core residue important for SUMO binding at site K282 and K890. However, the flanking amino acids in both these cases were distinct from the class A-ARF, suggesting low likelihood of a conserved SUMO motif. The class-C ARF in *M. polymorpha* showed low conservation at the SUMO site. These results reveal that the SUMO sites of only class A-ARF in *M. polymorpha* is conserved.

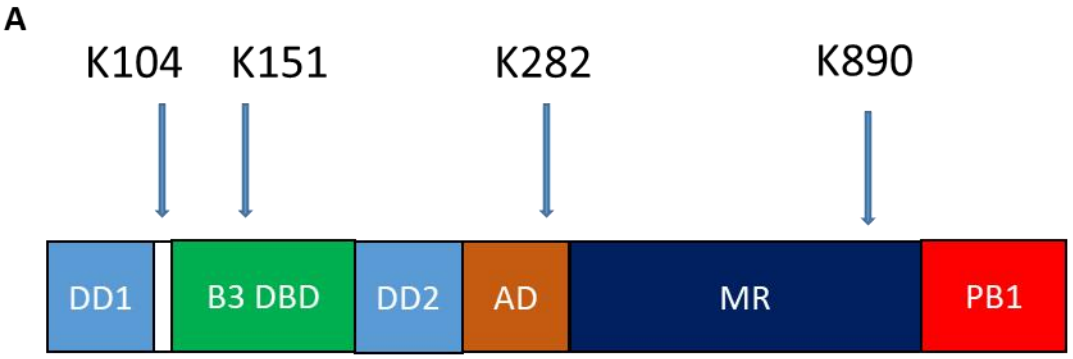
A
K104
K151
K282
K890
DD1
B3 DBD
DD2
AD
MR
PB1

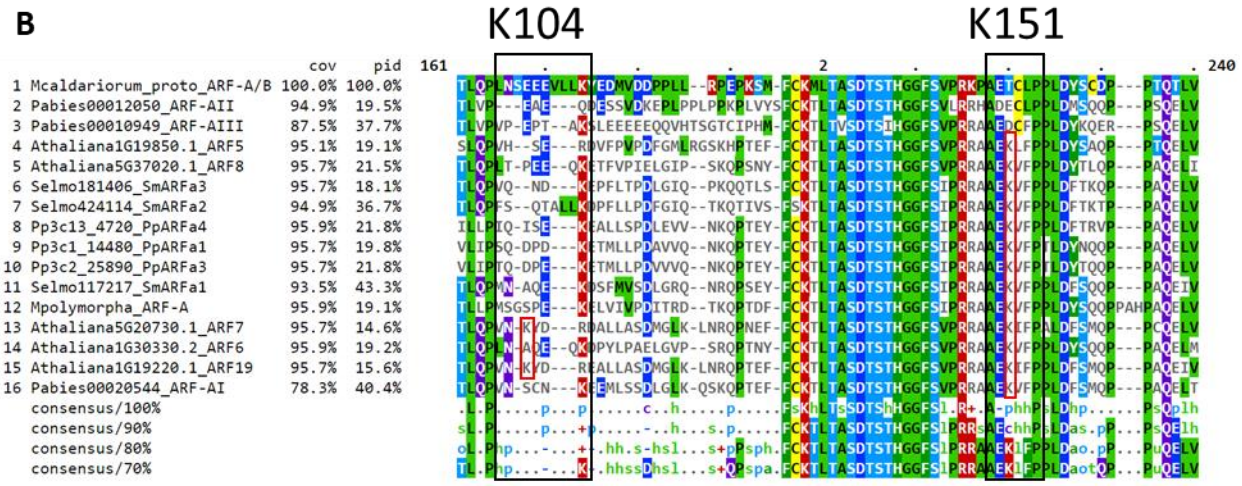
B
K104
K151
cov pid
1 Mcaldariorum_proto_ARF-A/B 100.0% 100.0%
2 Pabies00012050_ARF-AII 94.9% 19.5%
3 Pabies00010949_ARF-AIII 87.5% 37.7%
4 Athaliana1G19850.1_ARF5 95.1% 19.1%
5 Athaliana5G37020.1_ARF8 95.7% 21.5%
6 Selmo181406_SmARFa3 95.7% 18.1%
7 Selmo424114_SmARFa2 94.9% 36.7%
8 Pp3c13_4720_PpARFa4 95.9% 21.8%
9 Pp3c1_14480_PpARFa1 95.7% 19.8%
10 Pp3c2_25890_PpARFa3 95.7% 21.8%
11 Selmo117217_SmARFa1 93.5% 43.3%
12 Mpolymorpha_ARF-A 95.9% 19.1%
13 Athaliana5G20730.1_ARF7 95.7% 14.6%
14 Athaliana1G30330.2_ARF6 95.9% 19.2%
15 Athaliana1G19220.1_ARF19 95.7% 15.6%
16 Pabies00020544_ARF-AI 78.3% 40.4%
consensus/100%
consensus/90%
consensus/80%
consensus/70%
161
240

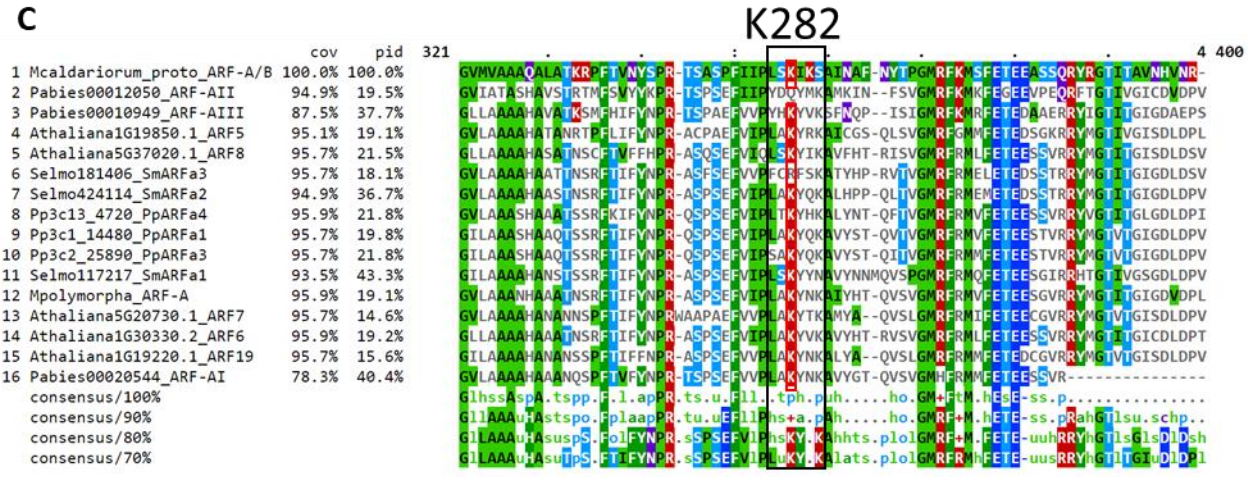
C
K282
cov pid
1 Mcaldariorum_proto_ARF-A/B 100.0% 100.0%
2 Pabies00012050_ARF-AII 94.9% 19.5%
3 Pabies00010949_ARF-AIII 87.5% 37.7%
4 Athaliana1G19850.1_ARF5 95.1% 19.1%
5 Athaliana5G37020.1_ARF8 95.7% 21.5%
6 Selmo181406_SmARFa3 95.7% 18.1%
7 Selmo424114_SmARFa2 94.9% 36.7%
8 Pp3c13_4720_PpARFa4 95.9% 21.8%
9 Pp3c1_14480_PpARFa1 95.7% 19.8%
10 Pp3c2_25890_PpARFa3 95.7% 21.8%
11 Selmo117217_SmARFa1 93.5% 43.3%
12 Mpolymorpha_ARF-A 95.9% 19.1%
13 Athaliana5G20730.1_ARF7 95.7% 14.6%
14 Athaliana1G30330.2_ARF6 95.9% 19.2%
15 Athaliana1G19220.1_ARF19 95.7% 15.6%
16 Pabies00020544_ARF-AI 78.3% 40.4%
consensus/100%
consensus/90%
consensus/80%
consensus/70%
321
400

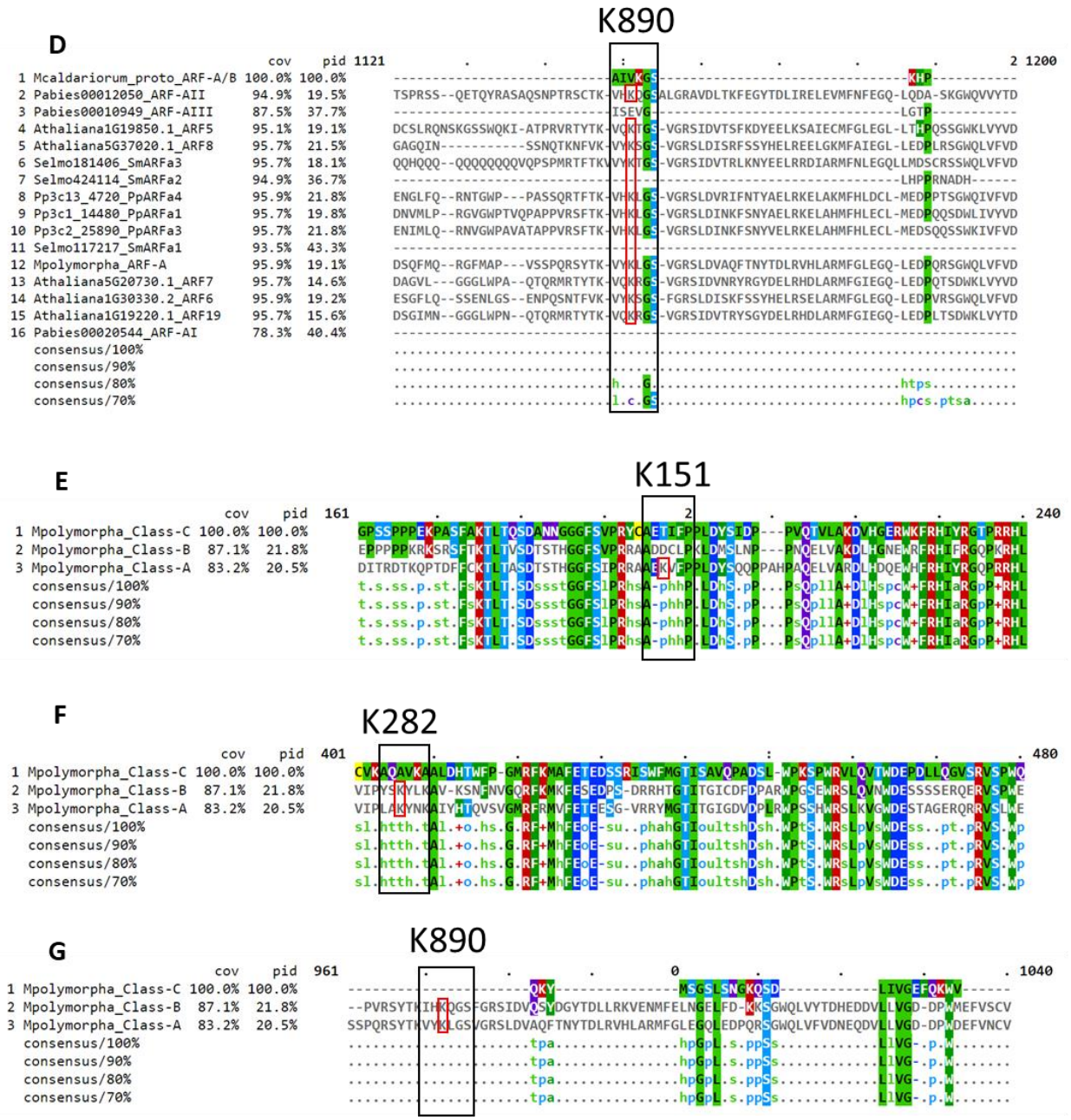

Figure 4.7 – SUMO sites K151 and K282 are highly conserved in multiple evolutionary lineages. Domain structure of the ARF7 protein indicates the localisation of four SUMO sites (A). Protein alignment of ARFs in *Arabidopsis thaliana* (angionsperms), *Picea abies* (Gymnosperms), *Selaginella moellendorffii* (Lycophytes), *Physcomitrella patens* (Mosses), *Marcantia polymorpha* (Liverworts) and *Mesotaenium caldariorum* (Charophytes) visualized the evolutionary conservation of the four SUMO sites on K104 (B), K151 (B), K282 (C) and K890 (D). Black boxes indicate SUMO sites and red boxes indicate conservation of the crucial lysine necessary for SUMO binding. Furthermore, the crucial lysine residue and flanking sites of SUMO site K151, K282 and K809 where not conserved in class B and class C-ARF's in *M. polymorpha* and only present in the class A-ARF (E, F, G). The 'cov' percentage applies to full alignment coverage between target alignment and *M. caldariorum* ARF protein sequence, whilst 'pid'

percentage indicates the identical residues in the covered alignment between *M. caldariorum* ARF and target alignment. Abbreviations: DD1&2: Dimerization domains 1 and 2. B3 DBD: B3 DNA-interaction Domain. AD: Ancillary Domain. MR: Middle Region. PB1: Phox and Bem 1.

4.3 Discussion

4.3.1 Lateral root hydropatterning is regulated by an ARF7-LBD16 dependent pathway

Lateral roots are crucial for the exploration of soil for water and nutrients (Morris et al. 2017). LRs preferentially emerge towards water employing an adaptive response termed LR hydropatterning (Bao et al. 2014; Orosa-Puente et al. 2018). In this chapter, the importance of ARF7 SUMOylation on asymmetric expression of its target, the transcription factor *LBD16,* in the root elongation zone during LR hydropatterning is shown.

The *lbd16-1 loss-of-function* mutant exhibits a clear LR hydropatterning defect similar to *arf7*-1 mutants. However, mutants in other LBD family members involved in lateral root formation with confirmed knock-out alleles, such as *lbd18-1* and *lbd29-1,* did not show a hydropatterning defect (Supp. Fig. S4.1A, B). Future studies should assess LR hydropatterning in higher order LBD mutants to evaluate the role gene redundancy might play in this family of transcription factors. Of the LR expressed LBD genes, only *LBD16, LBD18* and *LBD29* have been confirmed as direct targets of ARF7, whilst other family members such as *LBD17*, and *LBD33* are likely indirect targets (Lavenus et al. 2015; Pandey et al. 2018). If these five LBD's are regulated directly or indirectly by ARF7 then why is LR hydropatterning only dependent on *LBD16*?

One possibility that could explain why *LBD16* is so important during LR hydropatterning is its expression pattern. GUS expression analysis of the five LBD genes involved in LR formation, *LBD16, LBD17, LBD18, LBD29* and *LBD33*, revealed varying levels of expression in LRP. *LBD33* is the outlier in this list of LBD genes as it exhibits a strongly reduced expression and is not found in the adjacent vasculature (Lee et al. 2009; Goh et al. 2012a). Furthermore, *LBD16* GUS reporter intensity is stronger compared to other LBD genes, suggesting there is a difference in promoter activity, rather than spatial expression pattern. Together this expression data suggests limited difference in

expression pattern between the five LBDs. Thus, the expression of these genes does not explain the importance of *LBD16* in LR hydropatterning.

Another possibility is a difference in protein stability or activity due to a difference in protein sequence between the four LR expressed LBDs. Interestingly, all five previously mentioned LBD members can be classified in the same class (IA) and same subtype (C), indicating a high degree of sequence similarity between lateral root developmental LBD genes (Iwakawa et al. 2002). Interestingly, *LBD16* and *LBD29* are a result of a gene duplication event 24-40 million years ago and thus contain a very similar LOB domains (Blanc et al. 2003; Matsumura et al. 2009). Similarly, *LBD17* showed the greatest sequence similarity with *LBD29*. Additionally, *LBD17* is located next to *LBD16* on the genome and thus *LBD29* and *LBD17* are likely to be the result of a more recent gene duplication event. The N-terminal LOB domain of these three genes are quite similar, however the C-terminal domains are very different shown by the difference in tree scale comparing the LOB domain and the C-terminal phylogenetic tree (Fig 4.8A-C) (Matsumura et al. 2009). The variable C-terminal could explain the difference seen in transcriptional control of downstream genes. Research on multiple orthologs of the LBD family suggested possible transcriptional activation domains on the C-terminal as well as a possible role in inhibition of LOB dependent homodimerization (Liu et al. 2005; Majer et al. 2012). Further analysis of the C-terminal sequence similarity showed highest similarity between *LBD17* and *LBD29* of 38%, whilst between *LBD16* and *LBD29* this is only 23% (Matsumura et al. 2009). The C-terminal of *LBD16* is thus very different from most other LBD gene duplicates and, according to MUSCLE alignment, most closely related to *LBD18* (Fig 4.8C). Additionally, LBD16 targets have potential binding sites for both LBD16 or LBD18, indicating similar DNA binding sites (O'Malley et al. 2016; Goh et al. 2019). Yet not all transcriptional targets of LBD18 are also regulated by LBD16, suggesting some level of distinction in DNA binding motif (Lee et al. 2013a). Research related to LBD18's C-terminal domain showed its importance in binding to the PB1 domain on ARF7 and ARF19 to enhance transcriptional activity (Lee et al. 2017; Pandey et al. 2018). This binding was also shown to compete with the binding of IAA repressor protein on ARF (Pandey et al. 2018), revealing a possible positive feedback loop to construct a robust feedback mechanism during lateral root development. Future

research will have to reveal if the C-terminal domain of LBD16 contributes in a similar way as LBD18's to stabilize ARF7 and if this provides a positive feedback loop during LR hydropatterning. LBD16 and LBD18 might bind similar DNA motifs, their C-terminal domain varies greatly which might explain differences in gene targets and clarify why LBD16 is key during LR hydropatterning.

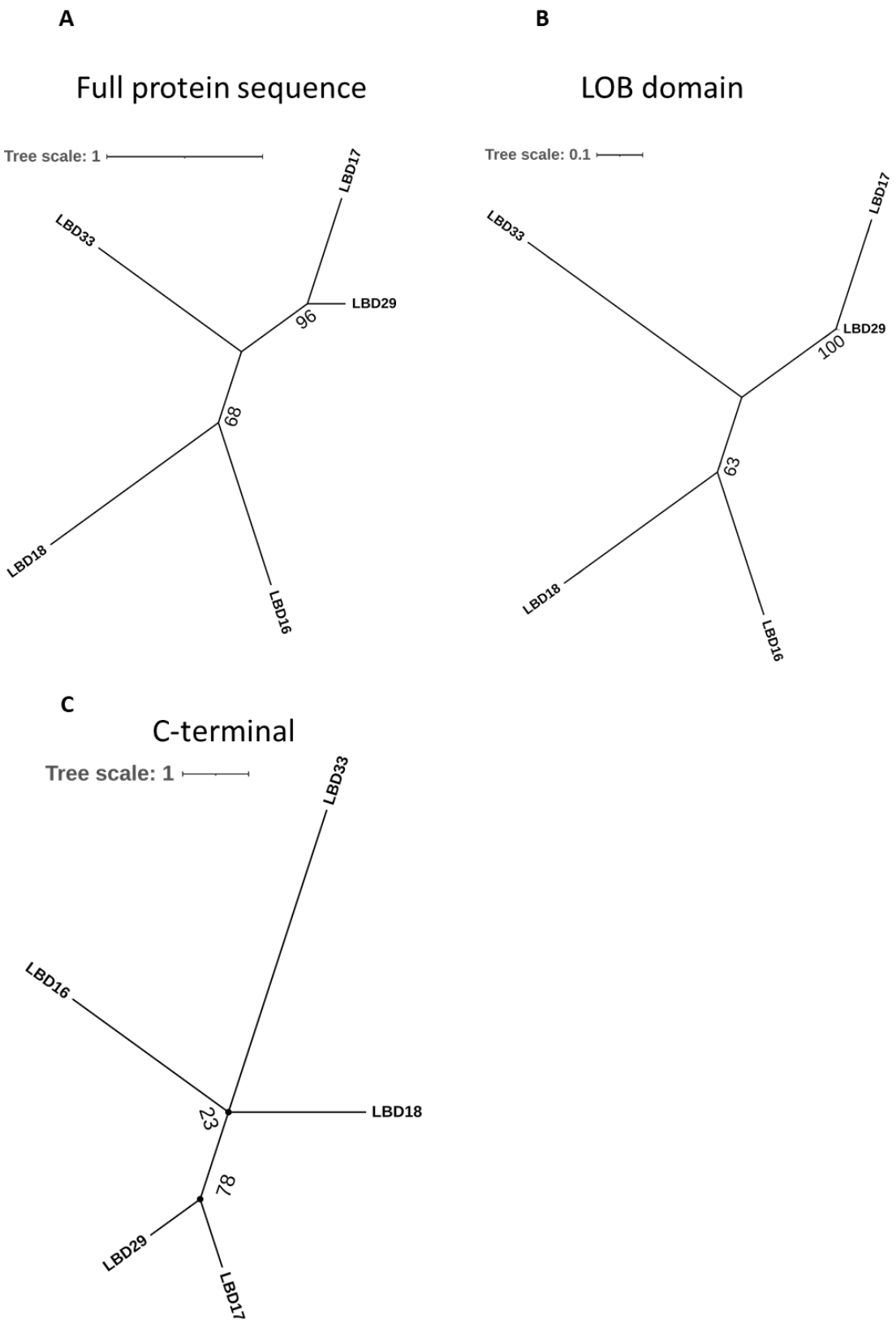

Figure 4.8 – Protein sequence alignment of LBD family members involved in lateral root primordia initiation and development. Comparison of LBD16, LBD17, LBD18, LBD29 and LBD33 full protein sequence (A), LOB domain sequence (B) and C-terminal sequence (C) alignment using MUSCLE alignment. Phylogenetic trees were made using iTol software (Letunic and Bork 2019). Tree scale

indicates the branch length, representing the evolutionary time between two nodes. Numbers near nodes indicate bootstrap value, the times out of a 100 tests the same tree was constructed.

4.3.2 SUMOylation regulates ARF7 activity during lateral root hydropatterning

The transcription factor ARF7 directly binds to the promoter of *LBD16,* thereby regulating its auxin inducible asymmetric gene expression pattern during LR hydropatterning. Both ARF7-Venus and gLBD16-GFP translational reporters were used to study if localisation differs between the agar and the air side of the root during a hydropatterning stimuli. A new Light Sheet Fluorescent Microscopy (LSFM) protocol was employed to distinguish the agar and air sides of roots grown on agar. Use of these tools demonstrated that all root cells expressed *ARF7-Venus* and no difference in relative fluorescence between agar and air side was apparent (Orosa-Puente et al. 2018). However, gLBD16-GFP displayed a strong asymmetrical expression in root elongation zone pericycle cells, indicating an early preference for one xylem pole that promotes LR initiation.

To assess the role of ARF7 on gLBD16-GFP asymmetrical expression, a cross was made between *arf7-1* and gLBD16-GFP. This line showed a strong reduction in asymmetry of the GFP signal. This result revealed two key points. Firstly, hydropatterning is dependent on a functional ARF7-LBD16 pathway to create an asymmetrical localisation of LBD16. This data is supported by earlier research showing a loss of oscillation of DR5 expression in *arf7-1* mutants, which resulted in irregular locations of pre branch sites (Moreno-Risueno et al. 2010). Demonstrating the importance of ARF7 in regulation of periodic oscillations in order to space out LRP initiation sites, possibly doing so by asymmetrical expression of downstream targets. Secondly, all root cells contain stabilized ARF7, as demonstrated with the ARF7-Venus line, but not all root cells actively transcribe *LBD16*. Additionally, the hydropatterning response could be restored by over expressing *ARF7*, indicating that neither the level nor expression pattern is crucial for hydropatterning (Orosa-Puente et al. 2018). Instead, it suggests that ARF7 activity is regulated during LR hydropatterning.

The previous results led to research on possible post-translational modification of ARF7 (Orosa-Puente et al. 2018). Post-translational modification (PTM) of proteins represents a major field of study, with >100 types being described to date (Barber and Rinehart

2018). One of these classes of PTM, SUMOylation, was shown to be critical for controlling ARF7 during hydropatterning. Sequence analysis of ARF7 identified four lysines that can bind SUMO, so called SUMO sites (Orosa-Puente et al. 2018). Mutating all of these SUMO sites resulted in the creation of a non-SUMOylatable ARF7^{4KR} protein (Orosa-Puente et al. 2018). Additionally, when both *ARF7^{WT}* (containing the Col-0 ARF7 coding sequence) and *ARF7^{4KR}* were transformed into *arf7-1* mutants, the hydropatterning response could only be restored with the *ARF7^{WT}* transgene (Orosa-Puente et al. 2018), thereby demonstrating the necessity of SUMOylation of ARF7 during LR hydropatterning.

To further analyse how SUMOylation affects ARF7 function, we analysed in which domains these sites were located. The first SUMO site on the ARF7 protein sequence, K104, is located in the flanking region of the dimerization domain 1 (DD1). This domain together with DD2 regulates ARF dimerization which might be critical for biological function (Boer et al. 2014). SUMOylation of this residue might affect the dimerization ability of ARFs thereby potentially preventing regulation of transcription by ARF dimers. The next SUMO site, K151, is sited in the B3 DNA-interaction domain (B3 DBD), which is critical for interaction with AuxRE motifs (Boer et al. 2014). Hypothetically SUMOylation of this site might distort DNA binding ability of ARF7 and therefore reduce transcriptional output. The ARF7^{4KR} showed increased AuxRE binding on *LBD29* and *LBD16* promoter compared to ARF7^{WT}, suggesting that the unSUMOylatable version of ARF7 has a higher DNA binding affinity (Orosa-Puente et al. 2018). However, this result does not distinguish between the role of the multiple SUMO sites on ARF7. Further work on combinations of 1K/R and 3K/R ARF7 lines will reveal the importance of each SUMO site on ARF7 transcriptional activity. The SUMO site K282 is positioned on the Ancillary Domain (AD) of ARF7. The function of this domain is still unknown, although it is thought to tightly interact with the DD1 and 2 domains. SUMOylation of K282 might therefor also affect homo and hetero-dimerization of ARFs to control transcriptional activity. The last SUMO site, K890, sits in the 3' end of the middle region, near the PB1 domain. The middle region is important for the transcriptional activity of A class ARFs and is highly distinct from Class B and C ARFs (Ulmasov et al. 1999). SUMOylation of K890 might affect binding of SWI/SNF chromatin remodellers, which binds on the middle region in

ARF5 (Wu et al. 2015). The SWI/SNF complex is important for opening up the chromatin around the DNA binding site to allow transcription. Without binding of these important complexes ARF transcription activity will be diminished. The SUMOylation of ARF on these four SUMO sites might be a way of rapidly controlling auxin response levels. SUMOylation could also serve as an extra checkpoint in which an auxin response can only occur when auxin is available and ARFs are deSUMOylated.

To further study the effect of SUMOylation on downstream targets of ARF7, the *ARF7^{WT}* and *ARF7^{4KR}* transgenics were crossed with gLBD16-GFP. The asymmetrical localisation of LBD16 could be restored by complementing with the *ARF7 ^{WT}* transgene, yet not by complementing with the *ARF7^{4KR}*. Additional ChIP and expression data revealed a stronger binding and induction of *ARF7* direct targets, such as *LBD16, LBD29 and IAA19,* in the *ARF7^{4KR} line* compared to the *ARF7^{WT}.* This fits with fluorescence data shown here (Fig. 4.5E) that demonstrate a higher level of relative fluorescence in gLBD16-GFP *ARF7 ^{4KR}* compared to *ARF7 ^{WT}*. Thus, we hypothesize that SUMOylation of ARF7 causes a reduction in transcriptional activity.

How is the SUMO status of ARF7 controlled and how does this affect the activity of the protein? ARF7 is rapidly SUMOylated when roots are removed from agar plates and placed on paper (Orosa-Puente et al. 2018). Hence, ARF7 SUMOylation status is responsive to local moisture levels. Mathematical modelling predicts that growth sustained by uptake and elongation of cells in the elongation zone serves as a biophysical cue to determine where to pattern the roots (Robbins and Dinneny 2018). This theory was verified by treating maize roots with growth inhibitors and observing a direct negative correlation between root growth and LR hydropatterning. Differences in water potential between air and agar exposed side was especially severe near the, as the authors termed, competent zone of maize roots, what equates to the elongation zone in *A. thaliana* roots. In the elongation zone water uptake directly affects cell elongation, making this an excellent zone for integration of water availability cues. The radial difference in water potential in this zone could be the driving force behind the formation of a gradient of SUMOylated ARF7 across the root radial axis, with high SUMOylated ARF7 on the air side and free active ARF7 on the agar side.

The activity of ARF7 is dependent on binding to AUX/IAA repressor proteins, which prevents activation of auxin induced genes when auxin levels are low (Goh et al. 2012b). Binding of ARF7 and IAA3 was shown to be dependent on SUMOylation of ARF7 as the 4KR non-SUMOylatable version of ARF7 showed decreased interaction with IAA3, whilst still being able to bind IAA14 (Orosa-Puente et al. 2018). Analysis of IAA3 and IAA14 protein sequences revealed a SIM site in the former, but not latter. This could promote interaction between SUMOylated ARF7 and SIM containing IAA3 proteins. Mutating the SIM site in IAA3 completely abolished IAA3 and ARF7 interaction. Further analysis uncovered that the SIM site was localized in the PB1 domain. This domain shares high homology with the PB1 domain of ARF7 and regulates the interaction between Aux/IAA and ARF (Chapman and Estelle 2009). Mutating the SUMO sites on ARF7 can abolish SUMO and SIM binding. However, binding between the two PB1 domains is still possible. However, mutating the IAA3 SIM site completely blocked ARF7 binding and IAA3 interaction, indicating a more profound effect of SIM mutation on this interaction. This mutation might block SUMO-SIM interaction as well as prevent PB1 binding, preventing all ARF7 and IAA3 interactions. SUMOylation thus inhibits ARF7 activity by binding to IAA3 repressor proteins through SIM, causing it to become inactive.

Interestingly, in the case of ARF7^{4KR}-GFP, auxin (NAA) treatment could still strongly increase promoter binding to *LBD16* and *LBD29* than without NAA (Orosa-Puente et al. 2018). This suggests that the combination of deSUMOylated ARF7 and auxin treatment have an additive effect on the expression of downstream targets. Thus, ARF7 SUMOylation provides the plant with a wider range of regulatory options to control auxin response output.

This leads to the following model in which SUMOylated ARF7 on the air side of the primary root will recruit IAA3 and repress expression of auxin responsive genes like *LBD16* associated with LR initiation. On the agar side ARF7 is free from SUMO and activates *LBD16* as seen in this chapter.

4.3.3 Asymmetric LBD16 expression is key to lateral root hydropatterning

The asymmetric expression of *LBD16* by ARF7 appears to be critical during a LR hydropatterning response. Significantly, lines over-expressing *LBD16* (LBD16 OE)

showed the strongest hydropatterning defect seen in published and unpublished work. Indeed, LBD16 OE lines shared a lot of similarities with *ARF7* ^{4KR}. This prompted studying the radial expression of *LBD16* in more detail. Both lines showed an increased *LBD16* expression and hydropatterning defect. This could be caused by an inability to create an asymmetric gLBD16-GFP expression pattern, causing an unbiased initiation of LRs. In this case the hyperactive *ARF7*^{4KR} works in a similar fashion as over-expressing *LBD16*, but on a smaller scale as ARF7 activity is controlled by more than SUMO alone. Likely the longitudinal and radial specific expression of *LBD16* is key to re-programme specific XPP cells to differentiate and form LR Founder cells (LRFCs). Without proper cell specific induction of LBD16 expression, environmental cues cannot be translated into developmental outputs. Non-specific selection of LRFCs through over-expressing *LBD16* thus leads to a uniform distribution of LRs and a strong defect in hydropatterning.

Alternatively, the strong defect in *LBD16* OE could be caused by impaired root and shoot growth. Robbins and Dinneny established that when root growth is severely impaired, this in turn impairs the LR hydropatterning response (Robbins and Dinneny 2018). Potentially this is caused by the loss of water uptake at the root elongation zone, which is thought to be the region where water cues are detected. Without the proper inflow of water, that drives cell elongation in this zone, the root cannot establish where the water is available and would thus demonstrate a defect in its LR hydropatterning response.

Detailed analysis of the gLBD16-GFP LSFM datasets revealed another novel observation. Re-analysing the spatial localisation of gLBD16-GFP, we found a weak nuclear signal in vascular procambium cells next to the pericycle. These cells have recently been renamed as xylem-procambium cells (Smetana et al. 2019). Xylem-procambium cells, together with XPP cells, act as stem cells during vascular cambium formation. Interestingly, ARF genes, such as ARF7, promote the formation of these stem cells and likely induce LBD16 expression in a similar pattern to lateral root primordia formation. However, the formation of cambium is initiated at a later root developmental stage than the initiation of LRFCs (Smetana et al. 2019). It is likely that these two developmental processes, cambium formation and LRFC initiation, deploy a similar genetic pathway for cell division and differentiation.

The remaining question is if and how the localisation of LBD16 in these cells contribute to the selection of LRFC? Is the expression of the *LBD16* in both neighbouring cells independent of each other or is there some movement of this protein between xylem-procambium and pericycle cells that orchestrates the positioning of LRFC's according to the availability of water in the surroundings. Another possibility is that LBD16 drives expression of target genes, which then move to neighbouring cells. To test the first hypothesis, we are collaborating with Joop Vermeer (Université de Neuchâtel, previously University of Zurich) to construct a 3xmCherry tagged LBD16 construct to block plasmodesmatal transport of this protein. The transcription factor LBD16 is a relatively small protein with 245 amino acids and protein size of approximately 27 kDa. According to studies on plasmodesmatal transport in the root tip, the size exclusion limit of proteins moving freely is ~16 kDa, but movement from the endodermis to pericycle and vasculature is limited to proteins which are ~60 kDa (Rim et al. 2011). This research classifies LBD16 as a protein with limited movement. Fusing LBD16 coding sequence with GFP increases its size to 54 kDa, which should theoretically still be able to move through the plasmodesmata and fit the same size exclusion limit classification. However, when LBD16 is tagged with 3xmCherry the resulting protein size becomes 108 kDa. At this size plasmodesmatal transport of LBD16-3xmCherry would be blocked, allowing us to distinguish between transport of LBD16 protein and the site of *LBD16* expression. Transforming LBD16-3xmCherry into *ldb16-1* background will allow us to assess if the immobile form of LBD16 can restore the LR number to Col-0 levels similar to LBD16-GFP. If LR number is not restored in LBD16-3xmCherry lines than the mobility of this protein is crucial for LR formation. Furthermore, dipping LBD16-3xmCherry in LBD16-GFP reporter lines will aid in understanding in which cell types LBD16 is expressed (where mCherry is present) and where it moves to (where the GFP is present). This experiment will inform us in which stage of LRP development the mobility of LBD16 is important. These future experiments will aid our understanding of the role of mobile transcription factors in LR formation.

4.3.4 Evolutionary conservation of ARF SUMOylation

To assess if SUMOylation of ARFs is a more recent modification or if this is conserved across different plant lineages, A-class ARFs of multiple evolutionary lineages were aligned. Thereafter, the conservation of the *A. thaliana* SUMO sites was assessed. This analysis revealed strong conservation of two SUMO sites, K151 and K282, which were conserved in a variety of evolutionary lineages from the Liverworts onwards. K151 sits in the B3 DNA-binding domain, whilst K282 is located in the ancillary domain. Likely the K151 SUMO site affects DNA binding ability of ARF7. This could explain the increased binding of ARF7 ^{4KR} to the promoters of *LBD16* and *LBD29* and the increased level of fluorescence in *gLBD16-GFP* ARF7 ^{4KR}. In this model, SUMOylation of K151 results in decreased binding efficiency to AuxRE. K282 is located in the ancillary domain of unknown function, which might be involved in interaction with the dimerization domain (Roosjen et al., 2018). Likely dimerization is important for ARF activity, as the mutation of the dimerization domain in ARF5 could not restore the phenotype of *loss-of-function* mutants (Boer et al., 2014). K890 showed high conservation of the lysine residue, but high variability in the two flanking residues, which could affect SUMOylation of this site. K890 is located on the middle region near the PB1 domain. Potentially K890 could affect binding with the SIM on the PB1 domain of IAA3/SHY2. This SUMO-SIM interaction might strengthen the binding affinity between these two proteins. Another possibility is that SUMOylation of K890 affects binding of chromatin regulatory proteins such as SWI/SNF chromatin remodelling ATPases that were shown to bind to the middle region of ARF5. Blocking the binding of SWI/SNF complex will affect the open chromatin state and reduce transcriptional activity. In contrast, K104 exhibits low conservation. This site is located between DD1 and B3 DBD and as a result might impact ARF hetero- and homodimerization in a similar manner as previously described for K282. As this site is only conserved in ARF7 and ARF19 it likely evolved most recent. Potentially SUMOylation of K104 acts to strengthen the regulation of ARF7 and ARF19 dimerization during abiotic stress. Future work with point mutations in each of these SUMO sites will have to decipher the precise contribution each site plays in regulating ARF7 activity.

Only the charophycean algae *Mesotaenium caldariorum* showed no conservation of the lysine residue at K151 and K282. Possibly the proto-ARF in this species does not function

as an ARF. Charophytes, *Klebsormidium nitens* and *Spirogyra pratensis* showed a strong transcriptional responses to auxin treatment, even though some charophytes in this study contained no auxin signalling pathway components (i.e. *TIR1/AFB*, *Aux/IAA* and *ARF*) (Mutte et al. 2018). It is likely this response is not specific to auxin treatment but due to the similarity of auxin to indole and tryptophan, which instead could lead to a metabolic response towards nutrient acquisition (Mutte et al. 2018). Future studies should increase the number of protein sequence databases used, to confirm if these residues are conserved in other species within the lineages.

In the liverwort *M. polymorpha*, the genome contains all three auxin signalling components; one TIR1, one Aux/IAA and four ARFs (one from each class and a non-coding ARF that does not contain the B3 DBD domain). The limited number of auxin signalling genes makes this an ideal model species to investigate the distinct biological functions of the ARF classes. The *M. polymorpha* class A-ARF, *MpARF1*, was confirmed as a transcriptional activator (Kato et al. 2015) and mutations in *MpARF1* led to a reduced auxin sensitivity and developmental defects (Kato et al. 2017). In contrast, *MpARF2* classified as a transcriptional repressor (Kato et al. 2017) and potentially functions by competing for the same DNA binding sites as MpARF1 and repressing transcription by binding TPL co-repressors (Kato et al. 2020). *MpARF3* mutants exhibit developmental defects, this mutation has no effect on the auxin response (Kato et al. 2020). Likely C-class ARFs have an auxin independent function in plants as in *A. thaliana* this class has a weak affinity for Aux/IAAs (Piya et al. 2014). Intriguingly, only MpARF1 contained a conserved lysine on K151, K282 and K890 when aligned with *A. thaliana* ARF7, whilst MpARF2 and MpARF3 had low conservation at these sites. Could deSUMOylation of activating ARFs have evolved as a rapid on/ off switch for the auxin response. ARF7 ^{4KR} is more transcriptionally active than ARF ^{WT}, but these experiments did not reveal which sites of ARF7 are SUMOylated *in planta* in a given cell or tissue at a given time. This problem would be solved by making a constitutively SUMOylated ARF7, but this is, at this time, impossible. More likely SUMOylation is a tool to fine-tune the auxin response. Likely ARF7 is mostly SUMOylated in cells as pools of free SUMO are low (Johnson 2004), allowing a diminished auxin response. When an increased auxin response is necessary, ARF7 can rapidly be deSUMOylated, thereby activating an

increased auxin response. Hence, deSUMOylation might be important in managing the amplitude of the auxin response. It could also be used to quickly shut down the auxin response through SUMOylation of key domains when the plant perceives stress (Kurepa et al. 2003). SUMOylation of ARFs might have enabled plants to rapidly regulate the level of auxin response, which is a critical for controlling transcriptional activators.

Supplemental figure

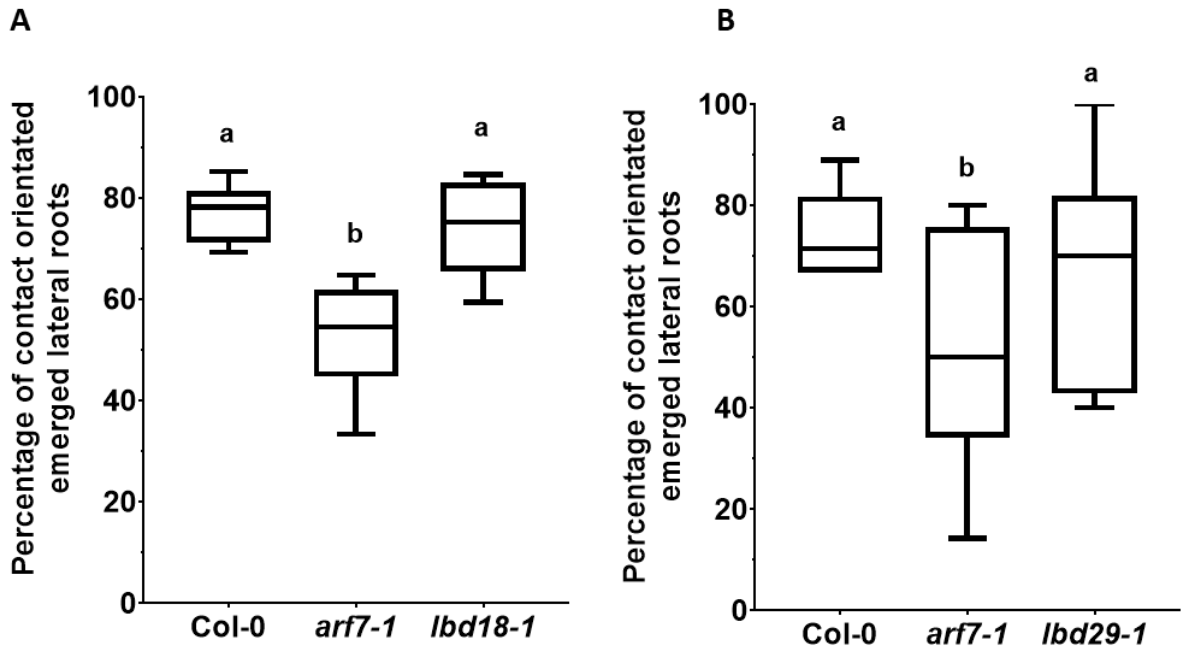

Figure S4.1 – *lbd18-1* and *lbd29-1* mutants exhibited Col-0 levels of LR hydropatterning. In two separate experiments both *lbd18-1* (A) and *lbd29-1* (B) did not show an altered LR hydropatterning response compared to Col-0. Box plots were used to display data distribution. Different letters indicate significant difference between lines ($p \leq 0.05$, one-way ANOVA, Tukey's HSD test) n=9-12 seedlings.

5. SUMO protease OTS1 regulates hydropatterning

5.1 Introduction

Plants have evolved root adaptive responses to forage the heterogenous soil environment more efficiently for resources such as water and nutrients (Gruber et al. 2013; Orman-Ligeza et al. 2018). For example, a barley root growing through a macropore, devoid of contact with water, adapts by blocking branching using its xerobranching response (Orman-Ligeza et al. 2018), whilst maize growing along a macropore only exhibit branching towards the water containing soil using its lateral root hydropatterning response (Bao et al. 2014). Recent work has demonstrated lateral root hydropatterning is dependent on the SUMO-mediated post-translational modification of the key regulator ARF7 (Orosa-Puente et al. 2018). We hypothesize that in root cells exposed on the air side (i.e. the side opposite to the agar) ARF7 is SUMOylated and therefore inactive, whereas ARF7 is un-modified in root cells in contact with agar. However, how ARF7 SUMOylation status is asymmetrically controlled by external water availability remains unclear.

SUMOylation status is controlled by the rate of addition and cleavage of SUMO peptides from its target proteins. This requires the maturation of immature SUMO, followed by the activation, conjugation and ligation of SUMO to target substates (Morrell and Sadanandom 2019). This is potentially followed by poly-SUMO formation involving PIAL proteins or deSUMOylation by SUMO proteases. Together these steps form the SUMO cycle as discussed in more detail in Chapter 1. As most cellular SUMO consists in a conjugated state, it is believed that deSUMOylation of substrates is key to how SUMO regulates cellular processes (Johnson 2004). Additionally, a limited number of SUMO E1 activators and E2 conjugators are found in the *A. thaliana* genome. SUMO E1 activators and E2 conjugators showed no specificity for the various SUMO proteins, thus these do not discriminate during conjugation reactions (Chosed et al. 2006). In contrast, 14 SUMO proteases have been identified in the *A. thaliana* genome, although not all have confirmed SUMO peptidase activity (Morrell and Sadanandom 2019). In plants all identified SUMO proteases are cysteine proteases, which are named after the cysteine residue in the heart of their catalytic site functioning as a nucleophile during proteolytic

cleavage (Gillies and Hochstrasser 2012; Mossessova and Lima 2000). They can be split up in two families based on the amino acid order of the active site: ULP and DeSI. The DeSI family in *A. thaliana* remains largely understudied due to its quite recent identification in mouse (Shin et al. 2012). Recent studies have confirmed the role of DeSI3a in the immune response, indicating DeSI have confirmed isopeptidase activity in plants (Orosa et al. 2018).

The ULP family of SUMO proteases are evolutionary distinct from DeSI's. They can be subdivided into four classes: (I) ELS, (II) OTS, (III) SPF and (IV) FUG types (Castro et al. 2018). Exact evolutionary classification between these classes is difficult due to their amino acid sequence divergence. A lot of variation in activity exist between these classes as the OTS type have confirmed isopeptidase (SUMO cleavage of substrate) and peptidase activity (SUMO maturation) for SUMO1 and 2, whilst the SPF type have medium isopeptidase and low peptidase activity for SUMO1 and cannot process SUMO2 (Conti et al. 2008; Liu et al. 2017). Likely, different classes of ULP proteases are involved with maturation and deSUMOylation of particular SUMO proteins, thereby regulating their specific functioning. Additional specificity to the SUMO machinery is provided by subcellular localisation signals determined by their N-terminal sequences (Li & Hochstrasser, 2003; Kroetz et al., 2009). Most ULP proteases are localised in the nucleus or nuclear envelop, where they can directly control deSUMOylation of nuclear proteins like transcription factors. However, ELS1 is specifically expressed in the cytoplasm, suggesting this protease has distinct targets. Another level of specificity is provided by expression of these proteases. SUMO proteases are expressed ubiquitously in *A. thaliana* (Morrell and Sadanandom 2019). However, the level of expression of the different genes varies per organ, suggesting different developmental roles for the different classes.

The OTS class of deSUMOylating proteases has a strong link with environmental regulation. The role of these proteases was first identified through use of an activation-tagging screen where enhanced expression of *OTS1* led to increased resilience to salt stress (Conti et al. 2008). This phenotype appeared due to a reduction in SUMO1/SUMO2 conjugates found in *OTS1* over-expression lines. The closest homologue to OTS1 was OTS2, with 56% of its amino acid identical to OTS1 and 72%

identical to the OTS1 protease domain. These two homologues are more distant related to other SUMO proteases (Morrell and Sadanandom 2019). In contrast to *OTS1* over-expression lines, the *ots1-1 ots2-1* double mutant exhibited an increased sensitivity to salt, whilst single mutants showed a Col-0 phenotype (Conti et al. 2008). This revealed the genetic redundancy between both OTS SUMO proteases in response to salt stress. Salt exposure did not alter *OTS1* transcript levels, but increased proteasome mediated degradation of OTS1, which as a result enhanced levels of SUMO conjugates (Conti et al. 2008). As OTS proteases are exclusively located in the nucleoplasm, increased levels of SUMOylation of transcription factors can affect gene expression during salt exposure. Potentially, the increased SUMOylation response could decrease gene transcription and decelerate plant growth to cope with local stress. Further evidence in favour of this model, revealed that over-expression of *SUMO1* in *ots1-1 ots2-1* background could severely limit growth similar to salt-stressed *ots1-1 ots2-1* plants (Conti et al. 2009). Interestingly, OTS1 and OTS2 activity only affected SUMO1/2 conjugation upon salt stress and no effect on SUMO3 conjugate levels was observed (Conti et al. 2008). This suggests that different classes of SUMO proteases can have different SUMO targets to control during abiotic and biotic stress responses. Subsequently, the difference in protease-to-target specificity may also reflect the organ and sub-cellular localisation of distinct SUMO proteases. Especially the organ specific expression pattern of the SUMO proteases remains unresolved and might reveal tissue specific protease-substrate interactions.

The OTS1 rice ortholog, OsOTS1, controls salt tolerance in a similar manner, where high salt exposure results in a breakdown of OsOTS1 (Srivastava et al. 2016b). Similar to *A. thaliana*, rice plants over-expressing OsOTS1 had increased salt resilience, whilst RNAi lines repressing OsOTS1 protein levels had decreased resilience (Srivastava et al. 2016a). In contrast, researchers observed a drought sensitive phenotype of rice lines over-expression *OsOTS1*, whilst *OsOTS1-RNAi* lines were more drought resilient (Srivastava et al. 2017). OsOTS1 levels dropped significantly after treatment with drought and ABA, a major regulator of drought response. The drought sensitivity of OTS1 abundance makes it a likely candidate for a role during lateral root hydropatterning.

In this chapter, *loss-of-function* mutants in both *OTS1* and *OTS2* are analysed to establish their role in LR hydropatterning. The *ots1-1 ots2-1* double mutant exhibited a severe defect in LR hydropatterning, and LR initiation and emergence. Complementation of the double mutant with *OTS1-mVenus* could partially restore Col-0 phenotype and fully restore LR hydropatterning. Additionally, *OTS1* expression could be visualized in pericycle cells of the late elongation zone involved in LRFC initiation. However, *OTS1-mVenus* levels were not affected by external water distribution in this zone. Data in this chapter suggests LR hydropatterning is dependent on OTS1 activity rather than OTS1 than stability.

5.2 Results

5.2.1 Mutants in *OTS1* and *OTS2* exhibit a hydropatterning defect

To decipher which gene(s) control ARF7 deSUMOylation, we re-analysed expression of ULP SUMO proteases in LR formation using a transcriptomic time course data set of LR development (Voß et al. 2015). This data revealed highest expression in LRP of OTS1 and no relative change of expression during LR development (Supp. Fig. S5.1A,B). As it was earlier observed that OTS1 plays a role in abiotic stress responses (Conti et al. 2008), we decided to further study OTS1 and its close homolog OTS2's role in LR hydropatterning. *ots1-1 ots2-1* double mutants were provided by prof. Ari Sadanandom and genotyped for the SALK insertion (Supp Fig. S5.2A-D).

Double mutants with SALK insertions in two highly related SUMO proteases, *OTS1* and *OTS2,* exhibited severe root phenotypes including wavy primary roots, impaired primary root growth as well as a decrease in lateral root emergence and density (Fig 5.1 A-D). Additionally, *ots1-1 ots2-1* seedlings exhibit a significant hydropatterning defect (Fig 5.1 E). Expression data for each root zone revealed *OTS1* transcripts are detected in elongation and differentiation zones where LRs initiate, whereas OTS2 is mainly expressed in the lateral root zone where LRP develop and emerge (Supp. Fig. S5.3A). As hydropatterning is sensed in the elongation and early differentiation zone, we specifically focused on OTS1. Interestingly, both *OTS* genes had comparable expression in roots of *arf7 arf19* mutant compared to Col-0, indicating limited control by ARF7 and ARF19 on *OTS1* expression (Supp. Fig. S5.3B).

To determine the spatial-temporal regulation of the OTS1 protein, we constructed a *OTS1* (coding sequence only) translational reporters fused to mVENUS. To validate if either of the OTS1-mVENUS reporters were functional, complementation assays in the *ots1-1 ots2-1* background were performed. *pOTS1::mVenus:OTS1* (N-terminal tagged reporter) and a *pOTS1::OTS1::mVenus* (C-terminal tagged reporter) were constructed and transformed into *ots1-1 ots2-1* plants. Lines expressing either transgene exhibited partial restoration of primary root length and complete restoration of lateral root number, density and hydropatterning, indicating these LR traits were dependent on OTS1 (Fig 5.1 A,B,E; Supp. Fig. S5.4A-D). Furthermore, the complementation lines showed similar phenotypes, indicating no effect of the position of the mVenus tag on OTS1 protein function. Expression analysis shows partial restoration of *OTS1* transcript levels in complementation lines compared to *ots1-1 ots2-1* mutant (Fig. 5.1F). Surprisingly, over-expression of *OTS1* does not affect root growth nor LR hydropatterning, suggesting either strong regulation of *OTS1* mRNA translation or OTS1 protein stability and/or activity as key in hydropatterning rather than *OTS1* transcript abundance (Fig. 5.1A-F). Taken together these results reveal that OTS1 is crucial for LR hydropatterning and suggests possible regulation of LR hydropatterning through OTS1 protein abundance and/or activity.

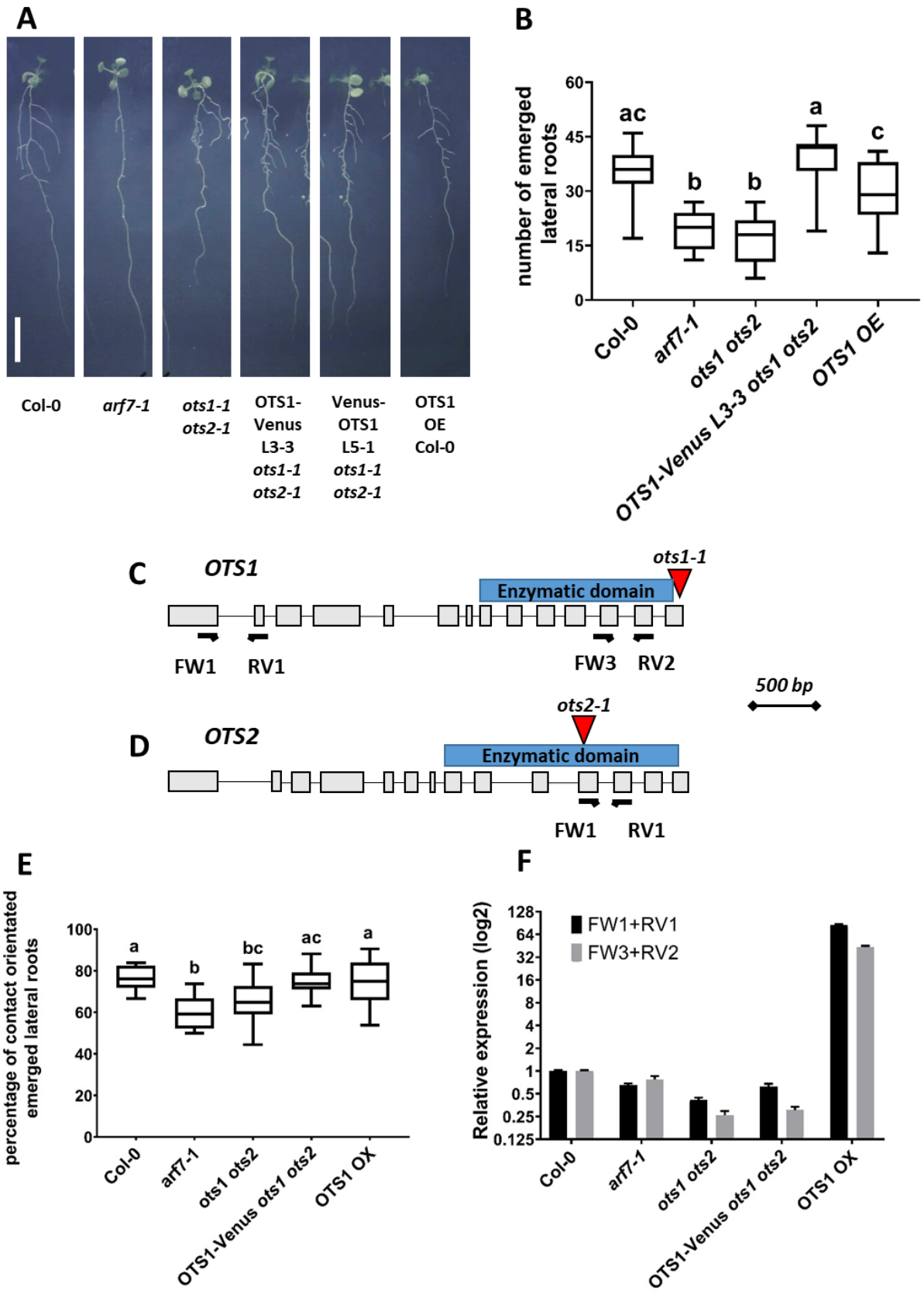

Figure 5.1 – The *ots1 ots2* double mutant displays a severe impairment in root growth and is defective in its lateral root hydropatterning. The *ots1 ot2* double mutant exhibits reduced primary root growth

and lateral root emergence (A, B). This is restored in the OTS1-Venus and Venus-OTS1 complementation lines (A, B). The genome map indicates the T-DNA insertion positions on *OTS1* (C) and *OTS2* (D) and the location of the enzymatic domain containing the C48 peptidase. FW1, RV1, FW3 and RV2 indicate the position of RT-qPCR primers used in this chapter. The double mutant has a significant defect in lateral root patterning, which is rescued by complementation with the OTS1-Venus construct (E). Overexpressing *OTS1* does not seem to have an impact on hydropatterning (E). Expression analysis of these lines indicates that *OTS1* has decreased expression in *ots1-1 ots2-1* mutants and this is only partly restored in the complementation line OTS1-Venus (F). The OX lines clearly showed an enhanced expression of *OTS1* (F). Different letters indicate significant difference between lines (error bars are SEM, p≤0.05, one-way ANOVA, Tukey's HSD test, n=10-14. Expression analysis was done on three biological replicates each containing 15 whole roots. Scale bars represents 1 cm.

To confirm whether regulation of LR hydropatterning by OTS1 is crucial, a second independent *OTS1* allele was characterised. This second allele, termed *ots1-2 gk*, contained a Gabi-Kat (GK) insertion in the 6th exon, whereas the *ots1-1* allele features a mutation in its last exon (Fig. 5.2A). *ots1-2 gk* mutants exhibited a significant reduction in primary root growth and lateral root density, whilst *ots1-1* single mutants showed no difference compared to Col-0 (Fig. 5.2B-D). This new allele also showed a significant defect in LR hydropatterning comparable to *ots1-1 ots2-1* double mutants (Fig. 5.2E), strengthening the evidence that LR hydropatterning is dependent on OTS1 (and to a lesser extent on OTS2).

Further investigation was necessary to explain the difference in hydropatterning response visible in the two single mutants, *ots1-1* and *ots1-2 GK*. Expression analysis of *OTS1* in both these alleles, using FW1 and RV1 primers located at the 5' end of the transcript, led to the surprising discovery that *ots1-1* had decreased levels of *OTS1*, but in *ots1-2 GK* expression levels were increased (Fig. 5.3A). To confirm that the expression change is uniform in the entire transcript and not only increased the transcript levels upstream of the GK insertion, a second RT-qPCR primer pair (FW3 + RV2) was used that amplifies the 3' end of the transcript. This second primer pair displayed similar *OTS1* transcript levels in Col-0, *ots1-1* and *ots1-1 ots2-1* mutants as the 5' primer pair, which confirmed earlier expression results. However, *OTS1* 3' transcript levels where even higher than the over expression already visible in the 5' end of the transcript in *ots1-2*

GK. This data suggests that the GABI-KAT insert causes an over-expression of the gene and might cause a *gain-of-function* mutation.

To verify the position of the GK insert, GK specific border primer and *OTS1* gene specific primers were used. T-DNA map of GK insert (https://www.gabi-kat.de/) was used to find a border primer named o8760 (Fig. 5.3C). To investigate the position and direction of the T-DNA insert PCR was employed by using two *OTS1* gene specific primers, one that amplifies towards the 3' end and one amplifying towards the 5' end (Fig. 5.3B). Surprisingly, both primer pairs resulted in a PCR product, suggesting a possible double GK insertion in the same location (Fig. 5.3D). Sequencing and alignment of both PCR products highlighted the same location on the OTS1 gene map as the position of the GK insert (Fig. 5.3B,E). In contrast with what was defined as the position of the insert on TAIR, this insert is located further downstream in the 7th intron. Potentially, the 35CaMV promoter from the first GK insert drives the over-expression of the enzymatic domain (ULP protease) of OTS1, thus leading to the increased expression of the 3' end.

Further analysis showed no new in-frame ATG codes in the sequencing results. However, exon 8 contains two in-frame ATG codes that could potentially start translation and form 90% of the protease domain, without the entire OTS1 N-terminal. Taken together, this data shows a potential for *ots1-2 GK* as a *gain-of-function* mutant, resulting in over-expression of the C terminal OTS1 protease domain.

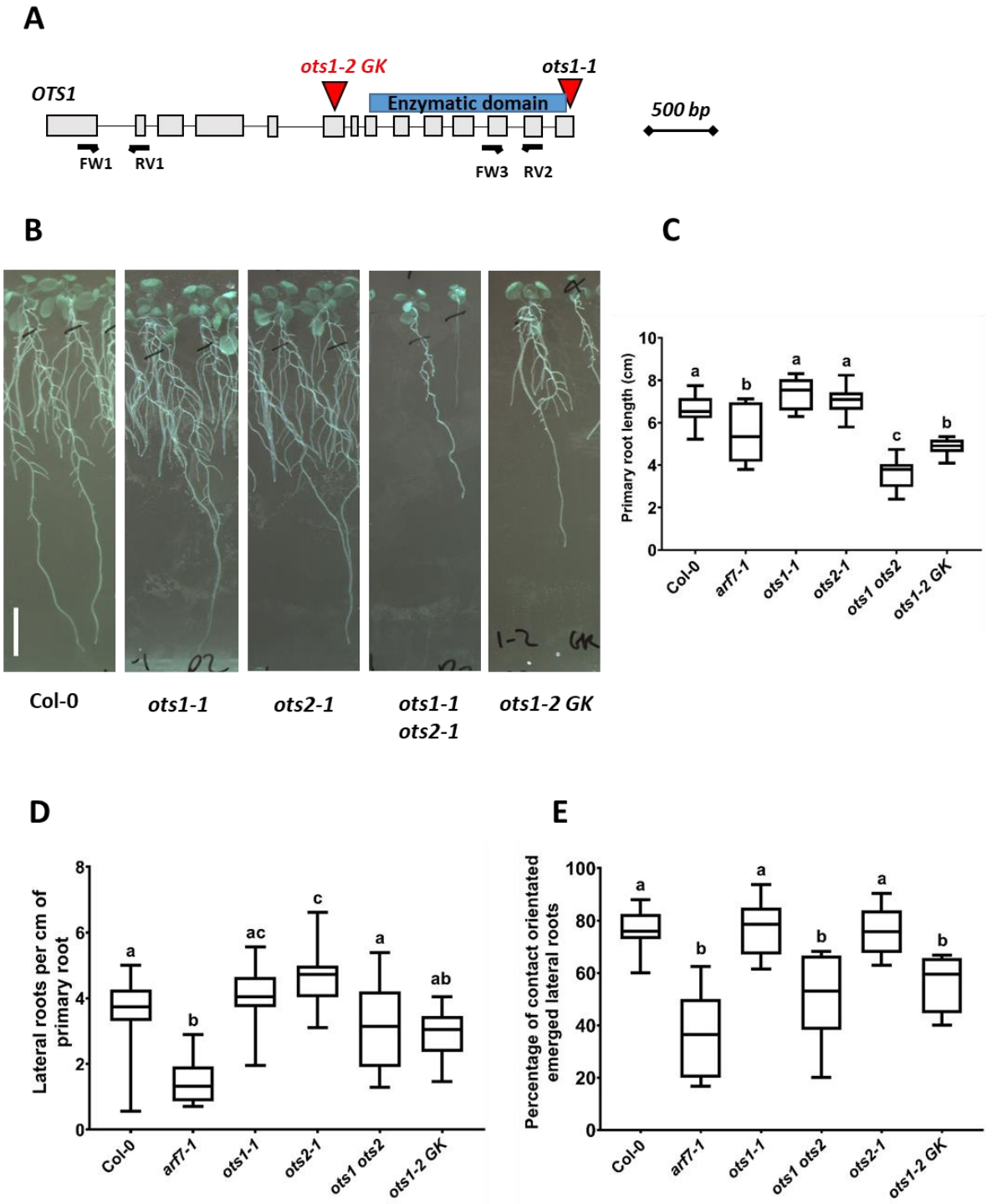

Figure 5.2 – Newly established *ots1-2gk* allele has a severe hydropatterning defect. The Gabi-Kat insertion of the ots1-2 GK allele is, according to TAIR database, positioned on the sixth exon of *OTS1* (A). *ots1-2gk* displays an impaired root growth and reduced LR density (B-D). Additionally, this new allele has a significant defect in its lateral root hydropatterning (E). Different letters indicate significant difference between lines (error bars are SEM, p≤0.05, one-way ANOVA, Tukey's HSD test, n=12-15 roots replicates containing a minimal of 6 lateral roots. Scale bar represents 1 cm.

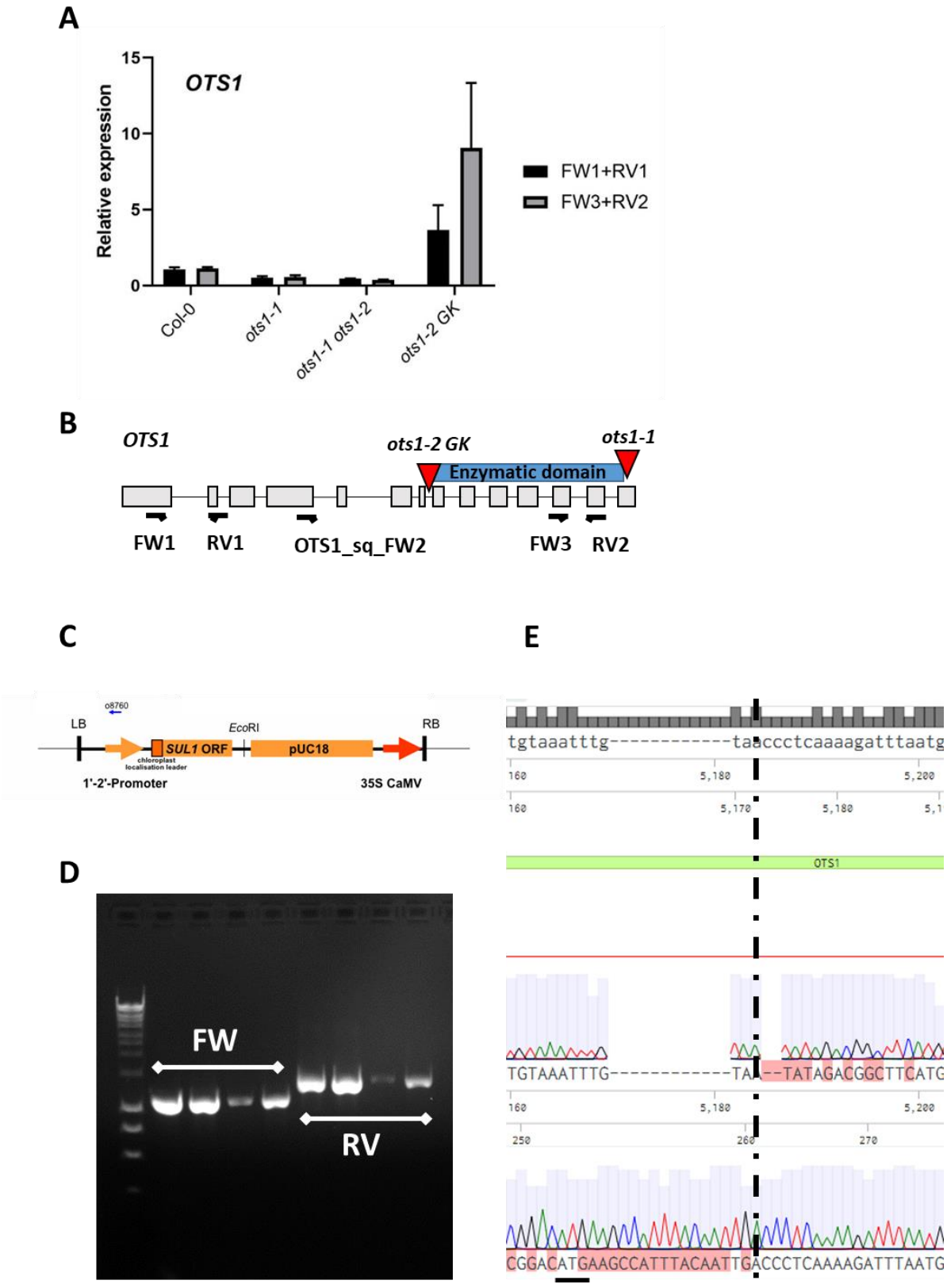

Figure 5.3 – The *ots1-2gk* allele causes a gain-of-function mutation which results in over-expression of *OTS1* transcript. OTS1 expression in *ots1-1* and *ots1-1 ots2-1* mutants is repressed, whilst expression

is increased in *ots1-2gk* (A). The genome map visualizes the location of SALK insertion and new location of the GK insert, location of RT-qPCR primers used as well as the primer used to sequence GK insertion position on *OTS1* (B). Overview of the T-DNA used in GABI-KAT lines, including left border primer used in sequencing of the insertion position (data from https://www.gabi-kat.de/)(C). PCR amplification using *OTS1* gene specific and GK insert specific primers used for sequencing of insert position (D). Note that both use of FW and RV gene specific primers in combination with the Gabi-Kat specific primer results in a band. Alignment of sequencing results on *OTS1* gene map (E).

5.2.2 Lateral root initiation is dependent on OTS1

Next, the effect of *OTS* mutations on LRP initiation and development was investigated. All *OTS* mutant lines were subjected to a 90 degrees 'root bending' assay, in which lateral root initiation is induced and synchronized at the resulting root bend (Péret et al. 2012). Roots were harvested at 18 hours and 42 hours after a gravitropic stimulus to examine the speed of initiation and development of LRP. LR initiation was strongly reduced in *ots1-1 ots2-1* double mutants, revealing a role for the OTS class of SUMO proteases in LR initiation, specifically in early stages of division of the LRP (Fig. 5.4A, B). LRP in the single mutants initiated in a Col-0 manner. Complementation with *OTS1-Venus* transgene could restore LR initiation in *ots1-1 ots2-1* background.

Data for the second 42 hour timepoint provides an indication about how fast the primordium emerges through overlaying tissue layers. In addition to abnormal LRP initiation in *ots1-1 ots2-1*, this mutant also displayed delayed LR emergence (Fig. 5.4C, D). However, this delay is possibly a consequence of the delay in LR initiation. Surprisingly, *ots1-1* and *ots2-1* single mutants showed a slight increase in speed of emergence compared to Col-0. The same is true for the mVenus-OTS1 and OTS1-mVenus rescue lines. Interestingly, the *ots1-2 GK* line exhibited an accumulation of stage 3 and stage 4 LRP, suggesting a problem with passing through the endodermis. Taken together, data presented here reveals an important role for OTS proteases in regulating LRP initiation and emergence processes.

A more detailed histological study assessed which LRP stages were specifically affected in the various *ots* mutant lines. LRP were staged according to Malamy and Benfey's criterion (1997) (Malamy and Benfey 1997). This data was visualized as the LRP density per stage per mutant. Only two lines significantly differed from Col-0, *ots1-1* and *ots1-*

2gk. *ots1-1* displayed an increased initiation of LRP that caused significant increased LRP density of stage1, 2, 3, 4, 6 and 7. Likely this is caused by an increase in initiation events that results in increased number of subsequent stages. In the case of *ots1-2gk* it was specifically stage 3 and 4 that were significantly increased in LRP density compared to Col-0. Stage 3 and 4 are often highlighted as having an important role in endodermis and LRP signalling. Data suggest this signalling might be defective in these mutants, causing accumulation of stage 3 and 4 LRP.

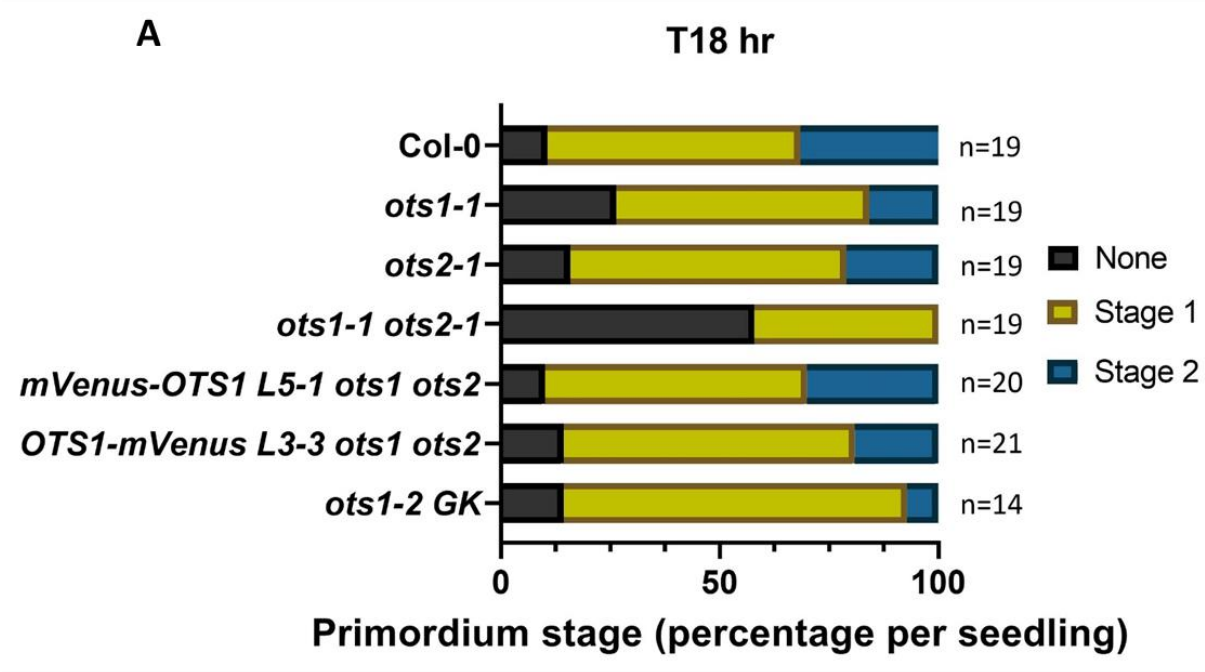

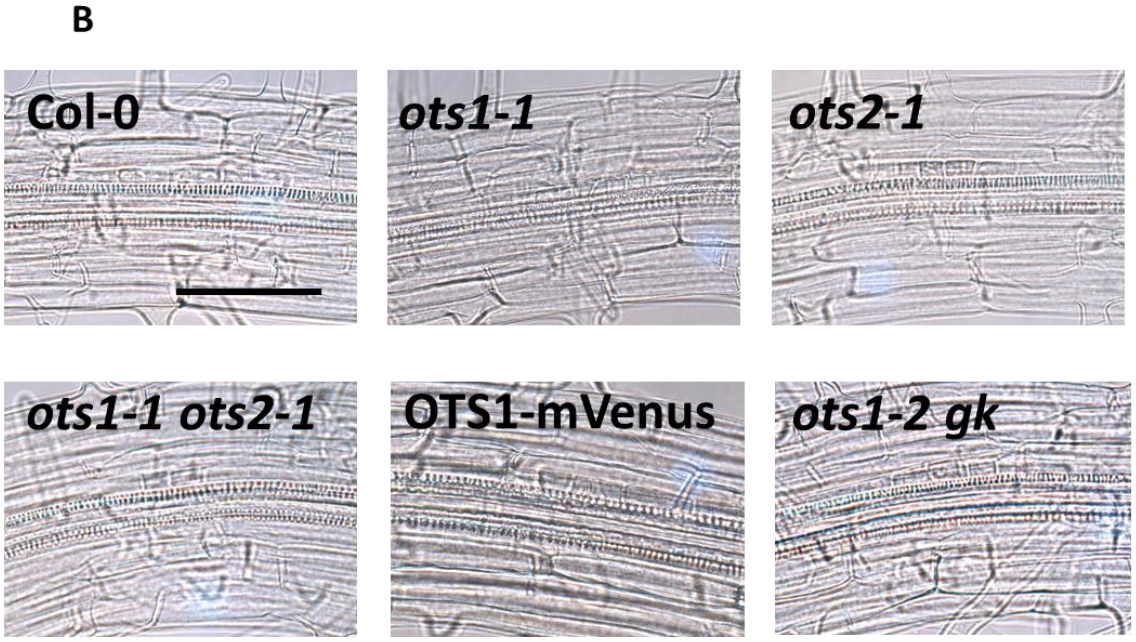

C

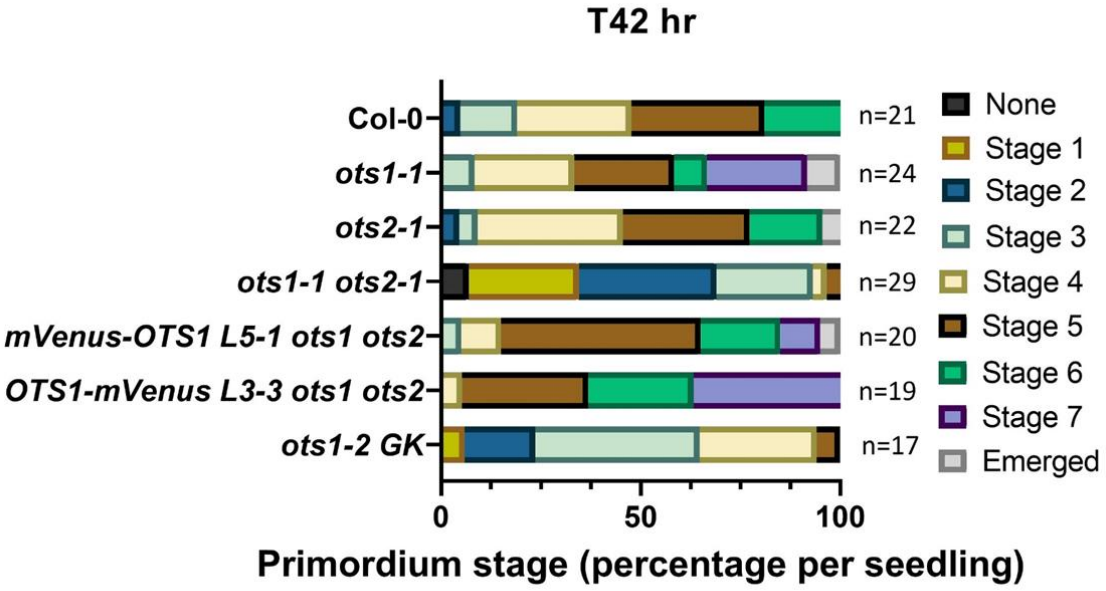
T42 hr
Col-0
ots1-1
ots2-1
ots1-1 ots2-1
mVenus-OTS1 L5-1 ots1 ots2
OTS1-mVenus L3-3 ots1 ots2
ots1-2 GK
n=21
n=24
n=22
n=29
n=20
n=19
n=17
None
Stage 1
Stage 2
Stage 3
Stage 4
Stage 5
Stage 6
Stage 7
Emerged
0
50
100
Primordium stage (percentage per seedling)

D

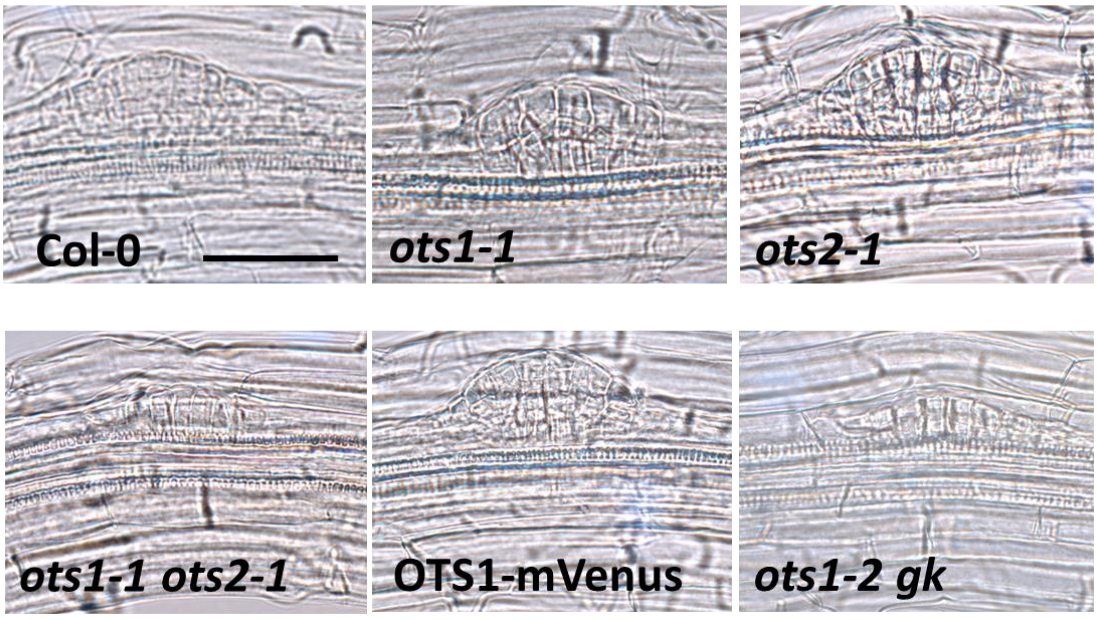
Col-0
ots1-1
ots2-1
ots1-1 ots2-1
OTS1-mVenus
ots1-2 gk

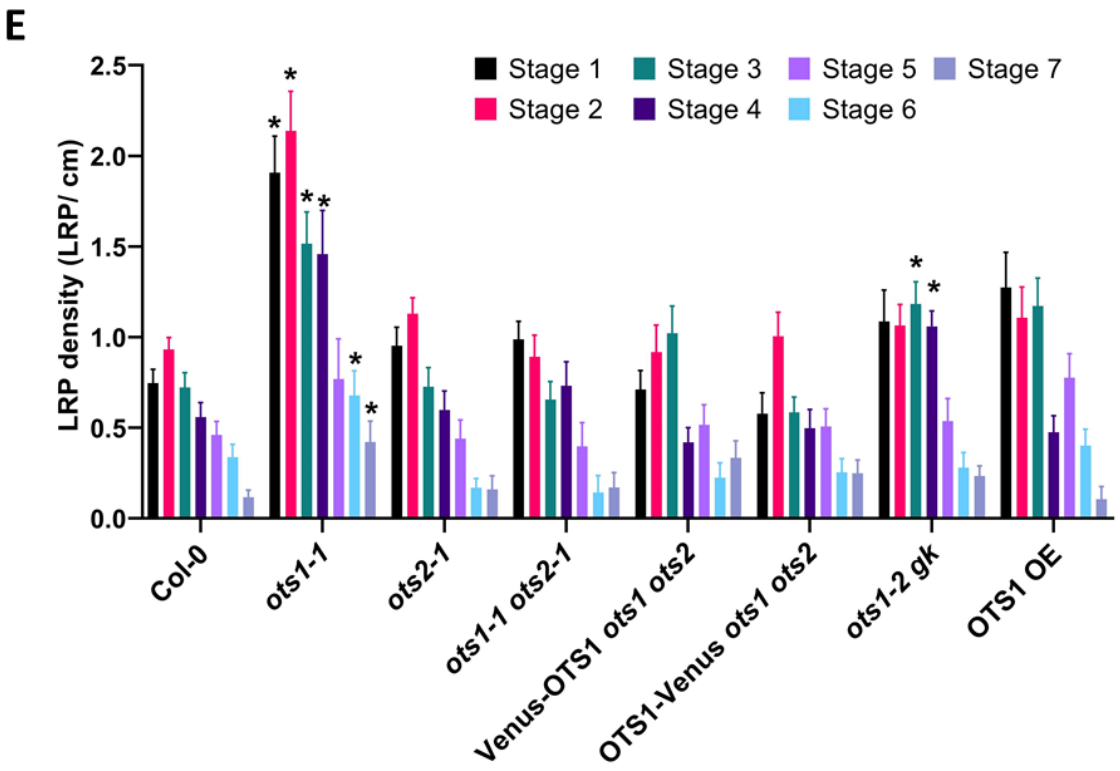

Figure 5.4 – Lateral root initiation is delayed in *ots1-1 ots2-1* double mutants and emergence is delayed in *ots1-1 ots2-1* and the *ots1-2gk* mutant. To synchronize LR development plates containing several OTS mutants were bent 90°. LRP initiation and development was then analysed at 18 and 48 hour after bending and classified in LRP developmental stages as described in Malamy and Benfey (1997). 18 hours after bending the Col-0 showed accumulation of stage 1 and stage 2 primordia, while *ots1-1 ots2-1* double mutants showed a greater number of non-initiated LR (A). LRP images illustrate the developmental stage in which the median of the measurement of each line is 18 hours after bending (B) and 42 hours after bending (D). 42 hours after bending the root, LRP in Col-0 are in stage 4 or 5 of development, while *ots1-1 ots2-1* mutants still lag behind. Furthermore, *ots1-2gk* lines show a decrease in emergence rate and are found mostly in stage 3 and 4 of LRP development. Bars indicate the frequency of seedlings with a LRP in a certain stage of development 18 hours after bending (A, C). Different colours indicate different stages of LRP development. Number of seedings is indicated on the right side of the bar for every line. The density of all primordium stages based on Malamy and Benfey (1997) in the various OTS mutants grown for 12 days on 1/2MS media (E). Bars show means, error bars are SEM. Data of mutants was statistically compared to Col-0 and analysed using one-way ANOVA, p≤0.05, n=7-15 seedlings. Scale bars, 50µm.

5.2.3 *ots1-2gk* is a gain of function mutation causing OTS1 overexpression

To understand the molecular basis for the contrasting lateral root phenotypes of *ots1-1* versus *ots1-2 gk*, levels of *OTS1* transcripts in various *ots1* mutant backgrounds were quantified. Additionally, expression of *OTS1* in *arf7-1* was analysed as hydropatterning is dependent on the SUMOylation of ARF7 and might feedback to *OTS1* transcript levels (Orosa-Puente et al. 2018). *OTS1* levels in *arf7-1* were comparable to Col-0, which suggests that ARF7 does not control *OTS1* levels (Fig. 5.5A). As expected, expression of *OTS1* was reduced in the *ots1-1* single and *ots1-1 ots2-1* double mutant and partially restored in the mVenus-OTS1 and OTS1-mVENUS complementation lines. In contrast, in the *ots1-2 gk* line the expression was increased 9-fold, marking this as a potential *gain-of-function* mutation. Furthermore, the expression of *OTS2* is significantly reduced in *ots1-2 gk*, whilst increased in *ots1-1* (Fig. 5.5B). These results further highlight that each *ots1* mutation have an opposing effect on *OTS1* expression. Additionally, OTS1 and OTS2 show partial redundancy, as *OTS2* levels are increased in *ots1-1,* but no increase of *OTS1* expression is visible in *ots2-1*. This result suggests a possible role for OTS1 in feedback regulation of *OTS2* expression.

Next, the expression of key genes involved in LR hydropatterning, such as *ARF7* and *LBD16*, were analysed in various *ots1* mutant backgrounds to assess their possible genetic regulation. Levels of *ARF7* expression were stable in all *OTS* mutants (Fig. 5.5C). Although a slight (1.6-fold) increase in expression was visible in *ots1-2 GK.* The expression of *LBD16* (a direct ARF7 downstream target) was altered in *ots1* mutants (Fig. 5.5D). As expected, *arf7-1* exhibited a reduced expression of *LBD16.* The reduction in expression in *ots1-1 ots2-1* could be restored to Col-0 levels by complementation with mVenus-OTS1 or OTS1-mVenus. Opposite to *ots1-1*, *ots1-2 GK* line exhibited increased levels of *LBD16*. Hence, OTS1 can affect levels of *LBD16* expression in a similar level as *arf7-1* mutants.

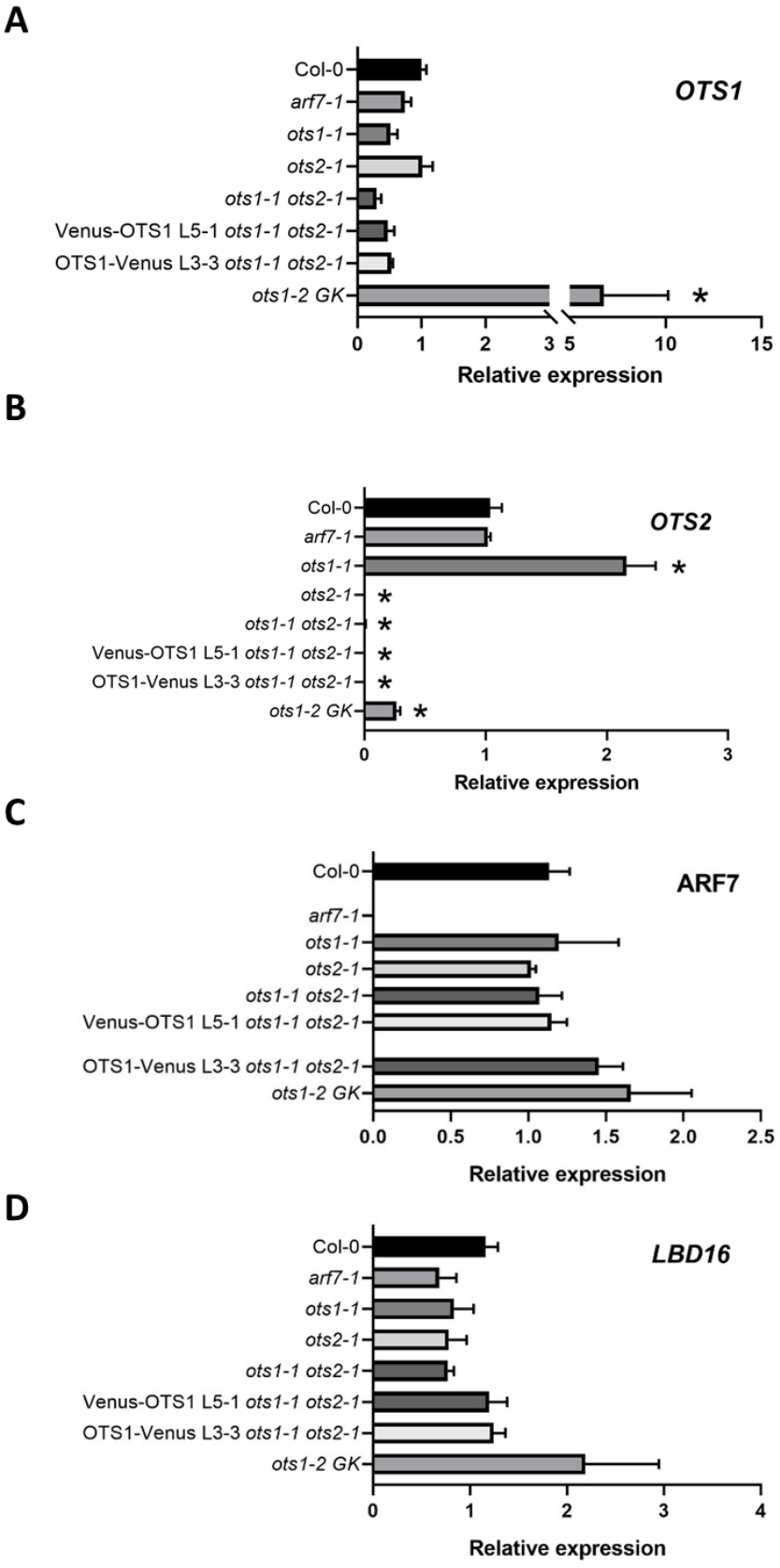

Figure 5.5 – The new *ots1-2gk* allele is a possible *gain-of-function* mutation with increased levels of *OTS1* expression in the root. Expression levels of *OTS1* decrease in *ots1-1 ots2-1* double mutants but

increase in *ots1-2gk* (A). In contrast, levels of *OTS2* go down in *ots1-2gk* (B). Levels of *ARF7* expression are stable in the multiple *OTS* mutants (C). The level of *LBD16* transcript drops in *arf7-1* and *ots1-1 ots2-1* mutants but are restored in the translational reporter lines (D). However, in the *ots1-2gk* lines the levels of *LBD16* are increased (D). Values are relative to Col-0 expression. Asterisks indicate significant difference between mutant line and Col-0 (error bars are SEM, p≤0.05, one-way ANOVA, Tukey's HSD test, n=3 replicates containing ~15 roots per sample.

5.2.4 OTS1 OE and *ots1-2gk* lines exhibit increased salt tolerance

OTS1 and OTS2 were first identified as being involved in the regulation of the salt stress response (Conti et al. 2008). Therefore, salt stress would be a valid way of testing the functional complementation of the mVenus-OTS1 and OTS1-mVenus translational reporters, while also investigating how salt stress affects the new *gain-of-function ots1-2 gk* line. All assembled lines were grown for 5 days on normal ½ MS media, after 5 days plants were transferred to plates containing either ½ MS (Mock) or 100mM of NaCl. After 7 days of growth, a total of 12 days, plates were imaged, and several root parameters measured (Fig. 5.6A, B). Raw data of primary root growth, LR number and LR density was analysed as well as the relative change in these parameters between mock and 100mM NaCl treatment.

ots1-1 and *ots2-1* single mutants exhibited Col-0 growth of primary root and number and density of LRs under normal (mock) conditions (Fig. 5.6C, E, G). However, *ots2-1* showed a significant increase in number and density of LRs when treated with salt, suggesting a higher degree of salt tolerance (Fig. 5.6E, G). This trend was not observed in the relative data (Fig. 5.6F, H). The *ots1-1 ots2-1* double mutant exhibits severe root growth defects in mock conditions but responded similar to salt treatment as Col-0 as seen by the relative growth and LR number (Fig. 5.6C-H). Complementation with mVenus-OTS1 and OTS1-mVenus could partially restore primary root growth and fully restore LR number and density under control conditions (Fig. 5.6C, E, G). The effect of salt response was similar to Col-0, implying full functionality of these transgenes (Fig. 5.6D, F, H).

The *gain-of-function* mutant *ots1-2gk* showed decreased primary root growth and a slight decrease in LR number under mock conditions (Fig. 5.6C, E, G). However, *ots1-2gk* was less affected by salt treatment, shown by the significant increase in relative growth

of primary root and number and density of LRs (Fig. 5.6D, F, H). This trend is very similar to what is observed in the *OTS1* OE line, where a relative increase in LR number and density was observed after salt treatment (Fig. 5.6F, H). This data suggests that *ots1-2gk* and OTS1 OE are less sensitive to salt treatment.

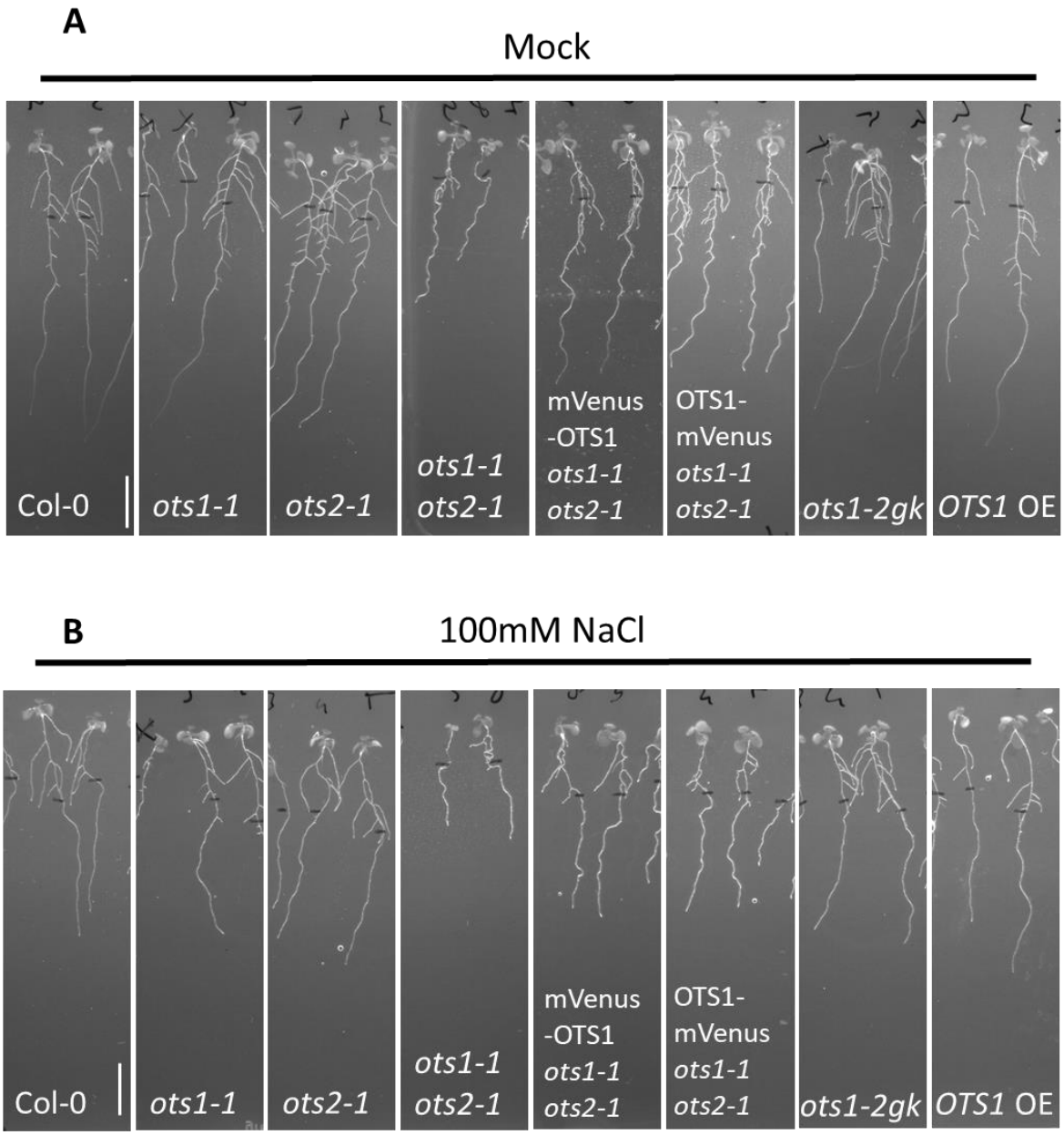

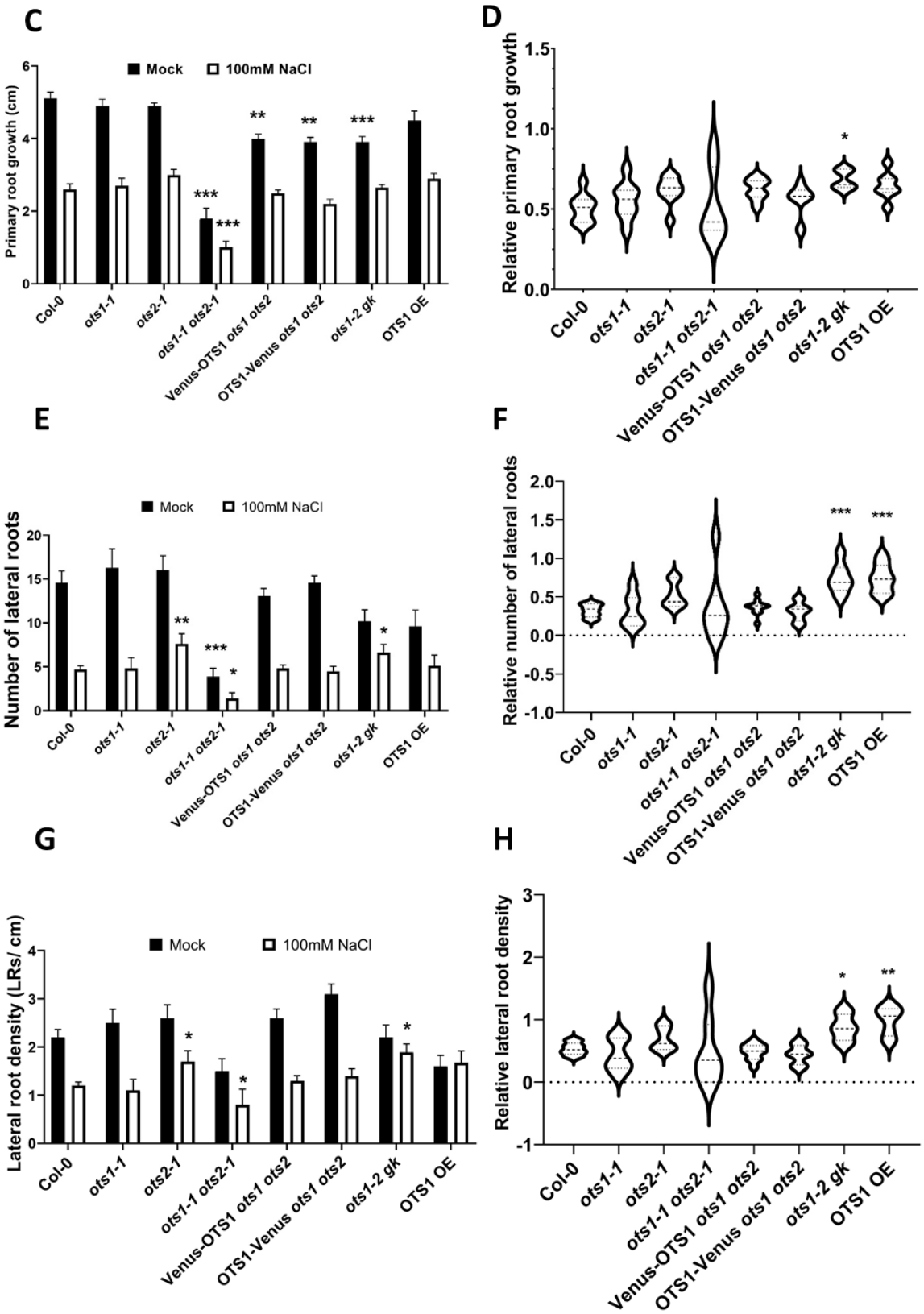

Figure 5.6 – *ots1-2gk* and *OTS1* OE are more tolerant to salt stress. Seedlings were germinated on 1/2MS and transferred 5 dpg to plates containing mock or 100mM NaCl. These seedlings were grown for another 7 days before images were taken (A, B) and root parameters, i.e. primary root growth,

lateral root number and lateral root density, analysed. *ots1-1 ots2-1*, mVenus-OTS1, OTS1-Venus and *ots1-2gk* lines showed reduced primary root growth (A). On salt (100mM NaCl) media *ots1-2gk* and *OTS1* OE exhibit stronger tolerance to salt resulting in increased primary root growth and LR formation (B). Root parameters where analysed in two ways, absolute data and relative data comparing to mock treatment. *ots1-1 ots2-1* exhibits significant primary root growth reduction compared to Col-0 in both mock and salt treatment (C). However, relatively this is not statistically significant (D). Only *ots1-2gk* showed a significant increase in primary root growth under salt stress. Number of LRs is significantly increased in *ots2-1* mutants, yet this does not lead to a significant relative increase in LR number (E). *ots1-2gk* and *OTS1* OE lines, in comparison, have a significant increase in relative LR number (F). Again *ots2-1* and *ots1-2gk* display increased LR density under salt stress conditions compared to Col-0 (G). However, only *ots1-2gk* and *OTS1* OE have a relative increase in LR density (H). Bars of absolute data show means, error bars are SEM. Black bars indicate mock transferred and grown seedlings, while white bars indicate seedlings transferred to plates containing (100mM NaCl). Violin plots show relative data distribution. Data of mutants was statistically compared to Col-0 grown in the same conditions and analysed using one-way ANOVA, * p≤0.05, ** p≤0.01, *** p≤0.001, n=8-10 seedlings. Scale bars indicate 1cm.

5.2.5 *OTS1* is expressed in meristem, elongation zone and lateral root primordia

OTS1 transcription was visualized by fusing a nuclear localized 3xmVenus reporter to the *OTS1* promoter sequence, employing a ~2Kb promoter fragment upstream of the OTS1 open reading frame's start codon. Note that this regulatory sequence included the first intron of *OTS1* (263 bp) and 5' untranslated sequence up until the start of the second exon (Fig. 5.7A). The first intron was included since this can potentially enhance or change many gene's expression patterns (Truskina et al. 2020). Transgenic roots expressing the *OTS1pro::3xmVenus* transcriptional fusion showed strong expression in the meristematic zone, especially epidermal and cortex cells, whereas weaker expression was visible in elongation and differentiation zone epidermal cells. Furthermore, OTS1 in the elongation zone was also expressed in inner root tissues.

OTS1 translational reporter fusions were constructed by tagging either the N- or C-terminal of the OTS1 coding sequence (Fig. 5.7C). As the enzymatic ULP domain is located near the C-terminal, possible interference of the mVenus tag with protein function may occur (Fig. 5.7C). Plants expressing these OTS1-mVenus and mVenus-OTS1 construct in *ots1-1 ots2-1* double mutant background exhibited partial rescue of OTS1 expression levels (Fig. 5.4A). Phenotypically, partial restoration of primary root growth,

and full restoration of LR hydropatterning and lateral root initiation and emergence defects were observed (Fig. 5. 1A,B,E and Fig. 5.5 A-B). Analysis of the fluorescent signal in reporter lines employing confocal microscopy detected very weak marker expression (Fig. 5.7D), consistent with low *OTS1* expression in complementation lines (Fig 5.4A). This could potentially be due to the use (largely) of the exonic *OTS1* coding sequence, instead of the full genomic (intron/exon) sequence. Expression of *OTS1* was strongest in the meristem epidermal cells, although expression was also visible in meristematic cortex cells (Fig. 5.7D). In the late elongation and differentiation zone the expression moved into the vasculature and possibly the pericycle. The signal was only sporadically found in the epidermis in these two root zones.

To confirm whether *pOTS1::3xmVenus* and OTS1-mVenus were expressed in the pericycle, Light Sheet Fluorescent Microscopy (LSFM) was employed to give a detailed view of radial localisation. Similar to the hydropatterning assay in Chapter 4, six images were made in different angles around the root on the LSFM. These were then fused using multi-view reconstruction software in Fiji. Propidium iodide (PI) was used to stain cell walls in these images. Expression of the transcriptional reporter for *OTS1* was observed in all cell types in the basal meristem (Fig. 5.8A, D). In this max projection cross section the PI staining is not greatly visible, probably due to the close proximity of so many cells in the meristem. Next a cross section was taken through the early elongation zone (Fig. 5.8C) where expression was observed in epidermal cells, cortical and endodermal cells. At the top of the elongation zone, expression was reduced in the epidermis and weakly visible in endodermis and pericycle (Fig. 5.8B).

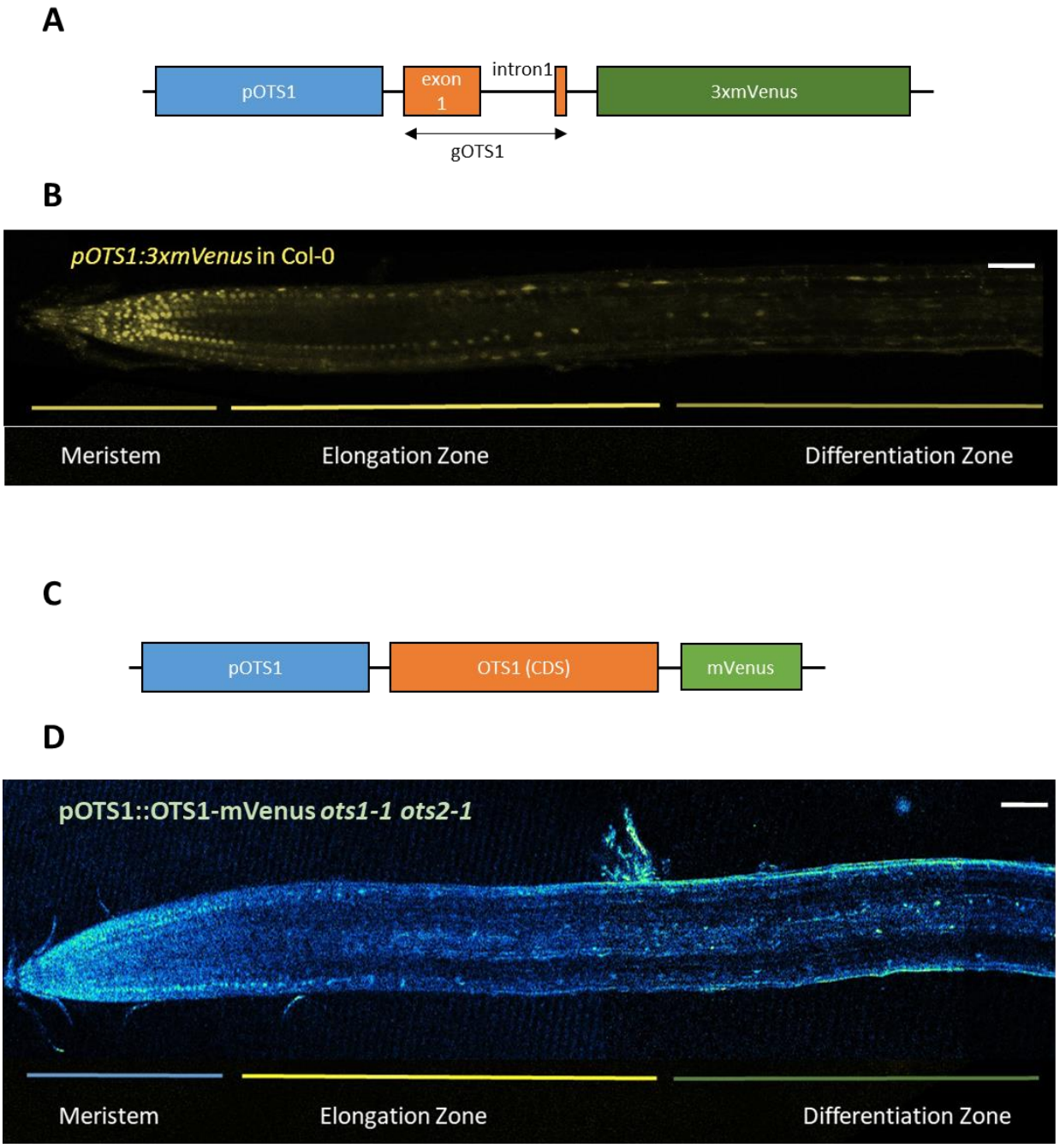

Figure 5.7 – *OTS1* is expressed at the root tip meristem cortex and epidermis cells as shown by the transcriptional and translational reporter lines. Transcriptional reporter was constructed using a ~2Kb promoter upstream from translational start codon plus the addition of first exon, first intron and part of second exon of *OTS1* (A). Confocal image visualizing *OTS1* expression in meristem, elongation and early differentiation zone (B). Translational reporter was constructed using *OTS1* coding sequence and tagged with mVenus fluorophore (C). Nuclear expression of OTS1-mVenus was visible in meristem, late elongation zone and the differentiation zone (D). Scale bar represents 50 µm.

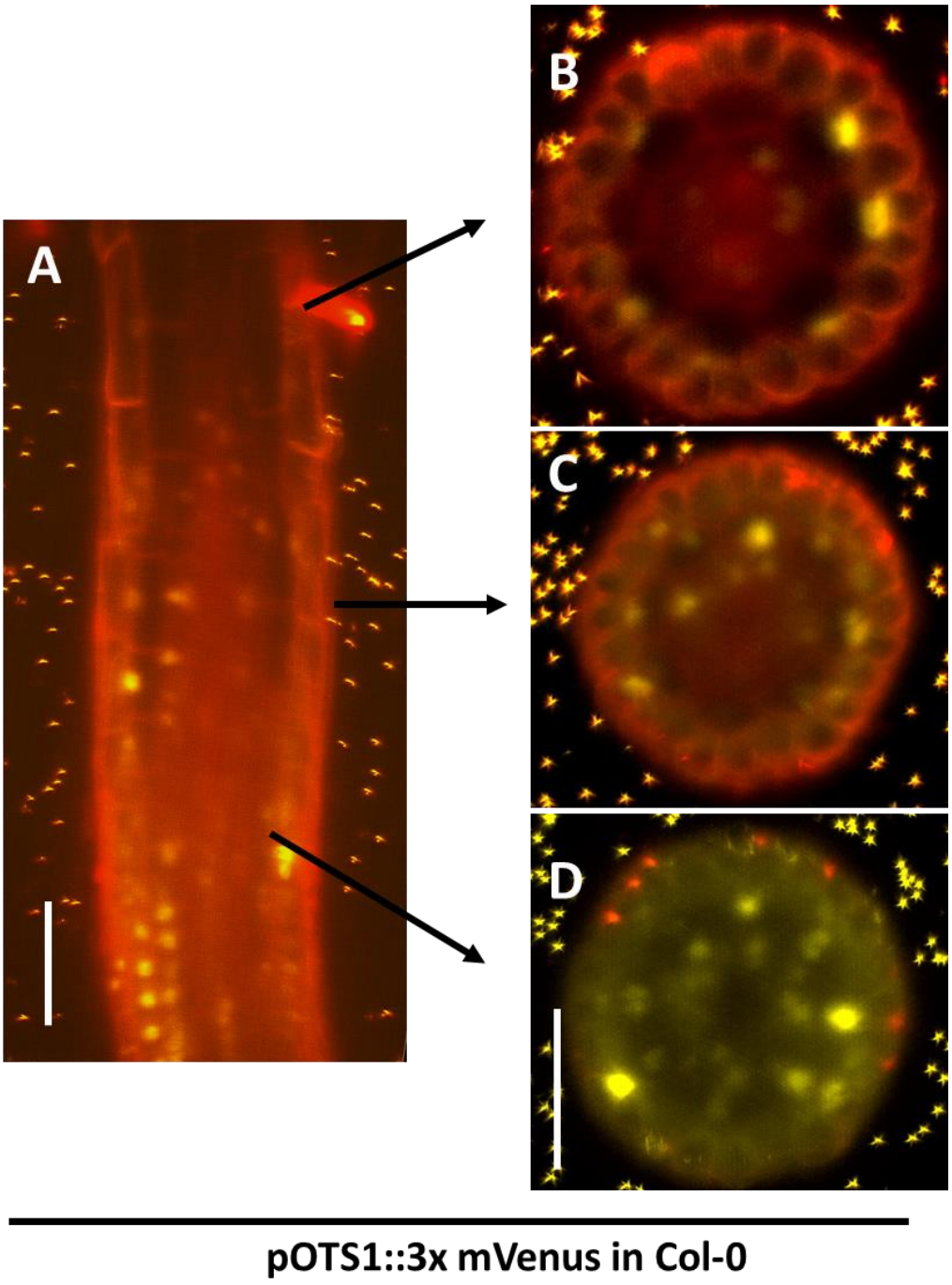

Figure 5.8 – Light Sheet Fluorescent Microscopy (LSFM) was used to visualize radial expression of the pOTS1::3xmVenus (yellow) transcriptional reporter. Longitudinally, *OTS1* is highly expressed in the basal meristem in multiple tissue layers, while this expression is reduced in the elongation zone (A). Max projections of radial cross sections were analysed to observe tissue specific expression. In the basal meristem *OTS1* expression can be found in all tissue layers except the central pro-vasculature cells (D). Levels of expression are reduced in the early elongation zone and expression minimized to epidermis, cortex and endodermis (C). In the later elongation zone expression is found in epidermis

and low levels in endodermis and pericycle (B). Propidium iodide (red) was used to stain the cell walls. Scale bar represents 50 µm.

Detailed LSFM analysis of the transgenic roots expressing the OTS1-mVenus translational fusion detected the reporter in quiescent centre, cortex and epidermal cells in the root meristem zone (Fig. 5.9A). Radial cross sections strengthen this observation (Fig. 5.9B, C). Note that the red membrane marker is a genetically encoded membrane marker (pUBQ10:: RCI2A-tdTomato; Segonzac et al., 2012) crossed into OTS1-mVenus. This enhances the contrast and gives clearer cell outlines, especially in elongation and differentiation zones. Analysis of the weak OTS1-mVenus signal in the late elongation zone, revealed expression confined to the epidermis and vasculature cells (Fig. 5.9D). Radial cross and maximum projections aided in visualizing OTS1-mVenus in the protoxylem and pericycle (Fig. 5.9E, F).

Furthermore, *OTS1* reporter expression was detected during multiple stages of LRP development. Confocal analysis using both transcriptional and translation *OTS1* reporters detected nuclear expression at all stages of LRP development and in every primordia cell (Fig. 5.10 A-F), revealing a potential role for OTS1 in regulating LR initiation and development.

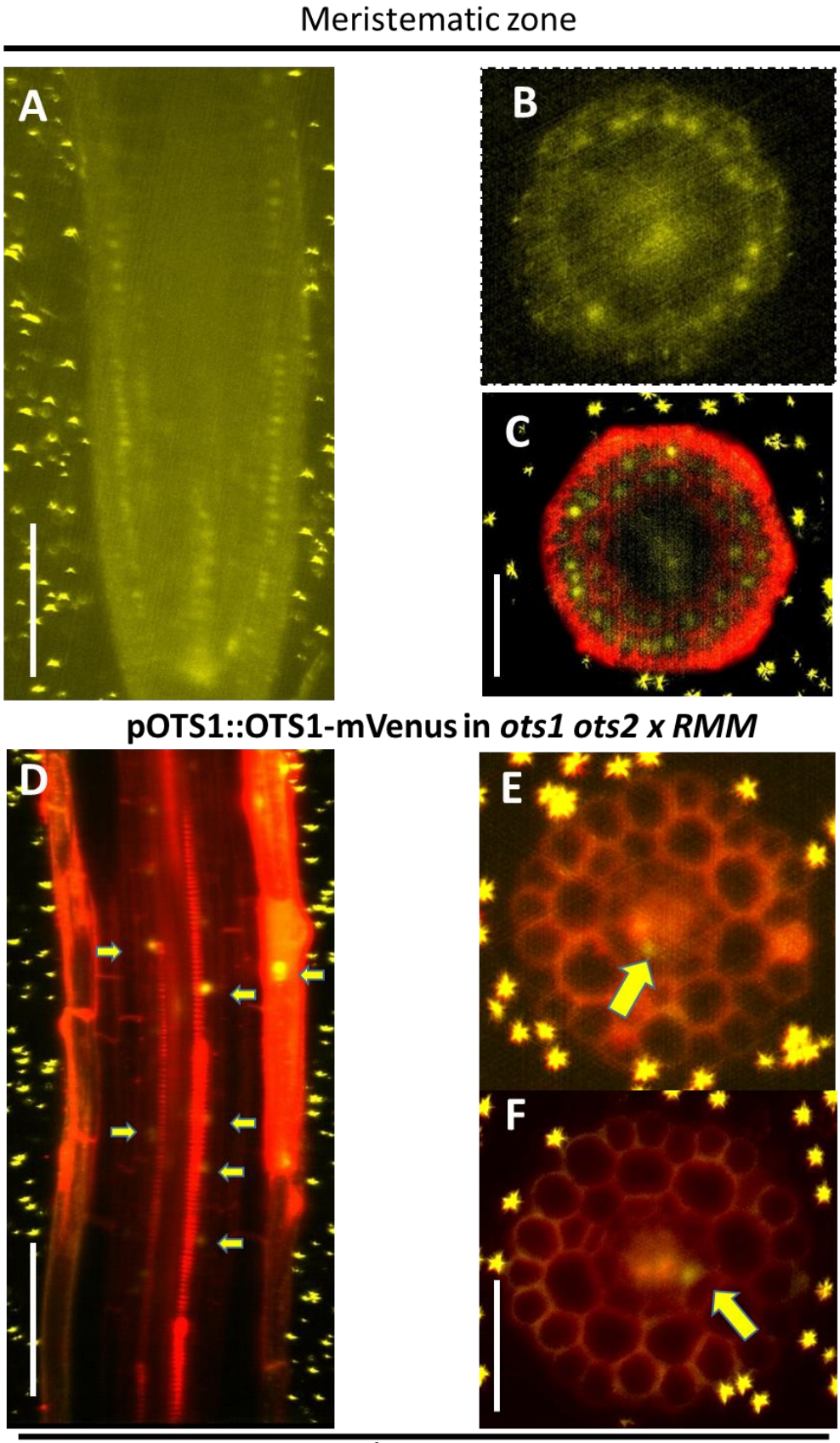
Meristematic zone
A
B
C
pOTS1::OTS1-mVenus in ots1 ots2 x RMM
D
E
F
Late elongation zone

Figure 5.9 – LSFM was used to visualize radial expression of the pOTS1::OTS1-mVenus x Red Membrane Marker (yellow) translational reporter. In the meristematic root zone, OTS1-mVenus is expressed in quiescence centre, proto vasculature cells, epidermis, and cortex cells (A, B, C). In the late elongation zone OTS1-mVenus is localised in protoxylem cells, pericycle cells and sporadically in the epidermis (D, E, F). Maximum projection radial cross sections more clearly demonstrate the radial localisation pattern (B, C, E, F). Scale bar represents 50 µm.

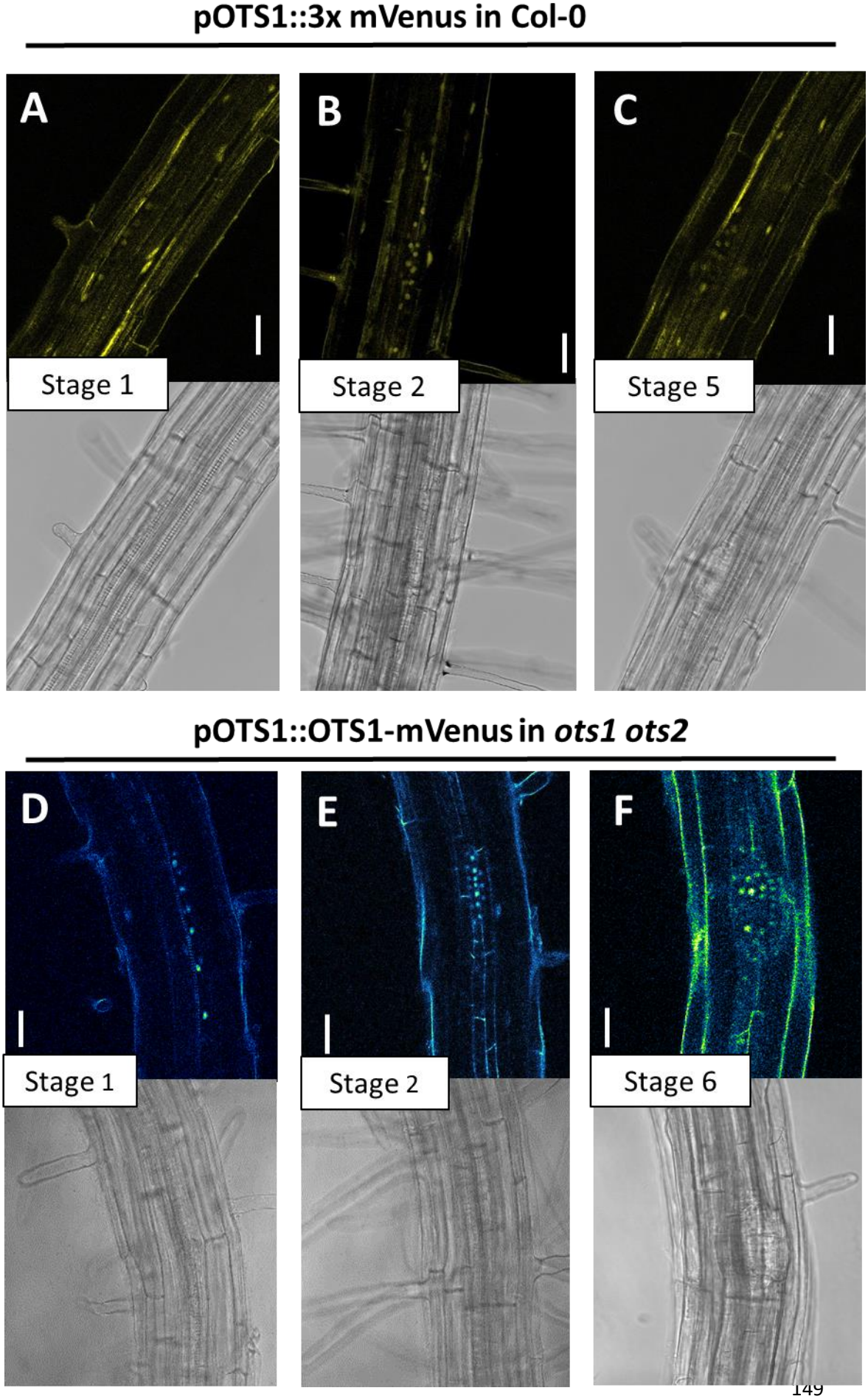
pOTS1::3x mVenus in Col-0
A
B
C
Stage 1
Stage 2
Stage 5
pOTS1::OTS1-mVenus in ots1 ots2
D
E
F
Stage 1
Stage 2
Stage 6

Figure 5.10 – *pOTS1::3xmVenus* and pOTS1::OTS1-mVenus expression in LR primordia stages. Confocal microscopy images demonstrating the localisation of the transcriptional reporter of OTS1 (*pOTS1-3xmVenus*) in several stages of LRP (A, B ,C). The translational reporter, POTS1::OTS1-mVenus, showed expression in the very first stage of primordia development and in subsequent stage 2 and 6 (D,E,F). Upper image displays confocal images, bottom images were taken using brightfield. Scale bar represents 50 µm.

5.2.6 OTS1 stability is not affected by external water distribution

The OTS1 translational reporter was next used to investigate if levels of *OTS1* expression are influenced by external water distribution. An LSFM approach was adopted identical to that used in Chapter 4 with the *gLBD16-GFP* translational reporter (Fig. 4.2). Low levels of nuclear fluorescence can be detected in two cell files in the late elongation zone. The elongation zone is considered to sense changes in water potential driven by the external water environment. These nuclei are in the tissue overlaying either xylem pole pericycle (XPP), the protoxylem and pericycle (Fig. 5.11A). Results revealed stable expression of *OTS1-mVenus* on both sides of the xylem pole, near and distant to the agar (Fig 5.11B). Furthermore, analysis of relative fluorescence of these nuclei demonstrated no change in expression levels of *OTS1-mVenus* between agar and air side of the root (Fig 5.11C). Hence, results suggest that *OTS1* expression and/or stability is not affected by external water availability.

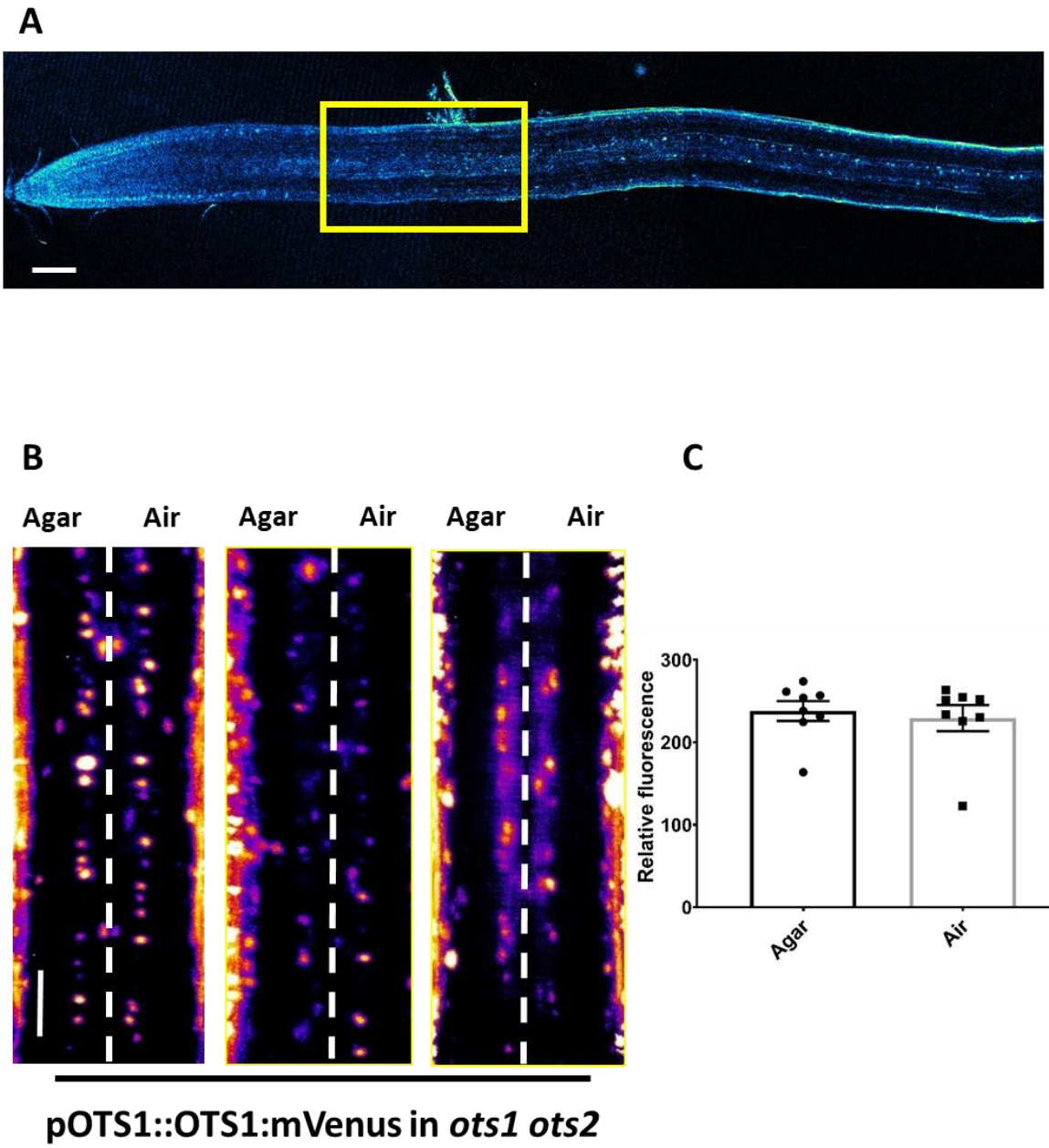

Figure 5.11 – OTS1-mVenus is not asymmetrically expressed in the elongation zone. OTS1-mVenus is expressed in protoxylem and pericycle cells in the late elongation and differentiation zone (A). The yellow border indicates the location of the late elongation zone in which Multiview images were taken using LSFM. Multiview images from six angles were fused and radially sliced to separate based on xylem pole position relative to the agar. Maximum projections reveal no asymmetric expression of OTS1-mVenus in the late elongation zone (B). Relative fluorescence measurements comparing nuclei on the agar and air side display no difference, indicating similar levels of OTS1-mVenus fluorescence (C). n=8. Scale bar represents 50 µm.

5.2.7 Auxin induced lateral root formation in *ots2-1* mutants

Auxin is a major regulator of LR formation (Casimiro et al, 2001). As *ots1-1 ots2-1* mutants showed such a strong LR initiation defect, we further wanted to investigate how these mutants respond to increased exogenous auxin levels. For this, a similar approach was used as with the salt stress experiment. Plants were germinated on 1/2MS plates and after 5 days transferred to mock, 50nM NAA (medium doses) or 200nM NAA (high doses) plates. After seven days of growth these plates were imaged, and several root traits assessed (Fig. 5.12A, B, C).

Col-0 showed reduced primary root growth after auxin addition, an increase of LR number after 50 NAA treatment and increased LR density after 50 and 200nM NAA treatment (Fig. 5.12D, G, I). *ots1-1* single mutants exhibited a similar trend in all these root traits (Fig. 5.12D-J). In contrast, *ots2-1* single mutants showed significantly increased primary root growth after 200nM NAA treatment, as well as increased LR formation and increased LR density after 50nM NAA treatment (Fig. 5.12D, G, I). Indicating less auxin sensitivity in the primary, but increased auxin inducibility of LR formation. This did not result in a significant relative increase in these parameters (Fig. 5.12F, H, J). *ots1-1 ots2-1* double mutants showed an increase in primary root growth after 50nM NAA treatment and reduction after 200nM NAA (Fig. 5.12D, G, I). LR formation was also shown to be inducible in these double mutants after auxin treatment, indicated by a strong relative increase in LR number. The complementation lines mVenus-OTS1 and OTS1-mVenus showed a similar root response to auxin as Col-0, suggesting these proteins are fully functional (Fig. 5.12D-J). *ots1-2gk* lines showed similar response to both Col-0 and *ots1-1* (Fig. 5.12D-J). In contrast, *OTS1* over-expression led to increased primary root growth after 200nM NAA treatment (Fig. 5.12D, F). Furthermore, a strong relative increase in LR number and density was observed when these lines were treated with both auxin concentrations (Fig. 5.12G-J). This data indicates a stronger auxin inducibility of LR formation when *OTS1* is over-expressed.

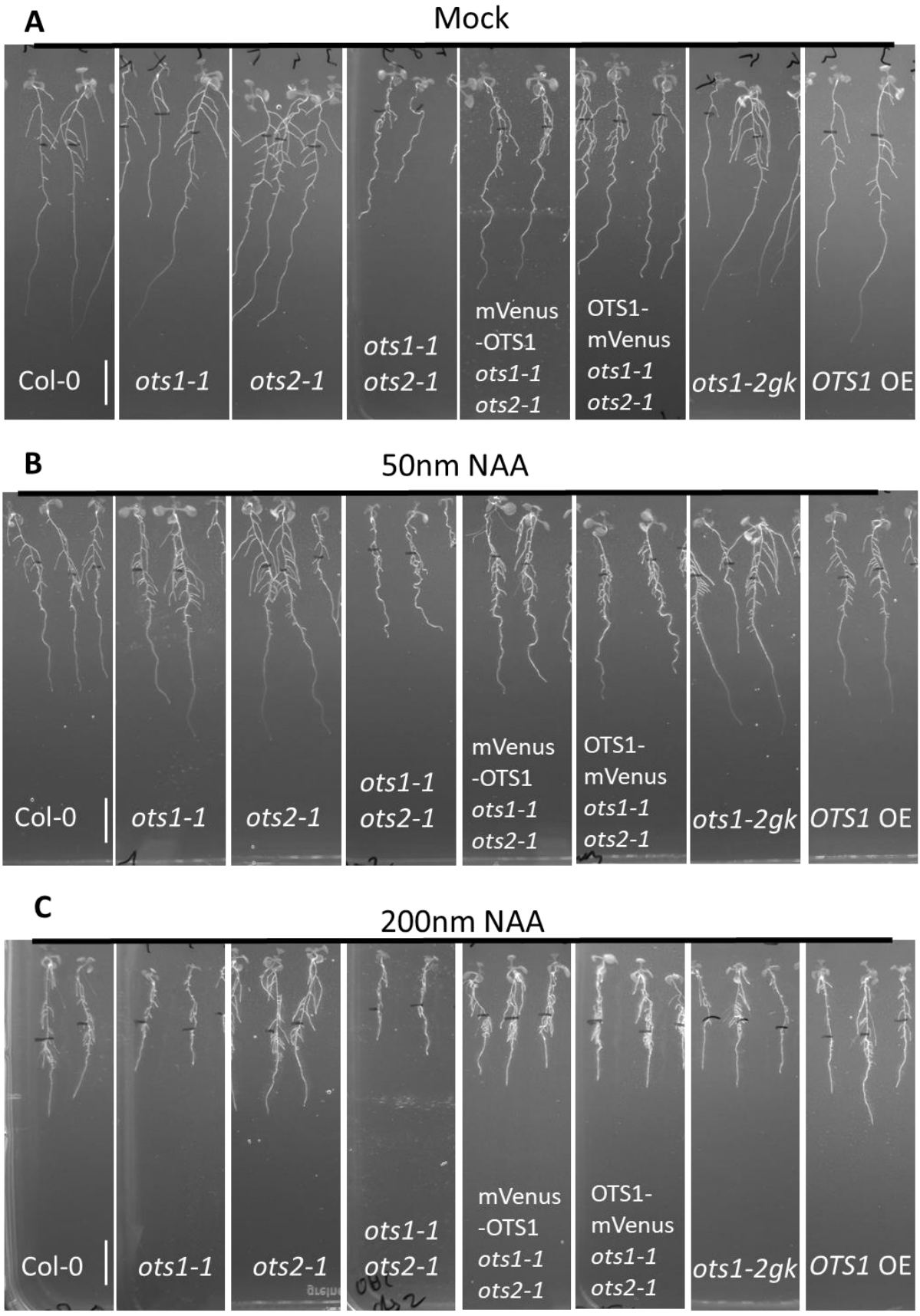
A
Mock
Col-0
ots1-1
ots2-1
ots1-1 ots2-1
mVenus -OTS1 ots1-1 ots2-1
OTS1- mVenus ots1-1 ots2-1
ots1-2gk
OTS1 OE
B
50nm NAA
Col-0
ots1-1
ots2-1
ots1-1 ots2-1
mVenus -OTS1 ots1-1 ots2-1
OTS1- mVenus ots1-1 ots2-1
ots1-2gk
OTS1 OE
C
200nm NAA
Col-0
ots1-1
ots2-1
ots1-1 ots2-1
mVenus -OTS1 ots1-1 ots2-1
OTS1- mVenus ots1-1 ots2-1
ots1-2gk
OTS1 OE

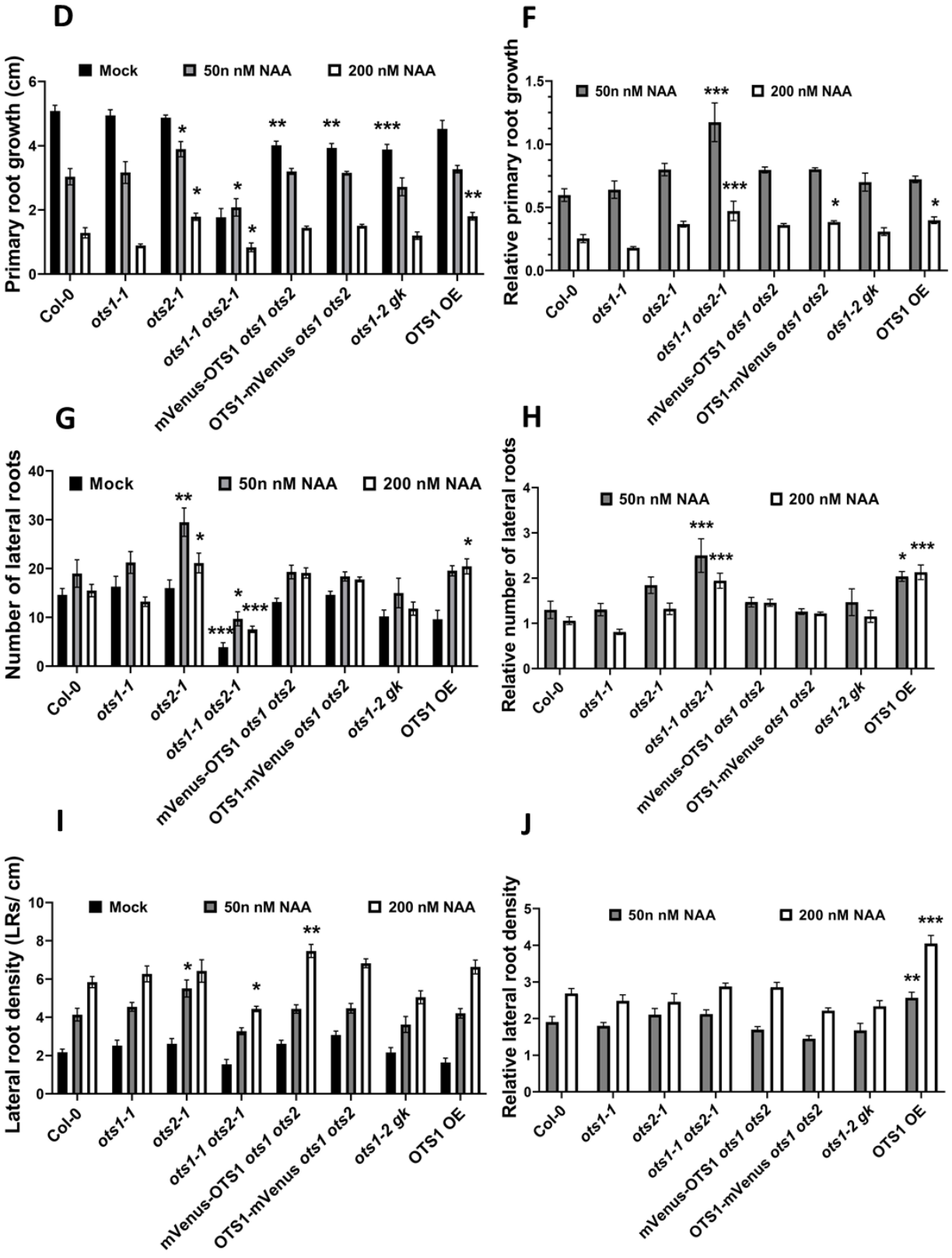

Figure 5.12 – ots1-1 ots2-1 mutants are still able to form auxin induced LRs. Seedlings were germinated on 1/2MS and transferred 5 dpg to plates containing mock (A) or 50nM NAA (B) or 200nM NAA (C) plates. These seedlings were grown for another 7 days before images were taken and root parameters,

i.e. primary root growth, lateral root number and lateral root density, analysed. All mutant lines showed a reduction in primary root growth after auxin treatment, except the ots1-1 ots2-1 mutants which showed increased primary root growth after 50nM NAA treatment compared to mock treatment (D). OTS1 OE had a significantly higher primary root growth after growth on 200nM NAA plates compared to Col-0 in the same conditions observed both in absolute and relative data (F). LR numbers significantly increased in ots2-1 mutants after 50nM NAA treatment and OTS1 OE after 200nM NAA treatment (G). In ots1-1 ots2-1 background the absolute number of LRs was significantly lower than Col-0, but relatively they grew more LRs (H). The LR density increased in ots2-1 after 50nM treatment, and in mVenus-OTS1 after 200nM NAA treatment, while ots1-1 ots2-1 had significantly decreased number of LR density after 200nM NAA treatment (I). Only OTS1 OE has significantly increased relative LR density after both auxin treatment compared to Col-0 (J). Bars of absolute data show means, error bars are SEM. Black bars indicate mock transferred and grown seedlings, while grey bars indicate 50nM NAA and white bars indicate seedlings transferred to plates containing 200nM NAA. Same bar colour scheme was used for the relative data minus the mock data. Data of mutants was statistically compared to Col-0 grown in the same conditions and analysed using one-way ANOVA, * p≤0.05, ** p≤0.01, *** p≤0.001, n=8-10 seedlings. Scale bars indicate 1cm.

To further analyse if the difference observed in LR number is due to an increase or decrease in LR initiation, the root zone below the last emerged LR was cut out and cleared. Afterwards LRP in this zone were counted and compared to auxin treated roots. A significant increase in the number and density of LRP was observed in *ots1-1* grown on mock plates compared to Col-0 (Fig. 5.13A). In contrast, *ots1-1* did not show a significant increase in LR number, suggesting this mutation specifically impacts number of initiation events. After treatment with 50nM NAA LR number and density were comparable to Col-0 (Fig. 5.13C, D). In contrast, *ots1-2* showed Col-0 levels of LR formation in mock conditions, but increased LR and LRP formation after auxin addition (Fig. 5.13C). Hence, *ots1-1* and *ots2-1* have opposing effects as a response to auxin treatment. The *ots1-1 ots2-1* double mutant exhibited reduced number of LRs and LRP, but no difference compared to Col-0 when looking at LR and LRP density (Fig. 5.13A, B). Auxin treatment of *ots1-1 ots2-1* lines revealed limited auxin inducibility of LR and LRP formation as numbers were significantly reduced (Fig. 5.13C, D). LR density was comparable to Col-0, whilst LRP density was significant decreased after auxin treatment, suggesting a limited auxin inducibility of LRP in this line.

Complementation of *ots1-1 ots2-1* with mVenus-OTS1 and OTS1-mVenus restored levels of LR and LRP number and density to Col-0 levels after mock treatment, but could not restore the auxin induced LRP formation and density (Fig. 5.13A-D). This data reveals partial restoration of the auxin induced LRP induction in complementation lines.

ots1-2gk lines showed increased levels of LRP density in control conditions similar to *ots1-1*(Fig. 5.13A, B). However, no difference was observed after auxin treatment in LR and LRP formation or density (Fig. 5.13C, D). *OTS1* OE lines displayed Col-0 levels of LR number and density after mock and auxin treatment (Fig. 5.13A-D).

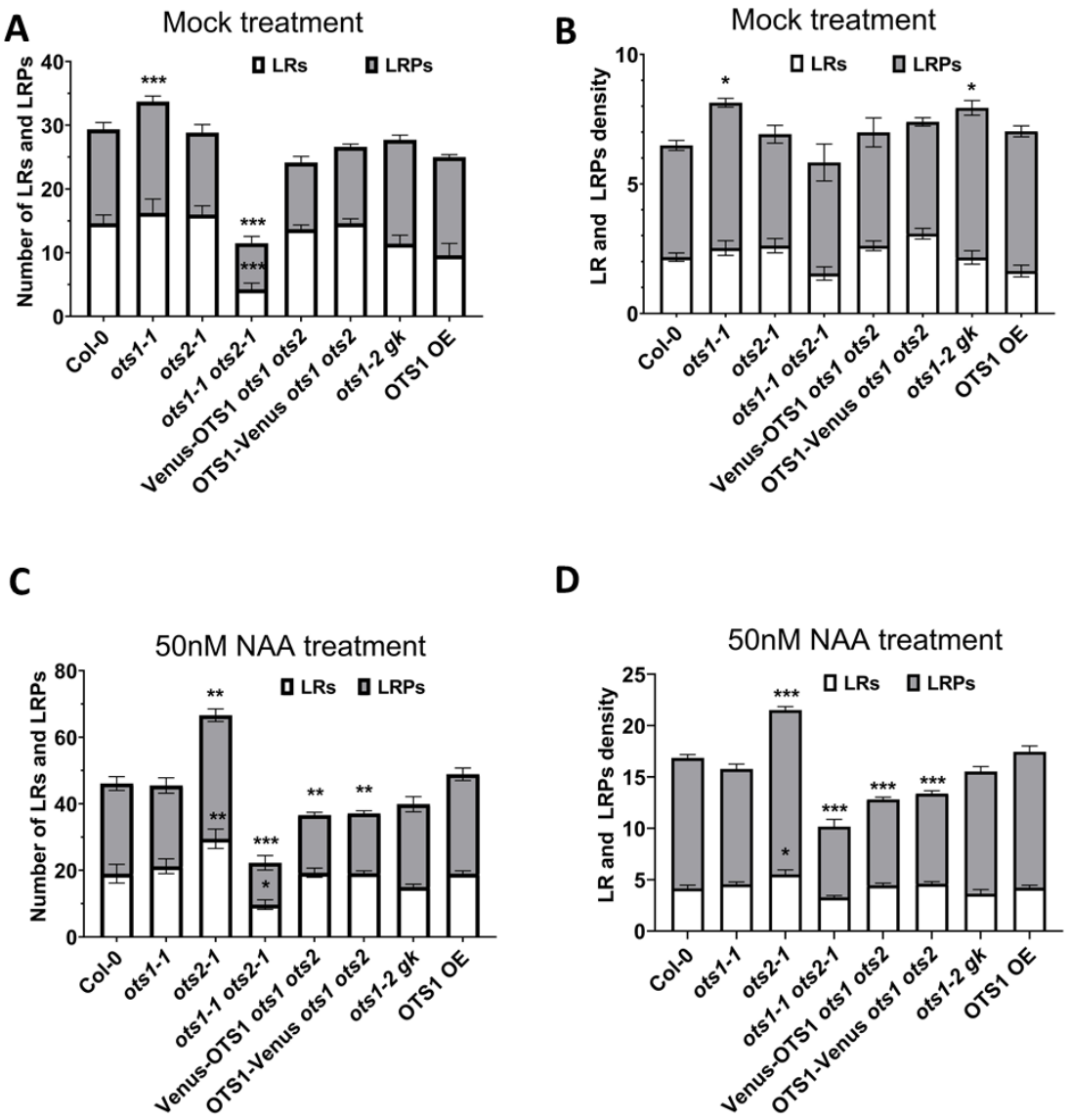

Figure 5.13 – LRP density is increased in *ots1-1* and *ots1-2gk* mutants. Number of LRs and LRP and the density of LRs and LRP in the root zone below the first fully emerged LR in OTS mutants (A, B) and on 50nM NAA (C, D). The number of LRP and the LRP density significantly increases in ots1-1 mutants in comparison with Col-0 (A, B). *ots1-1 ots2-1* mutants showed decreased LR and LRP numbers, but no significant difference in LR or LRP density. 50nM NAA treated seedlings showed significant reduced LRP number and density in *ots1-1 ots2-1*, mVenus-OTS1 and OTS1-mVenus lines (C, D). Contrary, *ots2-1* mutants showed increased LRP number and density after 50nM NAA treatment. Stacked bars show means, error bars are SEM. White bars indicate number or density of LRs, while black bars indicate number or density of LRP. LR data of mutants was statistically compared to Col-0 LR number and the LRP were compared to Col-0 LRP number and density. This data was analysed using one-way ANOVA, * p≤0.05, ** p≤0.01, *** p≤0.001, n=8-10 seedlings.

5.2.8 OTS1 exhibits differential stability to selected hormone signals

To determine if *OTS1* expression, localisation and/or stability is controlled by phytohormone signalling pathways, OTS1 transcriptional and translational reporters were subjected to treatment with the following phytohormones: Auxin (NAA), Abscisic acid (ABA), Cytokinin (BA), Salicylic acid (SA) and an Ethylene precursor (ACC). A drop (~20 µl) of phytohormone or mock solution was added to the root tip, covering the meristem and elongation zone, of *OTS1* transcriptional and translational reporters. After four hours of treatment, confocal microscopy was employed to take z-stacks of root meristems. Relative fluorescence levels were measured over an area in the epidermis using ImageJ/Fiji software.

Relative fluorescence in the two independent transcriptional reporter lines, line 1-2-1 and 2-2-3, were analysed based on expression in the epidermal cells in the centre of the root. None of the used phytohormones had any significant effect on the expression levels of OTS1 (Fig. 5.14A, B). Additionally, the expression pattern remained unaltered after hormone treatment (Fig. 5.14C). These results indicate that OTS1 is not directly regulated by any of the tested phytohormones.

Subsequently, the regulation of OTS1 protein level by the same hormones was investigated. Both the N-terminal and C-terminal OTS1 translational reporters were used in this study. BA (cytokinin) treatment significantly lowered the expression of both mVenus-OTS1 and OTS1-mvenus in epidermal cells of the root meristem (Fig. 5.15A, B). ABA and SA treatment significantly lowered expression in the mVenus-OTS1 lines, yet not in the OTS1-mVenus line. Other hormone treatment had limited influence on level or pattern of the translational reporters (Fig. 5.15B). This data reveals a novel OTS1 protein degradation mediated by cytokinin and potentially ABA signalling.

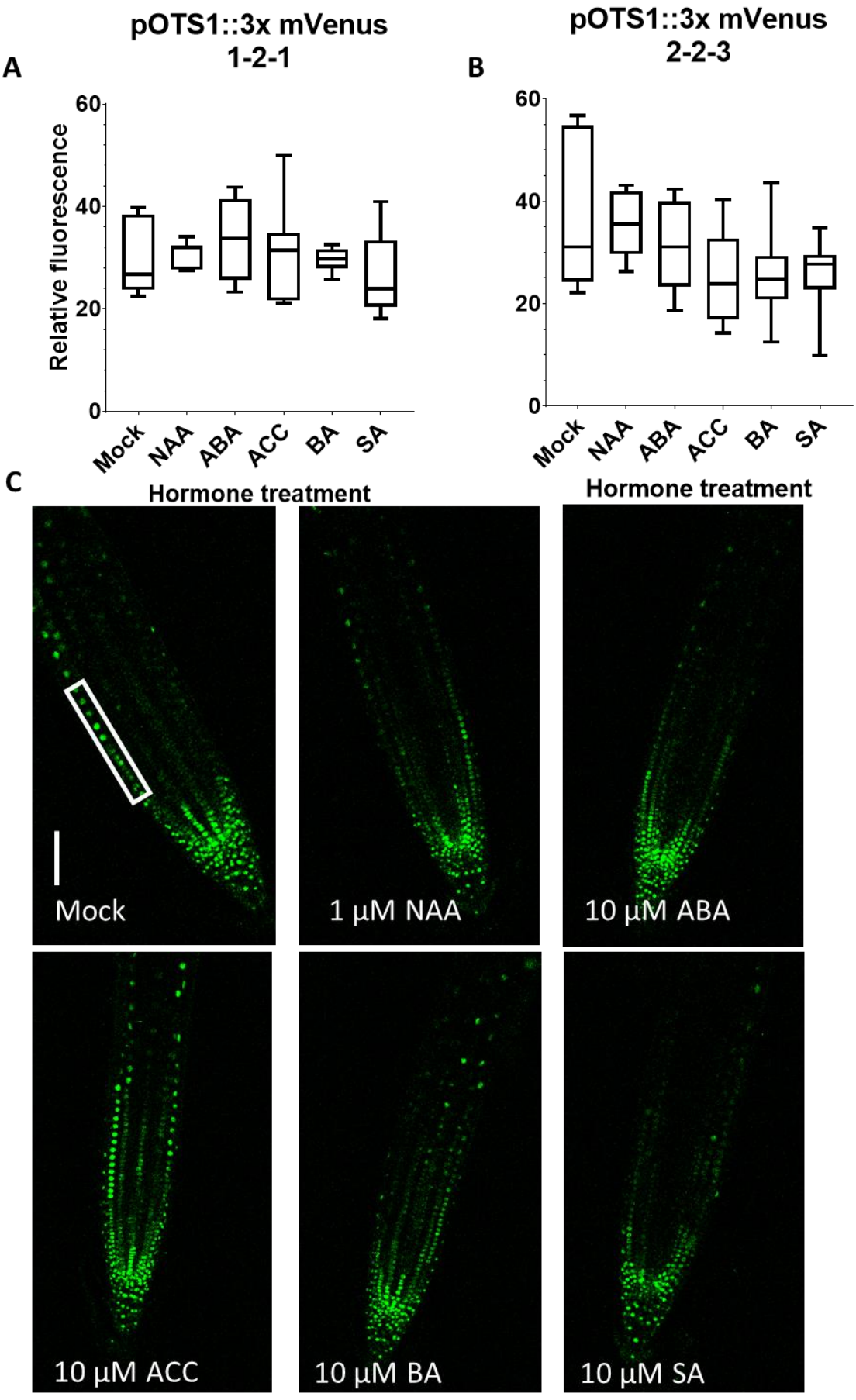
A
pOTS1::3x mVenus
1-2-1
Relative fluorescence
60
40
20
0
Mock
NAA
ABA
ACC
BA
SA
Hormone treatment
B
pOTS1::3x mVenus
2-2-3
60
40
20
0
Mock
NAA
ABA
ACC
BA
SA
Hormone treatment
C
Mock
1 µM NAA
10 µM ABA
10 µM ACC
10 µM BA
10 µM SA

Figure 5.14 – Expression level of *OTS1* remains unchanged after phytohormone treatment when measuring fluorescence in the epidermal tissue. The mean fluorescence in an equal area containing 10 nuclei of the epidermis at the centre of the root was measured after treatment. Four hour treatment with 1 µM NAA, 10µM ABA, 10 µM BA, 10 µM SA and 10 µM ACC had no effect on relative fluorescence levels of *pOTS1::3xmVenus* in two independent reporter (1-2-1 and 2-2-3) lines compared to mock treatment (A, B). Furthermore, tissue specific expression pattern remained unaltered by hormonal treatment (B). Data presented in box-plots with n=7. Scale bar represents 50 µm. Data of different hormone treatments was statistically compared to mock treatment and analysed using one-way ANOVA, asterisks indicate p≤0.05.

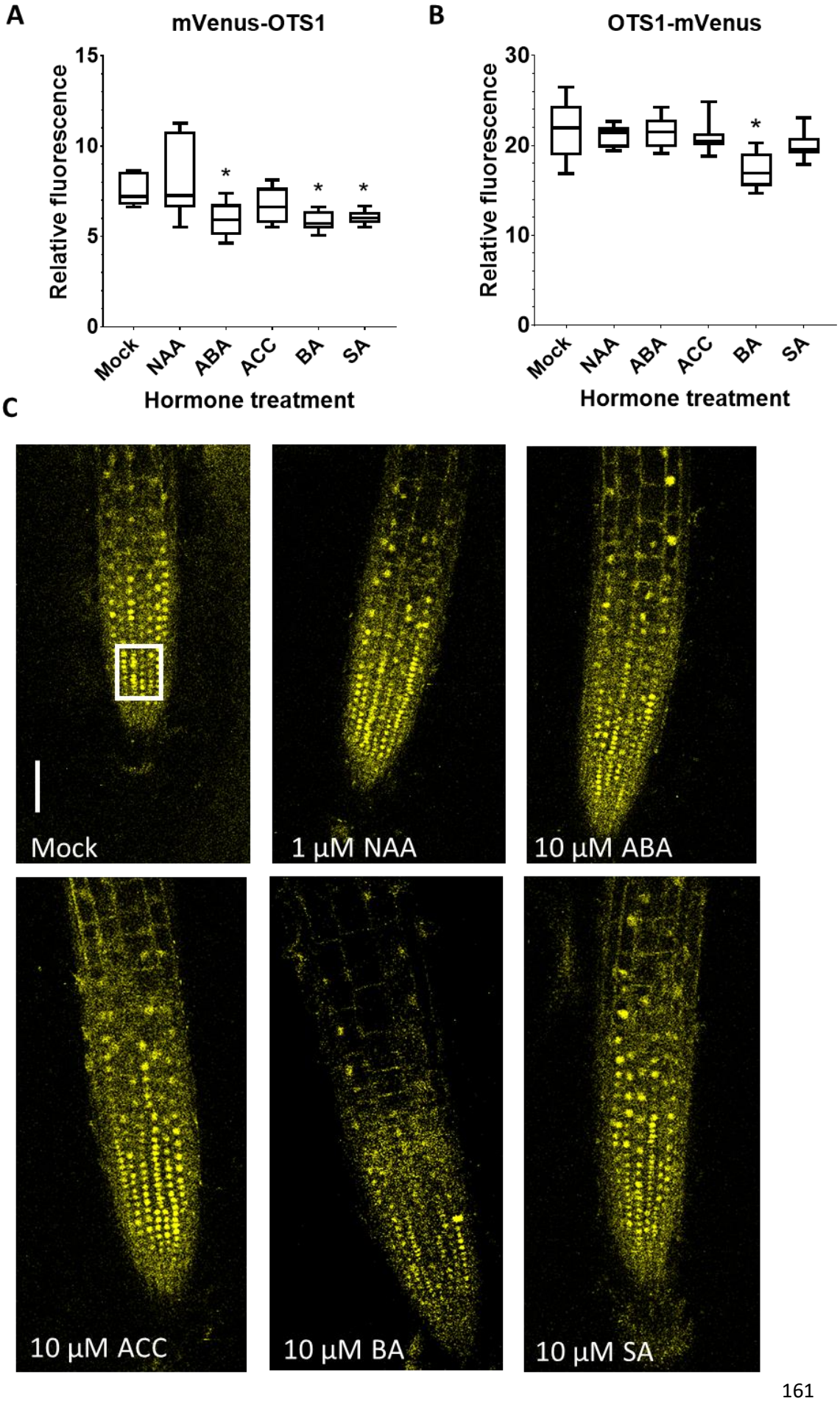
A
mVenus-OTS1
Relative fluorescence
15
10
5
0
*
*
*
Mock
NAA
ABA
ACC
BA
SA
Hormone treatment
B
OTS1-mVenus
Relative fluorescence
30
20
10
0
*
Mock
NAA
ABA
ACC
BA
SA
Hormone treatment
C
Mock
1 µM NAA
10 µM ABA
10 µM ACC
10 µM BA
10 µM SA

Figure 5.15 – Expression levels of the OTS1 translational reporter are reduced after cytokinin (BA) treatment. The mean fluorescence in an equal area of the epidermis at the root side near the laser was measured after hormone treatment. Four hour treatment with 1 µM NAA, 10µM ABA, 10 µM SA and 10 µM ACC had no effect on OTS1-mVenus fluorescence levels (A). However, 10 µM BA treatment caused a drop in fluorescence level of OTS1-mVenus. A clear reduction of OTS1-mVenus nuclear fluorescence levels was visible after BA treatment, whilst the pattern is not affected after the other hormone treatments. n=7. Scale bar represents 50 µm. Data of different hormone treatments was statistically compared to mock treatment and analysed using one-way ANOVA, asterisks indicate p≤0.05.

5.3 Discussion

5.3.1 Lateral root hydropatterning is dependent on OTS1

Plants use an adaptive response termed lateral root hydropatterning to branch only when in contact with water. Branching towards available water is regulated by SUMOylation of ARF7. On the primary root side opposing the water, termed here the air side, ARF7 is predicted to be in a SUMOylated state. SUMOylated ARF7 has repressed transcriptional activity (via interaction with the SIM site on the Aux/IAA repressor IAA3) leading to reduced expression of ARF7 targets like LR activator *LBD16*. In contrast, on the root side in contact with water, ARF7 is unmodified by SUMO and free to transcribe its downstream gene targets and activate LR initiation. Exactly how the SUMOylation status of ARF7 is controlled by external water availability remains unclear. In this chapter we demonstrate that lateral root initiation and hydropatterning is dependent on the SUMO protease OTS1. We propose a model in which OTS1 preferentially deSUMOylates ARF7 on the root side in contact with water, thereby activating ARF-dependent auxin response and LR initiation.

Hydropatterning analysis of multiple mutants in the OTS SUMO protease class demonstrated a significant defect in the *ots1-1 ots2-1* double mutant. *ots1-1 ots2-1* seedlings exhibited a general delay in seedling development with reduced primary root length and lateral root number. In contrast, *ots1-1* and *ots2-1* single mutants did not show a strong phenotypic difference from Col-0. This could be attributed to redundancy between these *OTS* genes. Consistent with this, *ots1-1* roots featured increased OTS2 expression. However, *ots2-1* showed Col-0 levels of *OTS1* transcripts. This result

suggests that *OTS2* is not as critical for root development as *OTS1* and therefore does not need increased levels of *OTS1* in the *ots2-1* mutants. It might also indicate a feedback loop between these two *OTS* genes in which OTS1 indirectly reduced *OTS2* expression. Taken together these results suggest a major role for *OTS1* in root development.

Complementation of *ots1-1 ots2-1* with p*OTS1::mVenus-OTS1* and p*OTS1::OTS1-mVenus* could restore LR formation, LR density and partially restore primary root growth. Additionally, these transgenes could fully restore *ots1-1 ots2-1* hydropatterning to Col-0 levels, indicating that solely restoring *OTS1* expression is sufficient. This result also demonstrated that OTS1 function was not disrupted by the mVenus tag, as both N- and C-terminal tagged OTS1-Venus restore *ots1-1 ots2-1* phenotypes to Col-0. Furthermore, salt and auxin treatment showed similar root phenotypic responses as Col-0, indicating a functional OTS1 protein. Interestingly, *OTS1* transcript levels were not fully restored to Col-0 levels in either of the two complementation lines. This could be a consequence of using only the *OTS1* coding sequence, as introns in the genomic sequence might enhance expression or alter tissue specific expression pattern (Truskina et al. 2020). This could also be the basis for the partial rescue of primary root growth in complementation lines. In contrast to the translational reporter, the transcriptional reporter line showed increased expression in the meristem, especially in pro-vasculature cells (Note: the transcriptional reporter employed 3x Venus, which might explain the differences observed in meristematic *OTS1* expression with translational reporters). The transcriptional reporter of OTS1 did include the first intron, which might drive expression in the meristematic zone. Surprisingly, the two translational complementation lines displayed recovery of *LBD16* expression, indicating that OTS1 expression in LR related tissues, such as the pericycle, was restored. Future work should focus on constructing a genomic OTS1 transgene to determine if inclusion of introns could restore *OTS1* expression to Col-0 levels and (potentially) fully restore primary root growth.

ARF7 and OTS1 have been demonstrated to interact *in vivo* (Orosa-Puente et al. 2018). It is likely that OTS1 deSUMOylates ARF7 in root cells facing the agar side, thereby removing SUMO-dependent suppression by IAA3 and activating expression of ARF7

downstream targets such as *LBD16*. Consistent with this model, *LBD16* expression decreased in *ots1-1*, *ots2-1* and the double mutant, equivalent to the *arf7-1* knock-out. This reduction in *LBD16* expression could be restored in the mVenus-OTS1 and OTS1-mVenus complementation lines validating a regulatory role for OTS1 on *LBD16* expression. Additionally, *ARF7* transcript levels did not alter in these *OTS* mutants. This implies that OTS1 affects downstream targets of ARF7, potentially by deSUMOylation and re-activation of ARF7 transcriptional ability.

Intriguingly, over-expressing OTS1 did not disrupt LR hydropatterning. According to our hypothesized model of hydropatterning (where a gradient of OTS1 protein exists that mirrors water availability), overexpressing *OTS1* should deSUMOylate and activate ARF7 on both agar and air side, resulting in defective LR hydropatterning. However, the opposite response is seen experimentally. This could either be due to OTS1 SUMO protease activity, rather than abundance, controlling LR hydropatterning. What form of post-translational modification OTS1 undergoes remains unclear (Barber and Rinehart 2018).

5.3.2 A gradient of OTS1 activity rather than stability appears to regulate hydropatterning

To explore whether OTS1 SUMO protease activity, rather than abundance, controls LR hydropatterning, OTS1 translational reporter lines (mVenus-OTS1 and OTS1-mVenus) were exposed to a hydropatterning stimuli. The LSFM protocol (developed in Chapter 4) was employed to image mVenus-OTS1 and OTS1-mVenus roots in the late elongation and early differentiation zones. This revealed no clearly asymmetric reporter signal on wet versus air sides of the root for either reporter, suggesting OTS1 stability is not affected by external water availability. This result, when combined with phenotypic data for *OTS1* over-expressing lines (detailed above), independently validated that a gradient of OTS1 protein stability on air versus water side does not control LR hydropatterning. Instead, a gradient of OTS1 SUMO protease activity could provide the basis for its role during the LR hydropatterning response.

OTS1, is a cysteine protease, which are known to be affected by the cellular redox environment as the thiol group of the cysteine is a target for oxidation (Berlett and

Stadtman 1997). Oxidation of the cysteine can lead to reversible and irreversible changes to protein function (Stankovic-Valentin and Melchior 2018). A close ULP family member in humans, SENP3, can recruit the chaperone protein (Hsp90) after oxidation of two of its cysteines (Yan et al. 2010). SENP3 was also shown to re-localize from the nucleolus to the nucleoplasm after hydrogen peroxide treatment, enabling it to act on new targets after mild oxidative stress (Huang et al. 2009). These results suggest a potential OTS1 activity gradient may exist which is regulated through the oxidation of cysteines, potentially involving a redox gradient between agar and air side of the primary root. Further proteomic-based studies on cell specific OTS1 redox status needs to be performed to address this question.

5.3.3 OTS1 promotes early initiation of lateral root primordia

Both OTS1 and OTS2 play important roles during lateral root branching. The *ots1-1 ots2-1* double mutants exhibit a severe reduction in LR number due to a severe delay in LR initiation. The *ots1-1* and *ots2-1* single mutants have no LR initiation defect, revealing redundancy. However, complementation of *ots1-1 ots2-1* with mVenus-OTS1 and OTS1-mVenus could restore initiation of LRP to Col-0 levels, suggesting OTS1 is important during LR initiation. As OTS1 binds ARF7, we hypothesize that OTS1 deSUMOylation of ARF7 appears necessary for the activation of LRFC through the IAA3-ARF-LBD module (Orosa-Puente et al. 2018).

Staging data revealed a distinct effect of mutating *OTS1*. *ots1-1* displayed a significant increase in LRP density in *ots1-1*, yet no difference in LR number was observed. This observation suggests that the spacing of lateral roots is altered, as no difference is observed between primary root length of *ots1-1* and Col-0. Treating *ots1-1* with 50nM NAA increased the LRP number and density but abolished the difference between Col-0 and *ots1-1*. This result might indicate an increase in pre-branch site formation or LR initiation by higher levels of endogenous NAA in *ots1-1* roots. The difference in NAA level or auxin response between *ots1-1* and Col-0 is reduced after exogenous application of NAA. Interestingly, *ots1-2gk* demonstrated a similar increase in LRP density as *ots1-1*, implying this response is specific to alterations in OTS1.

Contrary to *ots1-1*, *ots2-1* single mutants exhibited increased LRP number and LRP density when treated with 50nM NAA. This mutant seemed to be hypersensitive to auxin in LR initiation yet has only a limited primary root response to auxin. Furthermore, *OTS1* expression levels are not enhanced in *ots2-1* under normal growth conditions, indicating a less vital role for *OTS2* in LR formation. Potentially, OTS1 expression is auxin inducible over longer time frames then were observed in these experiments (4hr), which would explain why *ots2-1* but not *ots1-1* mutants show auxin induced LRP formation. The auxin inducible promoter element could potentially lie in the first intron, explaining why the OTS1 complementation lines only showed partial restoration of LRP induction after exogenous auxin treatment.

To further specify which LR developmental process OTS1 is involved in, the translational reporter was imaged in root tip tissues. This revealed OTS1-mVenus expression from late elongation zone onwards in protoxylem and xylem-pole pericycle (XPP) cells. This coincides with the tissue specific expression of *DR5::GUS* in protoxylem and XPP cells (De Smet et al. 2007). One important difference is that *DR5::GUS* expression starts in the basal meristem, whilst OTS1 showed transcription in this zone, but no translational reporter expression. This might be explained by slow maturation time of mVenus in comparison to GUS reporter lines. Hence, OTS1 might play a role in the LR oscillation zone, but this will have to be further confirmed by crossing it with *DR5::Luc* lines and observing pre-branch site formation.

Lateral root developmental stages were imaged to determine OTS1-mVenus localisation during lateral root initiation and development. OTS1-mVenus showed expression in all stages of LRP, starting from stage 1 after the first asymmetric cell division. Imaging reveal that both pOTS1::3xmVenus and OTS1-mVenus are detected after the first asymmetric cell division (De Rybel et al. 2010). This fits with the model in which OTS1 deSUMOylates ARF7, activating transcription of LR regulatory genes and primordium development. However, from this confocal data we cannot conclude if OTS1 is stable in early LRFCs and regulates nuclear migration.

OTS1 and OTS2 appeared to play a role during LRP emergence. In addition to a severely diminished rate of initiation in *ots1-1 ots2-1*, this double mutant also displayed a strong

delay in LR development. In contrast, *ots1-1* and *ots2-1* showed very similar emergence to Col-0, which revealed redundancy between OTS1 and OTS2. The *gain-of-function* mutation *ots1-2 gk* resulted in an accumulation of stage 3 and 4 primordia. These stages correspond with when the LRP has to grow through the overlying endodermis. This process involves auxin crosstalk between the growing LRP and the endodermis. This was visualised by creating the *pCASP::shy2-2* line that makes use of an undegradable Aux/IAA expressed in the endodermis resulting in an unresponsive endodermis (Vermeer et al. 2014). Over-expressing a truncated form of OTS1 could affect deSUMOylating of many proteins that might be controlling auxin induced or cell wall related processes. Key to the exact role of OTS1 in the endodermis would be to make tissue specific expressed *OTS1* lines that only express *OTS1* only in the pericycle and endodermis. This would allow investigation of tissue specific functioning of deSUMOylation. Results in this chapter clearly demonstrate the crucial role of OTS-class proteases on LR initiation and, to a lesser extent, LR emergence.

5.3.4 Could other SUMO proteases affect lateral root hydropatterning?

This chapter has mostly focussed on the OTS class of SUMO proteases, as *OTS1* is the highest expressed ULP protease in root tissues. However, other SUMO proteases could contribute to ARF7 deSUMOylation. Of the six ULP family members tested for iso- and peptidase activity, ESD4, OTS1 and OTS2 have both high peptidase and isopeptidase activity on SUMO1 and SUMO2 (Chosed et al. 2006; Conti et al. 2008). ELS1 has a greater peptidase activity than isopeptidase, suggesting a limited role in SUMO deconjugation (Chosed et al. 2006; Hermkes et al. 2011). Likely, SPF1 and SPF2 mature only SUMO1 and have isopeptidase activity limited to the inflorescence (Liu et al. 2017). Contrary to the ULP family, the DeSI family did not show any peptidase activity in mouse and are hypothesized to be only involved in SUMO deconjugating (Shin et al. 2012; Suh et al. 2012). The only functionally studied DeSI member in plants, DeSI3a, suggests a similar deconjugating function in plants (Orosa et al. 2018). Further analysis of under studied ULP and DeSI's family members could highlight potential unknown roles for these deSUMOylation protease in root development.

Next to the specificity of SUMO proteases, other components of the SUMOylation machinery could affect LR hydropatterning. In our hydropatterning bioassay no defect was found in *siz1-3* knock-out mutants, encoding a SUMO E3 ligase (Supp. Fig. S5.5A-D). However, no detailed analysis of *hpy2* mutants has been conducted yet. Additionally, no study has been undertaken in assessing the role of the E2 SUMO conjugator SCE1 in LR hydropatterning. This is mainly due to the embryo lethality when knocking out *SCE1* expression, demonstrating the importance of SUMOylation in embryo development (Saracco et al. 2007). Three T-DNA lines in the promoter of SCE1 are available for further root development analysis, as these displayed reduced SCE1 transcript and protein levels as well as exhibit reduced levels of SUMOylated conjugates. However, these mutants did not show an altered phenotype and this suggests that the reduced levels of SCE1 can be tolerated (Saracco et al. 2007). A lot of questions still remain unanswered about components of the SUMO machinery and their importance in LR hydropatterning. Studying the effect of mutants in the SUMO pathway and resolving their expression pattern in the root will reveal the importance of SUMOylation in root development and LR hydropatterning.

Supplemental figures

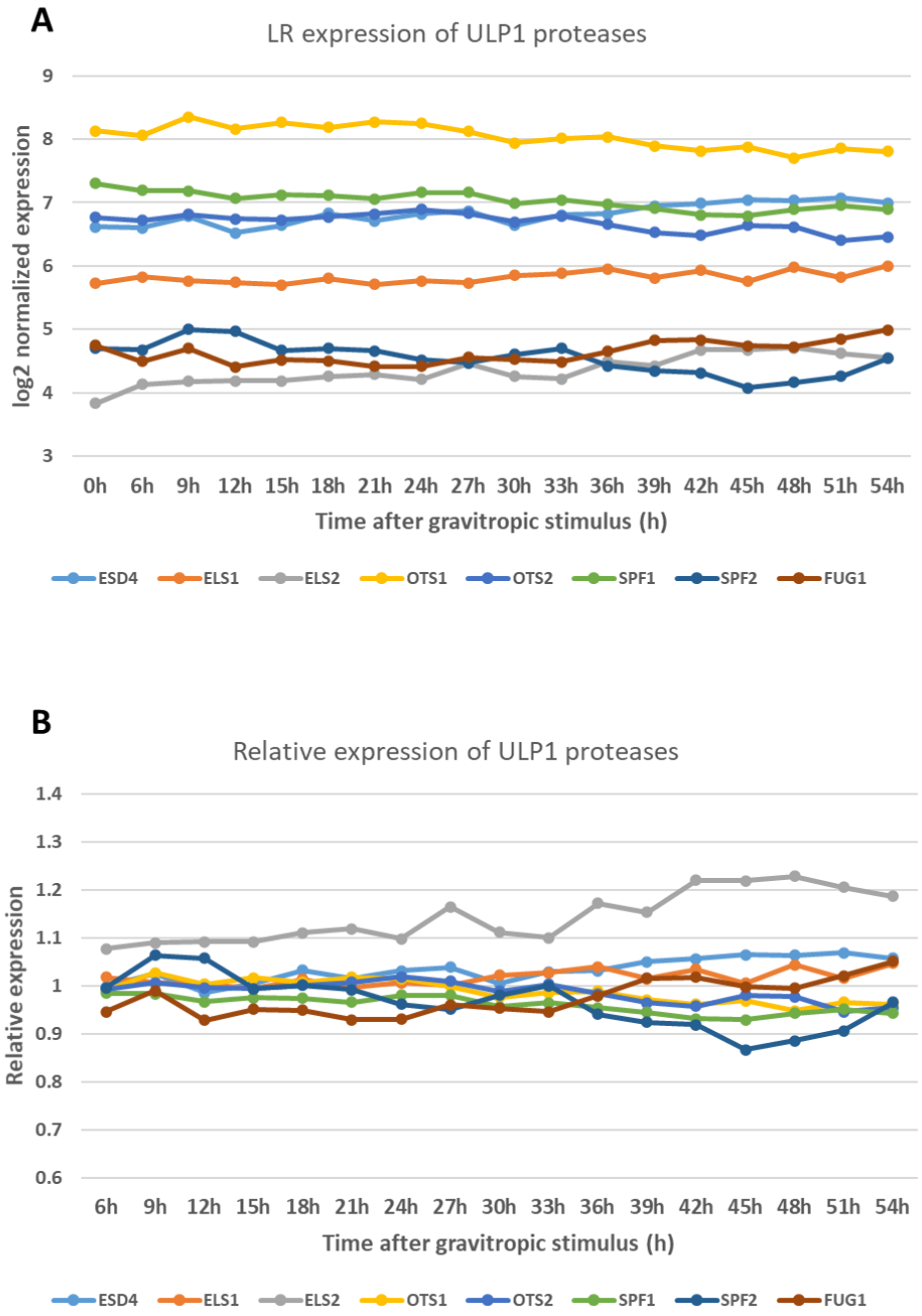

Figure S5.1 – Normalized and relative expression data of ULP1 proteases during LR development. Normalized expression of all eight ULP1 SUMO proteases during LR development, which was synchronised by a gravitropic stimuli (A). Relative expression of the same gene targets relative to time point 0h. Expression data was shared from previously published material (Voβ et al., 2015).

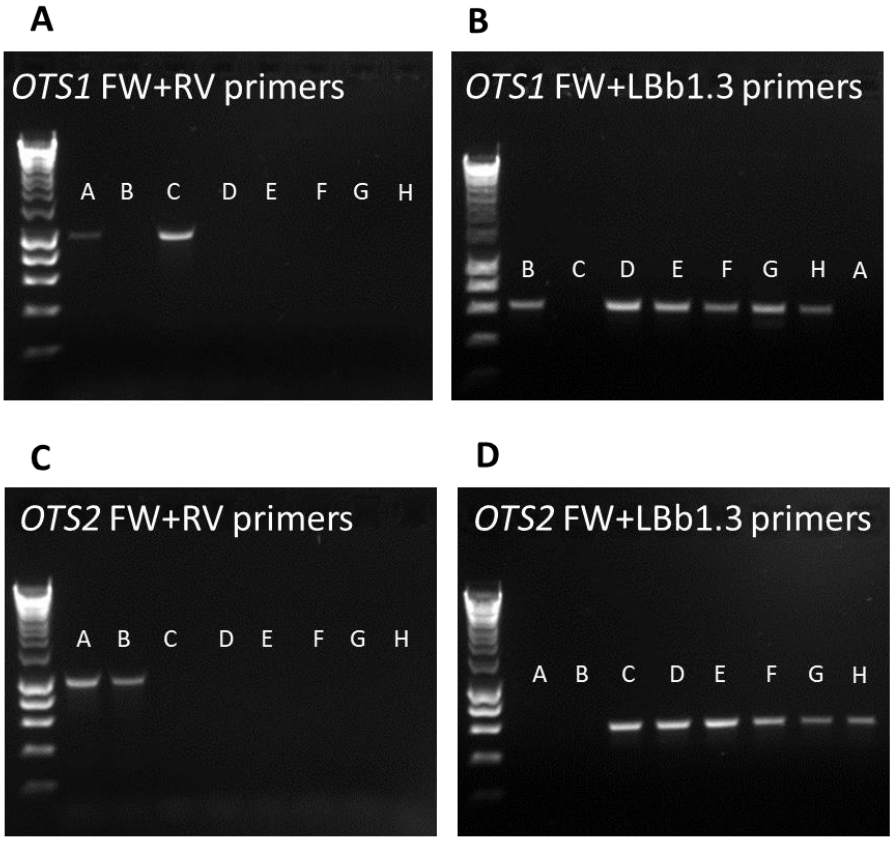

A. Col-0
B. ots1-1
C. ots2-1
D. ots1-1 ots2-1
E. pOTS1::Venus-OTS1 *ots1-1 ots2-1*
F. pOTS1::OTS1-Venus *ots1-1 ots2-1*
G. pOTS1::gOTS1-GFP *ots1-1 ots2-1*
H. XVE::OTS1-mVenus 6 *ots1-1 ots2-1*

Figure S5.2 – Genotyping for confirming SALK insertion lines. For primers used see Chapter 2. Note that no bands are visible in OTS1 restoration transgenics as the OTS1_RV primer is located in the 3' region.

A

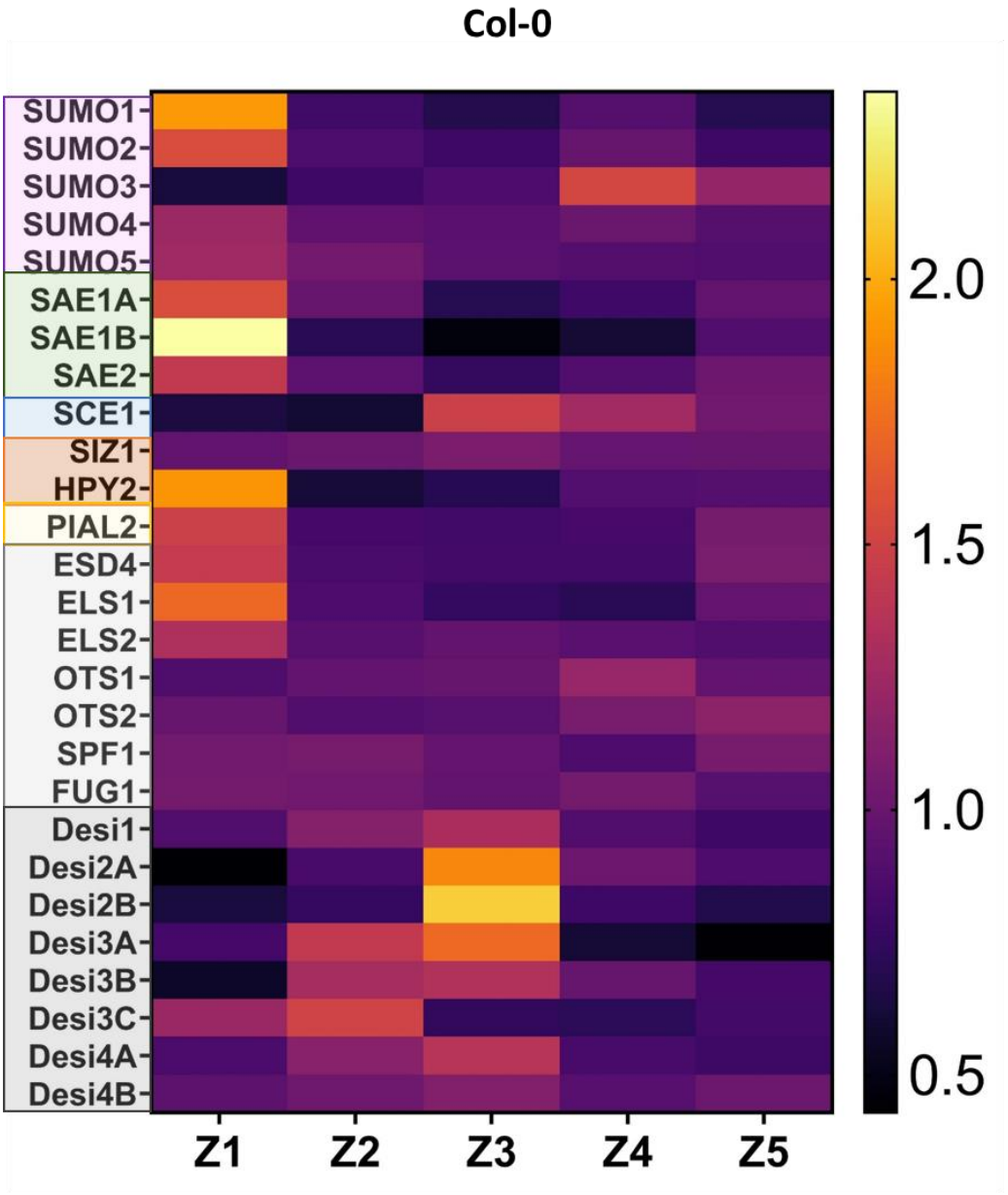

Z1 - Meristem (Until root cap)
Z2 - Rapid Elongation zone (until first root hair bulge)
Z3 - Late elongation zone (until first fully elongated hair)
Z4 - Differentiation zone (500um above Z3)
Z5 - lateral root zone

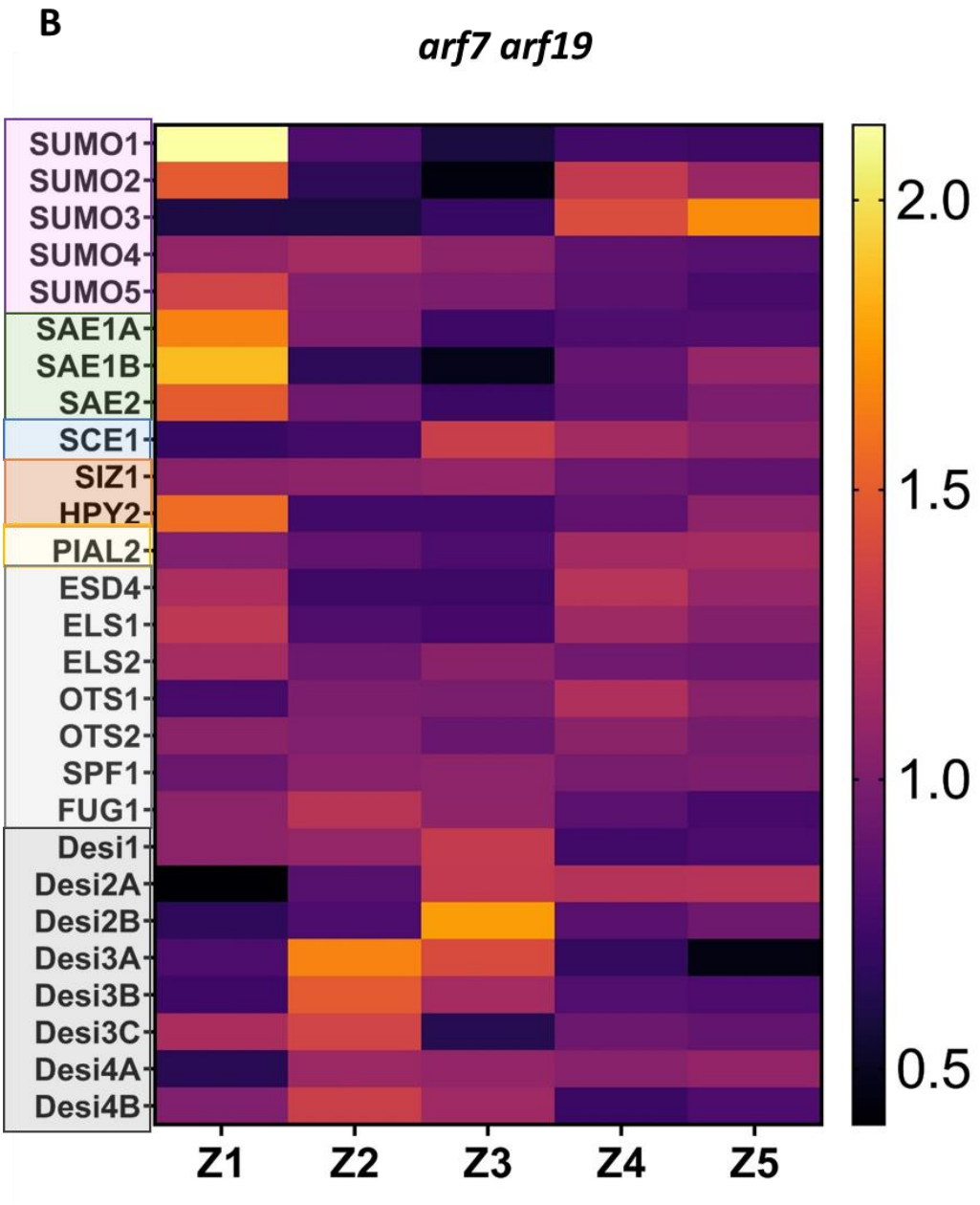

Figure S5.3 – Expression profile of SUMO related genes in specific root zones. The Brady (2007) microarray root dataset was re-analysed to visualize relative expression of SUMO related genes from meristematic zone (Z1) until lateral root zone (Z5). Different colours indicate difference in relative expression of each SUMO gene within the five zones compared to the average expression of that gene (A). The expression of these SUMO genes was also analysed in the arf7 arf19 five zone root dataset (B).

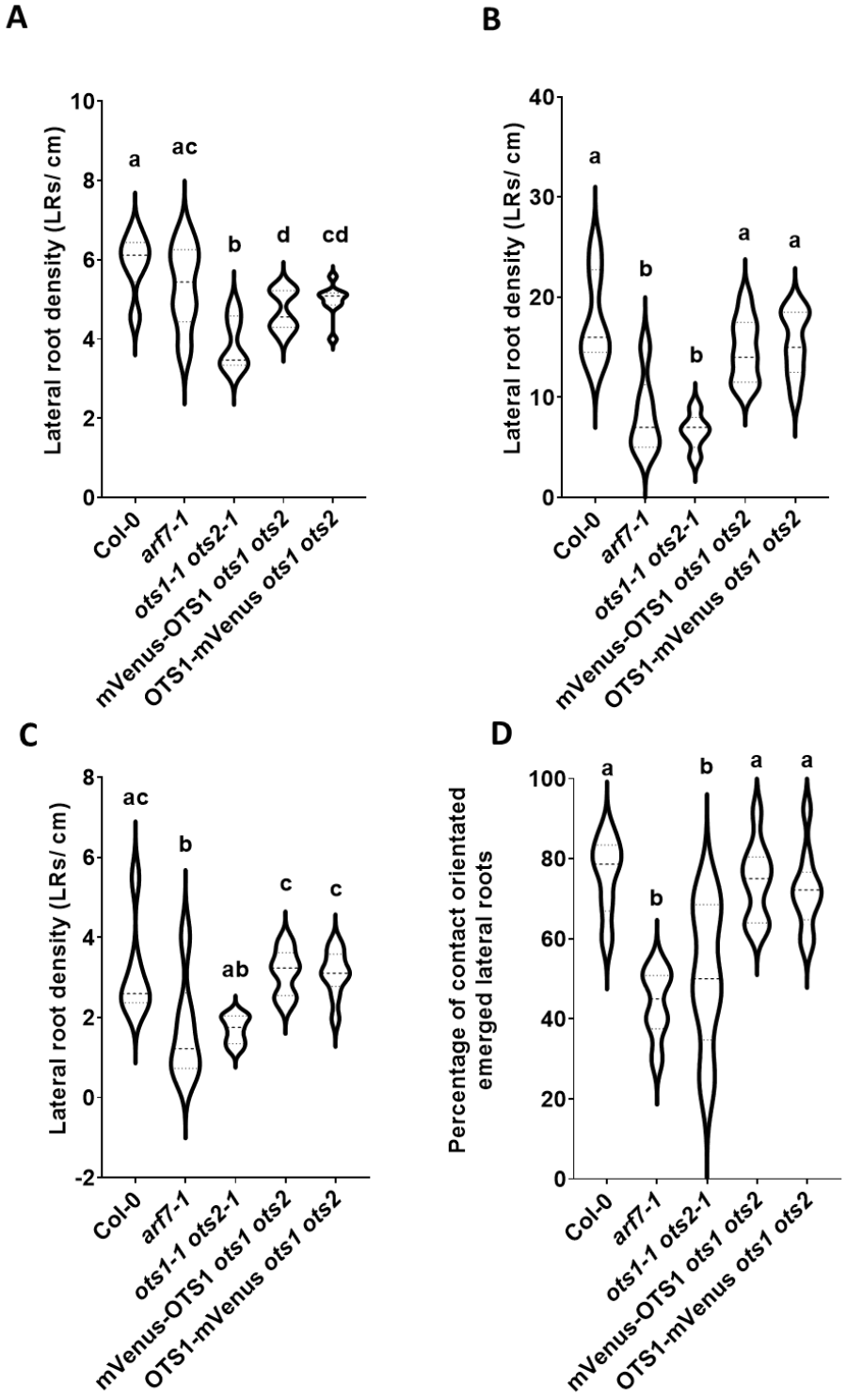

Figure S5.4 – mVenus-OTS1 and OTS1-mVenus transgene partially restores primary root growth and full restores lateral root number and density and contact orientated LRs. Primary root growth of mVenus-OTS1 and OTS1-mVenus is increased compared to ots1-1 ots2-1 but not to Col-0 levels (A). mVenus-OTS1 and OTS1-mVenus exhibits a restoration of number of LR (B), LR density (C) and LR hydropatterning (D) to Col-0 levels. Violin plots show relative data distribution. Different letters indicate significant difference between lines, p≤0.05, one-way ANOVA, Tukey's HSD test, n=8-10.

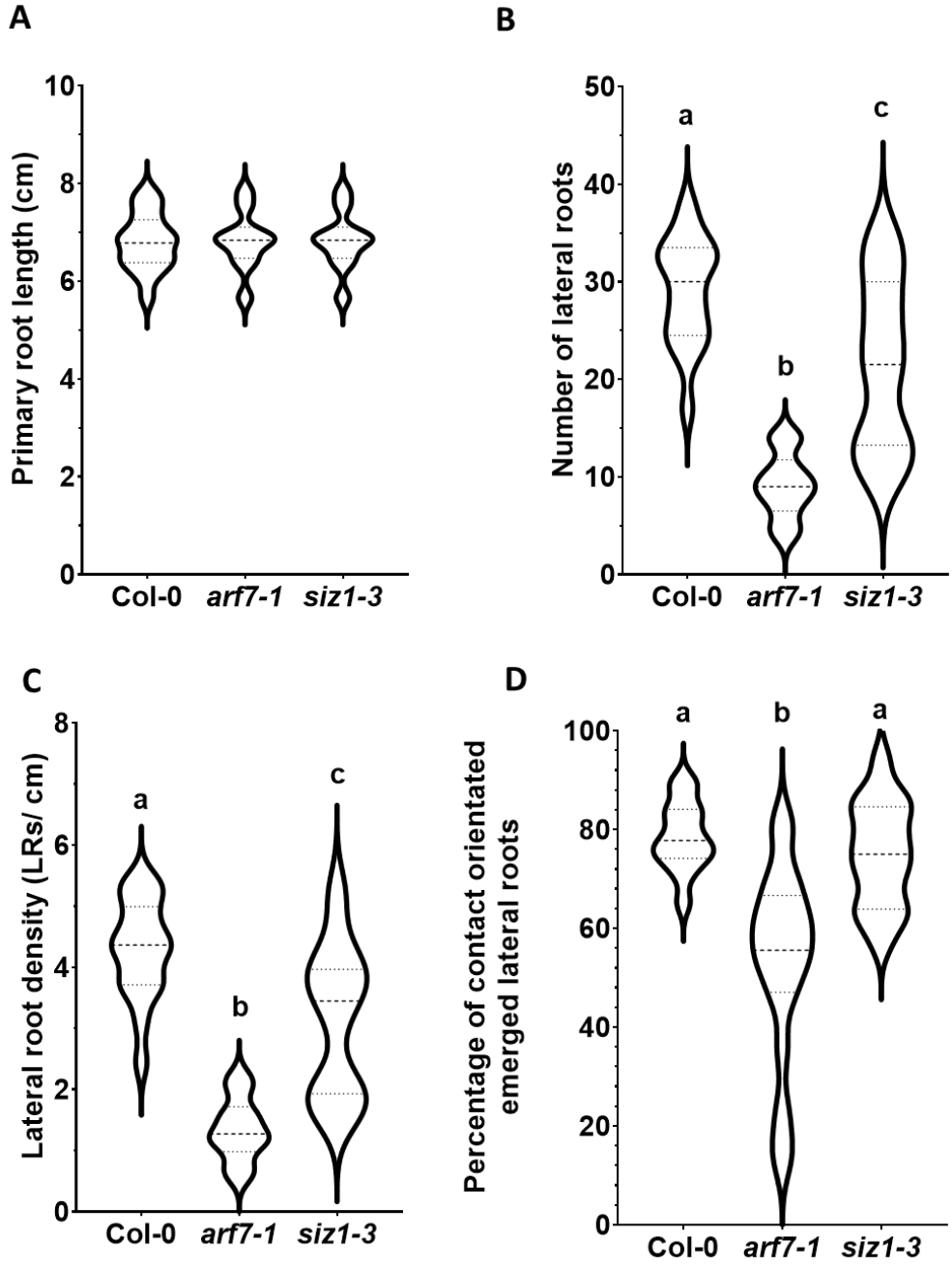

Figure 5.5 – *siz1-3* mutants display reduced number and density of LRs, but do not have a LR hydropatterning defect. Primary root growth of Col-0, *arf7-1* and *siz1-3* is similar (A). *siz1-3* exhibits a decreased number of LR (B) and LR density (C) but does not have a hydropatterning defect (D). Violin plots show relative data distribution. Different letters indicate significant difference between lines, p≤0.05, one-way ANOVA, Tukey's HSD test, n=10-12.

6. GENERAL DISCUSSION

The root system is crucial for plants to forage in soil for nutrient and water resources. The high plasticity of root development in response to the distribution of resources in soil enables plants to forage efficiently. Developmental plasticity in roots is controlled by multiple environmental sensing mechanisms. For example, several studies have discovered root adaptive traits that regulate root development plasticity in response to water distribution. Two of these water-related adaptive responses regulate root angle: hydrotropism controls primary root bending towards regions of high moisture content (Dietrich et al. 2017), whilst xerotropism contributes to the steepness of lateral root growth in response to drought conditions (Rellán-Álvarez et al. 2015). Both responses allow longitudinal changes in root growth direction in order to access areas of high water availability. Other related adaptive responses regulate lateral root branching. In the case of xerobranching, root exposure to an air gap inhibits lateral root initiation from the very first stage of development, thus preventing the plant from forming branches in zones without water (Orman-Ligeza et al. 2018). When a root is exposed to water on only one side, lateral roots preferentially emerge on this side, employing the adaptive mechanism termed lateral root hydropatterning (Bao et al. 2014). The combination of these and other root adaptive responses mould 3D root system architecture to improve its ability to efficiently forage for soil resources. In this thesis we focused on elucidating molecular, cellular and tissue scale pathways regulating lateral root hydropatterning.

6.1 Hydropatterning regulates lateral root initiation and emergence

Hydropatterning represents a fascinating water-related root adaptive response. Earlier work demonstrated that lateral roots preferentially emerge towards agar when seedling roots are grown along the surface of vertical petri plates (Bao et al. 2014). This study highlighted two working models for hydropatterning. In the first, xylem pole selection and LRFC specification are independent of water, leaving LR initiation and emergence to steer new root branches towards water. The second model predicts that the local radial water bias directs the selection of xylem pole and LRFC specification. Surprisingly, my thesis studies found that both models appeared incorrect. Light Sheet

Fluorescence Microscopy (LSFM) enabled imaging of LRP initiation and emergence relative to roots growing along vertical agar surfaces. This method revealed no bias in lateral root initiation between the xylem pole near agar and the pole near the air exposed side. This was further supported by the asymmetrical expression of gLBD16-GFP in the elongation zone. Instead, LRP have a higher degree of flexibility in terms of initiation and outgrowth angle. LRP did not initiate and emerge in a straight line with the xylem pole axis but could deviate significantly from this axis. When a LRP initiated near the xylem pole on the air side, the LRP showed a high degree of bending leading to emergence on the agar side. This LRP angle from the xylem pole axis was termed lateral root deviation angle. The LR deviation angle is a product of two developmental processes. Firstly, work with the gLBD16-GFP reporter displayed cases of strong deviation angles observed from the onset of LR initiation. This data implies that the selection of XPP cells to form LRFCs is highly flexible. Secondly, a bias in radial cell divisions in one flank of the developing LRP can steer LRP outgrowth. The combination of these developmental processes directs organ outgrowth.

The LR deviation angle is strongly affected by water availability, as roots grown in water or agar exhibited reduced deviation angles. LRP initiating in parallel to the agar surface displayed the smallest deviation angle, whilst LRP initiating near the agar or air side displayed strong deviations. This horizontal outgrowth of LRs could be caused by high water uptake through the meniscus. Potentially, signalling molecules that flow from the external environment towards the xylem pole driven by water influx influence LR angle. One target molecule for this role is auxin for two main reasons. Firstly, auxin levels accumulate in epidermal cells in the basal meristem and elongation zone (Band et al. 2014). Radial water influx may then co-mobilise water and auxin towards the inner root tissue via symplastic transport. Another reason is that auxin distribution has been shown to be affected by plasmodesmatal (PD) transport in the root apex, which is likely how water moves from epidermis to xylem pole tissues (Mellor et al. 2020). This led to a new model for LR hydropatterning (Fig. 6.1A) in which auxin, originating from epidermal cells in the elongation zone, moves through PD towards XPP cells driven by water influx from the meniscus. This would allow auxin accumulation in XPP cells in line

with the meniscus and would account for the flexibility of XPP selection observed in our assay.

The genetic pathway regulating LR hydropatterning still needs further elucidation. We began by assessing the hydropatterning response in ARF regulated genes as LR hydropatterning was shown to be dependent on auxin signalling (Bao et al. 2014). Multiple LBD knock-out mutants were screened as these genes are direct or indirect targets of ARF7 (Lavenus et al. 2015). Only *lbd16-1* mutants exhibited a hydropatterning defect on our plate based bioassay. Analysis of *LBD16* over-expression lines demonstrated a loss of LR hydropatterning more severe than observed in *lbd16-1* mutants. LSFM work demonstrated that *LBD16* over-expression reduced LRP deviation angle, which explains why this line exhibits such a strong LR hydropatterning phenotype as it cannot angle its LRP towards the agar when LRFCs are specified on the air side. Interestingly, no LRP deviation angle defect was observed in *lbd16-1*, suggesting genetic redundancy within this gene family. LBD16 is key in initiating nuclear migration and the coordination of the first asymmetric division of the LRFCs (Goh et al. 2012a). However, LBD16 has no established role in LRFC selection. The *LBD16* OE data indicates cell specific expression of *LBD16* in XPP cells is necessary to promote LR deviation but likely LBD16 is not the key driving factor determining LRFC specification during hydropatterning. More likely upstream regulators of *LBD16* coordinate its XPP cell file specific expression, which is necessary for the flexibility observed in selection of LRFCs.

In the early elongation zone gLBD16-GFP reporter expression is first observed in the inner vasculature tissue. These cells are termed xylem-procambium cells and are located next to the xylem pole and proto-xylem cells (Smetana et al. 2019). Procambium cells act as stem cells for secondary vasculature growth through ARFs similar to LR initiation. Could xylem-procambium cells coordinate LRFC specification through mobile transcription factors? A likely candidate for this role is *LBD16* as its expression was observed in both xylem-procambium cells and XPP cells. LBD16 is a relatively small protein, approximately 27 kDa, which enables it to move through plasmodesmata between endodermis, pericycle and inner vasculature tissues even when tagged with GFP (Rim et al. 2011). Future experiments should focus on creating an immobile LBD16 construct by tagging it with 3xmCherry to assess how mobility affects LBD16 functioning

in LR formation. If we combine this with our previous model of root water uptake and LRFC selection it creates a two-component model (Fig. 6.1A). In this model xylem-procambium cells accumulate auxin, which stabilizes ARFs and induces expression of targets like *LBD16*. *LBD16* RNA or protein could be mobilised into adjacent XPP cells, where the combination of radial auxin inflow from the epidermis and mobile transcription factors from the adjacent xylem-procambium cells could function to specify XPP cells for LR initiation. This double checkpoint allows for greater flexibility of LRFCs and ensures optimal positioning of LRP to capture water.

Developing primordia emerge towards the agar driven by radial divisions in the flanking cells (Fig. 6.1B). Radially a primordium comprises of five to eight pericycle cell files (Von Wangenheim et al. 2016). The central file undergoes the first anticlinal division and in later stages forms the quiescent centre (Goh et al. 2016). The boundary of the flanking cell files is determined by the phloem pole pericycle (PPP) cells, which appear to lack the meristematic potential that XPP cells demonstrate (Torres-Martínez et al. 2020). Recruiting these PPP cells is invaluable for forming the new vascular connection between primary and lateral root. Recruitment of neighbouring cell files by the central cell file is dependent on auxin signalling and transport (Torres-Martínez et al. 2020). The highest auxin response is visible in the primordium tip, whilst a low auxin response is visible at the sides and base of the primordium (Benkova et al. 2003). This pattern is maintained by PIN auxin transporters which dynamic rearrangements drives auxin fluxes in the LRP (Benkova et al. 2003). Potentially these PINs are based in cells surrounding the tip to maximize the auxin flux towards the tip thereby regulating cell division. Alterations in PIN location or activity could lead to a bias in auxin distribution within the developing primordium (Fig. 6.1B). This could result in higher levels of auxin in one flank of the primordium which could drive increased cell division and steer the growth of the primordium towards one side. Another option is that the auxin flux in the overlying layers of the primordium steers the deviation angle. An auxin reflux controlled by LAX3 and PIN3 coordinates cell wall remodelling enzymes that enable emergence of the developing primordium (Peret et al. 2013). Could these transporters be affected by external water availability? Potentially auxin distribution in the overlying tissues by PIN3 and LAX3 could actively steer emergence towards external water (Fig. 6.1B). Future

work with fluorescent reporter and knock-out mutants in these transporters should focus on the precise role of auxin transport in enabling lateral root deviation towards water.

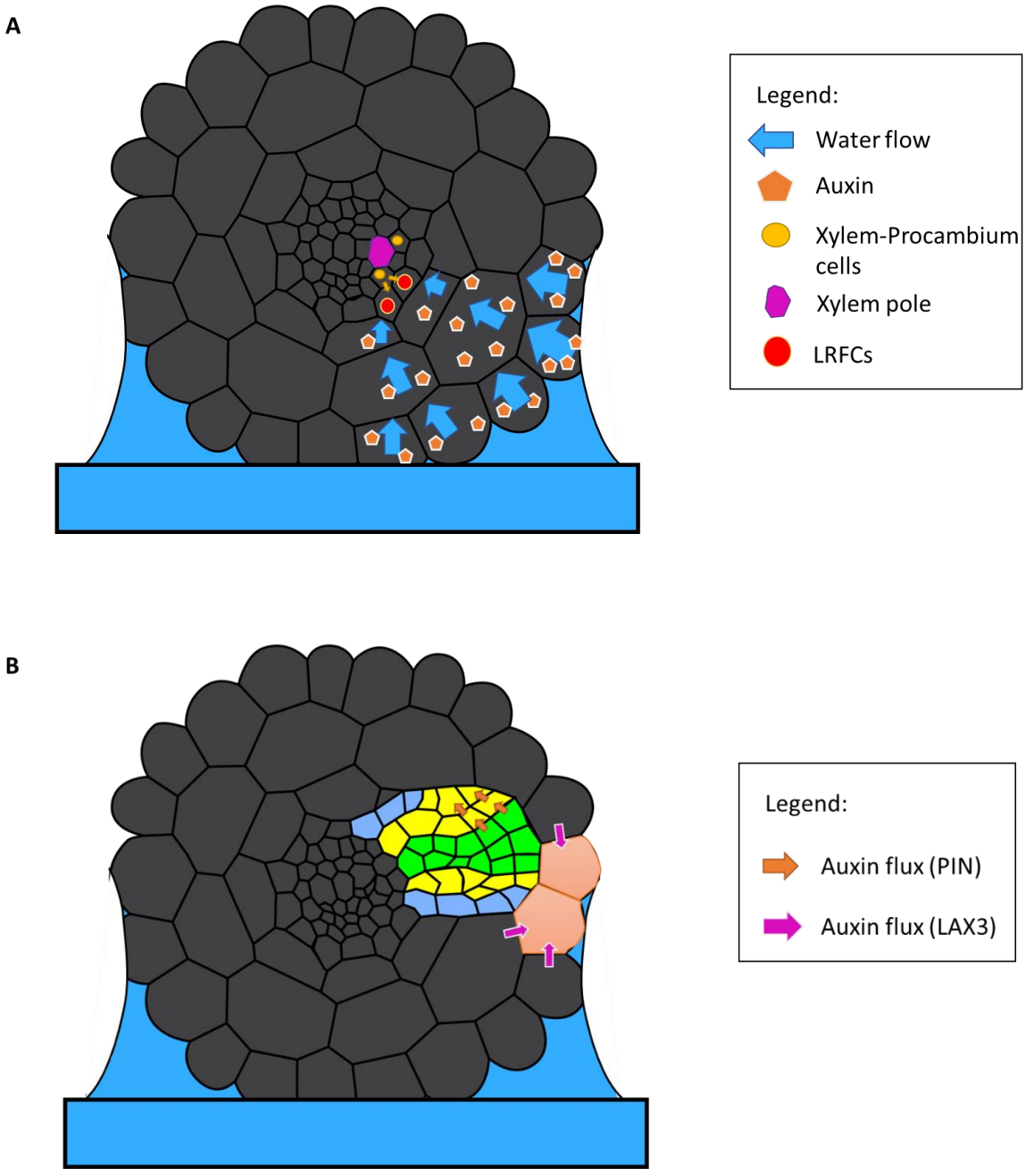

Figure 6.1 – The hypothesized model controlling LRFC specification and LRP angling affected by the external hydrological environment. We propose a model to explain the flexibility observed in LRFC selection, in which water movement from the external agar source, promotes the symplastic movement of water (blue arrows), and soluble such as auxin (orange pentagon), towards the xylem pole (purple). This generates auxin accumulation in XPP cells neighbouring the xylem pole, which mark a subset of XPP cells for LRFC initiation (red circles). Additionally, *LBD16* expressed in the xylem-

procambium cells (yellow circles) could move to adjacent cells to further stimuli the first asymmetric division to generate a lateral root. In the second model we propose that LRP deviation angle is also altered at the later developmental stage through increased cell division in the flanking cell files. Here, the green LRP cells represent the central cell file derived from the first periclinal cell that undergoes asymmetric cell division. The flanking cell files are indicated in yellow and blue. Increased radial division are observed in the yellow cell file exposed to the air side, forcing the LRP towards the agar. This developmental process might be steered by PIN efflux carriers (orange arrow), which orchestrate the distribution of auxin through the LRP. Another possibility is that the overlying tissue steers the emergence path. PIN3 and LAX3 auxin transport (purple arrow) could direct auxin into overlying cells near the agar side, thereby influencing the deviation angle of the developing primordium.

6.2 SUMOylation regulates ARF7 activity during lateral root hydropatterning

One of the major regulators of LR formation and *LBD16* is AUXIN RESPONSE FACTOR7 (ARF7) (Lavenus et al. 2015). *A. thaliana* contains five transcriptional activating ARFs termed *ARF 5, 6, 7, 8* and *19* (Ulmasov et al. 1999; Tiwari et al. 2003). When mutants in these activating ARF's were screened for LR hydropatterning defects, only *arf7-1* exhibited radially unbiased LR emergence (Orosa-Puente et al. 2018). Hence, LR hydropatterning is dependent on ARF7. Over-expression of *ARF7* could restore LR hydropatterning in *arf7-1* background, which confirmed the importance of ARF7 in this response (Orosa-Puente et al. 2018). In addition, *ARF7-Venus* was observed in all root cells and no asymmetry of fluorescent signal was visible, contrary to what was detected with gLBD16-GFP. These observations indicate that rather than tissue-specific expression of *ARF7*, LR hydropatterning is most likely driven by protein activity (Orosa-Puente et al. 2018). In collaboration with prof. Ari Sadanandom, University of Durham, we identified four small ubiquitin-like modifier (SUMO) sites on the ARF7 protein sequence and confirmed that ARF7 was target for SUMO modification (Orosa-Puente et al., 2018; Fig. 6.2A). This post-translational modification enables substrates to rapidly alter their subcellular localisation, stability, 3-D protein structure and interaction partners (Morrell and Sadanandom 2019). Mutating the four lysine cores of these SUMO sites could completely inhibit ARF7 and SUMO interaction (Orosa-Puente et al. 2018). This non-SUMOylatable ARF7 construct, termed ARF7^{4KR}, was unable to restore LR hydropatterning in the *arf7-1* background, whilst full restoration was observed in the

ARF7^{WT} transgene, indicating that SUMOylation of ARF7 regulates LR hydropatterning. ARF7^{4KR} crossed with the gLBD16-GFP translational reporter, showed increased fluorescence levels in the root elongation zone relative to ARF7^{WT}. Furthermore, ChIP-PCR detected higher levels of ARF7^{4KR} binding to *LBD16* and *LBD29* promoters (Orosa-Puente et al. 2018). These results indicate that ARF7^{4KR} is more active than the SUMOylatable ARF7^{WT}.

Protein immunoprecipitation data showed increased ARF7 SUMOylation after 20 min of transient drought stress, suggesting that the absence of water promotes ARF7 SUMOylation (Orosa-Puente et al. 2018). Modelling approaches of LR hydropatterning reveal a strong difference in water potential between agar and air exposed side across the root axis driven by root elongation (Robbins and Dinneny 2018). The difference in water potential might drive the SUMOylation of ARF7 on the air exposed side of the root, thereby limiting the auxin response. SUMOylated ARF7 can interact with the SUMO interaction domain (SIM) site on IAA3/SHY2. However, ARF7^{4KR} and IAA3 with mutated SIM site could no longer interact, indicating the importance of this SUMO-SIM interaction. TPL repressor proteins and the TIR1/AFB auxin receptor could still bind mutated IAA3, suggesting that this mutation specifically affects ARF7-IAA3 interaction (Orosa-Puente et al. 2018). Increased levels of ARF7 SUMOylation on the air exposed side would lead to increased interaction of ARF7 and IAA3 repressor proteins causing ARF7 proteasomal-mediated degradation and reduced expression of target genes like *LBD16*. This would result in decreased LR formation on the air exposed side. In contrast, low levels of ARF7 SUMOylation on the agar exposed side diminishes ARF7 and IAA3 interaction. This would translate to higher ARF7 transcriptional activity and increased expression of LR formation genes such as *LBD16* and *LBD29*.

LR hydropatterning is dependent on the asymmetric expression of ARF7 direct target *LDB16*. The asymmetric expression of gLBD16-GFP was absent in *arf7-1* background, suggesting it is driven by ARF7 activity. Additionally, ARF7-Venus was expressed in most root cells and did not exhibit an asymmetry. Hence, gLBD16-GFP asymmetry is dependent on the activity of ARF7. The expression of *LBD16* is partially regulated by SUMOylation. ARF7^{4KR} crossed with gLBD16-GFP lines revealed a decline in asymmetry compared to gLBD16-GFP in ARF7^{WT} background. The asymmetry in gLBD16-GFP

expression is established in the elongation zone, suggesting it might be the result of DR5 oscillations starting at the basal meristem (De Smet et al. 2007; Moreno-Risueno et al. 2010). The oscillating DR5 signal is the driving force behind alternating left-right LR patterning which fits with the observed asymmetrical expression of *LBD16*. LBD16 is important for inducing nuclear polarisation and the first asymmetric cell division but does not play a role in LRFC specification (Goh et al. 2012a). If the asymmetric expression of *LBD16* is perturbed in *arf7-1* and ARF7 ^{4KR} lines in the elongation zone, this implies SUMOylation of ARF7 affects later stages of DR5 oscillation and possibly LRFC specification. *arf7-1* mutants were shown to exhibit reduced pre-branch site formation as a result of reduced DR5 oscillation (Moreno-Risueno et al. 2010). It would be interesting to observe if ARF7 ^{WT} and ARF7 ^{4KR} can increase pre-branch site numbers, or if SUMOylation of ARF7 affects DR5 oscillation. ARF7 SUMOylation might affect LRFC specification which would fit data from Chapter 3 where we observed high flexibility in LRFC selection affected by radial water availability. The selection of LRFCs is controlled by another auxin signalling module consisting of IAA28-ARF7-GATA23 (De Rybel et al. 2010). Hydropatterning could affect the radial localisation of GATA23 by inactivating ARF7 through SUMOylation on the air exposed side. Future confocal analysis will have to decipher if the expression of GATA23 in XPP cells is linked to water availability. From this data it is likely that SUMOylation of ARF7 targets LRFC specification, but we cannot rule out a role in the oscillation zone.

It is still unclear how the four SUMO sites on ARF7 regulate its transcriptional activity. Two SUMO sites, K151 and K282, exhibited strong conservation of the core lysine and surrounding residues in several evolutionary lineages stemming from *Marchantia polymorpha* (representing Liverworts). In contrast, these sites were not conserved in the proto-ARF of the charophyte *M. caldariorum*. Research into auxin signalling suggests that charophytes probably did not have a distinct response to auxin (Mutte et al. 2018). The auxin signalling network evolved in liverworts where the three components that make up the auxin signalling pathway are present, i.e. TIR1/AFB, AUX/IAA and ARF (Mutte et al. 2018). Intriguingly, K151 and K282 are only present in class-A activating ARFs in *M. polymorpha*. Could SUMOylation of activating ARFs have been evolved as a way to fine-tune levels of auxin response? Mutating these SUMO sites

in *M. polymorpha* class-A ARF could elaborate on the importance of SUMOylation of the activating class of ARFs.

K151 and K282 sit in the highly conserved DNA-binding domain (DBD) of ARF7. K151 is located in the B3 subdomain that controls ARF and DNA binding and could directly influence DNA binding affinity (Fig. 6.2B). This would fit with ChIP-PCR data of non-SUMOylatable ARF7^{4KR} which showed increased binding to the promoter of *LBD16* and *LBD29* compared to ARF7^{WT} (Orosa-Puente et al. 2018). K282 is located in the ancillary domain of ARF7 and possibly affects dimerization of ARFs together with K104 in the flanking region of the DD1 (Fig. 6.2B). K104 is a less conserved SUMO site and probably evolved more recently in ARF7 and ARF19. This might have enabled tighter control of ARF7 and ARF19 homo- and heterodimerization. SUMO site K890, near the 3' of the middle region, is evolutionary well conserved and in ARF7 might affect binding to IAA3 through SUMO-SIM interaction (Fig. 6.2B). Another possibility is that SUMOylation of K890 inhibits binding of co-factors such as the SWI-SNF complex, which directs chromatin remodelling. Supressing this binding could lead to condensed chromatin around ARF7, supressing transcriptional ability. More detailed analysis of 1K/R and 3K/R lines will help to reveal the specific role(s) of each SUMO site on ARF7 activity.

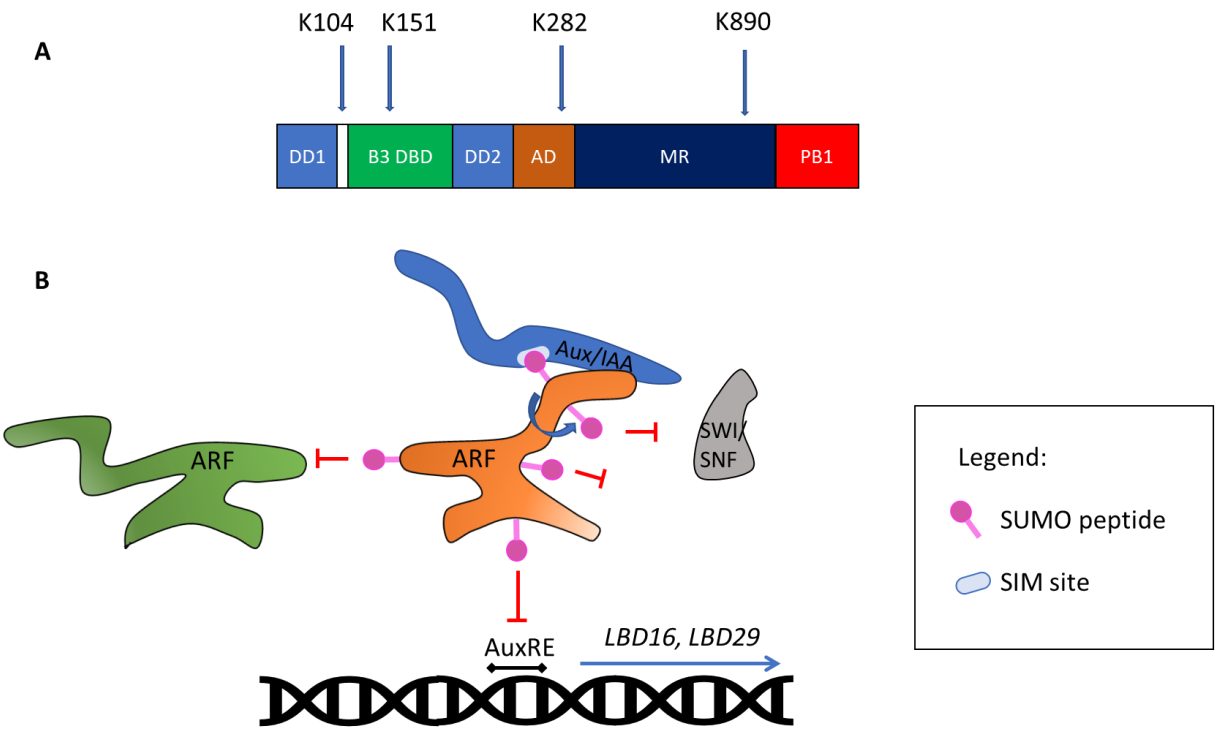

Figure 6.2 – ARF7 SUMOylation can affect protein activity in several ways. The protein domain structure of ARF7 indicates the positions of the SUMO sites, named after the lysine core amino acid (A). SUMOylation of K104 could affect homo- and heterodimerization of ARFs. K151, located on the DNA-binding domain, could affect binding to AuxRE and inducing transcription of targets likes *LBD16* and *LBD29*. The SUMO site on the Ancillary Domain (AD) could affect dimerization, but it is not yet known what the exact role of this domain is. SUMOylation of K890 could strengthen binding of IAA3 and ARF7, but could also inhibit binding of co-factors such as the SWI/SNF chromatin remodelling complex. Abbreviations: DD1&2: Dimerization domains 1 and 2. B3 DBD: B3 DNA-interaction Domain. AD: Ancillary Domain. MR: Middle Region. PB1: Phox and Bem 1.

6.3 SUMO protease OTS1 regulates LR hydropatterning

How is ARF7 SUMOylation status regulated in the elongation zone? SUMOylation of a target substrate is controlled by E1 activating, E2 conjugating and E3 ligating enzymes. Only a limited number of these enzymes can be found in the *A. thaliana* genome and only one of the crucial E2 conjugation enzyme. Hence, it is thought that deSUMOylation of substrates is key in regulating developmental processes. Many classes of deSUMOylating proteins can be found in the *A. thaliana* genome. They are divided into two groups: Ubiquitin-Like Proteases (ULP) and deSUMOylating isopeptidases (DeSi). Recent work suggests that the DeSi family only control deSUMOylation (Orosa et al. 2018), whilst the ULP's control both SUMO maturation and substrate deSUMOylation

(Chosed et al. 2006). The ULP family consists of eight family members that can be further divided into four classes based on their distinct N-terminal (Castro et al. 2018). The OTS class of ULP is highly expressed during LR development (Supp. Fig. 5.1) and *ots1-1 ots2-1* double mutants exhibit severe response to salt stress (Conti et al. 2008). However, over-expressing of *OTS1* led to an increased tolerance to salt, suggesting OTS1 might regulate osmotic responses (Conti et al. 2008). We further characterized the root architecture in *ots1-1 ots2-1* and observed severe primary and lateral root defects. Additionally, the double mutant was defective in hydropatterning, indicating a potential role in water sensing. The LR defect in *ots1-1 ots2-1* was caused by a severe delay in LR initiation and emergence. This delay was not observed in *ots1-1* and *ots2-1* single mutants, revealing redundancy between these genes. Interestingly, *ots1-1* and *ots1-2* gk single mutants displayed an increased number of LRP. This result could indicate a role for OTS1 in spacing of LRP in the oscillation zone. Addition of exogenous auxin could induce LR formation in *ots1-1 ots2-1,* suggesting auxin signalling is not fully dependent on these proteases for LR formation. *ots2-1* showed increased LRP initiation in response to auxin, whilst *ots1-1* demonstrated no auxin inducible phenotype. This data suggests a role for OTS1 under high auxin conditions. However, it is still unclear how as OTS1-mVenus pattern and fluorescence level were not directly influenced by short term (4hr) auxin treatment. Likely, auxin and deSUMOylation by OTS work together to fine-tune ARF activity (Fig. 6.3). In this model, auxin plays the main role as it is not fully dependent on OTS1 and OTS2. In turn, OTS1 finely tunes the auxin response by deSUMOylation of key ARF7 domains which affect transcriptional activity and protein stability.

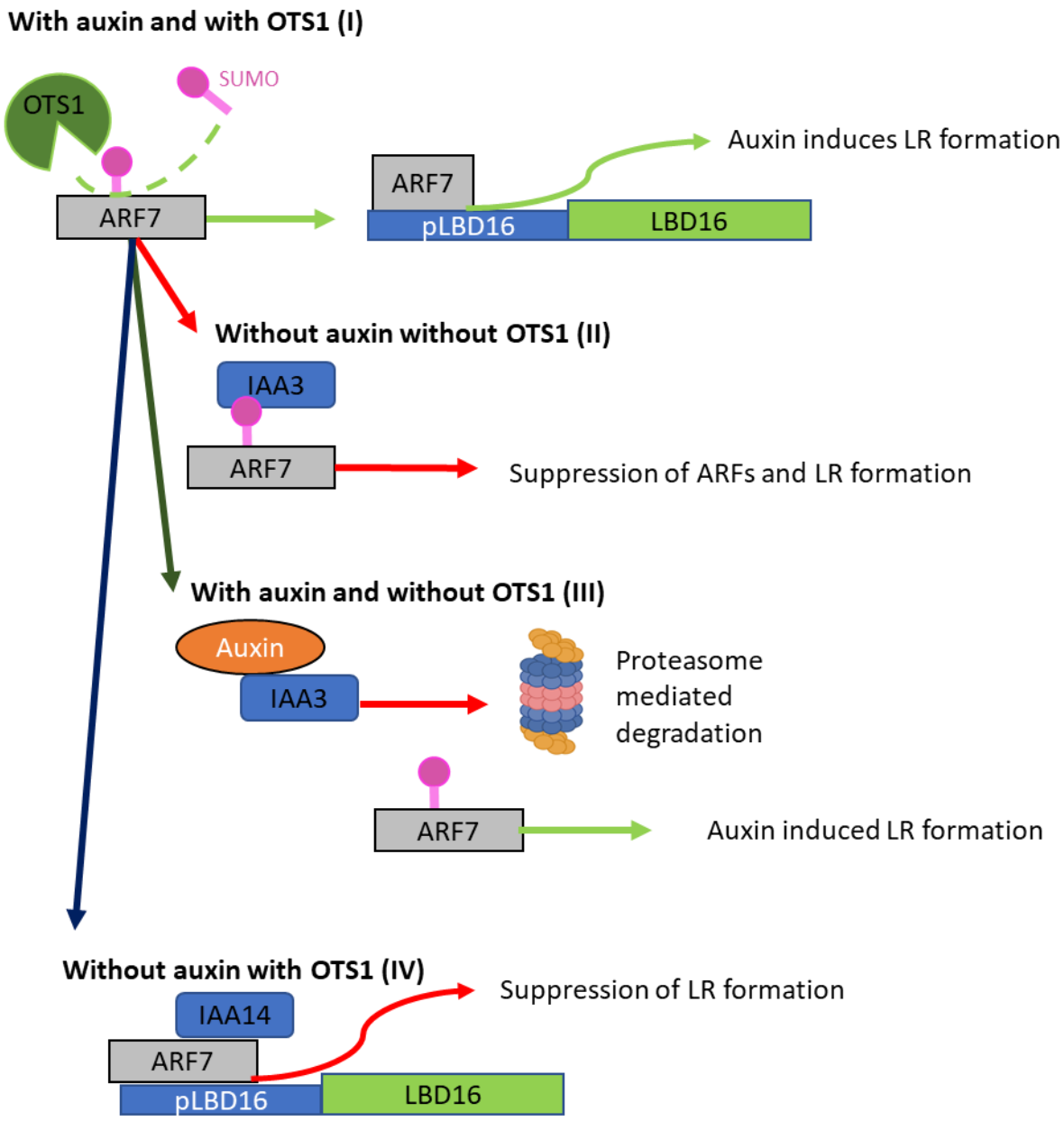

Figure 6.3 – Auxin and OTS1 work in tandem. Experimentally we tested the effect of auxin on lines with or without OTS1 and OTS2. In Col-0 (condition I) auxin induces LR formation by breaking down of Aux/IAA and deSUMOylation of ARF7 by OTS1 which activates transcription of targets such as LBD16. ots1-1 ots2-1 mutants showed multiple developmental defects including decreased LR number (II). This LR defect could be the result of reduced deSUMOylation of ARF7 by OTS1, causing increased binding of ARF7 to IAA3 repressor proteins and suppression of LR formation. LR formation was increased in *ots1-1 ots2-1* when exogenous auxin was added, suggesting OTS1 is not crucial for auxin induced LR formation (III). Without auxin addition LR formation is limited, potentially because ARF7 activity and stability is regulated by other Aux/IAA that do not depend on SUMOylated ARF7.

Complementation of the *ots1-1 ots2-1* double mutant with mVenus-OTS1 and OTS1-mVenus restored LR formation but did not fully restore primary root growth. Additionally, OTS1 transcript levels were not fully restored in roots. This is likely caused by using only the OTS1 coding sequence. The OTS1 transcriptional reporter, with the first intron included, showed a stronger signal in the primary root meristem than OTS1-mVenus, suggesting possible promoter elements in the first intron crucial for expression in the root meristem. Transgenic roots expressing OTS1-mVenus exhibited expression in XPP cells in the elongation zone. Expression of OTS1-mVenus occurs prior to gLBD16-GFP expression, which is visible in the late elongation zone. In our hypothesized model, OTS1 deSUMOylates ARF7, activating expression of target *LBD16*. gLBD16-GFP showed asymmetric expression, but this pattern was neither observed in ARF7-Venus nor OTS1-mVenus. Likely ARF7 activity is important in regulating hydropatterning not ARF7 protein stability. OTS1 is a cysteine protease and could therefore be affected by changes in cellular redox status. We hypothesize an altered model in which an OTS1 activity gradient exists between air and agar exposed root side (Fig. 6.4). This activity gradient directly affects the SUMOylation status of targets such as ARF7. DeSUMOylation of ARF7 on the agar side leads to activating transcription and inducing LR formation. Future work will have to: (1) assess the activity of OTS1 in different redox environments and (2) assess the redox potential differences between XPP cells on air versus water exposed root sides.

OTS1 and OTS2 are also involved in LRP development and emergence. *ots1-1 ots2-1* exhibited a severely reduced rate of emergence. Nuclear expression of OTS1-mVenus was observed in LRP from the onset of stage 1 till emergence. Additionally, *ots1-2gk* exhibited accumulation of stage 3 and 4 primordia, where the primordium pushes against the overlying endodermis. This might indicate an important role for OTS1 regulation of auxin signalling cross-talk between primordium and endodermis. Interestingly, *SHY2/IAA3* expression in the endodermis is crucial for LRP initiation (Vermeer et al. 2014). Could OTS1 activity regulate SUMO-SIM dependable interaction between ARF7 and IAA3 in endodermal tissue, thereby regulating LR initiation? Future work with tissue-specific expression of OTS1 in XPP and endodermal cells will have to explore the role of deSUMOylation by OTS1 in these different tissues.

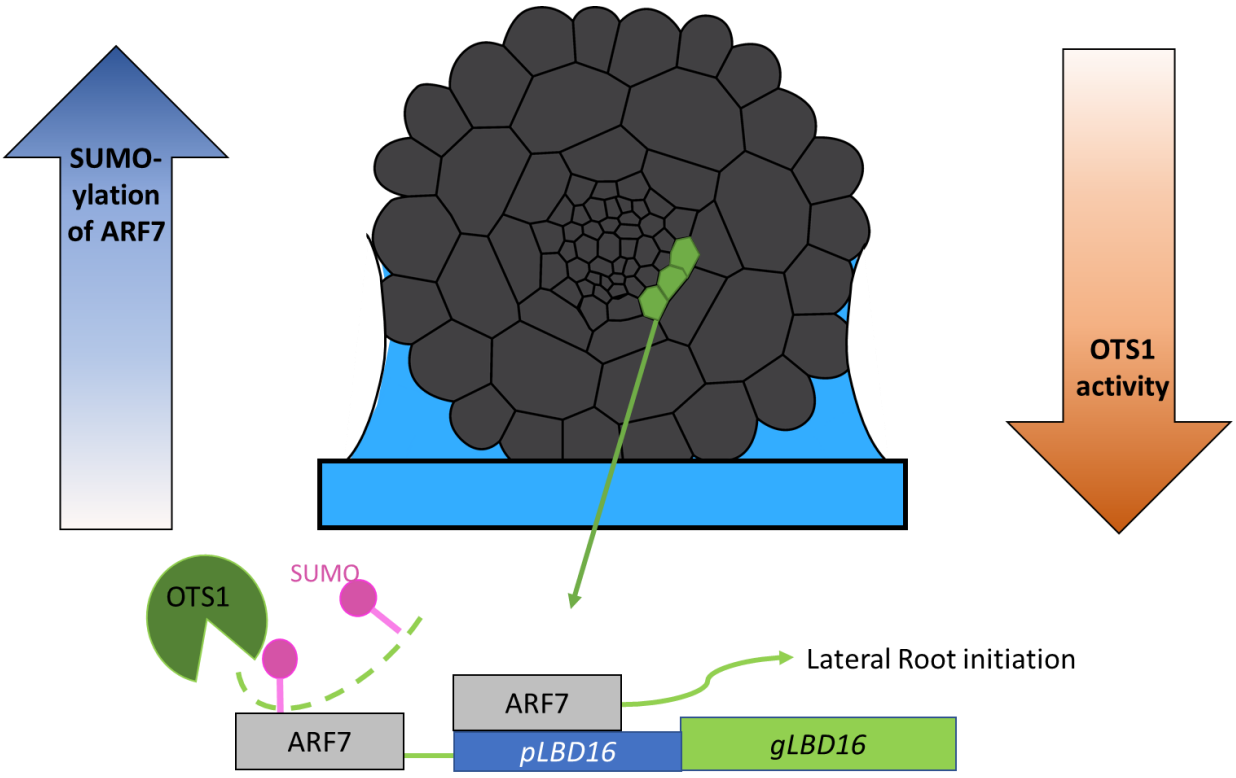

Figure 6.4 – OTS1 activity regulates ARF7 SUMOylation status and LR hydropatterning. We hypothesize a model in which OTS1 is more active on the agar side of the root, causing an opposite gradient in SUMOylated ARF7. This results in reduced ARF7 transcriptional activity on the air exposed side and thus reduced LR formation. On the agar exposed side OTS1 deSUMOylates ARF7 in XPP cells, activating transcription of downstream targets like *LBD16* to induce LR initiation.

6.4 Future Directions and Wider implications of the thesis findings

Water is key to plant growth and development. Crop growth under water deficit conditions is likely to become an increasing global trend as ground water is depleted and drought periods increase in frequency (Wheeler and von Braun 2013; Cotterman et al. 2017). To combat the detrimental effect that severe drought will have on crop yield, more research is needed to understand how plants sense and respond to prolonged drought stress. Root system architecture impacts foraging for water and other soil resources and is therefore a key target for crop improvement (Lynch 2011, 2013; Morris et al. 2017). Several water-related adaptive root responses have been described in this thesis (Orman-Ligeza et al. 2018; Rellán-Álvarez et al. 2015; Dietrich et al. 2017). In this work we focused on one adaptive root response: the branching of roots towards external water, termed LR hydropatterning (Bao et al. 2014). Prior studies revealed the importance of root water uptake in the elongation zone in order to generate a

hydropatterning response (Robbins and Dinneny 2018). In this thesis, a strong influence of the external hydrological environment on LR initiation and emergence was also observed. How do roots sense water availability in soil? One hypothesised model involves auxin acting as a 'hydrosignal' as it moves symplastically with radial water flow, triggering developmental outputs. However, auxin is not the only molecule that can act as a hydrosignal as many hormones and other classes of information containing molecule (e.g. miRNA) can move freely from cell-to-cell via plasmodesmata. Abscisic acid (ABA) is one hormone that is key to many water adaptive responses, such as hydrotropism and xerobranching. During xerobranching ABA was proposed to affect levels of free IAA, thereby inhibiting LR initiation (Orman-Ligeza et al. 2018). Does a similar signalling cascade take place during hydropatterning on the air exposed side through ABA accumulation? More generally, could hydrosignals function in other plant tissues and organs to monitor water fluxes, such as in leaves during drought stress? Further research is required to validate whether movement of putative hydrosignals like auxin and ABA can be directly linked with radial water fluxes.

Auxin regulates a multitude of shoot and root development processes through ARF transcription factors (Vanneste and Friml 2009). This thesis revealed many activating ARFs contain conserved SUMOylation sites, suggesting a more general role for SUMO in post-translational regulation of activating ARFs. Non-SUMOylatable ARF7^{4KR} showed increased transcriptional activity of *LBD16*. Hence, SUMOylation of key ARF domains provides a way to fine-tune levels of transcriptional output. Rapid SUMOylation of ARFs could also function to supress auxin response during stress conditions by increasing the affinity for SIM containing Aux/IAAs like IAA3. As class A-ARFs are expressed in a multitude of organs (Rademacher et al. 2011; Truskina et al. 2020), SUMOylation could impact a plethora of developmental processes. Mutating SUMO sites in individual class A-ARFs could reveal the importance of these conserved SUMO sites in the activity of each activating ARF. Furthermore, SUMOylation controls many abiotic developmental processes such as: competition for light (Sadanandom et al. 2015), salt stress (Conti et al. 2008), plant immunity (Orosa et al. 2018) and heat stress (Kurepa et al. 2003). Hence, SUMOylation or deSUMOylation of ARFs could be key to the developmental regulation of auxin responses to these stresses.

The deSUMOylation of target proteins appears critical in regulating many stress responses. For example, over-expressing SUMO protease *OTS1* decreases SUMO conjugate levels in response to salt, thereby increasing salt tolerance (Conti et al. 2008). In this thesis, we observed a hydropatterning defect in *ots1-1 ots2-1* double mutants. A translational reporter OTS1-mVenus rescued *ots1-1 ots2-1* hydropatterning, but no difference in reporter signal was observed in air versus agar exposed side. This suggests OTS1 activity (rather than its stability) is crucial for hydropatterning. If this is the case, how could OTS1 activity mirror water availability and hence serve as a 'water sensor'? As a cysteine protease, OTS1 activity could be regulated by cellular redox status (Berlett and Stadtman 1997) which is known to change under water-deficit conditions (Cruz De Carvalho 2008). The oxidation of the cysteine is especially important for the ULP protease family since the core of their catalytic triad contains a cysteine. Mutating this core cysteine results in a SUMO protease lacking deSUMOylation activity (Conti et al. 2008). As this SUMO protease is expressed throughout plant tissues, could OTS1 also function in other developmental responses to water stress such as stomatal opening? Increased ROS levels and ABA signalling play vital roles in closing stomata in response to drought (Kwak et al. 2003). Could this response be influenced by the regulation of OTS1 activity by ROS, for example? Hence, future research may discover that OTS1/OTS2 SUMO proteases play a far wider and more important role in water relations than currently understood.

BIBLIOGRAPHY

Agre P, Preston GM, Smith BL, Jung JS, Raina S, Moon C, Guggino WB, Nielsen S. 1993. Aquaporin CHIP: the archetypal molecular water channel. *Am J Physiol* **265**: F463–F476.

Aguilar-Martinez E, Chen X, Webber A, Mould AP, Seifert A, Hay RT, Sharrocks AD. 2015. Screen for multi-SUMO-binding proteins reveals a multi-SIM-binding mechanism for recruitment of the transcriptional regulator ZMYM2 to chromatin. *Proc Natl Acad Sci U S A* **112**: E4854–E4863.

Aharon R, Shahak Y, Wininger S, Bendov R, Kapulnik Y, Galili G. 2003. Overexpression of a plasma membrane aquaporin in transgenic tobacco improves plant vigor under favorable growth conditions but not under drought or salt stress. *Plant Cell* **15**: 439–447. http://www.plantcell.org/cgi/doi/10.1105/tpc.009225.

Ahmed MA, Zarebanadkouki M, Kaestner A, Carminati A. 2016. Measurements of water uptake of maize roots: the key function of lateral roots. *Plant Soil* **398**: 59–77.

Ahmed MA, Zarebanadkouki M, Meunier F, Javaux M, Kaestner A, Carminati A. 2018. Root type matters: Measurement of water uptake by seminal, crown, and lateral roots in maize. *J Exp Bot* **69**: 1199–1206.

Atkinson BS, Sparkes DL, Mooney SJ. 2009. The impact of soil structure on the establishment of winter wheat (Triticum aestivum). *Eur J Agron* **30**: 243–257.

Augustine RC, York SL, Rytz TC, Vierstra RD. 2016. Defining the SUMO System in Maize: SUMOylation Is Up-Regulated during Endosperm Development and Rapidly Induced by Stress. *Plant Physiol* **171**: 2191–2210. http://www.plantphysiol.org/lookup/doi/10.1104/pp.16.00353.

Babe a., Lavigne T, Severin J-P, Nagel K a., Walter a., Chaumont F, Batoko H, Beeckman T, Draye X. 2012. Repression of early lateral root initiation events by transient water deficit in barley and maize. *Philos Trans R Soc B Biol Sci* **367**: 1534–1541.

Ballas N, Wong L-M, Theologis A. 1993. Identification of the Auxin-responsive Element, AuxRE, in the Primary indoleacetic Acid-Inducible gene, PS-IAA4/5, of Pea (Pisum sativum). *J Mol Biol* **223**: 580–596.

Band LR, Wells DM, Fozard J a, Ghetiu T, French AP, Pound MP, Wilson MH, Yu L, Li W, Hijazi HI, et al. 2014. Systems analysis of auxin transport in the Arabidopsis root apex. *Plant Cell* **26**: 862–75. http://www.pubmedcentral.nih.gov/articlerender.fcgi?artid=4001398&tool=pmcentrez&rendertype=abstract (Accessed May 5, 2014).

Bao Y, Aggarwal P, Robbins NE, Sturrock CJ, Thompson MC, Tan HQ, Tham C, Duan L, Rodriguez PL, Vernoux T, et al. 2014. Plant roots use a patterning mechanism to position lateral root branches toward available water. *Proc Natl Acad Sci* **111**: 9319–9324. http://www.pnas.org/cgi/doi/10.1073/pnas.1400966111 (Accessed June 11, 2014).

Barber KW, Rinehart J. 2018. The ABCs of PTMs. *Nat Chem Biol* **14**: 188–192. http://dx.doi.org/10.1038/nchembio.2572.

Baxter A, Mittler R, Suzuki N. 2014. ROS as key players in plant stress signalling. *J Exp Bot* **65**: 1229–1240.

Beeckman T, Burssens S, Inze D. 2001. The peri-cell-cycle in Arabidopsis. *J Exp Bot* **52**: 403–411.

Benitez-Alfonso Y, Faulkner C, Pendle A, Miyashima S, Helariutta Y, Maule A. 2013. Symplastic Intercellular Connectivity Regulates Lateral Root Patterning. *Dev Cell* **26**: 136–147.

Benitez-Alfonso Y, Jackson D. 2009. Redox homeostasis regulates plasmodesmal communication in Arabidopsis meristems. *Plant Signal Behav* **4**: 655–659. http://www.pnas.org/content/106/9/3615.abstract%5Cnhttp://www.pnas.org/cgi/doi/10.1073/pnas.0808717106%5Cnhttp://www.tandfonline.com/doi/abs/10.4161/psb.4.7.8992.

Benkova E, Michniewicz M, Sauer M, Teichmann T, Pflanzen M Der. 2003. Local , Efflux-Dependent Auxin Gradients as a Common Module for Plant Organ Formation. *Cell* **115**: 591–602.

Bennett MJ, Marchant A, Green HG, May ST, Ward SP, Millner PA, Walker AR, Schulz B, Feldmann KA. 1996. Arabidopsis AUX1 gene: A permease-like regulator of root gravitropism. *Science (80-)* **273**: 948–950.

Berckmans B, Vassileva V, Schmid SPC, Maes S, Parizot B, Naramoto S, Magyar Z, Kamei CLA, Koncz C, Bogre L, et al. 2011. Auxin-Dependent Cell Cycle Reactivation through Transcriptional Regulation of Arabidopsis E2Fa by Lateral Organ Boundary Proteins. *Plant Cell* **23**: 3671–3683.

Berendzen KW, Weiste C, Wanke D, Kilian J, Harter K, Dröge-Laser W. 2012. Bioinformatic cis-element analyses performed in Arabidopsis and rice disclose bZIP- and MYB-related binding sites as potential AuxRE-coupling elements in auxin-mediated transcription. *BMC Plant Biol* **12**.

Berlett BS, Stadtman ER. 1997. Protein oxidation in aging and disease. *Free Radic Biol Med* **272**: 20313–20316.

Bienert GP, Moller ALB, Kristiansen KA, Schulz A, Moller IM, Schjoerring JK, Jahn TP. 2007. Specific Aquaporins Facilitate the Diffusion of Hydrogen Peroxide across Membranes. *J Biol Chem* **282**:

1183–1192. http://www.jbc.org/cgi/doi/10.1074/jbc.M603761200.

Blakely LM, Durham M, Evans TA, Blakely RM. 1982. Experimental Studies on Lateral Root Formation in Radish Seedling Roots. I. General Methods, Developmental Stages, and Spontaneous Formation of Laterals. *Bot Gaz* **143**: 341–352.

Blanc G, Hokamp K, Wolfe KH. 2003. A recent polyploidy superimposed on older large-scale duplications in the Arabidopsis genome. *Genome Res* **13**: 137–144.

Boer DR, Freire-Rios A, Van Den Berg WAM, Saaki T, Manfield IW, Kepinski S, López-Vidrieo I, Franco-Zorrilla JM, De Vries SC, Solano R, et al. 2014. Structural basis for DNA binding specificity by the auxin-dependent ARF transcription factors. *Cell* **156**: 577–589.

Boisson-Dernier A, Roy S, Kritsas K, Grobei MA, Jaciubek M, Schroeder JI, Grossniklaus U. 2009. Disruption of the pollen-expressed FERONIA homologs ANXUR1 and ANXUR2 triggers pollen tube discharge. *Development* **136**: 3279–3288.

Borlaug NE, Dowswell CR. 2003. Feeding a world of ten billion people: a 21st century challenge. *… Int Congr Wake …* 3–23. http://www.dista.unibo.it/doublehelix/proceedings/SECTION_I/HELIX pp 003-023.pdf.

Bourdais G, Burdiak P, Gauthier A, Nitsch L, Salojärvi J, Rayapuram C, Idänheimo N, Hunter K, Kimura S, Merilo E, et al. 2015. Large-Scale Phenomics Identifies Primary and Fine-Tuning Roles for CRKs in Responses Related to Oxidative Stress. *PLoS Genet* **11**: e1005373. http://www.ncbi.nlm.nih.gov/pubmed/26197346.

Brown NP, Leroy C, Sander C. 1998. MView: A web-compatible database search or multiple alignment viewer. *Bioinformatics* **14**: 380–381.

Caillaud M-C, Wirthmueller L, Sklenar J, Findlay K, Piquerez SJM, Jones AME, Robatzek S, Jones JDG, Faulkner C. 2014. The Plasmodesmal Protein PDLP1 Localises to Haustoria-Associated Membranes during Downy Mildew Infection and Regulates Callose Deposition. *PLoS Pathog* **10**: 1–13.

Calderón Villalobos LIA, Lee S, De Oliveira C, Ivetac A, Brandt W, Armitage L, Sheard LB, Tan X, Parry G, Mao H, et al. 2012. A combinatorial TIR1/AFB-Aux/IAA co-receptor system for differential sensing of auxin. *Nat Chem Biol* **8**: 477–485.

Casero PJ, Casimiro I, Rodriguez-Gallardo L, Martin-Partido G, Lloret PG. 1993. Lateral root initiation by asymmetrical transverse divisions of pericycle cells in adventitious roots ofAllium cepa. *Protoplasma* **176**: 138–144.

Casimiro I, Beeckman T, Graham N, Bhalerao R, Zhang H, Casero P, Sandberg G, Bennett MJ. 2003. Dissecting Arabidopsis lateral root development. *Trends Plant Sci* **8**: 165–71. http://www.ncbi.nlm.nih.gov/pubmed/12711228 (Accessed July 16, 2014).

Casimiro I, Marchant a, Bhalerao RP, Beeckman T, Dhooge S, Swarup R, Graham N, Inzé D, Sandberg G, Casero PJ, et al. 2001. Auxin transport promotes Arabidopsis lateral root initiation. *Plant Cell* **13**: 843–52. http://www.pubmedcentral.nih.gov/articlerender.fcgi?artid=135543&tool=pmcentrez&rendertype=abstract.

Castaño-Miquel L, Mas A, Teixeira I, Seguí J, Perearnau A, Thampi BN, Schapire AL, Rodrigo N, La Verde G, Manrique S, et al. 2017. SUMOylation Inhibition Mediated by Disruption of SUMO E1-E2 Interactions Confers Plant Susceptibility to Necrotrophic Fungal Pathogens. *Mol Plant* **10**: 709–720.

Castaño-Miquel L, Seguí J, Lois LM. 2011. Distinctive properties of Arabidopsis SUMO paralogues support the in vivo predominant role of AtSUMO1/2 isoforms. *Biochem J* **436**: 581–590.

Castro PH, Bachmair A, Bejarano ER, Coupland G, Maria Lois L, Sadanandom A, Van Den Burg HA, Vierstra RD, Azevedo H. 2018. Revised nomenclature and functional overview of the ULP gene family of plant deSUMOylating proteases. *J Exp Bot*.

Castro PH, Tavares RM, Bejarano ER, Azevedo H. 2012. SUMO,a heavyweight player in plant abiotic stress responses. *Cell Mol Life Sci* **69**: 3269–3283.

Catala R, Ouyang J, Abreu IA, Hu Y, Seo H, Zhang X, Chua N-H. 2007. The Arabidopsis E3 SUMO Ligase SIZ1 Regulates Plant Growth and Drought Responses. *Plant Cell Online* **19**: 2952–2966. http://www.plantcell.org/cgi/doi/10.1105/tpc.106.049981.

Causier B, Ashworth M, Guo W, Davies B. 2012. The TOPLESS interactome: A framework for gene repression in Arabidopsis. *Plant Physiol* **158**: 423–438.

Celenza Jr JL, Grisafi PL, Fink GR. 1995. A pathway for lateral root formation in Arabidopsis thaliana. **9**: 2131–2142.

Chapman EJ, Estelle M. 2009. Mechanism of auxin-regulated gene expression in plants. *Annu Rev Genet* **43**: 265–85. http://www.ncbi.nlm.nih.gov/pubmed/19686081.

Chosed R, Mukherjee S, Lois LM, Orth K. 2006. Evolution of a signalling system that incorporates both redundancy and diversity: Arabidopsis SUMOylation. *Biochem J* **398**: 521–529. papers2://publication/doi/10.1042/BJ20060426.

Christmann A, Grill E, Huang J. 2013. Hydraulic signals in long-distance signaling. *Curr Opin Plant Biol* **16**: 293–300. http://dx.doi.org/10.1016/j.pbi.2013.02.011.

Clough SJ, Bent AF. 1998. Floral dip: A simplified method for Agrobacterium-mediated transformation of Arabidopsis thaliana. *Plant J* **16**: 735–743.

Cochard H, Venisse JS, Barigah TS, Brunel N, Herbette S, Guilliot A, Tyree MT, Sakr S. 2007. Putative role of aquaporins in variable hydraulic conductance of leaves in response to light. *Plant Physiol* **143**: 122–133.

Conti L, Kioumourtzoglou D, O'Donnell E, Dominy P, Sadanandom A. 2009. OTS1 and OTS2 SUMO proteases link plant development and survival under salt stress. *Plant Signal Behav* **4**: 225–227.

Conti L, Price G, O'Donnell E, Schwessinger B, Dominy P, Sadanandom A. 2008. Small ubiquitin-like modifier proteases OVERLY TOLERANT TO SALT1 and -2 regulate salt stress responses in Arabidopsis. *Plant Cell* **20**: 2894–908. http://www.pubmedcentral.nih.gov/articlerender.fcgi?artid=2590731&tool=pmcentrez&rendertype=abstract (Accessed September 8, 2014).

Cotterman KA, Kendall AD, Basso B, Hyndman DW. 2017. Groundwater depletion and climate change: future prospects of crop production in the Central High Plains Aquifer. *Clim Change* **146**: 187–200.

Cruz De Carvalho MH. 2008. Drought stress and reactive oxygen species: Production, scavenging and signaling. *Plant Signal Behav* **3**: 156–165.

Cuevas-Velazquez CL, Saab-Rincón G, Reyes JL, Covarrubias AA. 2016. The unstructured n-terminal region of Arabidopsis group 4 late embryogenesis abundant (LEA) proteins is required for folding and for chaperone-like activity under water deficit. *J Biol Chem* **291**: 10893–10903.

De Rybel B, Audenaert D, Xuan W, Overvoorde P, Strader LC, Kepinski S, Hoye R, Brisbois R, Parizot B, Vanneste S, et al. 2012. A role for the root cap in root branching revealed by the non-auxin probe naxillin. *Nat Chem Biol* **8**: 798–805.

De Rybel B, Vassileva V, Parizot B, Demeulenaere M, Grunewald W, Audenaert D, Van Campenhout J, Overvoorde P, Jansen L, Vanneste S, et al. 2010. A novel Aux/IAA28 signaling cascade activates GATA23-dependent specification of lateral root founder cell identity. *Curr Biol* **20**: 1697–1706.

De Smet I, Tetsumura T, De Rybel B, Frei dit Frey N, Laplaze L, Casimiro I, Swarup R, Naudts M, Vanneste S, Audenaert D, et al. 2007. Auxin-dependent regulation of lateral root positioning in the basal meristem of Arabidopsis. *Development* **134**: 681–90.

http://www.ncbi.nlm.nih.gov/pubmed/17215297 (Accessed November 6, 2014).

De Smet I, Vanneste S, Inzé D, Beeckman T. 2006. Lateral root initiation or the birth of a new meristem. *Plant Mol Biol* **60**: 871–87. http://www.ncbi.nlm.nih.gov/pubmed/16724258 (Accessed December 13, 2014).

Dharmasiri N, Dharmasiri S, Estelle M. 2005a. The F-box protein TIR1 is an auxin receptor. *Nature* **435**: 441–445.

Dharmasiri N, Dharmasiri S, Weijers D, Lechner E, Yamada M, Hobbie L, Ehrismann JS, Jürgens G, Estelle M. 2005b. Plant development is regulated by a family of auxin receptor F box proteins. *Dev Cell* **9**: 109–119.

Dietrich D, Pang L, Kobayashi A, Fozard JA, Boudolf V, Bhosale R, Antoni R, Nguyen T, Hiratsuka S, Fujii N, et al. 2017. Root hydrotropism is controlled via a cortex-specific growth mechanism. *Nat Plants* **3**: 17057.

Dreher KA, Brown J, Saw RE, Callis J. 2006. The Arabidopsis Aux/IAA protein family has diversified in degradation and auxin responsiveness. *Plant Cell* **18**: 699–714.

Drew MC. 1975. Comparison of the effects of localized supply of phosphate, nitrate, ammonium and potassium on the growth of the seminal root system, and the shoot, in barley. *New Phytol* **75**: 479–490.

Du Y, Scheres B. 2018. Lateral root formation and the multiple roles of auxin. *J Exp Bot* **69**: 155–167.

Du Y, Scheres B. 2017. PLETHORA transcription factors orchestrate de novo organ patterning during Arabidopsis lateral root outgrowth. *Proc Natl Acad Sci* **114**: 11709–11714.

Duan Q, Kita D, Li C, Cheung AY, Wu H-M. 2010. FERONIA receptor-like kinase regulates RHO GTPase signaling of root hair development. *Proc Natl Acad Sci U S A* **107**: 17821–6. http://www.pubmedcentral.nih.gov/articlerender.fcgi?artid=2955125&tool=pmcentrez&rendertype=abstract%5Cnhttp://www.pnas.org/content/107/41/17821.short.

Dubrovsky JG, Sauer M, Napsucialy-Mendivil S, Ivanchenko MG, Friml J, Shishkova S, Celenza J, Benková E. 2008. Auxin acts as a local morphogenetic trigger to specify lateral root founder cells. *Proc Natl Acad Sci U S A* **105**: 8790–8794.

Dynowski M, Schaaf G, Loque D, Moran O, Ludewig U. 2008. Plant plasma membrane water channels conduct the signalling molecule H2O2. *Biochem J* **414**: 53–61.

Eberharter A, Becker PB. 2002. Histone acetylation: A switch between repressive and permissive

chromatin. Second in review on chromatin dynamics. *EMBO Rep* **3**: 224–229.

Edgar RC. 2004. MUSCLE: Multiple sequence alignment with high accuracy and high throughput. *Nucleic Acids Res* **32**: 1792–1797.

Ehlers K, Kollmann R. 2001. Primary and secondary plasmodesmata: structure, origin, and functioning. *Protoplasma* **216**: 1–30.

Ehlers K, van Bel AJE. 2010. Dynamics of plasmodesmal connectivity in successive interfaces of the cambial zone. *Planta* **231**: 371–385.

Elrouby N, Bonequi MV, Porri A, Coupland G. 2013. Identification of Arabidopsis SUMO-interacting proteins that regulate chromatin activity and developmental transitions. *Proc Natl Acad Sci U S A* **110**: 19956–19961.

Escamez S, André D, Sztojka B, Bollhöner B, Hall H, Berthet B, Voß U, Lers A, Maizel A, Andersson M, et al. 2020. Cell Death in Cells Overlying Lateral Root Primordia Facilitates Organ Growth in Arabidopsis. *Curr Biol* **30**: 455-464.e7.

Feng W, Kita D, Peaucelle A, Cartwright HN, Doan V, Duan Q, Liu MC, Maman J, Steinhorst L, Schmitz-Thom I, et al. 2018. The FERONIA Receptor Kinase Maintains Cell-Wall Integrity during Salt Stress through Ca2+ Signaling. *Curr Biol* **28**: 666-675.e5.

Feng W, Lindner H, Robbins NE, Dinneny JR. 2016. Growing Out of Stress: The Role of Cell- and Organ-Scale Growth Control in Plant Water-Stress Responses. *Plant Cell* **28**: 1769–1782. http://www.plantcell.org/lookup/doi/10.1105/tpc.16.00182.

Feng Z, Sun X, Wang G, Liu H, Zhu J. 2012. LBD29 regulates the cell cycle progression in response to auxin during lateral root formation in Arabidopsis thaliana. *Ann Bot* **110**: 1–10.

Fernández-Marcos M, Desvoyes B, Manzano C, Liberman LM, Benfey PN, del Pozo JC, Gutierrez C. 2017. Control of Arabidopsis lateral root primordium boundaries by MYB36. *New Phytol* **213**: 105–112.

Fernandez A, Drozdzecki A, Hoogewijs K, Nguyen A, Beeckman T, Madder A, Hilson P. 2013. Transcriptional and functional classification of the GOLVEN/ROOT GROWTH FACTOR/CLE-like signaling peptides reveals their role in lateral root and hair formation. *Plant Physiol* **161**: 954–70. http://www.ncbi.nlm.nih.gov/pubmed/23370719%0Ahttp://www.pubmedcentral.nih.gov/articlerender.fcgi?artid=PMC3561032.

Fernandez A, Drozdzecki A, Hoogewijs K, Vassileva V, Madder A, Beeckman T, Hilson P. 2015. The

GLV6/RGF8/CLEL2 peptide regulates early pericycle divisions during lateral root initiation. *J Exp Bot* **66**: 5245–5256.

Fernandez AI, Vangheluwe N, Xu K, Jourquin J, Alves L, Claus N, Morales-herrera S, Parizot B, Gernier H De, Yu Q, et al. 2020. GOLVEN peptide signalling through RGI receptors and MPK6 restricts asymmetric cell division during lateral root initiation. *Nat Plants*.

Franco-Zorrilla JM, López-Vidriero I, Carrasco JL, Godoy M, Vera P, Solano R. 2014. DNA-binding specificities of plant transcription factors and their potential to define target genes. *Proc Natl Acad Sci U S A* **111**: 2367–2372.

Friml J, Wisniewska J, Benkova E, Mendgen K, Palme K. 2002. Lateral relocation of auxin efflux regulator PIN3 mediates tropism in ArabidopsisFriml, Jiří; Wiśniewska, Justyna; Benková, Eva; Mendgen, Kur Lateral relocation of auxin efflux regulator PIN3 mediates tropism in Arabidopsis. *Lett to Nat* **415**: 1–4.

Fukaki H, Nakao Y, Okushima Y, Theologis A, Tasaka M. 2005. Tissue-specific expression of stabilized SOLITARY-ROOT/IAA14 alters lateral root development in Arabidopsis. *Plant J* **44**: 382–395.

Fukaki H, Tameda S, Masuda H, Tasaka M. 2002. Lateral root formation is blocked by a gain-of-function mutation in the SOLITARY-ROOT / IAA14 gene of Arabidopsis. *Plant J* **29**: 153–168.

Fukaki H, Taniguchi N, Tasaka M. 2006. PICKLE is required for SOLITARY-ROOT/IAA14-mediated repression of ARF7 and ARF19 activity during Arabidopsis lateral root initiation. *Plant J* **48**: 380–389.

Furuta K, Lichtenberger R, Helariutta Y. 2012. The role of mobile small RNA species during root growth and development. *Curr Opin Cell Biol* **24**: 211–216.

Gillies J, Hochstrasser M. 2012. A new class of SUMO proteases. *Nat Publ Gr* **13**: 284–285. http://dx.doi.org/10.1038/embor.2012.34.

Gilroy S, Suzuki N, Miller G, Choi WG, Toyota M, Devireddy AR, Mittler R. 2014. A tidal wave of signals: Calcium and ROS at the forefront of rapid systemic signaling. *Trends Plant Sci* **19**: 623–630. http://dx.doi.org/10.1016/j.tplants.2014.06.013.

Godfray HCJ, Beddington JR, Crute IR, Haddad L, Lawrence D, Muir JF, Pretty J, Robinson S, Thomas SM, Toulmin C. 2010. Food Security : The Challenge of Feeding 9 Billion People. *Science (80-)* **327**: 812–818.

Goh T. 2019. Long-term live-cell imaging approaches to study lateral root formation in Arabidopsis

thaliana. *Microscopy* **68**: 4–12.

Goh T, Joi S, Mimura T, Fukaki H. 2012a. The establishment of asymmetry in Arabidopsis lateral root founder cells is regulated by LBD16/ASL18 and related LBD/ASL proteins. *Development* **139**: 883–893.

Goh T, Kasahara H, Mimura T, Kamiya Y, Fukaki H. 2012b. Multiple AUX/IAA-ARF modules regulate lateral root formation: the role of Arabidopsis SHY2/IAA3-mediated auxin signalling. *Philos Trans R Soc B Biol Sci* **367**: 1461–1468.

Goh T, Toyokura K, Wells DM, Swarup K, Yamamoto M, Mimura T, Weijers D, Fukaki H, Laplaze L, Bennett MJ, et al. 2016. Quiescent center initiation in the Arabidopsis lateral root primordia is dependent on the SCARECROW transcription factor. *Development* **143**: 3363–3371.

Goh T, Toyokura K, Yamaguchi N, Okamoto Y, Uehara T, Kaneko S, Takebayashi Y, Kasahara H, Ikeyama Y, Okushima Y, et al. 2019. Lateral root initiation requires the sequential induction of transcription factors LBD16 and PUCHI in Arabidopsis thaliana. *New Phytol* **224**: 749–760.

Gomes D, Agasse A, Thiébaud P, Delrot S, Gerós H, Chaumont F. 2009. Aquaporins are multifunctional water and solute transporters highly divergent in living organisms. *Biochim Biophys Acta - Biomembr* **1788**: 1213–1228. http://dx.doi.org/10.1016/j.bbamem.2009.03.009.

González-Carranza ZH, Elliott KA, Roberts JA. 2007. Expression of polygalacturonases and evidence to support their role during cell separation processes in Arabidopsis thaliana. *J Exp Bot* **58**: 3719–3730.

Gonzalez-Guzman M, Pizzio GA, Antoni R, Vera-Sirera F, Merilo E, Bassel GW, Fernández MA, Holdsworth MJ, Perez-Amador MA, Kollist H, et al. 2012. Arabidopsis PYR/PYL/RCAR receptors play a major role in quantitative regulation of stomatal aperture and transcriptional response to abscisic acid. *Plant Cell* **24**: 2483–2496.

Goodstein DM, Shu S, Howson R, Neupane R, Hayes RD, Fazo J, Mitros T, Dirks W, Hellsten U, Putnam N, et al. 2012. Phytozome: A comparative platform for green plant genomics. *Nucleic Acids Res* **40**: 1178–1186.

Gray WM, Del Pozo JC, Walker L, Hobbie L, Risseeuw E, Banks T, Crosby WL, Yang M, Ma H, Estelle M. 1999. Identification of an SCF ubiquitin-ligase complex required for auxin response in Arabidopsis thaliana. *Genes Dev* **13**: 1678–1691.

Gray WM, Hellmann H, Dharmasiri S, Estelle M. 2002. Role of the Arabidopsis RING-H2 protein RBX1 in RUB modification and SCF function. *Plant Cell* **14**: 2137–2144.

Gray WM, Kepinski S, Rouse D, Leyser O, Estelle M. 2001. Auxin regulates SCFTIR1-dependent degradation of AUX/IAA proteins. *Nature* **414**: 271–276.

Gruber BD, Giehl RFH, Friedel S, von Wirén N. 2013. Plasticity of the Arabidopsis Root System under Nutrient Deficiencies. *Plant Physiol* **163**: 161–79. http://www.pubmedcentral.nih.gov/articlerender.fcgi?artid=3762638&tool=pmcentrez&rendertype=abstract.

Guilfoyle TJ. 2015. The PB1 domain in auxin response factor and aux/IAA proteins: A versatile protein interaction module in the auxin response. *Plant Cell* **27**: 33–43.

Guo H, Li L, Ye H, Yu X, Algreen A, Yin Y. 2009. Three related receptor-like kinases are required for optimal cell elongation in Arabidopsis thaliana. *Proc Natl Acad Sci U S A* **106**: 7648–7653. http://www.pubmedcentral.nih.gov/articlerender.fcgi?artid=2678668&tool=pmcentrez&rendertype=abstract%5Cnhttp://www.pubmedcentral.nih.gov/articlerender.fcgi?artid=2678668%7B&%7Dtool=pmcentrez%7B&%7Drendertype=abstract.

Gustavsson S, Lebrun AS, Nordén K, Chaumont F, Johanson U. 2005. A novel plant major intrinsic protein in Physcomitrella patens most similar to bacterial glycerol channels. *Plant Physiol* **139**: 287–295.

Hamant O, Haswell ES. 2017. Life behind the wall: sensing mechanical cues in plants. *BMC Biol* **15**: 59. http://bmcbiol.biomedcentral.com/articles/10.1186/s12915-017-0403-5.

Hamant O, Heisler MG, Jönsson H, Krupinski P, Uyttewaal M, Bokov P, Corson F, Sahlin P, Boudaoud A, Meyerowitz EM, et al. 2008. Developmental patterning by mechanical signals in Arabidopsis. *Science* **322**: 1650–5. http://classic.sciencemag.org/content/322/5908/1650.full.

Hamilton ES, Jensen GS, Maksaev G, Katims A, Sherp AM, Haswell ES. 2015. Mechanosensitive channel MSL8 regulates osmotic forces during pollen hydration and germination. *Science (80-)* **350**: 438–441.

Han M, Park Y, Kim I, Kim EH, Yu TK, Rhee S, Suh JY. 2014a. Structural basis for the auxin-induced transcriptional regulation by Aux/IAA17. *Proc Natl Acad Sci U S A* **112**: E602.

Han X, Hyun TK, Zhang M, Kumar R, Koh E ji, Kang BH, Lucas WJ, Kim JY. 2014b. Auxin-Callose-Mediated Plasmodesmal Gating Is Essential for Tropic Auxin Gradient Formation and Signaling. *Dev Cell* **28**: 132–146. http://dx.doi.org/10.1016/j.devcel.2013.12.008.

Haruta M, Sabat G, Stecker K, Minkoff BB, Sussman MR. 2014. A Peptide Hormone and Its Receptor. *Science (80-)* **343**: 408–411.

Haswell ES, Verslues PE. 2015. The ongoing search for the molecular basis of plant osmosensing. *J Gen Physiol* **145**: 389–94. http://jgp.rupress.org/content/145/5/389.

Hématy K, Sado P-E, Van Tuinen A, Rochange S, Desnos T, Balzergue S, Pelletier S, Renou J-P, Höfte H. 2007. A receptor-like kinase mediates the response of Arabidopsis cells to the inhibition of cellulose synthesis. *Curr Biol* **17**: 922–931.

Hermkes R, Fu YF, Nürrenberg K, Budhiraja R, Schmelzer E, Elrouby N, Dohmen RJ, Bachmair A, Coupland G. 2011. Distinct roles for Arabidopsis SUMO protease ESD4 and its closest homolog ELS1. *Planta* **233**: 63–73.

Himanen K, Vuylsteke M, Vanneste S, Vercruysse S, Boucheron E, Alard P, Chriqui D, Van Montagu M, Inzé D, Beeckman T. 2004. Transcript profiling of early lateral root initiation. *Proc Natl Acad Sci U S A* **101**: 5146–51.

Hodge A. 2004. The plastic plant: Root responses to heterogeneous supplies of nutrients. *New Phytol* **162**: 9–24.

Hofhuis H, Laskowski M, Du Y, Prasad K, Grigg S, Pinon V, Scheres B. 2013. Phyllotaxis and rhizotaxis in Arabidopsis are modified by three plethora transcription factors. *Curr Biol* **23**: 956–962. http://dx.doi.org/10.1016/j.cub.2013.04.048.

Hooijmaijers C, Rhee JY, Kwak KJ, Chung GC, Horie T, Katsuhara M, Kang H. 2012. Hydrogen peroxide permeability of plasma membrane aquaporins of Arabidopsis thaliana. *J Plant Res* **125**: 147–153.

Hou C, Tian W, Kleist T, He K, Garcia V, Bai F, Hao Y, Luan S, Li L. 2014. DUF221 proteins are a family of osmosensitive calcium-permeable cation channels conserved across eukaryotes. *Cell Res* **24**: 632–635.

Hua D, Wang C, He J, Liao H, Duan Y, Zhu Z, Guo Y, Chen Z, Gong Z. 2012. A Plasma Membrane Receptor Kinase, GHR1, Mediates Abscisic Acid- and Hydrogen Peroxide-Regulated Stomatal Movement in Arabidopsis. *Plant Cell* **24**: 2546–2561. http://www.plantcell.org/content/24/6/2546.full%5Cnhttp://www.plantcell.org/lookup/doi/10.1105/tpc.112.100107.

Huang C, Han Y, Wang Y, Sun X, Yan S, Yeh ETH, Chen Y, Cang H, Li H, Shi G, et al. 2009. SENP3 is responsible for HIF-1 transactivation under mild oxidative stress via p300 de-SUMOylation. *EMBO J* **28**: 2748–2762. http://dx.doi.org/10.1038/emboj.2009.210.

Idänheimo N, Gauthier A, Salojärvi J, Siligato R, Brosché M, Kollist H, Mähönen AP, Kangasjärvi J, Wrzaczek M. 2014. The Arabidopsis thaliana cysteine-rich receptor-like kinases CRK6 and CRK7

protect against apoplastic oxidative stress. *Biochem Biophys Res Commun* **445**: 457–462.

Iglesias VA, Meins F. 2000. Movement of plant viruses is delayed in a B-1,3-glucanase-deficient mutant showing a reduced plasmodesmatal size exclusion limit and enhanced callose deposition. *Plant J* **21**: 157–166.

Ishida T, Yoshimura M, Miura K, Sugimoto K. 2012. MMS21/HPY2 and SIZ1, Two Arabidopsis SUMO E3 Ligases, Have Distinct Functions in Development. *PLoS One* **7**: 1–10.

Iwakawa H, Ueno Y, Semiarti E, Onouchi H, Kojima S, Tsukaya H, Hasebe M, Soma T, Ikezaki M, Machida C, et al. 2002. The ASYMMETRIC LEAVES2 gene of Arabidopsis thaliana, required for formation of a symmetric flat leaf lamina, encodes a member of a novel family of proteins characterized by cysteine repeats and a leucine zipper. *Plant Cell Physiol* **43**: 467–478.

Jang JY, Lee SH, Rhee JY, Chung GC, Ahn SJ, Kang H. 2007. Transgenic Arabidopsis and tobacco plants overexpressing an aquaporin respond differently to various abiotic stresses. *Plant Mol Biol* **64**: 621–632.

Jocelyn E. Malamy and Philip N. Benfey. 1997. Organization and cell differentiation in lateral roots of Arabidopsis thaliana. *Development* **124**: 33–44.

Johnson ES. 2004. Protein Modification by SUMO. *Annu Rev Biochem* **73**: 355–382.

Kadam S, Abril A, Dhanapal AP, Koester RP, Vermerris W, Jose S, Fritschi FB. 2017. Characterization and Regulation of Aquaporin Genes of Sorghum [Sorghum bicolor (L.) Moench] in Response to Waterlogging Stress. *Front Plant Sci* **8**: 1–14. http://journal.frontiersin.org/article/10.3389/fpls.2017.00862/full.

Kapilan R, Vaziri M, Zwiazek JJ. 2018. Regulation of aquaporins in plants under stress. *Biol Res* **51**: 1–11. https://doi.org/10.1186/s40659-018-0152-0.

Kato H, Ishizaki K, Kouno M, Shirakawa M, Bowman JL, Nishihama R, Kohchi T. 2015. Auxin-Mediated Transcriptional System with a Minimal Set of Components Is Critical for Morphogenesis through the Life Cycle in Marchantia polymorpha. *PLoS Genet* **11**: 1–26.

Kato H, Kouno M, Takeda M, Suzuki H, Ishizaki K, Nishihama R, Kohchi T. 2017. The roles of the sole activator-type auxin response factor in pattern formation of marchantia polymorpha. *Plant Cell Physiol* **58**: 1642–1651.

Kato H, Mutte SK, Suzuki H, Crespo I, Das S, Radoeva T, Fontana M, Yoshitake Y, Hainiwa E, Berg W Van Den, et al. 2020. Design principles of a minimal auxin response system. *Nat Plants* **6**: Under

review. http://dx.doi.org/10.1038/s41477-020-0662-y.

Ke J, Ma H, Gu X, Thelen A, Brunzelle JS, Li J, Xu HE, Melcher K. 2015. Structural basis for recognition of diverse transcriptional repressors by the TOPLESS family of corepressors. *Sci Adv* **1**: 1–13.

Kim I, Cho E, Crawford K, Hempel FD, Zambryski PC. 2005. Cell-to-cell movement of GFP during embryogenesis and early seedling development in Arabidopsis. *Proc Natl Acad Sci U S A* **102**: 2227–2231. http://www.ncbi.nlm.nih.gov/entrez/query.fcgi?cmd=Retrieve&db=PubMed&dopt=Citation&list_uids=15668382.

Kim JY, Song JT, Seo HS. 2017. Post-translational modifications of Arabidopsis E3 SUMO ligase AtSIZ1 are controlled by environmental conditions. *FEBS Open Bio* **7**: 1622–1634.

Kohorn BD, Kobayashi M, Johansen S, Riese J, Huang LF, Koch K, Fu S, Dotson A, Byers N. 2006. An Arabidopsis cell wall-associated kinase required for invertase activity and cell growth. *Plant J* **46**: 307–316.

Kohorn BD, Kohorn SL. 2012. The cell wall-associated kinases, WAKs, as pectin receptors. *Front Plant Sci* **3**: 88. http://dx.doi.org/10.3389/fpls.2012.00088%5Cnhttp://www.ncbi.nlm.nih.gov/pubmed/22639672%5Cnhttp://www.ncbi.nlm.nih.gov/pmc/articles/PMC3355716%5Cnhttp://www.frontiersin.org/Journal/Abstract.aspx?s=907&name=plant_physiology&ART_DOI=10.3389/fpls.2012.00088.

Korasick DA, Westfall CS, Lee SG, Nanao MH, Dumas R, Hagen G, Guilfoyle TJ, Jez JM, Strader LC. 2014. Molecular basis for AUXIN RESPONSE FACTOR protein interaction and the control of auxin response repression. *Proc Natl Acad Sci U S A* **111**: 5427–5432.

Kramer PJ, Boyer JS. 1995. *Water relations of plants and soils.* Academic press.

Kroetz MB, Su D, Hochstrasser M. 2009. Essential Role of Nuclear Localization for Yeast Ulp2 SUMO Protease Function. *Mol Biol Cell* **20**: 2673–2683.

Kumpf RP, Shi C-L, Larrieu A, Stø IM, Butenko M a, Péret B, Riiser ES, Bennett MJ, Aalen RB. 2013. Floral organ abscission peptide IDA and its HAE/HSL2 receptors control cell separation during lateral root emergence. *Proc Natl Acad Sci* **110**: 5235–40. http://www.pubmedcentral.nih.gov/articlerender.fcgi?artid=3612645&tool=pmcentrez&rendertype=abstract.

Kurepa J, Walker JM, Smalle J, Gosink MM, Davis SJ, Durham TL, Sung DY, Vierstra RD. 2003. The small

ubiquitin-like modifier (SUMO) protein modification system in Arabidopsis. Accumulation of sumo1 and -2 conjugates is increased by stress. *J Biol Chem* **278**: 6862–6872.

Kurusu T, Nishikawa D, Yamazaki Y, Gotoh M, Nakano M, Hamada H, Yamanaka T, Iida K, Nakagawa Y, Saji H, et al. 2012. Plasma membrane protein OsMCA1 is involved in regulation of hypo-osmotic shock-induced Ca2+ influx and modulates generation of reactive oxygen species in cultured rice cells. *BMC Plant Biol* **12**: 11. http://www.biomedcentral.com/1471-2229/12/11.

Kwak JM, Mori IC, Pei ZM, Leonhard N, Angel Torres M, Dangl JL, Bloom RE, Bodde S, Jones JDG, Schroeder JI. 2003. NADPH oxidase AtrbohD and AtrbohF genes function in ROS-dependent ABA signaling in arabidopsis. *EMBO J* **22**: 2623–2633.

Lally D, Ingmire P, Tong HY, He ZH. 2001. Antisense expression of a cell wall-associated protein kinase, WAK4, inhibits cell elongation and alters morphology. *Plant Cell* **13**: 1317–1331.

Laskowski M, Biller S, Stanley K, Kajstura T, Prusty R. 2006. Expression profiling of auxin-treated Arabidopsis roots: Toward a molecular analysis of lateral root emergence. *Plant Cell Physiol* **47**: 788–792.

Laskowski M, Grieneisen VA, Hofhuis H, Hove CA ten, Hogeweg P, Marée AFM, Scheres B. 2008. Root System Architecture from Coupling Cell Shape to Auxin Transport. *PLoS Biol* **6**: e307.

Laskowski MJ, Williams ME, Nusbaum HC, Sussex IM. 1995. Formation of lateral root meristems is a two-stage process. *Development* **121**: 3303–3310.

Lavenus J, Goh T, Guyomarc'h S, Hill K, Lucas M, Voß U, Kenobi K, Wilson MH, Farcot E, Hagen G, et al. 2015. Inference of the Arabidopsis Lateral Root Gene Regulatory Network Suggests a Bifurcation Mechanism That Defines Primordia Flanking and Central Zones. *Plant Cell* **27**: 1368–1388. http://www.plantcell.org/lookup/doi/10.1105/tpc.114.132993.

Lavy M, Prigge MJ, Tao S, Shain S, Kuo A, Kirchsteiger K, Estelle M. 2016. Constitutive auxin response in Physcomitrella reveals complex interactions between Aux/IAA and ARF proteins. *Elife* **5**: 1–22.

Lee HW, Kang NY, Pandey SK, Cho C, Lee SH, Kim J. 2017. Dimerization in LBD16 and LBD18 transcription factors is critical for lateral root formation. *Plant Physiol* **174**: 301–311.

Lee HW, Kim J. 2013. EXPANSINA17 Up-Regulated by LBD18/ASL20 promotes lateral root formation during the auxin response. *Plant Cell Physiol* **54**: 1600–1611.

Lee HW, Kim MJ, Kim NY, Lee SH, Kim J. 2013a. LBD18 acts as a transcriptional activator that directly binds to the EXPANSIN14 promoter in promoting lateral root emergence of Arabidopsis. *Plant J*

73: 212–224.

Lee HW, Kim NY, Lee DJ, Kim J. 2009. LBD18/ASL20 regulates lateral root formation in combination with LBD16/ASL18 downstream of ARF7 and ARF19 in Arabidopsis. *Plant Physiol* **151**: 1377–1389.

Lee J-Y, Wang X, Cui W, Sager R, Modla S, Czymmek K, Zybaliov B, van Wijk K, Zhang C, Lu H, et al. 2011. A Plasmodesmata-Localized Protein Mediates Crosstalk between Cell-to-Cell Communication and Innate Immunity in Arabidopsis. *Plant Cell Online* **23**: 3353–3373. http://www.plantcell.org/cgi/doi/10.1105/tpc.111.087742.

Lee Y, Rubio MC, Alassimone J, Geldner N. 2013b. A mechanism for localized lignin deposition in the endodermis. *Cell* **153**: 402–412. http://dx.doi.org/10.1016/j.cell.2013.02.045.

Levy A, Erlanger M, Rosenthal M, Epel BL. 2007. A plasmodesmata-associated β-1,3-glucanase in Arabidopsis. *Plant J* **49**: 669–682.

Li SJ, Hochstrasser M. 2003. The Ulp1 SUMO isopeptidase: Distinct domains required for viability, nuclear envelope localization, and substrate specificity. *J Cell Biol* **160**: 1069–1081.

Li Y, Liu Z Bin, Shi X, Hagen G, Guilfoyle TJ. 1994. An auxin-inducible element in soybean SAUR promoters. *Plant Physiol* **106**: 37–43.

Litwack G. 2020. Chapter 12 - Hormonal Regulation of Epithelial Sodium Channel (ENaC) and Other Nonneuronal Epithelial Ion Channels. In *Hormonal Signaling in Biology and Medicine*, pp. 283–309.

Liu H, Wang S, Yu X, Yu J, He X, Zhang S, Shou H, Wu P. 2005. ARL1, a LOB-domain protein required for adventitious root formation in rice. *Plant J* **43**: 47–56.

Liu HL, Wang GC, Feng Z, Zhu J. 2010. Screening of genes associated with dedifferentiation and effect of LBD29 on pericycle cells in Arabidopsis thaliana. *Plant Growth Regul* **62**: 127–136.

Liu J, Perumal NB, Oldfield CJ, Su EW, Uversky VN, Dunker AK. 2006. Intrinsic disorder in transcription factors. *Biochemistry* **45**: 6873–6888.

Liu L, Jiang Y, Zhang X, Wang X, Wang Y, Han Y, Coupland G, Jin JB, Searle I, Fu YF, et al. 2017. Two SUMO proteases SUMO PROTEASE RELATED TO FERTILITY1 and 2 are required for fertility in arabidopsis. *Plant Physiol* **175**: 1703–1719.

Liu X, Wang J, Sun L. 2018. Structure of the hyperosmolality-gated calcium-permeable channel OSCA1.2. *Nat Commun* **9**. http://dx.doi.org/10.1038/s41467-018-07564-5.

Livak KJ, Schmittgen TD. 2001. Analysis of relative gene expression data using real-time quantitative PCR and the 2-ΔΔCT method. *Methods* **25**: 402–408.

Lobell DB, Schlenker W, Costa-Roberts J. 2011. Climate Trends and Global Crop Production Since 1980. *Science (80-)* **333**: 616–621.

Long JA, Ohno C, Smith ZR, Meyerowitz EM. 2006. TOPLESS regulates apical embryonic fate in Arabidopsis. *Science (80-)* **312**: 1520–1523.

Lucas M, Kenobi K, von Wangenheim D, Voβ U, Swarup K, De Smet I, Van Damme D, Lawrence T, Péret B, Moscardi E, et al. 2013. Lateral root morphogenesis is dependent on the mechanical properties of the overlaying tissues. *Proc Natl Acad Sci U S A* **110**: 5229–34. http://www.pubmedcentral.nih.gov/articlerender.fcgi?artid=3612681&tool=pmcentrez&rendertype=abstract.

Luxmoore RJ. 1981. Micro-, Meso-, and Macroporosity of Soil. *Soil Sci Soc Am J* **45**: 671–672.

Lynch JP. 2011. Root phenes for enhanced soil exploration and phosphorus acquisition: Tools for future crops. *Plant Physiol* **156**: 1041–1049.

Lynch JP. 2007. Roots of the second green revolution. *Aust J Bot* **55**: 493–512.

Lynch JP. 2013. Steep, cheap and deep: An ideotype to optimize water and N acquisition by maize root systems. *Ann Bot* **112**: 347–357.

Mähönen AP, Bishopp A, Higuchi M, Nieminen KM, Kinoshita K, Törmäkangas K, Ikeda Y, Oka A, Kakimoto T, Helariutta Y. 2006. Cytokinin signaling and its inhibitor AHP6 regulate cell fate during vascular development. *Science (80-)* **311**: 94–98.

Majer C, Hochholdinger F. 2011. Defining the boundaries: Structure and function of LOB domain proteins. *Trends Plant Sci* **16**: 47–52. http://dx.doi.org/10.1016/j.tplants.2010.09.009.

Majer C, Xu C, Berendzen KW, Hochholdinger F. 2012. Molecular interactions of Rootless Concerning Crown and Seminal Roots, a LOB domain protein regulating shoot-borne root initiation in maize (Zea mays L.). *Philos Trans R Soc B Biol Sci* **367**: 1542–1551.

Malamy JE, Benfey PN. 1997. Organization and cell differentiation in lateral roots of Arabidopsis thaliana. *Development* **124**: 33–44.

Mangalassery S, Sjögersten S, Sparkes DL, Sturrock CJ, Craigon J, Mooney SJ. 2014. To what extent can zero tillage lead to a reduction in greenhouse gas emissions from temperate soils? *Sci Rep* **4**: 1–8.

Manzano C, Pallero-Baena M, Casimiro I, De Rybel B, Orman-Ligeza B, Van Isterdael G, Beeckman T, Draye X, Casero P, Del Pozo JC. 2014. The Emerging Role of Reactive Oxygen Species Signaling during Lateral Root Development. *Plant Physiol* **165**: 1105–1119. http://www.ncbi.nlm.nih.gov/pubmed/24879433.

Marhavý P, Montesinos JC, Abuzeineh A, Van Damme D, Vermeer JEM, Duclercq J, Rakusová H, Nováková P, Friml J, Geldner N, et al. 2016. Targeted cell elimination reveals an auxin-guided biphasic mode of lateral root initiation. *Genes Dev* **30**: 471–83.

Marhavý P, Vanstraelen M, De Rybel B, Zhaojun D, Bennett MJ, Beeckman T, Benková E. 2013. Auxin reflux between the endodermis and pericycle promotes lateral root initiation. *EMBO J* **32**: 149–58. http://emboj.embopress.org/content/32/1/149.abstract.

Marín-Rodríguez MC, Orchard J, Seymour GB. 2002. Pectate lyases, cell wall degradation and fruit softening. *J Exp Bot* **53**: 2115–2119.

Martinka M, Dolan L, Pernas M, Abe J, Lux A. 2012. Endodermal cell-cell contact is required for the spatial control of Casparian band development in Arabidopsis thaliana. *Ann Bot* **110**: 361–371.

Matasci N, Hung LH, Yan Z, Carpenter EJ, Wickett NJ, Mirarab S, Nguyen N, Warnow T, Ayyampalayam S, Barker M, et al. 2014. Data access for the 1,000 Plants (1KP) project. *Gigascience* **3**: 1–10.

Matsumura Y, Iwakawa H, MacHida Y, MacHida C. 2009. Characterization of genes in the ASYMMETRIC LEAVES2-LATERAL ORGAN BOUNDARIES (AS2-LOB) family in Arabidopsis thaliana, and functional and molecular comparisons between AS2 and other family members. *Plant J* **58**: 525–537.

Maurel C. 1997. Aquaporins and Water Permeability of Plant Membranes. *Annu Rev Plant Physiol Plant Mol Biol* **48**: 399–429. http://www.annualreviews.org/doi/10.1146/annurev.arplant.48.1.399.

Maurel C, Kado RT, Guern J, Chrispeels MJ. 1995. Phosphorylation regulates the water channel activity of the seed-specific aquaporin alpha-TIP. *EMBO J* **14**: 3028–35. http://www.pubmedcentral.nih.gov/articlerender.fcgi?artid=394363&tool=pmcentrez&rendertype=abstract.

Mellor NL, Voß U, Janes G, Bennett MJ, Wells DM, Band LR. 2020. Auxin fluxes through plasmodesmata modify root-tip auxin distribution. *Development* **147**: dev181669.

Miller MJ, Scalf M, Rytz TC, Hubler SL, Smith LM, Vierstra RD. 2013. Quantitative Proteomics Reveals Factors Regulating RNA Biology as Dynamic Targets of Stress-induced SUMOylation in *Arabidopsis*. *Mol Cell Proteomics* **12**: 449–463. http://www.mcponline.org/lookup/doi/10.1074/mcp.M112.025056.

Miura K, Okamoto H, Okuma E, Shiba H, Kamada H, Hasegawa PM, Murata Y. 2013. SIZ1 deficiency causes reduced stomatal aperture and enhanced drought tolerance via controlling salicylic acid-induced accumulation of reactive oxygen species in Arabidopsis. *Plant J* **73**: 91–104.

Miyazaki S, Murata T, Sakurai-Ozato N, Kubo M, Demura T, Fukuda H, Hasebe M. 2009. ANXUR1 and 2, Sister Genes to FERONIA/SIRENE, Are Male Factors for Coordinated Fertilization. *Curr Biol* **19**: 1327–1331. http://dx.doi.org/10.1016/j.cub.2009.06.064.

Monshausen GB, Haswell ES. 2013. A force of nature: Molecular mechanisms of mechanoperception in plants. *J Exp Bot* **64**: 4663–4680.

Moreno-Risueno M a, Van Norman JM, Moreno A, Zhang J, Ahnert SE, Benfey PN. 2010. Oscillating gene expression determines competence for periodic Arabidopsis root branching. *Science* **329**: 1306–1311.

Morrell R, Sadanandom A. 2019. Dealing With Stress: A Review of Plant SUMO Proteases. *Front Plant Sci* **10**.

Morris EC, Griffiths M, Golebiowska A, Mairhofer S, Burr-Hersey J, Goh T, von Wangenheim D, Atkinson B, Sturrock CJ, Lynch JP, et al. 2017. Shaping 3D Root System Architecture. *Curr Biol* **27**: R919–R930. http://dx.doi.org/10.1016/j.cub.2017.06.043.

Moss BL, Mao H, Guseman JM, Hinds TR, Hellmuth A, Kovenock M, Noorassa A, Lanctot A, Calderón Villalobos LIA, Zheng N, et al. 2015. Rate motifs tune auxin/indole-3-acetic acid degradation dynamics. *Plant Physiol* **169**: 803–813.

Mossessova E, Lima CD. 2000. Ulp1-SUMO crystal structure and genetic analysis reveal conserved interactions and a regulatory element essential for cell growth in yeast. *Mol Cell* **5**: 865–876.

Murthy SE, Dubin AE, Whitwam T, Jojoa-Cruz S, Cahalan SM, Mosavi SAR, Ward AB, Patapoutian A. 2018. OSCA/TMEM63 are an Evolutionarily Conserved Family of Mechanically Activated Ion Channels. *eLi* **7**: 1–17.

Mutte SK, Kato H, Rothfels C, Melkonian M, Wong GKS, Weijers D. 2018. Origin and evolution of the nuclear auxin response system. *Elife* **7**: 1–25.

Nakagawa Y, Katagiri T, Shinozaki K, Qi Z, Tatsumi H, Furuichi T, Kishigami A, Sokabe M, Kojima I, Sato S, et al. 2007. Arabidopsis plasma membrane protein crucial for Ca2+ influx and touch sensing in roots. *Proc Natl Acad Sci U S A* **104**: 3639–44. http://www.pubmedcentral.nih.gov/articlerender.fcgi?artid=1802001&tool=pmcentrez&rendertype=abstract.

Naseer S, Lee Y, Lapierre C, Franke R, Nawrath C, Geldner N. 2012. Casparian strip diffusion barrier in Arabidopsis is made of a lignin polymer without suberin. *Proc Natl Acad Sci U S A* **109**: 10101–10106.

O'Malley RC, Huang SSC, Song L, Lewsey MG, Bartlett A, Nery JR, Galli M, Gallavotti A, Ecker JR. 2016. Cistrome and Epicistrome Features Shape the Regulatory DNA Landscape. *Cell* **165**: 1280–1292. http://dx.doi.org/10.1016/j.cell.2016.04.038.

Okushima Y, Fukaki H, Onoda M, Theologis A, Tasaka M. 2007. ARF7 and ARF19 regulate lateral root formation via direct activation of LBD/ASL genes in Arabidopsis. *Plant Cell* **19**: 118–130.

Okushima Y, Overvoorde PJ, Arima K, Alonso JM, Chan A, Chang C, Ecker JR, Hughes B, Lui A, Nguyen D, et al. 2005. Functional Genomic Analysis of the AUXIN RESPONSE FACTOR Gene Family Members in Arabidopsis thaliana: Unique and Overlapping Functions of ARF7 and ARF19. **17**: 444–463.

Orman-Ligeza B, Morris EC, Parizot B, Lavigne T, Babé A, Ligeza A, Klein S, Sturrock C, Xuan W, Novák O, et al. 2018. The Xerobranching Response Represses Lateral Root Formation When Roots Are Not in Contact with Water. *Curr Biol* **28**: 3165-3173.e5.

Orman-Ligeza B, Parizot B, de Rycke R, Fernandez A, Himschoot E, Van Breusegem F, Bennett MJ, Périlleux C, Beeckman T, Draye X. 2016. RBOH-mediated ROS production facilitates lateral root emergence in Arabidopsis. *Development* dev.136465. http://dev.biologists.org/lookup/doi/10.1242/dev.136465.

Orosa-Puente B, Leftley N, von Wangenheim D, Banda J, Srivastava AK, Hill K, Truskina J, Bhosale R, Morris E, Srivastava M, et al. 2018. Root branching toward water involves posttranslational modification of transcription factor ARF7. *Science (80-)* **362**: 1407–1410.

Orosa B, Yates G, Verma V, Srivastava AK, Srivastava M, Campanaro A, De Vega D, Fernandes A, Zhang C, Lee J, et al. 2018. SUMO conjugation to the pattern recognition receptor FLS2 triggers intracellular signalling in plant innate immunity. *Nat Commun* **9**: 1–12. http://dx.doi.org/10.1038/s41467-018-07696-8.

Ovečka M, von Wangenheim D, Tomančák P, Šamajová O, Komis G, Šamaj J. 2018. Multiscale imaging of plant development by light-sheet fluorescence microscopy. *Nat Plants* **4**: 639–650. http://dx.doi.org/10.1038/s41477-018-0238-2.

Pandey SK, Lee HW, Kim MJ, Cho C, Oh E, Kim J. 2018. LBD18 uses a dual mode of a positive feedback loop to regulate ARF expression and transcriptional activity in Arabidopsis. *Plant J* **95**: 233–251.

Parizot B, Laplaze L, Ricaud L, Boucheron-Dubuisson E, Bonke M, Chriqui D, Haseloff J, De Smet I, Helariutta Y, Bayle V, et al. 2008. Diarch Symmetry of the Vascular Bundle in Arabidopsis Root Encompasses the Pericycle and Is Reflected in Distich Lateral Root Initiation. *Plant Physiol* **146**: 140–148.

Parry G, Calderon-Villalobos LI, Prigge M, Peret B, Dharmasiri S, Itoh H, Lechner E, Gray WM, Bennett M, Estelle M. 2009. Complex regulation of the TIR1/AFB family of auxin receptors. *Proc Natl Acad Sci U S A* **106**: 22540–5. http://www.pubmedcentral.nih.gov/articlerender.fcgi?artid=2799741&tool=pmcentrez&rendertype=abstract.

Passot S, Gnacko F, Moukouanga D, Lucas M, Guyomarc'h S, Ortega BM, Atkinson JA, Belko MN, Bennett MJ, Gantet P, et al. 2016. Characterization of pearl millet root architecture and anatomy reveals three types of lateral roots. *Front Plant Sci* **7**: 1–11.

Paultre DSG, Gustin M-P, Molnar A, Oparka KJ. 2016. Lost in transit: long-distance trafficking and phloem unloading of protein signals in Arabidopsis homografts. *Plant Cell* **28**: tpc.00249.2016. http://www.plantcell.org/lookup/doi/10.1105/tpc.16.00249.

Péret B, Li G, Zhao J, Band LR, Voß U, Postaire O, Luu D-T, Da Ines O, Casimiro I, Lucas M, et al. 2012. Auxin regulates aquaporin function to facilitate lateral root emergence. *Nat Cell Biol* **14**: 991–998. http://dx.doi.org/10.1038/ncb2573.

Peret B, Middleton AM, French AP, Larrieu A, Bishopp A, Njo M, Wells DM, Porco S, Mellor N, Band LR, et al. 2013. Sequential induction of auxin efflux and influx carriers regulates lateral root emergence. *Mol Syst Biol* **9**: 699–699.

Perianez-rodriguez J, Rodriguez M, Marconi M, Bustillo-avendaño E, Wachsman G, Sanchez-corrionero A, Gernier H De, Cabrera J, Perez-garcia P, Gude I, et al. 2021. An auxin-regulable oscillatory circuit drives the root clock in Arabidopsis. 1–11.

Pietrosemoli N, García-Martín JA, Solano R, Pazos F. 2013. Genome-Wide Analysis of Protein Disorder in Arabidopsis thaliana: Implications for Plant Environmental Adaptation. *PLoS One* **8**.

Piya S, Shrestha SK, Binder B, Neal Stewart C, Hewezi T. 2014. Protein-protein interaction and gene co-expression maps of ARFs and Aux/IAAs in Arabidopsis. *Front Plant Sci* **5**: 1–9.

Porco S, Larrieu A, Du Y, Gaudinier A, Goh T, Swarup K, Swarup R, Kuempers B, Bishopp A, Lavenus J, et al. 2016. Lateral root emergence in Arabidopsis is dependent on transcription factor LBD29 regulation of auxin influx carrier LAX3. *Dev* **143**: 3340–3349.

Preibisch S, Amat F, Stamataki E, Sarov M, Singer RH, Myers E, Tomancak P. 2014. Efficient bayesian-based multiview deconvolution. *Nat Methods* **11**: 645–648.

Preibisch S, Saalfeld S, Schindelin J, Tomancak P. 2010. Software for bead-based registration of selective plane illumination microscopy data. *Nat Methods* **7**: 418–419.

Rademacher EH, Lokerse AS, Schlereth A, Llavata-Peris CI, Bayer M, Kientz M, FreireRios A, Borst JW, Lukowitz W, Jürgens G, et al. 2012. Different Auxin Response Machineries Control Distinct Cell Fates in the Early Plant Embryo. *Dev Cell* **22**: 211–222.

Rademacher EH, Möller B, Lokerse AS, Llavata-Peris CI, Van Den Berg W, Weijers D. 2011. A cellular expression map of the Arabidopsis AUXIN RESPONSE FACTOR gene family. *Plant J* **68**: 597–606.

Reinhardt H, Hachez C, Bienert MD, Beebo A, Swarup K, Voss U, Bouhidel K, Frigerio L, Schjoerring JK, Bennett MJ, et al. 2016. Tonoplast aquaporins facilitate lateral root emergence. *Plant Physiol* **170**. http://www.plantphysiol.org/lookup/doi/10.1104/pp.15.01635.

Rellán-Álvarez R, Lobet G, Lindner H, Pradier PL, Sebastian J, Yee MC, Geng Y, Trontin C, Larue T, Schrager-Lavelle A, et al. 2015. GLO-Roots: An imaging platform enabling multidimensional characterization of soil-grown root systems. *Elife* **4**: e07597.

Richter GL, Monshausen GB, Krol A, Gilroy S. 2009. Mechanical stimuli modulate lateral root organogenesis. *Plant Physiol* **151**: 1855–1866.

Rim Y, Huang L, Chu H, Han X, Cho WK, Jeon CO, Kim HJ, Hong JC, Lucas WJ, Kim JY. 2011. Analysis of Arabidopsis transcription factor families revealed extensive capacity for cell-to-cell movement as well as discrete trafficking patterns. *Mol Cells* **32**: 519–526.

Robbins NE, Dinneny J. 2018. Growth is required for perception of water availability to pattern plant root branches. *Proc Natl Acad Sci* **115**: E822–E831.

Rogers ED, Benfey PN. 2015. Regulation of plant root system architecture: Implications for crop advancement. *Curr Opin Biotechnol* **32**: 93–98. http://dx.doi.org/10.1016/j.copbio.2014.11.015.

Rogg LE, Lasswell J, Bartel B. 2001. A gain-of-function mutation in IAA28 suppresses lateral root development. *Plant Cell* **13**: 465–480.

Roosjen M, Paque S, Weijers D. 2018. Auxin Response Factors: Output control in auxin biology. *J Exp Bot* **69**: 179–188.

Rutschow HL, Baskin TI, Kramer EM. 2011. Regulation of solute flux through plasmodesmata in the root meristem. *Plant Physiol* **155**: 1817–1826.

Rytz TC, Miller MJ, McLoughlin F, Augustine RC, Marshall RS, Juan YT, Charng YY, Scalf M, Smith LM, Vierstra RD. 2018. SUMOylome profiling reveals a diverse array of nuclear targets modified by the SUMO ligase SIZ1 during heat stress. *Plant Cell* **30**: 1077–1099.

Sadanandom A, Ádám É, Orosa B, Viczián A, Klose C, Zhang C, Josse EM, Kozma-Bognár L, Nagy F. 2015. SUMOylation of phytochrome-B negatively regulates light-induced signaling in Arabidopsis thaliana. *Proc Natl Acad Sci U S A* **112**: 11108–11113.

Sager R, Wang X, Hill K, Yoo BC, Caplan J, Nedo A, Tran T, Bennett MJ, Lee JY. 2020. Auxin-dependent control of a plasmodesmal regulator creates a negative feedback loop modulating lateral root emergence. *Nat Commun* **11**: 1–10. http://dx.doi.org/10.1038/s41467-019-14226-7.

Santoni V, Verdoucq L, Sommerer N, Vinh J, Pflieger D, Maurel C. 2006. Methylation of aquaporins in plant plasma membrane. *Biochem J* **400**: 189–197.

Saracco SA, Miller MJ, Kurepa J, Vierstra RD. 2007. Genetic analysis of SUMOylation in Arabidopsis: Conjugation of SUMO1 and SUMO2 to nuclear proteins is essential. *Plant Physiol* **145**: 119–134.

Scheres B, Krizek BA. 2018. Coordination of growth in root and shoot apices by AIL/PLT transcription factors. *Curr Opin Plant Biol* **41**: 95–101. http://dx.doi.org/10.1016/j.pbi.2017.10.002.

Segonzac C, Nimchuk ZL, Beck M, Tarr PT, Robatzek S, Meyerowitz EM, Zipfel C. 2012. The shoot apical meristem regulatory peptide CLV3 does not activate innate immunity. *Plant Cell* **24**: 3186–3192.

Sheng L, Hu X, Du Y, Zhang G, Huang H, Scheres B, Xu L. 2017. Non-canonical WOX11-mediated root branching contributes to plasticity in arabidopsis root system architecture. *Dev* **144**: 3126–3133.

Shih HW, Miller ND, Dai C, Spalding EP, Monshausen GB. 2014. The receptor-like kinase FERONIA is required for mechanical signal transduction in Arabidopsis seedlings. *Curr Biol* **24**: 1887–1892. http://dx.doi.org/10.1016/j.cub.2014.06.064.

Shin EJ, Shin HM, Nam E, Kim WS, Kim JH, Oh BH, Yun Y. 2012. DeSUMOylating isopeptidase: A second class of SUMO protease. *EMBO Rep* **13**: 339–346. http://dx.doi.org/10.1038/embor.2012.3.

Shuai B, Reynaga-pen CG, Springer PS. 2002. Lateral organ boundaries. *Plant Physiol* **129**: 747–761.

Smetana O, Mäkilä R, Lyu M, Amiryousefi A, Sánchez Rodríguez F, Wu M-F, Solé-Gil A, Leal Gavarrón M, Siligato R, Miyashima S, et al. 2019. High levels of auxin signalling define the stem-cell organizer of the vascular cambium. *Nature* **565**: 485–489. http://dx.doi.org/10.1038/s41586-018-0837-0.

Srivastava AK, Zhang C, Caine RS, Gray J, Sadanandom A. 2017. Rice SUMO protease Overly Tolerant

to Salt 1 targets the transcription factor, OsbZIP23 to promote drought tolerance in rice. *Plant J* **1**: 1031–1043.

Srivastava AK, Zhang C, Sadanandom A. 2016a. Rice OVERLY TOLERANT TO SALT 1 (OTS1) SUMO protease is a positive regulator of seed germination and root development. *Plant Signal Behav* **11**: 1–3. http://dx.doi.org/10.1080/15592324.2016.1173301.

Srivastava AK, Zhang C, Yates G, Bailey M, Brown A, Sadanandom A. 2016b. SUMO Is a critical regulator of salt stress responses in rice. *Plant Physiol* **170**: 2378–2391.

Stankovic-Valentin N, Melchior F. 2018. Control of SUMO and Ubiquitin by ROS: Signaling and disease implications. *Mol Aspects Med* **63**: 3–17. https://doi.org/10.1016/j.mam.2018.07.002.

Steffens B, Rasmussen A. 2016. The physiology of adventitious roots. *Plant Physiol* **170**: 603–617.

Suh HY, Kim JH, Woo JS, Ku B, Shin EJ, Yun Y, Oh BH. 2012. Crystal structure of DeSI-1, a novel deSUMOylase belonging to a putative isopeptidase superfamily. *Proteins Struct Funct Bioinforma* **80**: 2099–2104.

Swarup K, Benková E, Swarup R, Casimiro I, Péret B, Yang Y, Parry G, Nielsen E, De Smet I, Vanneste S, et al. 2008. The auxin influx carrier LAX3 promotes lateral root emergence. *Nat Cell Biol* **10**: 946–54. http://www.ncbi.nlm.nih.gov/pubmed/18622388 (Accessed October 12, 2014).

Swarup R, Kramer EM, Perry P, Knox K, Leyser HMO, Haseloff J, Beemster GTSS, Bhalerao R, Bennett MJ, Leyser O, et al. 2005. Root gravitropism requires lateral root cap and epidermal cells for transport and response to a mobile auxin signal. *Nat Cell Biol* **7**: 1057–1065. http://dx.doi.org/10.1038/ncb1316.

Szemenyei H, Hannon M, Long JA. 2008. TOPLESS mediates auxin-dependent transcriptional repression during Arabidopsis embryogenesis. *Science (80-)* **319**: 1384–1386.

Tan X, Calderon-Villalobos LIA, Sharon M, Zheng C, Robinson C V., Estelle M, Zheng N. 2007. Mechanism of auxin perception by the TIR1 ubiquitin ligase. *Nature* **446**: 640–645.

Tang LP, Zhou C, Wang SS, Yuan J, Zhang XS, Su YH. 2017. FUSCA3 interacting with LEAFY COTYLEDON2 controls lateral root formation through regulating YUCCA4 gene expression in Arabidopsis thaliana. *New Phytol* **213**: 1740–1754.

Tardieu F, Davies WJ. 1993. Integration of hydraulic and chemical signalling in the control of stomatal conductance and water status of droughted plants. *Plant Cell Environ* **16**: 341–349.

Thomas CL, Bayer EM, Ritzenthaler C, Fernandez-Calvino L, Maule AJ. 2008. Specific targeting of a

plasmodesmal protein affecting cell-to-cell communication. *PLoS Biol* **6**: 0180–0190.

Tian Q, Reed JW. 1999. Control of auxin-regulated root development by the Arabidopsis thaliana SHY2/AA3 gene. *Development* **126**: 711–721.

Tian Q, Uhlir NJ, Reed JW. 2002. Arabidopsis SHY2 / IAA3 Inhibits Auxin-Regulated Gene Expression. **14**: 301–319.

Tiwari SB, Hagen G, Guilfoyle T. 2003. The roles of auxin response factor domains in auxin-responsive transcription. *Plant Cell* **15**: 533–543.

Tomanov K, Zeschmann A, Hermkesc R, Eifler K, Ziba I, Grieco M, Novatchkova M, Hofmann K, Hesse H, Bachmaira A. 2014. Arabidopsis PIAL1 and 2 promote SUMO chain formation as e4-type SUMO ligases and are involved in stress responses and sulfur metabolismc w open. *Plant Cell* **26**: 4547–4560.

Torres-Martínez HH, Hernández-Herrera P, Corkidi G, Dubrovsky JG. 2020. From one cell to many: Morphogenetic field of lateral root founder cells in Arabidopsis thaliana is built by gradual recruitment. *Proc Natl Acad Sci U S A* **117**: 20943–20949.

Torres-Martínez HH, Rodríguez-Alonso G, Shishkova S, Dubrovsky JG. 2019. Lateral Root Primordium Morphogenesis in Angiosperms. *Front Plant Sci* **10**: 1–19.

Tournaire-Roux C, Sutka M, Javot H, Gout E, Gerbeau P, Luu D, Bligny R, Maurel C. 2003. Cytosolic pH regulates root water transport during anoxic stress through gating of aquaporins. *Nature* **425**: 393.

Toyokura K, Goh T, Shinohara H, Shinoda A, Kondo Y, Okamoto Y, Uehara T, Fujimoto K, Okushima Y, Ikeyama Y, et al. 2019. Lateral Inhibition by a Peptide Hormone-Receptor Cascade during Arabidopsis Lateral Root Founder Cell Formation. *Dev Cell* **48**: 64-75.e5. https://doi.org/10.1016/j.devcel.2018.11.031.

Trachsel S, Kaeppler SM, Brown KM, Lynch JP. 2013. Maize root growth angles become steeper under low N conditions. *F Crop Res* **140**: 18–31. http://dx.doi.org/10.1016/j.fcr.2012.09.010.

Tracy SR, Daly K., Sturrock CJ, Crout NM., Mooney SJ, Roose T. 2015. Water Resources Research. *Water Resour Res* **51**: 1006–1022.

Truskina J, Jingyi H, Galvan-Ampudia CS, Laine S, Brunoud G, Porco S, Bagman A-M, Smit ME, Bennett MJ, Roudier F, et al. 2020. A network of transcriptional repressors mediates auxin response specificity. *Nature* 1–4. http://e-journal.uajy.ac.id/14649/1/JURNAL.pdf.

Ulmasov T, Hagen G, Guilfoyle TJ. 1999. Activation and repression of transcription by auxin-response factors. *Proc Natl Acad Sci U S A* **96**: 5844–5849.

Ulmasov T, Hagen G, Guilfoyle TJ. 1997a. ARF1, a transcription factor that binds to auxin response elements. *Science (80-)* **276**: 1865–1868.

Ulmasov T, Murfett J, Hagen G, Guilfoyle TJ. 1997b. Aux/IAA proteins repress expression of reporter genes containing natural and highly active synthetic auxin response elements. *Plant Cell* **9**: 1963–1971. http://www.pubmedcentral.nih.gov/articlerender.fcgi?artid=157050&tool=pmcentrez&rendertype=abstract.

Van Bel M, Diels T, Vancaester E, Kreft L, Botzki A, Van De Peer Y, Coppens F, Vandepoele K. 2018. PLAZA 4.0: An integrative resource for functional, evolutionary and comparative plant genomics. *Nucleic Acids Res* **46**: D1190–D1196.

Van Norman JM, Xuan W, Beeckman T, Benfey PN. 2013. To branch or not to branch: the role of pre-patterning in lateral root formation. *Development* **140**: 4301–10. http://www.ncbi.nlm.nih.gov/pubmed/24130327 (Accessed November 28, 2014).

Vanneste S, Friml J. 2009. Auxin: a trigger for change in plant development. *Cell* **136**: 1005–16. http://www.ncbi.nlm.nih.gov/pubmed/19303845 (Accessed March 21, 2014).

Vatén A, Dettmer J, Wu S, Stierhof YD, Miyashima S, Yadav SR, Roberts CJ, Campilho A, Bulone V, Lichtenberger R, et al. 2011. Callose Biosynthesis Regulates Symplastic Trafficking during Root Development. *Dev Cell* **21**: 1144–1155.

Vera-Estrella R, Barkla BJ, Bohnert HJ, Pantoja O. 2004. Novel regulation of aquaporins during osmotic stress. *Plant Physiol* **135**: 2318–29. http://www.plantphysiol.org/content/135/4/2318.short.

Verbelen J-P, De Cnodder T, Le J, Vissenberg K, Baluska F. 2006. The Root Apex of Arabidopsis thaliana Consists of Four Distinct Zones of Growth Activities. *Plant Signal Behav* **1**: 296–304.

Vermeer JEM, van Wangenheim D, Barberon M, Lee Y, Stelzer EHK, Maizel A, Geldner N. 2014. A spatial accomodation by neighboring cells is required for organ initiation in Arabidopsis. *Science (80-)* **343**: 178–183.

Vernoux T, Brunoud G, Farcot E, Morin V, Van Den Daele H, Legrand J, Oliva M, Das P, Larrieu A, Wells D, et al. 2011. The auxin signalling network translates dynamic input into robust patterning at the shoot apex. *Mol Syst Biol* **7**.

Von Wangenheim D, Fangerau J, Schmitz A, Smith RS, Leitte H, Stelzer EHK, Maizel A. 2016. Rules and self-organizing properties of post-embryonic plant organ cell division patterns. *Curr Biol* **26**: 439–449.

Voß U, Wilson MH, Kenobi K, Gould PD, Robertson FC, Peer WA, Lucas M, Swarup K, Casimiro I, Holman TJ, et al. 2015. The circadian clock rephases during lateral root organ initiation in Arabidopsis thaliana. *Nat Commun* **6**: 7641.

Wheeler T, von Braun J. 2013. Climate Change Impacts on Global Food Security. *Science (80-)* **341**: 508–513.

White PJ, George TS, Gregory PJ, Bengough AG, Hallett PD, McKenzie BM. 2013. Matching roots to their environment. *Ann Bot* **112**: 207–222.

Wilmoth J, Wang S, Tiwari S, Joshi A, Hagen G, Guilfoyle T. 2005. NPH4/ARF7 and ARF19 promote leaf expansion and auxin-induced lateral root formation. *Plant J*.

Wu MF, Yamaguchi N, Xiao J, Bargmann B, Estelle M, Sang Y, Wagner D. 2015. Auxin-regulated chromatin switch directs acquisition of flower primordium founder fate. *Elife* **4**: 1–20.

Xie H, Vucetic S, Iakoucheva LM, Oldfield CJ, Dunker AK, Obradovic Z, Uversky VN. 2007. Functional anthology of intrinsic disorder. 3. Ligands, post-translational modifications, and diseases associated with intrinsically disordered proteins. *J Proteome Res* **6**: 1917–1932.

Xu A, Cui K, Wang W, Wang Z, Huang J, Nie L, Yong L, Peng S. 2017. Differential Responses of Water Uptake Pathways and Expression of Two Aquaporin Genes to Water-Deficit in Rice Seedlings of Two Genotypes. *Rice Sci* **24**: 187–197.

Xu C, Luo F, Hochholdinger F. 2016. LOB Domain Proteins: Beyond Lateral Organ Boundaries. *Trends Plant Sci* **21**: 159–167.

Xuan W, Audenaert D, Parizot B, Möller BK, Njo MF, De Rybel B, De Rop G, Van Isterdael G, Mähönen AP, Vanneste S, et al. 2015. Root Cap-Derived Auxin Pre-patterns the Longitudinal Axis of the Arabidopsis Root. *Curr Biol* 1381–1388. http://linkinghub.elsevier.com/retrieve/pii/S0960982215003991.

Xuan W, Band LR, Kumpf RP, Van Damme D, Parizot B, De Rop G, Opdenacker D, Moller BK, Skorzinski N, Njo MF, et al. 2016. Cyclic programmed cell death stimulates hormone signaling and root development in Arabidopsis. *Science (80-)* **351**: 384–387. http://www.sciencemag.org/cgi/doi/10.1126/science.aad2776.

Yan S, Sun X, Xiang B, Cang H, Kang X, Chen Y, Li H, Shi G, Yeh ETH, Wang B, et al. 2010. Redox regulation of the stability of the SUMO protease SENP3 via interactions with CHIP and Hsp90. *EMBO J* **29**: 3773–3786. http://dx.doi.org/10.1038/emboj.2010.245.

Yuan F, Yang H, Xue Y, Kong D, Ye R, Li C, Zhang J, Theprungsirikul L, Shrift T, Krichilsky B, et al. 2014. OSCA1 mediates osmotic-stress-evoked Ca2+ increases vital for osmosensing in Arabidopsis. *Nature*. http://www.nature.com/doifinder/10.1038/nature13593 (Accessed August 28, 2014).

Zarebanadkouki M, Kim YX, Carminati A. 2013. Where do roots take up water? Neutron radiography of water flow into the roots of transpiring plants growing in soil. *New Phytol* **199**: 1034–1044.

Zemlyanskaya E V., Wiebe DS, Omelyanchuk NA, Levitsky VG, Mironova V V. 2016. Meta-analysis of transcriptome data identified TGTCNN motif variants associated with the response to plant hormone auxin in Arabidopsis thaliana L. *J Bioinform Comput Biol* **14**: 1–16.

Zenser N, Ellsmore A, Leasure C, Callis J. 2001. Auxin modulates the degradation rate of Aux/IAA proteins. *Proc Natl Acad Sci U S A* **98**: 11795–11800.

APPENDICES

PIPS reflective statement

Note to examiners:

This statement is included as an appendix to the thesis in order that the thesis accurately captures the PhD training experienced by the candidate as a BBSRC Doctoral Training Partnership student.

The Professional Internship for PhD Students is a compulsory 3-month placement which must be undertaken by DTP students. It is usually centred on a specific project and must not be related to the PhD project. This reflective statement is designed to capture the skills development which has taken place during the student's placement and the impact on their career plans it has had.

PIPS statement:

For my industrial placement I worked for 3 months at KWS, a seed breeding company. I joined their Pre-Breeding R&D group, specialising on wheat yield improvement using wild wheat varieties. These wild varieties often have strong biotic and abiotic stress resistant but lack the high yield that is often found in wheat inbred lines. By crossing these stress resilient wild varieties with high yielding inbred lines adapted to UK climate and soil, KWS aims to create high yielding, high stress resilient lines that will increase wheat yield in the UK in the oncoming climate instable future in which a higher degree of extreme weather is expected.

During my internship with KWS I participated in preparing for the annual winter wheat trials, including seed processing, sowing and drilling, seed treating as well as field preparation and upkeep. This gave me a clear view on how these big field trials are set up and managed. Something I completely was oblivious of before, since most of my work takes place in the lab with often smaller sample sizes. The sheer size of the work opened my eyes to what these companies are managing year in year out.

Next to sowing preparations, I worked on so called grab (harvest samples). These are samples of around 30 wheat ears taken from F4 generation crosses that were analysed by a genome wide association study (GWAS). To completely understand what a GWAS was I first started my own literature study on this, for me, unknown topic. At the same time, I started counting ears, spikelet's and thresh these to analyse seed yield for all these crosses. All this data was put into the phenotype data of the GWAS analysis and run using earlier acquired SNP data and a genomic map. The output of this study presented a handful of loci that significantly affected a certain trait. These loci will be further investigated once they consistently show up in data from last year and the next year.

At the end of this analysis, I was asked to present this data to the Pre-Breeding group and any other staff interested. By having to explain the GWAS and the following results to an audience, it led me to understand it better myself. GWAS is a very commonly used tool in plant science research, where I have read a lot about, but never completely grasped the underlying assumptions and theory behind it. This internship at KWS gave me the time to sit down and read up about this topic, while also giving me a direct way of using it with the data I gathered.

Next to the skill to analyse and interpret GWAS data, I also learned how to grow wheat, how KWS sows (drills) seed for winter- and spring wheat trials and how to process harvested samples. I also got a better idea of how company dynamics work. Before this internship I had no idea of how big an organisation is necessary to do Breeding and Pre-Breeding research. Looking at the interaction between the different teams, gave me a better understanding of the day by day work that his to be done to manage these massive field plots. This led me to believe that in the future I would still like to work in science, but maybe on a more applicable topic like crop improvement.

Publications arising from this thesis

Orosa-Puente, B., Leftley, N., von Wangenheim, D., **Banda, J.,** Srivastava, A.K., Hill, K., Truskina, J., Bhosale, R., Morris, E., Srivastava, M., Kümpers, B., Goh, T., Fukaki, H., Vermeer, J.E.M., Vernoux, T., Dinneny, J.R., French, A.P., Bishopp, A., Sadanandom, A., Bennett, M.J., 2018. Root branching toward water involves posttranslational modification of transcription factor ARF7. ***Science*** 362, 1407–1410.

Banda, J., Bellande, K., von Wangenheim, D., Goh, T., Guyomarc'h, S., Laplaze, L., Bennett, M.J., 2019. Lateral Root Formation in Arabidopsis: A Well-Ordered LRexit. ***Trends in Plant Science*** 24, 826–839.

von Wangenheim, D., **Banda, J**., Schmitz, A., Boland, J., Bishopp, A., Maizel, A., Stelzer, E.H.K., Bennett, M., 2020. Early developmental plasticity of lateral roots in response to asymmetric water availability. ***Nature Plants*** 6, 73–77.

<u>Accepted for publication:</u>

Leftley, N., **Banda, J**., Pandey, B., Bennett, M.J., Voss, U. Uncovering how auxin optimises root systems architecture in response to environmental stresses., 2021***.*** ***Auxin Signaling, second edition.*** CSHL Perspectives.

PLANT SCIENCE

Root branching toward water involves posttranslational modification of transcription factor ARF7

Beatriz Orosa-Puente[1]*†, Nicola Leftley[2]†, Daniel von Wangenheim[2]†, Jason Banda[2], Anjil K. Srivastava[1], Kristine Hill[2]‡, Jekaterina Truskina[2,3], Rahul Bhosale[2], Emily Morris[2], Moumita Srivastava[1], Britta Kümpers[2], Tatsuaki Goh[2,4]§, Hidehiro Fukaki[4], Joop E. M. Vermeer[5,6], Teva Vernoux[3], José R. Dinneny[7], Andrew P. French[2,8], Anthony Bishopp[2], Ari Sadanandom[1]¶, Malcolm J. Bennett[2]¶

Plants adapt to heterogeneous soil conditions by altering their root architecture. For example, roots branch when in contact with water by using the hydropatterning response. We report that hydropatterning is dependent on auxin response factor ARF7. This transcription factor induces asymmetric expression of its target gene *LBD16* in lateral root founder cells. This differential expression pattern is regulated by posttranslational modification of ARF7 with the small ubiquitin-like modifier (SUMO) protein. SUMOylation negatively regulates ARF7 DNA binding activity. ARF7 SUMOylation is required to recruit the Aux/IAA (indole-3-acetic acid) repressor protein IAA3. Blocking ARF7 SUMOylation disrupts IAA3 recruitment and hydropatterning. We conclude that SUMO-dependent regulation of auxin response controls root branching pattern in response to water availability.

The soil resources plants require, such as water, are often distributed heterogeneously (*1*). To aid foraging, root development is responsive to the spatial availability of soil signals (*2*, *3*). Microcomputed tomography imaging revealed that soil-water contact affects root architecture, causing lateral roots (LRs) to form when roots are in direct contact with moisture (*4*, *5*). This adaptive branching response is termed hydropatterning (*4*, *5*). In this current study, we report the molecular mechanism controlling hydropatterning, revealing that core components of the auxin response machinery are targets for posttranslational regulation.

The hydropatterning response can be mimicked in vitro by growing seedling roots vertically on the surface of agar plates (*4*). Opposite sides of a root are either in contact with moisture (directly with the plate or via the meniscus) or exposed to air (fig. S1). To visualize whether primordia preferentially form on the side in contact with moisture, we transferred a root, including the gel it was growing on, into a light sheet fluorescence microscope to image young primordia and measure their angle of outgrowth with respect to the agar surface (fig. S1). This revealed that LRs preferentially emerge from the side of the root in contact with moisture (Fig. 1A).

What causes new primordia to form on the water-contact side of a root? Seedlings exposed to a hydropatterning stimulus exhibit an auxin response gradient across the root radius (*4*). Auxin regulates LR development (*6*). Auxin-responsive gene expression is regulated by a family of transcription factors termed auxin response factors (ARFs) (*7*). The model plant *Arabidopsis thaliana* contains five *ARF* transcriptional activating genes termed *ARF5*, *-6*, *-7*, *-8*, and *-19* (*8*). To determine which ARF gene(s) controls hydropatterning, we phenotyped loss-of-function alleles. ARF7 mutants (*8*, *9*) were all impaired (Fig. 1, A to C, and fig. S2), whereas hydropatterning was normal in mutants of other ARF family members tested (fig. S3). Hence, hydropatterning appears ARF7 dependent.

ARF7 regulates LR initiation (*6*, *8*, *10*, *11*). Network inference, chromatin immunoprecipitation–polymerase chain reaction (ChIP-PCR) validation, and transcriptomic studies have revealed that ARF7 controls the auxin-dependent expression of LR regulatory genes such as *LBD16* (fig. S4) (*12*). Like *ARF7*, *LBD16* loss-of-function alleles *lbd16-1* and *lbd16-2* exhibit a hydropatterning defect (fig. S5). ARF7 may therefore control hydropatterning in an *LBD16*-dependent manner. *LBD*-like genes are differentially expressed in maize during hydropatterning (*5*). To determine whether *LBD16* is differentially expressed in response to a hydropatterning stimulus by ARF7, we monitored spatial expression of a *gLBD16–green fluorescent protein* (*GFP*) reporter (*13*). *LBD16-GFP* was first detected in the elongation zone (Fig. 1D and movie S1) in a subset of cells [termed xylem pole pericycle (XPP) founder cells, from which primordia originate], consistent with this reporter being an early marker for LR development (*13*). In *Arabidopsis*, LRs originate from pericycle cells positioned above either xylem pole (*6*). We tested whether *gLBD16-GFP* was differentially expressed in XPP cell files closest to the agar. To mark which side of a root was exposed to air, we overlaid samples with agar with a low melting point and containing fluorescent beads and then imaged from multiple angles using light sheet microscopy (figs. S6 to S8). Reconstructed root images revealed preferential *gLBD16-GFP* expression in XPP cell nuclei earlier on one side of wild-type (WT) roots (Fig. 1E). Asymmetric *gLBD16-GFP* expression was disrupted in *arf7-1* (Fig. 1F), consistent with the mutant's hydropatterning defect (Fig. 1C). Quantification of *LBD16-GFP* distribution in WT and *arf7-1* revealed this reporter was differentially expressed in an ARF7-dependent manner (fig. S8, A to D and F). To test whether asymmetric *LBD16* expression is essential for hydropatterning, the constitutive 35S promoter was used to drive *LBD16* expression in *lbd16* (fig. S9). Expression of *35S:LBD16* failed to rescue the *lbd16* hydropatterning defect (in contrast to *LBD16:LBD16-GFP*). Hence, asymmetric *LBD16* expression is essential for hydropatterning.

We next tested whether LBD16-dependent hydropatterning was controlled by means of differential ARF7 expression by using transcriptional and translational *ARF7pro::ARF7-VENUS* reporters (figs. S10 and S11). In contrast to *gLBD16-GFP* (Fig. 1, E and F), ARF7 reporters did not exhibit differential expression in LR stem cells (Fig. 1G). To test whether ARF7 was a target of posttranslational regulation, ARF7 was constitutively expressed (using the 35S promoter) in *arf7-1*. This revealed *35S:ARF7* could rescue *arf7-1* hydropatterning (Fig. 1C and fig. S12). Hence, ARF7 appears to control hydropatterning by means of a posttranslational (rather than transcriptional) mechanism.

ARF7 contains posttranslational regulatory motifs including four putative sites for addition of small ubiquitin-like modifier (SUMO) proteins at lysine residues (K104, K151, K282, and K889) (Fig. 2A). SUMO, unlike ubiquitin, can modify the function (rather than abundance) of target proteins (*14*). We confirmed ARF7 is a target for SUMOylation by coexpressing GFP- and hemagglutinin (HA) epitope–tagged ARF7 and SUMO sequences (Fig. 2B). Addition of SUMO to ARF7 is abolished after replacing lysine with arginine in all four ARF7 SUMOylation motifs (in *gARF7-*$^{4K/R}$; Fig. 2B).

[1]Department of Biosciences, University of Durham, Durham DH1 3LE, UK. [2]Plant and Crop Sciences, School of Biosciences, University of Nottingham, Sutton Bonington LE12 5RD, UK. [3]Laboratoire Reproduction et Développement des Plantes, Univ Lyon, ENS de Lyon, F-69342, Lyon, France. [4]Department of Biology, Graduate School of Science, Kobe University, Kobe 657-8501, Japan. [5]Department of Plant and Microbial Biology, University of Zurich, CH-8008 Zurich, Switzerland. [6]Developmental Biology, Wageningen University and Research, Wageningen, Netherlands. [7]Department of Biology, Stanford University, Stanford, CA 94305, USA. [8]School of Computer Science, Jubilee Campus, University of Nottingham, Nottingham NG8 1BB, UK.
*Present address: School of Biological Sciences, University of Edinburgh, Edinburgh EH9 3FF, UK. †These authors contributed equally to this work. ‡Present address: Center for Plant Molecular Biology – ZMBP, University of Tübingen, D - 72076 Tübingen, Germany. §Present address: Graduate School of Science and Technology, Nara Institute of Science and Technology, 8916-5 Takayama, Ikoma 630-0192, Japan. ¶Corresponding author. Email: ari.sadanandom@durham.ac.uk (A.S.); malcolm.bennett@nottingham.ac.uk (M.J.B.)

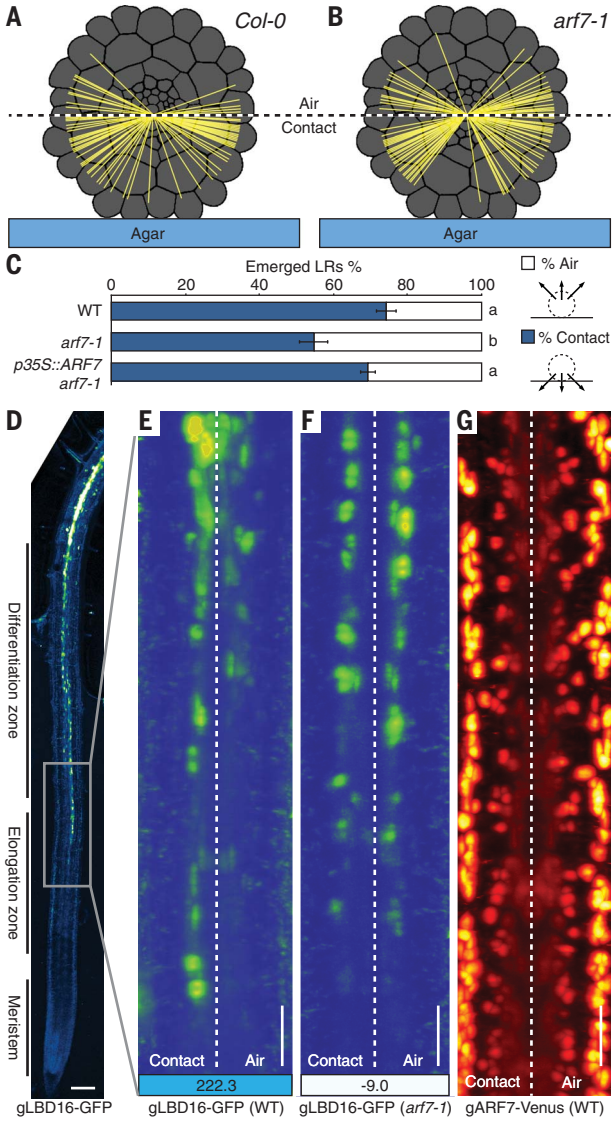

Fig. 1. *Arabidopsis* root branching toward water is ARF7 dependent. (**A** and **B**) Cross-section schematic of a root growing on agar. The LR primordia outgrowth angle (yellow lines) in respect to the agar surface is quantified from 3D light sheet microscopy images of WT (A) and *arf7-1* (B) plants. (**C**) Hydropatterning bioassay of WT, *arf7*, and *arf7* overexpressing ARF7 (*p35S::ARF7*). Data shown are mean values ± SE. Statistical differences were analyzed on the percent of emerged LRs emerging toward either contact or air using an analysis of variance, Tukey's HSD test ($P < 0.05$); statistically similar groups are indicated using the same letter. (**D**) Confocal image of *Arabidopsis* root tip expressing *gLBD16-GFP*. Gray boxed area highlights onset of *LBD16-GFP* expression in the elongation zone. (**E** to **G**) Maximum intensity projections of radial reslices obtained from light sheet fluorescent microscopy–multiview imaging show the gene expression pattern of *LBD16-GFP* in WT (E), *arf7* (F), and *ARF7::ARF7-Venus* (G) on the contact versus air sides. The numbers at the bottom of (E) and (F) display the index of asymmetry. Positive values correspond to an earlier expression beginning on the contact side; negative values show asymmetry toward the air side. Details are explained in figs. S1 and S6 to S8. Scale bars, 50 μm.

To test the importance of ARF7 SUMOylation for LR development and hydropatterning, we expressed SUMOylatable gARF7 and non-SUMOylatable *gARF7-*$^{4K/R}$ transgenes in *arf7-1*. Bioassays revealed *arf7* hydropatterning could be rescued by WT *gARF7* (Fig. 2, C and D, and fig. S13) but not by *gARF7-*$^{4K/R}$ (Fig. 2, E and F, and fig. S14). Nevertheless, *gARF7-*$^{4K/R}$ (like *gARF7*) remained capable of restoring *arf7* LR density to a WT level (Fig. 2F). Hence, ARF7-$^{4K/R}$ remained functional but unable to regulate hydropatterning. Quantification of *LBD16-GFP* distribution in *gARF7* versus *gARF7-*$^{4K/R}$ *arf7-1* revealed that this reporter was differentially expressed only in the presence of SUMOylatable ARF7 (fig. S8, A to C and E and G). We conclude ARF7 SUMOylation is required for hydropatterning.

How does SUMOylation modify ARF7 activity? ARF7 is rapidly SUMOylated after auxin treatment (Fig. 2G). One ARF7 SUMOylation site (K151) is located within the DNA binding domain (Fig. 2A) (*15*). SUMOylation may attenuate auxin-induced ARF7 DNA binding activity. Time course ChIP-PCR analysis revealed ARF7 transiently interacts with the *LBD16* promoter after auxin treatment (fig. S15). Furthermore, ChIP-PCR assays performed on *LBD16* and *LBD29* target promoters detected higher DNA binding by ARF7-$^{4K/R}$-GFP than WT ARF7-GFP (fig. S16). Hence, SUMOylation negatively regulates ARF7 DNA binding activity.

ARF7 transcriptional activity is negatively regulated by Aux/IAA (indole-3-acetic acid) repressor proteins (*16*). Aux/IAA proteins such as IAA3/SHY2 and IAA14/SLR control ARF7 activity during LR development (*16*, *17*). Like *arf7-1*, *IAA3* loss-of-function allele *shy2-31* causes an LR hydropatterning defect (Fig. 3A and fig. S17). Thus, we tested whether interactions among ARF7, IAA3/SHY2, and IAA14/SLR were SUMO dependent. Pull-down assays revealed that ARF7-GFP interacted with IAA3/SHY2 and IAA14/SLR proteins (fig. S18). In contrast, non-SUMOylatable ARF7-$^{4K/R}$ largely failed to pull down IAA3/SHY2. However, both forms of ARF7 interacted with IAA14/SLR (fig. S19). Hence, interaction between ARF7 and IAA3/SHY2 (but not IAA14/SLR) depends on the residues that regulate ARF7 SUMOylation.

Bioinformatic analysis revealed that *IAA3/SHY2* (but not *IAA14/SLR*) contained a SUMO interaction motif (SIM) (Fig. 3B). With its SIM domain mutated, interaction between IAA3 and WT ARF7 was abolished (Fig. 3C). Nevertheless, the IAA3 SIM mutant protein could interact with the TIR1 auxin receptor and TPL transcriptional repressor (figs. S19 and S20). Hence, mutating the SIM site differentially affects IAA3's ability to interact with SUMOylated ARF7 but not with other partners.

To assess the functional importance of the *IAA3* SIM sequence in planta, we engineered transgenic plants overexpressing *shy2-2* with or without SIM sequences. We examined the impact of the SIM sequence on the suppression of root branching characteristic of *shy2-2* mutant plants (*18*), a phenotype not dependent on hydropatterning. We drove overexpression of the *shy2-2* gene with the endodermal-specific CASP promoter. More root branching is evident in roots of plants expressing p*CASP:shy2-2* without the SIM sequence than in plants expressing p*CASP:shy2-2* with the SIM sequence (Fig. 3D). Thus, overexpression of shy2-2 in endodermis can block ARF7-dependent LR development, but only if the SIM sequence is included.

SUMO modifiers are added and removed from target proteins by E3 ligases and SUMO proteases, respectively. In *Arabidopsis*, OTS1 and OTS2 proteases cleave off SUMO from nuclear localized proteins (*19*). Pull-down assays revealed ARF7 is a direct target for OTS1 (fig. S21). Our bioassays revealed that the *ots1 ots2* mutant exhibits a hydropatterning defect (fig. S22). Hence, hydropatterning appears dependent on OTS1 and OTS2 function. These SUMO proteases are labile when plants are exposed to abiotic stress, causing their SUMOylated target proteins to accumulate (*19*, *20*). Indeed, transiently exposing *gARF7-GFP* seedlings to 20 minutes outside an agar plate resulted in a rapid increase in ARF7 SUMOylation (Fig. 2H). Hence, the absence (rather than the presence) of water stimulates this posttranslational response. Modeling suggests a substantial differential in water potential is generated across the air and contact axis of the root (*5*). We hypothesize that this triggers SUMOylated ARF7 on the air side of roots to recruit IAA3 and create a transcriptional repressor complex, thereby blocking auxin-responsive gene expression associated with LR initiation (Fig. 3E). Conversely, because IAA3 cannot be recruited by non-SUMOylated ARF7 in root cells on the contact side, this population of transcription factors can induce expression of genes like *LBD16* to trigger organ initiation (Fig. 3E).

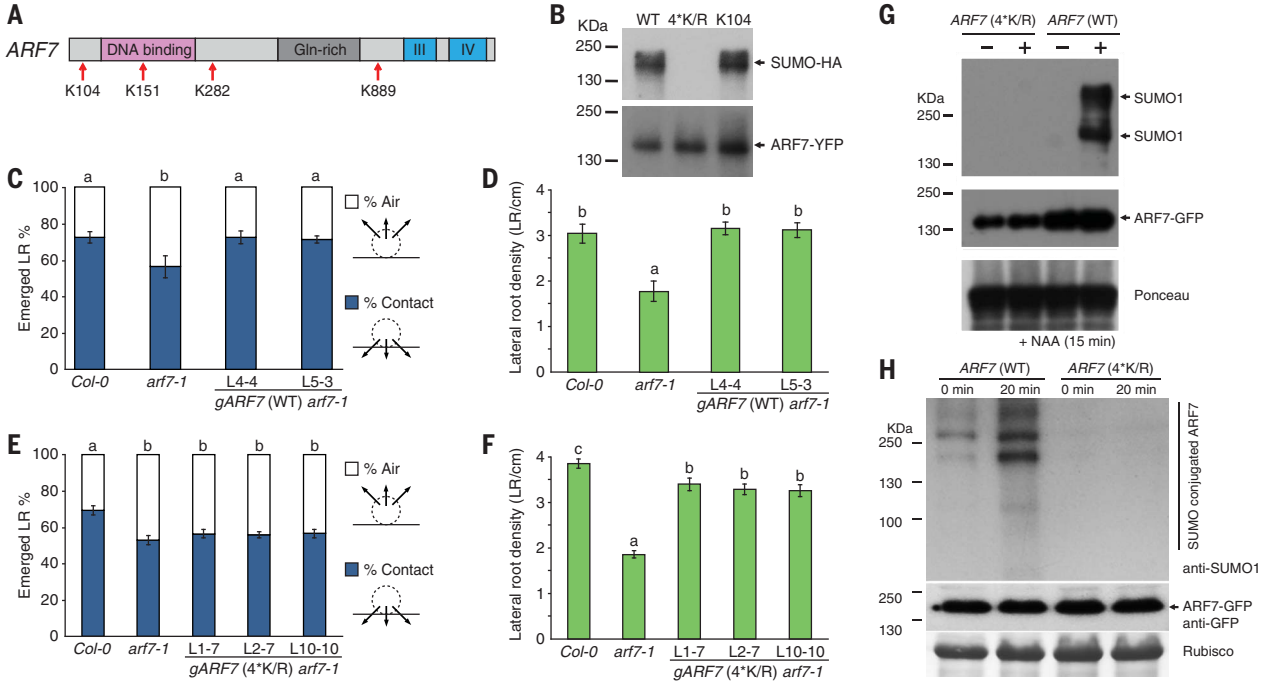

Fig. 2. ARF7 SUMOylation regulates hydropatterning and DNA binding affinity. (**A**) Schematic of ARF7 domains and four predicted SUMO sites K104, K151, K282, and K889. (**B**) Replacing all ARF7 SUMO site lysine with arginine residues in ARF7-GFP(4*K/R) blocks SUMOylation with HA-SUMO1 (but not WT ARF7 or single SUMO K104) in transient expression assays. YFP, yellow fluorescent protein. (**C** and **D**) Bioassays reveal that two independent transgenic lines expressing WT gARF7 can rescue *arf7-1* hydropatterning (C) and LR density defects (D). *n* LR = 196 (Col-0), 78 (arf7-1), 292 (L4-4), and 231 (L5-3); *n* plants = 7 (Col-0), 5 (arf7-1), 10 (L4-4), and 9 (L5-3). (**E** and **F**) Bioassays reveal that three independent transgenic lines expressing gARF7(4*K/R) cannot rescue *arf7-1* hydropatterning (E) but do restore LR density (F). *n* LR = 374 (Col-0), 268 (arf7-1), 198 (L1-7), 286 (L2-7), and 206 (L10-10); *n* plants = 12 (Col-0), 16 (arf7-1), 8 (L4-4), 11 (L5-3), and 8 (L10-10). Data are mean values ± SE, and statistics were performed as in Fig. 1C. (**G**) Immunoprecipitation reveals that ARF7-GFP [but not ARF7-GFP(4*K/R)] is rapidly SUMOylated 15 min after naphthaleneacetic acid (NAA) treatment. (**H**) Immunoprecipitation reveals that ARF7-GFP [but not ARF7-GFP(4*K/R)] is rapidly SUMOylated 20 min after seedlings were removed from their agar plates.

Fig. 3. SHY2 interacts with ARF7 in a SUMO-dependent manner to control hydropatterning. (**A**) Bioassay reveals that *IAA3/SHY2* mutant allele *shy2-31* does not exhibit a hydropatterning response. Data shown are mean ± SE. Letters indicate a significant difference compared with WT (*Ler*) roots based on Student's *t* test ($P < 0.05$). *n* LR = 208 (Ler) and 604 (shy2-31); *n* plants = 7 (Ler) and 19 (shy2-31). (**B**) The *IAA3* (but not *IAA14*) sequence contains a putative SIM, suggesting that IAA3 could bind SUMOylated ARF7. (**C**) Transient expression of IAA3/SHY2–HA (WT-SIM) or IAA3/SHY2–HA (SIM mutant) with ARF7-GFP or ARF7-GFP(4*K/R), followed by immunoprecipitation and western analysis, revealed that IAA3 interacts with ARF7 in a SIM- and SUMO-dependent manner. (**D**) Phenotyping *Arabidopsis* seedlings expressing *shy2-2* ± SIM by using the endodermal *CASP1* promoter revealed *CASP1:shy2-2* (WT) blocks LR branching (top), whereas *CASP1:shy2-2* (non-SIM) branch normally (bottom). Seedlings are from six independent lines termed SIM-containing *CASP1:shy2-2* (WT L1, L2, and L3) and non–SIM-containing *CASP1:shy2-2* (SIML1, L2, and L3). (**E**) Schematic summarizing the SUMO-dependent ARF7 model for hydropatterning, in which ARF7 is SUMOylated on the air side of the root, resulting in an interaction with IAA3 that inhibits LR initiation. On the contact side of the root, ARF7 is not SUMOylated, enabling the transcriptional factor to activate expression of genes involved in LR initiation.

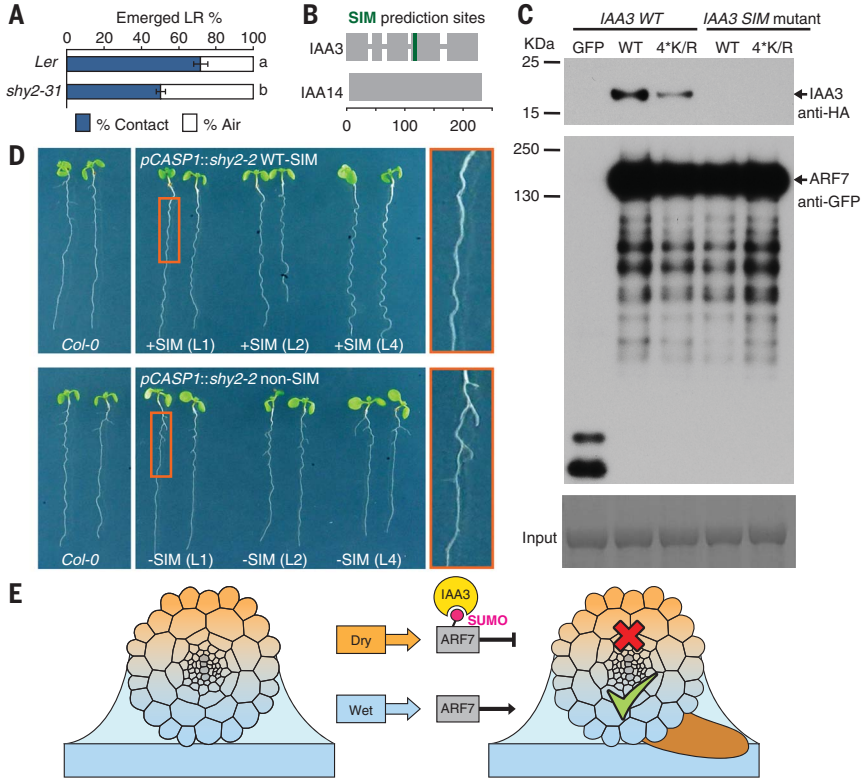

Our study has revealed how environmental inputs modulate the auxin response machinery. The SUMO-mediated posttranslational regulation of auxin signaling operates on top of the specificity provided from distribution of the hormone itself and the expression patterns of individual regulatory components. Thus, auxin regulation controls root branching pattern in response to water availability, building a root architecture that optimizes access to water.

REFERENCES AND NOTES

1. A. Hodge, *New Phytol.* **162**, 9–24 (2004).
2. B. D. Gruber, R. F. H. Giehl, S. Friedel, N. von Wirén, *Plant Physiol.* **163**, 161–179 (2013).
3. E. C. Morris *et al.*, *Curr. Biol.* **27**, R919–R930 (2017).
4. Y. Bao *et al.*, *Proc. Natl. Acad. Sci. U.S.A.* **111**, 9319–9324 (2014).
5. N. E. Robbins 2nd, J. R. Dinneny, *Proc. Natl. Acad. Sci. U.S.A.* **115**, E822–E831 (2018).
6. J. Lavenus *et al.*, *Trends Plant Sci.* **18**, 450–458 (2013).
7. T. Ulmasov, J. Murfett, G. Hagen, T. J. Guilfoyle, *Plant Cell* **9**, 1963–1971 (1997).
8. Y. Okushima *et al.*, *Plant Cell* **17**, 444–463 (2005).
9. R. M. Harper *et al.*, *Plant Cell* **12**, 757–770 (2000).
10. M. A. Moreno-Risueno *et al.*, *Science* **329**, 1306–1311 (2010).
11. B. Péret *et al.*, *Nat. Cell Biol.* **14**, 991–998 (2012).
12. J. Lavenus *et al.*, *Plant Cell* **27**, 1368–1388 (2015).
13. T. Goh, S. Joi, T. Mimura, H. Fukaki, *Development* **139**, 883–893 (2012).
14. E. S. Johnson, *Annu. Rev. Biochem.* **73**, 355–382 (2004).
15. D. R. Boer *et al.*, *Cell* **156**, 577–589 (2014).
16. T. Goh, H. Kasahara, T. Mimura, Y. Kamiya, H. Fukaki, *Philos. Trans. R. Soc. Lond. B Biol. Sci.* **367**, 1461–1468 (2012).
17. K. Swarup *et al.*, *Nat. Cell Biol.* **10**, 946–954 (2008).
18. J. E. M. Vermeer *et al.*, *Science* **343**, 178–183 (2014).
19. L. Conti *et al.*, *Dev. Cell* **28**, 102–110 (2014).
20. L. Conti *et al.*, *Plant Cell* **20**, 2894–2908 (2008).

ACKNOWLEDGMENTS

We acknowledge T. Guilfoyle for insightful discussions and dedicate this manuscript in his memory. We thank J. Dewick for assisting with the submission of this manuscript and C. Testerink for providing seed for the *lbd16-2* mutant allele. **Funding:** This work was supported by awards from the Biotechnology and Biological Sciences Research Council (grants no. BB/G023972/1, BB/R013748/1, BB/L026848/1, BB/M018431/1, BB/P016855/1, BB/M001806/1, BB/M012212); European Research Council (ERC) FUTUREROOTS Advanced grant 294729; ERC SUMOrice Consolidator grant 310235; Leverhulme Trust grant RPG-2016-409; ANR 2014-CE11-0018 Serrations grant; AuxID PICS grant from the CNRS; a joint INRA/University of Nottingham PhD grant to J.T.; J.E.M.V. is supported by the Swiss National Science Foundation (PP00P3_157524 and 316030_164086) and the Netherlands Organization for Scientific Research (NWO 864.13.008). H.F. was supported by a Grant-in-Aid for Scientific Research on Priority Areas (19060006) from the MEXT, Japan. **Author contributions:** B.O.-P., N.L., D.v.W., J.B., K.H., H.F., J.E.M.V., T.V., J.R.D., A.P.F., A.B., A.S., and M.J.B. designed experiments; B.O.-P., N.L, D.v.W., J.B., A.K.S., K.H., J.T., R.B., E.M., M.S., B.K., and T.G. performed experiments; and B.O.-P., N.L., D.v.W., A.B., A.S., and M.J.B. wrote the manuscript. **Competing interests:** Authors declare no competing interests. **Data and materials availability:** No restrictions are placed on materials, such as materials transfer agreements. Details of all data, code, and materials used in the analysis are available in the main text or the supplementary materials.

SUPPLEMENTARY MATERIALS

www.sciencemag.org/content/362/6421/1407/suppl/DC1
Materials and Methods
Figs. S1 to S22
Tables S1 to S3
References (*21–28*)
Movie S1

19 June 2018; accepted 6 November 2018
10.1126/science.aau3956

Root branching toward water involves posttranslational modification of transcription factor ARF7

Beatriz Orosa-Puente, Nicola Leftley, Daniel von Wangenheim, Jason Banda, Anjil K. Srivastava, Kristine Hill, Jekaterina Truskina, Rahul Bhosale, Emily Morris, Moumita Srivastava, Britta Kümpers, Tatsuaki Goh, Hidehiro Fukaki, Joop E. M. Vermeer, Teva Vernoux, José R. Dinneny, Andrew P. French, Anthony Bishopp, Ari Sadanandom and Malcolm J. Bennett

Science **362** (6421), 1407-1410.
DOI: 10.1126/science.aau3956

Rooting out the mechanism of asymmetry

Plant roots grow not in response to architectural blueprints but rather in search of scarce resources in the soil. Orosa-Puente *et al.* show why a new lateral root emerges on the damp side of a root rather than the dry side (see the Perspective by Giehl and von Wirén). The transcription factor ARF7 is found across the whole root but acquires a posttranslational modification on the dry side of the root, which represses its function. ARF7 on the damp side remains functional and is thus able to initiate the signaling cascade that leads to a new lateral root.

Science, this issue p. 1407; see also p. 1358

Trends in Plant Science

CellPress REVIEWS

Review

Lateral Root Formation in *Arabidopsis*: A Well-Ordered LRexit

Jason Banda,[1,4] Kevin Bellande,[2,4] Daniel von Wangenheim,[1] Tatsuaki Goh,[3] Soazig Guyomarc'h,[2] Laurent Laplaze,[2,*] and Malcolm J. Bennett[1,*]

Lateral roots (LRs) are crucial for increasing the surface area of root systems to explore heterogeneous soil environments. Major advances have recently been made in the model plant arabidopsis (*Arabidopsis thaliana*) to elucidate the cellular basis of LR development and the underlying gene regulatory networks (GRNs) that control the morphogenesis of the new root organ. This has provided a foundation for understanding the sophisticated adaptive mechanisms that regulate how plants pattern their root branching to match the spatial availability of resources such as water and nutrients in their external environment. We review new insights into the molecular, cellular, and environmental regulation of LR development in arabidopsis.

Highlights

Major advances have recently been made in arabidopsis to elucidate the cellular basis of LR development and the underlying GRNs.

New 4D imaging approaches are revolutionizing the perspective of the field on LR morphogenesis.

Recent studies reveal that biomechanical interactions between the new primordia and overlying tissues impact on organ initiation and morphogenesis. We propose a new mechanism, termed the developmental traffic light model, to explain how mechanical signals influence the patterning of the LR primordium.

LR research has progressed beyond studying individual genes to characterizing GRNs by exploiting innovative systems and omics-based approaches.

Arabidopsis roots employ regulatory mechanisms to sense the availability of water and nutrients so as to adapt their pattern of branching to optimize resource capture.

New Dimensions to Lateral Root Morphogenesis in Arabidopsis

Lateral roots (LRs) originate primarily from pericycle tissue in angiosperm species [1,2]. The pericycle consists of a single-cell layer surrounding the vascular tissues and which is overlain by endodermal, cortex, and epidermal tissues (Figure 1). In arabidopsis, LRs derive from six pericycle cell files overlying the xylem pole (Figure 1) [3–5]. Phloem-pole pericycle (PPP) cells are reported to be mitotically dormant, whereas xylem-pole-pericycle (XPP) cells retain stem cell activity after leaving the primary root meristem, and can therefore form LRs [6].

In arabidopsis, LR development can be divided into five main steps (Figure 1A): (i) pre-branch site formation, which takes place in the basal meristem/elongation zone [7,8]; (ii) LR initiation, which features pericycle nuclear migration to a common cell wall between pairs of LR founder cells (LRFCs) followed by asymmetric cell division in the differentiation zone [9,10]; (iii) LR morphogenesis in which the LRFCs divide further to form a lateral root primordium (LRP) that eventually acquires a root meristem organization [11,12]; (iv) concomitant LR emergence where the new organ grows through overlying tissue layers to emerge from the parent root in the differentiation zone [13], and finally (v) LR meristem activation corresponding to the initiation of cell divisions in the newly emerged LR meristem [14].

Until recently, arabidopsis LR development was studied in a 2D manner, primarily by visualizing primordia stages from a 'side on' viewpoint (Figure 1) and not considering wider 3D morphogenic events taking place. Advanced microscopy approaches such as confocal imaging and light sheet fluorescence microscopy (LSFM [15]) have helped to revolutionize the perspective of the field by providing static [16–19] or real-time [5,16,19,20] 3D visualization of LR development (Figure 1B). For example, LR formation features a stereotypical sequence of cell layer generation [5,11]. However, 4D time-lapse imaging studies of LR morphogenesis revealed that, after the first anticlinal cell division, the pattern of divisions does not follow a specific sequence [5,12,21]. There is a high level of plasticity in the spatiotemporal regulation of cell divisions, and a higher order of rules governs the shape of a new root tip.

[1]Plant and Crop Sciences, School of Biosciences, University of Nottingham, Sutton Bonington Campus, UK
[2]Unité Mixte de Recherche (UMR) Diversité, Adaptation, et Developpement des Plantes (DIADE), Institut de Recherche pour le Développement (IRD), Université de Montpellier, Montpellier, France
[3]Graduate School of Science and Technology, Nara Institute of Science and Technology, 8916-5 Takayama, Ikoma 630-0192, Japan
[4]Joint first authors

*Correspondence:
laurent.laplaze@ird.fr (L. Laplaze) and
malcolm.bennett@nottingham.ac.uk (M.J. Bennett).

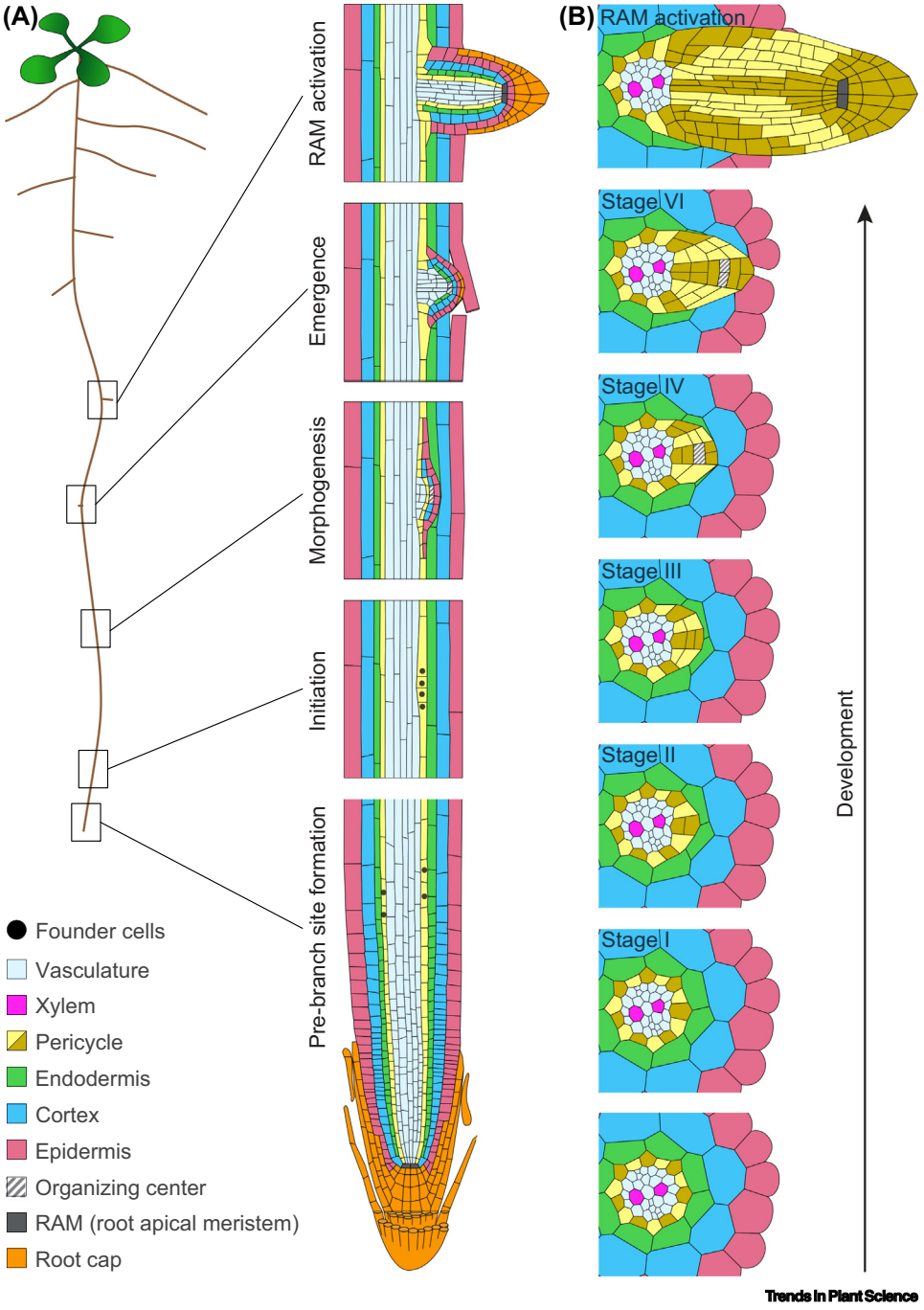

Figure 1. The Birth of a New Lateral Root (LR). The five main steps of LR formation in the classic longitudinal view (A). The process begins with the formation of the pre-branch sites in the meristem and elongation zone, followed by the initiation of LR founder cells (LRFCs) by the nuclear migration of two pericycle cells and their first anticlinal division in the differentiation zone. During morphogenesis the LRFCs divide periclinally as well as radially to form a 3D lateral root primordium (LRP). The LRP grows through the overlying tissue layers to emerge from the primary root. After emergence the LR acquires an active meristem. Color coding is according to the model described by Malamy and Benfey [11]. Six files of pericycle cells contribute to the LRP seen in a radial perspective (B) [5]. Common colors (yellow or dark yellow) highlight daughter cells derived from individual pericycle founder cell files.

Patterning under Pressure

LRPs originate from pericycle cells located deep within the parental root, and must therefore pass through overlying endodermal, cortical, and epidermal tissues before emerging [22] (Figure 1). This involves complex biomechanical interactions between the overlying tissues and the LRP that impact organ initiation and morphogenesis [21,23–25].

During LR initiation, root cells surrounding new primordia actively adapt and remodel their properties to accommodate organ emergence [21]. For instance, during organ initiation LRFCs swell before asymmetric division, and this would require adjacent xylem and/or endodermal cells to adjust their volumes to allow the radial growth of pericycle cells (Figure 1) [25]. Intercellular connectivity between the LRFC and surrounding cells are likely to be involved in coordinating cell volume adjustments through control of callose deposition by plasmodesmata remodeling enzymes which regulate LR initiation [26]. Interestingly, endodermal cell ablation is sufficient to trigger mitosis in the underlying pericycle cell [27]. Nevertheless, auxin cotreatment is necessary to observe an anticlinal division of the induced pericycle cells and initiate the LR organogenesis program [27]. In addition, the cell wall remodeling enzyme EXPANSIN A1 (EXPA1), which may modulate the mechanical properties of the pericycle cell wall, is also required for radial expansion of LRFCs and to ensure the correct positioning of the first anticlinal divisions (Table 1) [28]. Hence, sufficient pericycle width appears to be necessary to trigger asymmetric pericycle cell divisions during LR initiation [28].

During LR morphogenesis, primordia develop under mechanical pressure from surrounding tissues. These mechanical constraints, rather than a stereotypical pattern of cell division, are responsible for determining LRP shape [5,21]. Plants, like animals, regulate morphogenesis of new organs by employing a stem cell niche regulated by a mitotically inactive organizing center [29]. Interestingly, the organizing center appears once LRPs form four cell layers (stage IV, Figure 2C) and just prior to growing through the endodermis [12]. The endodermis contains an impermeable barrier, termed the Casparian strip (Figure 2), that was originally thought to regulate elemental and nutrient movement between inner and outer root tissues. However, the mechanical properties of the Casparian strip may also provide information that impacts on LRP development. During the time-course of LRP development, the mechanical properties of the endodermis cells are remodeled via an auxin-dependent pathway, and this is necessary for LRP development to progress from stage V onwards in a wild-type fashion [21]. We suggest that the Casparian strip could behave as a 'developmental traffic light' that holds back new LRs (red light) until the organizing center and stem cell niche are set up (amber light), allowing the new organ to break through the endodermis and overlying tissues before emerging into the soil (green light) (Figure 2). This checkpoint system could also provide a mechanism for regulating LR development by endogenous or environmental signals, only allowing LRPs to emerge in optimal conditions [30].

Breakthroughs in Lateral Root Emergence

New LRPs must reprogram overlying cells to aid organ emergence. The hormone auxin functions as a local signal released by new LRPs to facilitate this progression [22,25]. Key processes targeted by auxin in overlying cells include modifying their hydraulic properties, cell walls, and Casparian strip [21,23,25,31–33]. Regarding hydraulics, auxin represses the expression of almost every member of a family of water channels termed aquaporins [23]. Aquaporin genes encode plasma membrane (PIP class)- or tonoplast (TIP class)- localized water channels that regulate the hydraulic properties of plant cells. Auxin appears to fine-tune the hydraulic properties of cells in the LRPs and overlying tissues through its regulation of PIP and TIP gene spatial expression. Overexpressing and/or mutating PIP- and TIP-class aquaporins significantly delays LR

Table 1. Overview of Mutant and Transgenic Lines Affected in LR Development

Category	Mutant	Refs	LR phenotype	Stage affected
Auxin signaling	*35S:TOLS2*	[61]	Reduced number of LRs	LR initiation
	puchi	[90]	Reduced number of LRs	LRP development/emergence
	CASP::shy2-2	[25]	No LRs	LR initiation
Auxin transport	*aux1*	[91]	Reduced number of LRs	LR initiation
	lax3	[22]	Reduced number of LRs	Stage I development
Auxin conjugation/ degradation	*dao1*	[92]	Increased number of LRs	?
	gh3.1,2,3,4,5,6	[92]	Increased number of LRs	?
Auxin Biosynthesis	*yuc4*	[89]	Reduced number of LRs	?
Meristem establishment	*plt3 plt5 plt7*	[39]	Reduced emergence	Promotes initiation, reduces emergence
Transcription factors	*flp*	[93]	Reduced number of LRs	Delay in stage I
	fus3	[89]	Reduced number of LRs	Delayed emergence
	lec2	[89]	Reduced number of LRs	?
Peptides	*ralf34*	[58]	Increased number of LRs	Initiation
	irAtRALF1	[94]	Increased number of LRs	?
	ida	[24]	Decreased LR density	Delayed emergence
	CEP5	[59]	Decreased LR density	Stages I and II
Receptors	*xip1*	[59]	Decreased LR density	Initiation and development
	the1	[60]	Increased number of stage I LRP	Patterning and development of LRP
	GLV 1–11 overexpressor	[95]	Reduced LR density	Initiation and development
Kinases	*aur1-2 aur2-2*	[96]	Decreased LR density	Decreased initiation and emergence
	hae hsl2	[24]	Decreased LR density	Delayed emergence
	mkk4/mkk5	[97]	Reduced LR density	Delayed emergence
	MPK3SR and *MPK6SR*	[97]	Reduced LR density	Delayed emergence
Cell wall	*expa1*	[28]	Reduced number of LRs	Initiation
	gpat4 gpat8	[98]	Reduced number of LRs	Delayed emergence and deformation
	dcr	[98]	Reduced number of LRs	Delayed emergence and deformation
	bdg	[98]	Reduced number of LRs	Delayed emergence and deformation
	lrd5/xeg113	[31]	Increased rate of emergence	Emergence
Oxygen and ROS	*rap2.12,rap2.2,rap2.3,hre1,hre2*	[99]	Increased number of LRs	Delayed emergence
	erf VII	[99]	Increased number of LRs	Initiation
	robhc rbohd rbohe	[35]	Decreased LR density	Delayed emergence
	myb36	[37]	Decreased LR density	Delay in stage IV
	per7	[36]	Decreased LR density	Initiation
	per57	[36]	Decreased LR density	Initiation
Water transport	*pdbg1,2*	[26]	Increased LR density	Patterning and spacing
	pip2;1-1 and *pip2;1-2*	[23]	Reduced number of LRs	Delayed development
	tip1;1 tip2;1 tip2;1	[33]	Reduced number of LRs	Delayed emergence
Light sensing	*hyh/hy5*	[81]	Increased number of LRs	Initiation and emergence
SUMOylation	*ots1 ots2*	[68]	Reduced number of LRs	?
	siz1	[100]	Reduced number of LRs	?
Circadian clock	*toc1-1*	[46]	Decreased LR density	Delayed initiation and emergence

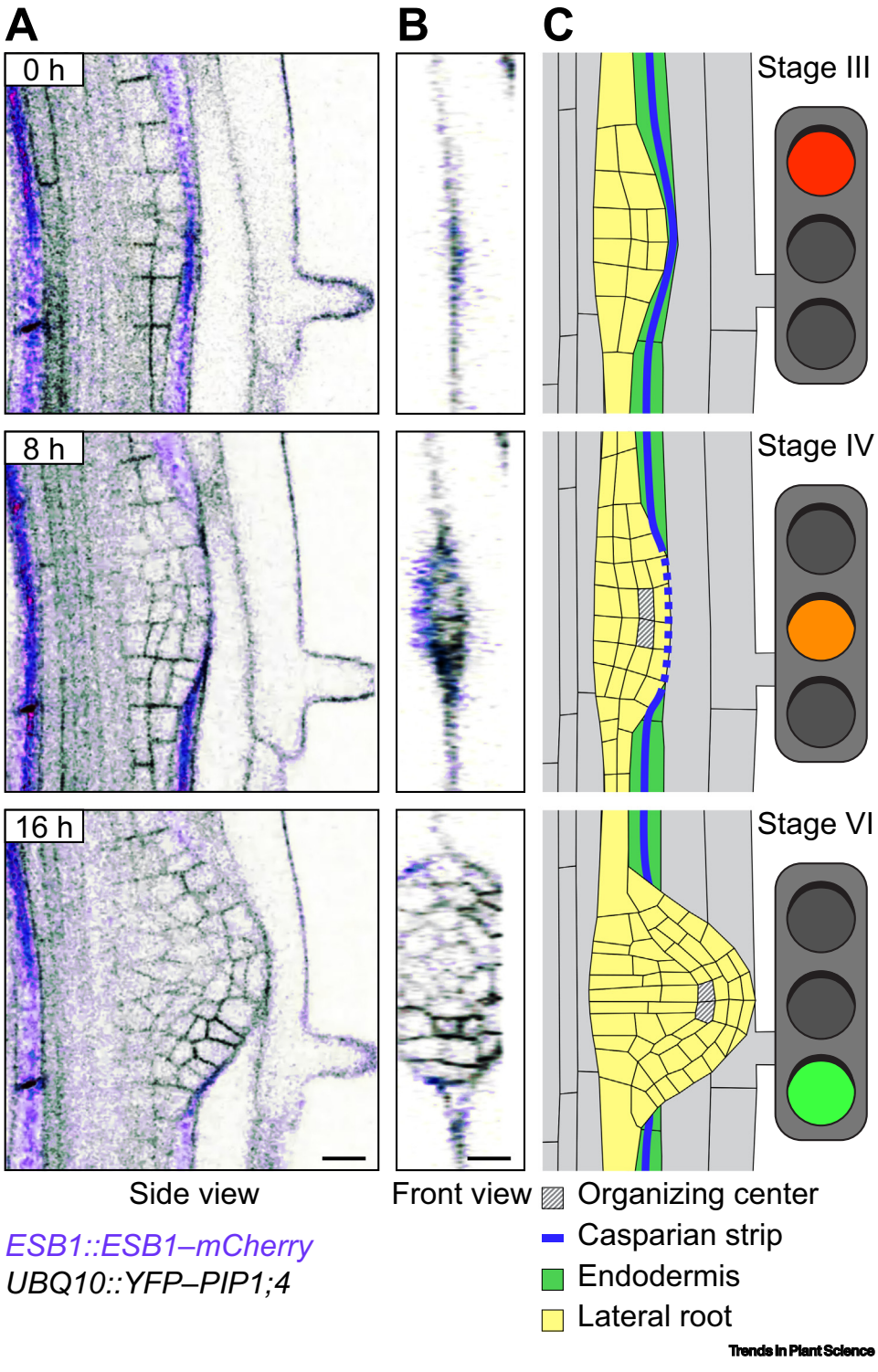

(See figure legend at the bottom of the next page.)

emergence (Table 1) [23,33]. Hence, auxin-dependent spatiotemporal regulation of aquaporin expression appears to be crucial for LRP emergence. The importance of these water channels results from new LRPs becoming symplastically isolated from surrounding tissues soon after initiation through the closure of plasmodesmata [26].

Auxin originating from new LRPs also causes overlying cells to modify their cell walls and undergo cell separation to enable new organs to emerge [22]. Auxin does this by triggering the sequential induction of the PIN3 auxin-efflux carrier and then the LAX3 influx carrier in cells directly overlying new LRPs [34]. A 3D root mathematical model indicated that, collectively, the distinct temporal patterns of induction of different classes of auxin carrier are necessary for preferential hormone accumulation in cells overlying LRPs. This functions to focus the auxin-dependent induction of cell wall remodeling enzymes, and consequentially cell separation, in advance of the emerging organ [22,34].

Reactive oxygen species (ROS) have also been proposed to function as important signals during auxin-regulated LR formation. ROS treatment increases LR density and can restore LR formation in lines in which auxin-mediated cell wall accommodation and remodeling in LRP-overlying cells are disrupted. ROS are deposited in the apoplast of overlying cells during LR emergence following the induction of RESPIRATORY BURST OXIDASE HOMOLOGs (RBOHs) (Table 1) [35]. Disrupting (or enhancing) the expression of RBOHs in LRPs or in overlying root tissues decelerates (or accelerates) LR development and emergence. Hence, RBOH-mediated ROS production appears to facilitate LR outgrowth by promoting the remodeling of overlying root cell walls. ROS generated within LRPs are also important for organ emergence [35,36]. The MYB36 transcription factor controls the expression of a subset of peroxidase genes (e.g., *PER9*) in boundary cells at the base of developing LRP. Mutating *MYB36* causes LRPs to adopt a flattened shape compared to the dome-like appearance of wild-type LRPs, resulting in slower organ emergence. Reducing the levels of hydrogen peroxide (H_2O_2) in *myb36-5* rescues the LR mutant phenotype (Table 1). This suggests that MYB36-dependent induction of peroxidases reduces H_2O_2 levels, thus defining the outer boundary of the growing LRP [37].

Lateral Root Gene Regulatory Networks: Learning Lessons from Primary Root Development

A large number of genes that regulate meristem patterning and maintenance in primary roots are also expressed during equivalent processes in LR development. For example, AP2-/ERF PLETHORA (PLT) transcription factors are major regulators of the gene regulatory network (GRN) controlling primary root meristem patterning and maintenance [38]. *PLT* genes are also expressed during LRP development [39]. Interestingly, *PLT3*, *PLT5*, and *PLT7* were shown to control the onset of *PLT1*, *PLT2*, and *PLT4* gene expression in developing LRPs (Figure 3). Accordingly, the triple *plt3 plt5 plt7* mutant exhibits a PLT-null phenotype in which the first round of periclinal cell divisions,

Figure 2. The Lateral Root Primordium (LRP) Must Break through the Overlying Endodermis Hardened with the Casparian Strip before Emergence. Three time-points of confocal time-lapse images highlight the thinning of the endodermis during lateral root (LR) morphogenesis and emergence (A). A 3D stack of images of an arabidopsis (*Arabidopsis thaliana)* root expressing a membrane marker (YFP–PIP1;4) and a Casparian strip marker (ESB1–mCherry) was captured every 10 minutes over a period of 20 h. Single-slice images are displayed in the side view (A) and front view (B). The process of emerging through the endodermal barrier could function as a 'developmental traffic light' in which the stage I–III LRP is initially stopped by the tough Casparian strip barrier in the overlying endodermal tissue (C). When the lights turn orange the Casparian strip receives cues from the LRP to slowly and locally break down to let the LRP pass, which gives the LRP time to form the organizing center and stem cell niche. When the lights turn green the LRP breaks through the endodermis and undergoes a drastic shape change from flat-topped to dome-shaped, while resuming its emergence through the cortex and epidermis.

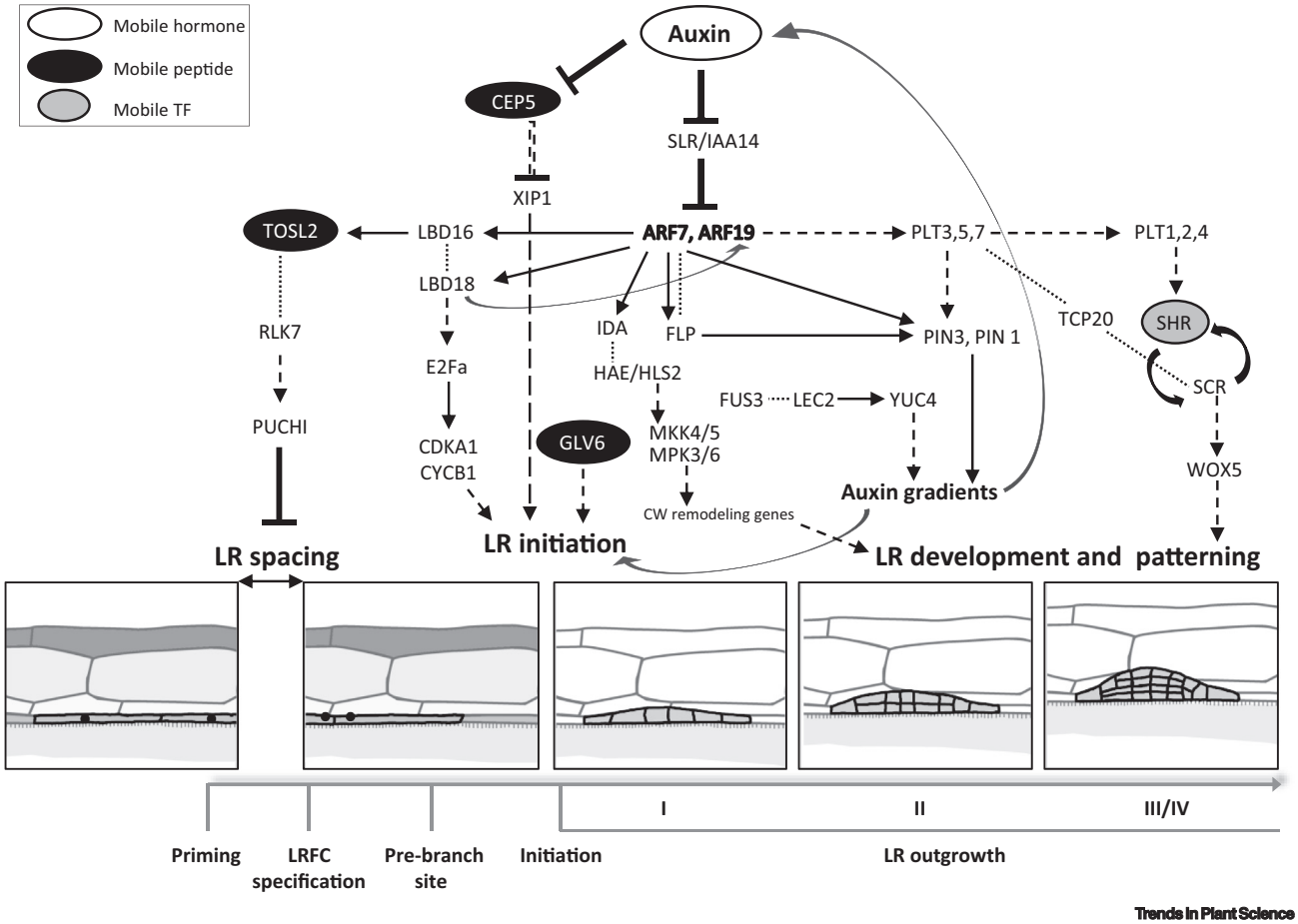

Figure 3. Feeding the Gene Regulatory Network (GRN) with Spatial and Temporal Information Results in Robust Spacing and Patterning of Developing Lateral Root Primordia (LRPs). Auxin synthesis, transport and response modules are sequentially triggered during lateral root (LR) initiation. The starting point for LR initiation is nuclear migration in lateral foot founder cells (LRFCs) that is controlled by the SLR/IAA14–ARF7 (ARF19) module. ARF7 and FLP control *PIN3* transcription and ARF7-regulated FLP transcription factors to form a coherent feed-forward loop controlling *PIN3* transcription. The LBD16 and LBD18 transcription factors control cell-cycle genes through transcription factor E2FA. LBD18 and ARFs form a double positive-feedback loop by binding directly to the *ARF19* promoter and through protein–protein interactions with ARF7 and ARF19 [88]. ARF7 and the ARF19 module control PLT-dependant responses through SHR/SCR turnover to control LR patterning [13]. TOLS2 peptide interacts with RLK7 to control PUCHI and LR spacing [61]. Plant-specific B3 transcription factors FUS3 and LEC2 interact together to induce the expression of the auxin biosynthesis gene *YUC4* through binding to its promoter elements in LRFCs [89]. The phloem pole-expressed CEP5 and its proposed leucine-rich repeat (LRR) receptor XIP1, as well as another peptide GOLVEN 6 (GLV6), might also be involved in the lateral root initiation (LRI) [57]. Abbreviations: ARF7/ARF19, AUXIN-RESPONSE FACTOR 7/19; CDKA1, A-type CYCLIN-DEPENDENT KINASE A1.1; CEP5, C-TERMINALLY ENCODED PEPTIDE 5; CW, cell wall; CYCB1, CYCLIN B1.1; FLP, FOURLIPS; FUS3, FUSCA 3; LBD16/LBD18, LATERAL ORGAN BOUNDARIES 16/18; LEC2, LEAFY COTYLEDON 2; RLK7, RECEPTOR-LIKE KINASE 7; SLR, SOLITARY-ROOT; TCP, TEOSINTE-BRANCHED CYCLOIDEA PCNA; TOLS2, TARGET OF LBD SIXTEEN 2; TF, transcription factor; WOX5, WUSCHEL-RELATED HOMEOBOX 5; XIP1, XYLEM INTERMIXED WITH PHLOEM 1; YUC4, YUCCA4.

which creates a two-layered LRP, is disrupted, resulting in a highly disorganized LRP with no properly defined meristem (Table 1). Surprisingly, transgenic expression of any PLT member from stage I onwards is sufficient to restore formative periclinal divisions and the subsequent organization of root meristem-like identities. This suggests that, rather than the target specificity of PLTs, the precise timing in *PLT* expression controls crucial events during LRP formation [13].

GRNs dependent on the GRAS-family SCARECROW (SCR)/SHORT-ROOT (SHR) transcription factors control the transition from stage II to stage III of LRP development (Figure 1), and thereby impact on the patterning of the quiescent center (QC) at stage IV/V [12,40]. The

observed onset of QC marker gene expression takes place concomitantly with a major transition from an early morphogenesis phase to a late meristem organization phase (Figure 1). Interestingly, the *scr* mutant is still able to establish a QC and a functional root meristem later in development, thus illustrating the robustness of the LR regulatory network [12]. In the primary root tip, SCR and PLT proteins were shown to directly induce the expression of QC marker *WOX5* by cooperative interaction with TCP to coordinate LR outgrowth in a time- and space-dependant manner (Figure 3) [41].

Lateral Root GRN: Emerging Properties

LR research has recently moved from studying the role of individual or a few genes to characterizing many genes that compose regulatory networks that control LR development by employing systems- and omics-based approaches. LR-related transcriptomic datasets have recently been produced in different conditions by monitoring gene expression dynamics during root branching in an unbiased fashion [42–46]. These offer unprecedented resources to explore single-gene expression dynamics and identify new candidate regulators of LR formation. More importantly, understanding how these components interact to form regulatory networks will be crucial if we aim to understand the emerging properties of LR development [47,48].

LRP can be induced in a highly synchronized manner by gravistimulation [23,46,49]. Researchers have therefore exploited gravistimulation-based LR induction to sequentially sample root bending zones every 3 h and to generate a high-resolution time-course transcriptomic dataset spanning LR induction to organ emergence and meristem activation [46]. This unique transcriptome resource offers unprecedented insights into expression dynamics during LR organogenesis, ranging from single genes to the network scale. More than 8000 (from 22 000) genes were differentially expressed during LRP formation. Clustering identified 77 distinct classes of gene expression profiles, highlighting the complex regulation of LR formation [46]. Interestingly, several circadian clock-regulated genes were identified, revealing a surprising clock-rephasing mechanism during LR initiation which was proposed to 'insulate' the LRP from diurnal fluctuations in water fluxes which might interfere with organ emergence [46].

This LR transcriptomic dataset has been used to infer the topology of the GRN coordinating LR morphogenesis [50]. The predicted GRN controlling primordia patterning was organized into two main auxin-regulated modules – an early network dependent on ARF7 and ARF19 (Figure 3), and a later network involving ARF5. In general, genes in the early ARF7-associated subnetwork are expressed in all primordia cells during the early stages of LRP development, and their expression then decreases and is confined to the base of the LRP. Concomitantly with this transition, the expression of genes associated with the ARF5 module increases. This module includes many transcription factors involved in primary root meristem organization whose expression is observed in central and tip LRP zones [13,50]. Interestingly, the inference approach indicated that these two subnetworks were linked by multiple mutual inhibition relationships [50]. This topology is predicted to confer a toggle-switch behavior on the GRN [51–53]. Together, this suggests that a switch between a module controlling the early stages of LR development and a second module regulating meristem organization takes place between 20 h and 30 h after gravistimulation, in other words at the transition from stage IV to stage V. Interestingly, this corresponds to the appearance of the organizing center identity in LRPs that marks a major transition in LRP cell divisions and expansion [12]. Thus, the predicted topology of the network suggests systems-scale mechanisms that contribute to LRP patterning. Network analysis further revealed an unexpected role for very long chain fatty acids (VLCFAs) that act downstream from the transcription factor PUCHI to control cell proliferation during LR formation [54].

LR transcriptome analysis and meta-analysis approaches have also contributed to the identification of numerous genes encoding small signaling peptides that are involved in intercellular communications during root branching [55,56]. Pairs of peptides and peptide–receptor complexes were shown to contribute to the spatial patterning of the LR initiation by mediating cell-to-cell signaling [24,57–60]. Recently, the secreted peptide TARGET OF LBD SIXTEEN 2/PAMP-INDUCED PEPTIDE-LIKE 3 (TOLS2/PIPL3) and its receptor RLK7 were shown to cooperate in inhibiting LR initiation near pre-existing LRFCs in a non-cell-autonomous manner, thus controlling minimal spacing between initiated LRs (Figure 3) [61]. Together with the intricate networks controlling hormone distribution and signaling across root tissues, peptide signaling pathways provide a new level of complexity in cell-to-cell communication that can contribute to the overall organization, especially spatial patterning, of the root branching process [62,63].

In summary, network-scale analyses have revealed that interconnectivity, redundancy, and multiple feedback loops provide plasticity at a cellular level, confer robustness to LRP development at a multicellular scale, and allow the integration of plant systemic cues. These network properties are likely to be crucial for the root developmental machinery to adapt to the myriad environment signals to which they are exposed in highly heterogeneous soil environments [17].

Divining Roots in Search of Moisture

Recent studies have revealed that plant roots employ sophisticated regulatory mechanisms to sense and respond to the availability of water and nutrients by branching. Soil consists of air pockets, stones, nutrient-rich and -poor patches, and the spatial and temporal distribution of moisture also varies. Regulating where a LR will form is therefore crucial to maximize the efficiency of foraging in soil. One of the most important soil resources for plant roots to obtain is water. It has long been known that osmotic stress can slow down LR emergence in arabidopsis and that this response is abscisic acid (ABA)-dependent [64]. In roots of barley (*Hordeum vulgare* cv.) and maize (*Zea mays*), water deficit caused LRs to no longer initiate [65]. A recent article revealed that this is controlled by an ABA-dependent regulatory mechanism termed xerobranching [66]. The effect of water deficit could be mimicked by ABA treatment, but mutants defective for key PYR/PYL ABA receptors were resistant to both signals. Additional experiments revealed that ABA accumulated in root tip tissues when exposed to water deficit, blocking LR initiation possibly by attenuating the oscillatory auxin-response network in the basal meristem.

A related adaptive response, termed LR hydropatterning, describes the ability of roots to differentiate between contact with moist soil or air, and then trigger preferential branching towards water. Xerobranching (inhibition of LR initiation by drought stress) and hydropatterning (preferential LR emergence towards the wettest side of the root) appear to be mechanistically distinct processes, because the latter response is unaffected in ABA mutant backgrounds [66,67]. Instead, modeling studies led authors to propose a 'sense-by-growth' mechanism for hydropatterning in which uptake of external water into the root elongation zone provides a means to perceive water availability [67]. Recent research has revealed that water availability controls LR initiation in the elongation zone via post-translational modification of AUXIN RESPONSE FACTOR 7 (ARF7). This key LR regulator encodes a transcription factor that contains four SUMO (small ubiquitin-like modifier) modification sites. Mutating all four ARF7 SUMOylation sites disrupts hydropatterning [68]. When roots are exposed to air, ARF7 SUMOylation rapidly increases. SUMOylation of ARF7 enables this transcription factor to recruit the Aux/IAA repressor protein, IAA3. This led to a model where the post-translational modification of ARF7 by SUMOylation on the dry side of a root causes IAA3 recruitment, repressing the expression of target genes such as *LBD16* that are required for LR initiation and hydropatterning (Figure 4) [68].

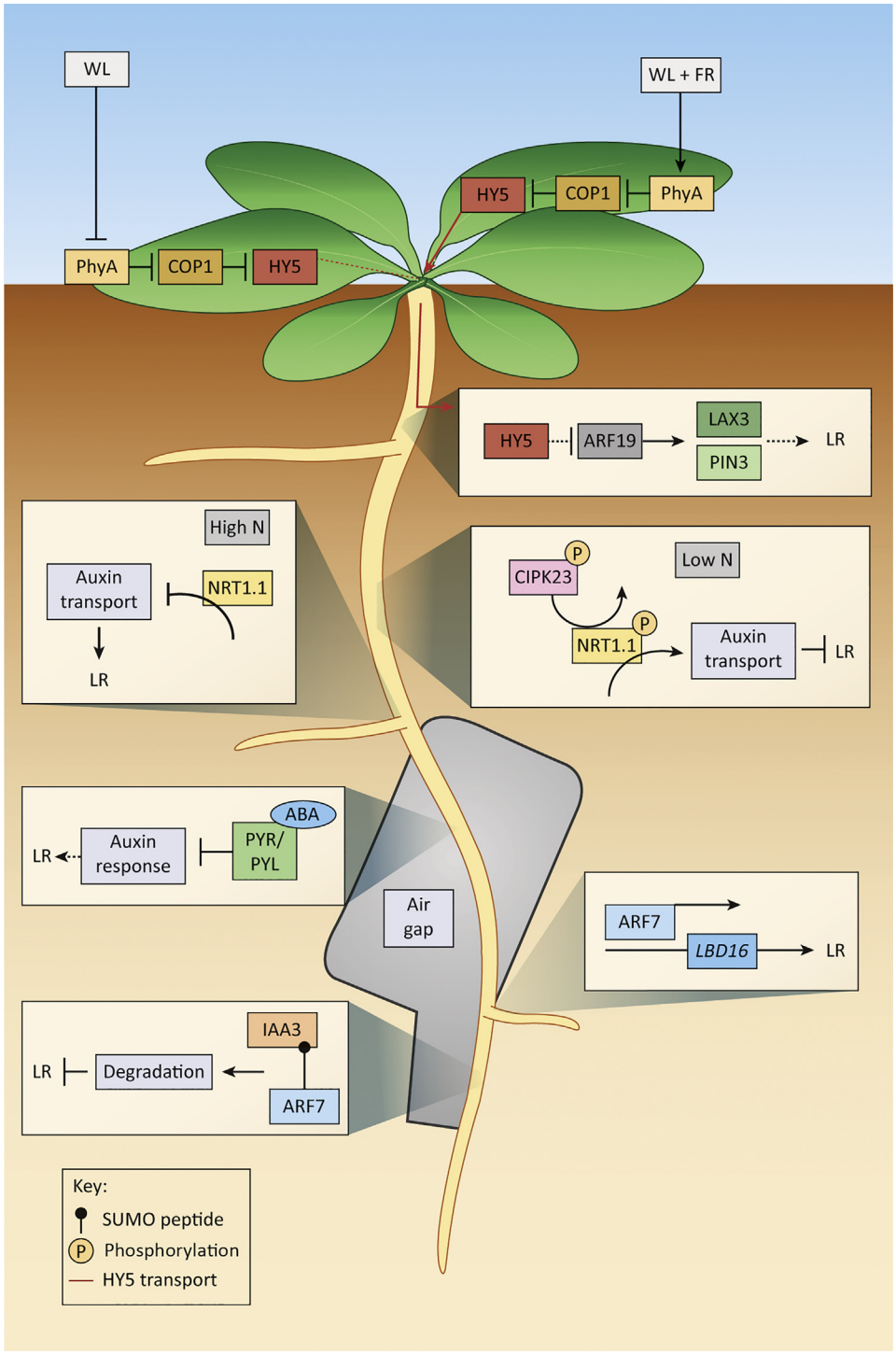

Figure 4. Soil and Light Environments Play a Key Role in Lateral Root (LR) Positioning. White light (WL) coming in from the top converts PhyA into its inactive form, leaving COP1 to break down HY5 [80]. However, under WL plus far-red (FR) light, COP1 is broken down through PhyA stabilization and PhyA-mediated degradation, and subsequently HY5

(Figure legend continued at the bottom of the next page.)

Branching Out in Search of Nitrogen (N)

The absorption of nutrients represents another crucial function of a root system, and of LRs in particular [17]. Nutrients are often dispersed in soil, and the ability by roots to sense nutrients is therefore vitally important for efficient resource acquisition. Nitrate is a key nutrient that has a profound effect on LR development, whose formation and elongation is induced under mild N stress, but this is impaired during exposure to high N or prolonged N stress (recently reviewed in [69–71]). A recent study reported the importance of C-TERMINALLY ENCODED PEPTIDES (CEPs) in roots experiencing low N, where root stele-expressed CEPs travel to the shoot and accumulate in the leaf phloem, where they bind to two leucine-rich receptor kinases (LRR-RKs), CEPR1 and CEPR2 [72]. This triggers the expression of *CEP DOWNSTREAM 1* (*CEPD1*) and *CEPD2*, which induce the expression of *NITRATE TRANSPORTER 2.1* (*NRT2.1*) in roots exposed to N-rich conditions [73]. This boosts N uptake, but inhibits LR growth, because *NRT2.1* knockout mutants have increased LR initiation [74]. A close family member, NRT1.1, coordinates a multitude of genes involved in the branching response to N [75]. This dual-affinity transporter and transceptor is phosphorylated under low-nitrate conditions by CBL-INTERACTING PROTEIN KINASE 23 (CIPK 23), turning the protein into a high-affinity nitrate carrier [76]. Interestingly, the non-phosphorylatable form of NRT1.1 no longer represses LR initiation [77]. Phosphorylation of NRT1.1 negatively effects local auxin buildup in LRP through its ability to cotransport auxin, which is inhibited in high nitrate patches, accounting for the local buildup of auxin, triggering the localized emergence of LRs (Figure 4) [77,78].

Shining Light on Lateral root Development

Recent studies have also revealed a key role for light in LR development. When roots were illuminated but the shoot was kept in the dark, root growth and LR emergence were reduced [79]. Interestingly, the bZIP transcription factor ELONGATED HYPOCOTYL 5 (HY5) knockout mutant is incapable of directing root growth in response to exposing the shoot to light. HY5 stability is regulated by the COP1 ubiquitin ligase, which degrades HY5 in the dark [80]. Accordingly, the *cop4-1* mutant showed no difference in root growth under different shoot and root light treatments. Stabilized HY5 in the shoot is transported down to the root via the phloem to induce LR formation [79]. However, adding far-red (FR) light could increase HY5 levels to a state in which LR primordia development was arrested [81]. The authors hypothesized that this is through the binding of HY5 to the *ARF19* promoter, thereby reducing its expression, which negatively effects PIN3 and LAX3 auxin-transport proteins in the overlying cortex (Figure 4) [81]. Hence, light perception in the shoot can finely regulate the auxin machinery locally in cells overlying LRPs to alter organ emergence. Interestingly, HY5 in shoots promotes carbon assimilation, and in roots can induce the expression of *NRT2.1* [79] while negatively regulating *AMT1;2* [82], which increase nitrate and reduces ammonium uptake, respectively. Collectively, this reveals novel root functions for HY5 and flags it as a key node in an array of plant environmental responses.

accumulates [81]. HY5 is transported through the phloem to inactivate lateral root primordium (LRP) development through inducing its own local expression and indirectly reducing LAX3 and PIN3 in the overlying tissue layers, possibly by interacting with ARF19. In areas of soil that are low in nitrogen (N), NTR1.1 becomes phosphorylated by CIPK23. Phosphorylation causes NRT1.1 to perform a dual function as a transporter of N and auxin, which blocks auxin accumulation in the LRP. In high-N soil, NRT1.1 is unphosphorylated, blocking its auxin-transport function and allowing auxin to build up in the LRP to promote emergence [75–78]. During periods of root growth through air gaps, xerobranching, abscisic acid (ABA) accumulates and binds to its receptor family, PYR/PYL, to indirectly reduce IAA levels and therefore lateral root founder cell (LRFC) initiation. However, when one side is in contact with water in the soil, ARF7 induces downstream targets such as LBD16 to initiate LRFC division on the side in contact with water, termed LR hydropatterning [68]. By contrast, on the air side ARF7 is SUMOylated, causing recruitment of IAA3 repressor proteins, resulting in ARF7 protein degradation and inhibition of LR formation. Abbreviations: IAA, indole acetic acid; SUMO, small ubiquitin-like modifier.

Concluding Remarks and Future Directions

Major advances have been made in elucidating the molecular and cellular basis of LR development using the model plant arabidopsis. Nevertheless, LR morphogenesis in other plant species such as maize and rice exhibits far greater anatomical variation than is observed in arabidopsis, reflecting the diversity of root classes [83]. However, very little is currently known about the underlying GRNs and mechanisms that drive the morphological diversity of these different LR classes in crops. Despite this, genetic studies in crop models such as maize and rice have identified common hormone signals and genes regulating LR development that are shared between these species and arabidopsis [84,85].

Surprisingly, limited attention has been paid to the role of biomechanics in the regulation of LR development to date. However, increasing evidence points to the central role of mechanical signals during development in both plants and animals [21,86]. LR development is a fascinating system in which to address these questions given that, unlike leaf primordia formation that takes place on the flanks of the shoot apical meristem, new root organs originate deep within parental root tissues. Live cell imaging (e.g., light sheet fluorescence microscopy) will further advance the field by allowing the dynamics of LR morphogenesis to be observed in real-time. Such research could generate fundamentally new knowledge about mechanical patterning and signaling in plants. For example, uncovering how LRP QC specification is synchronized with the new organ disrupting the Casparian strip could reveal novel mechanical signaling components and mechanisms linking cell walls and cell-cycle regulation.

The rich 'omic' resources available for arabidopsis have helped to initiate efforts to elucidate the underlying GRNs that control the morphogenesis of the new root organs. GRN approaches have revealed system properties that confer important features in LRP development: the ability to stabilize or, conversely, trigger changes in cell identity, the ability to organize those changes in time and space (patterning), the ability to reach a similar output from various transcriptomics scenarios (robustness) and, at the same time, the capability to integrate external cues that may influence the GRN final state. This latter property of plasticity plays a prominent role in root system adaptation to environmental signals. This will also provide a foundation on which to probe the sophisticated adaptive mechanisms that regulate how plants pattern root branching to match the spatial availability of resources such as water and nutrients in their external environment.

In parallel with omic data collection and studies, advances in cell tracking, sampling, and transcriptome analysis will generate a more detailed cartography of gene expression in developing LRPs at various stages. When combined with time-course transcriptomic datasets, this will allow exploration of GRNs at high temporal and spatial resolution. Moreover, cross-referencing with other omic datasets, such as epigenomics, or phosphoproteomics, will help to decipher the complex levels of regulation that result in the observed transcriptomic profiles and properties during LRP development [87]. Further studies will be needed in arabidopsis to explore and characterize the emerging properties of the LR GRN and how it integrates environmental signals, and also how it compares to mechanisms in other plant species (see Outstanding Questions).

Outstanding Questions

LR development is a two-step process that eventually leads to the formation of a new root meristem. Which cues control the organization of the LRP transition?

During LR morphogenesis, mechanical constraints from overlying endodermal, cortical, and epidermal tissues, rather than a stereotypical pattern of cell division, determine LRP shape. Does this mechanical information contribute to organ patterning? How does the LRP signal to the endodermal Casparian strip to induce local breakdown?

How are environmental and systemic signals integrated within the LR GRN to regulate root architecture at the whole-plant level?

How does the arabidopsis LR GRN differ compared to other plant species? Is it comparable to the different LR classes described in other species?

Can single-cell analysis increase our understanding of transcriptomics, lineage tracing, and epigenetics during LR morphogenesis?

Acknowledgments

J.B, D.v.W., T.G., and M.J.B. acknowledge the Biotechnology and Biological Sciences Research Council (BBSRC) for supporting doctoral training, responsive mode, and professorial fellowship awards (BB/G023972/1, BB/R013748/1, BB/L026848/1, BB/M018431/1, BB/PO16855/1, BB/M001806/1); K.B., S.G., and L.L. acknowledge support from the French National Research Agency (ANR) through the NewRoot project (ANR-17-CE13-0004-01); T.G. was supported by the Ministry of Education, Culture, Sports, Science, and Technology (MEXT) through a Japan Society for the Promotion of Science (JSPS) Research Fellowship for Young Scientists (12J02079).

References

1. Casimiro, I. *et al.* (2003) Dissecting *Arabidopsis* lateral root development. *Trends Plant Sci.* 8, 165–171
2. Torres-Martínez, H.H. *et al.* (2019) Lateral root primordium morphogenesis in angiosperms. *Front. Plant Sci.* 10, 1–19
3. Casero, P.J. *et al.* (1993) Lateral root initiation by asymmetrical transverse divisions of pericycle cells in adventitious roots of *Allium cepa*. *Protoplasma* 176, 138–144
4. Laskowski, M.J. *et al.* (1995) Formation of lateral root meristems is a two-stage process. *Development* 188, 49–58
5. von Wangenheim, D. *et al.* (2016) Rules and self-organizing properties of post-embryonic plant organ cell division patterns. *Curr. Biol.* 26, 439–449
6. Parizot, B. *et al.* (2008) Diarch symmetry of the vascular bundle in *Arabidopsis* root encompasses the pericycle and is reflected in distich lateral root initiation. *Plant Physiol.* 146, 140–148
7. De Smet, I. *et al.* (2007) Auxin-dependent regulation of lateral root positioning in the basal meristem of *Arabidopsis*. *Development* 134, 681–690
8. Moreno-Risueno, M.A. *et al.* (2010) Oscillating gene expression determines competence for periodic *Arabidopsis* root branching. *Science* 329, 1306–1311
9. Casimiro, I. *et al.* (2001) Auxin transport promotes *Arabidopsis* lateral root initiation. *Plant Cell* 13, 843–852
10. Goh, T. *et al.* (2012) The establishment of asymmetry in *Arabidopsis* lateral root founder cells is regulated by LBD16/ASL18 and related LBD/ASL proteins. *Development* 139, 883–893
11. Malamy, J.E. and Benfey, P.N. (1997) Organization and cell differentiation in lateral roots of *Arabidopsis thaliana*. *Development* 124, 33–44
12. Goh, T. *et al.* (2016) Quiescent center initiation in the *Arabidopsis* lateral root primordia is dependent on the SCARECROW transcription factor. *J. Cell Sci.* 129, e1.2
13. Du, Y. and Scheres, B. (2017) PLETHORA transcription factors orchestrate *de novo* organ patterning during *Arabidopsis* lateral root outgrowth. *Proc. Natl. Acad. Sci. U. S. A.* 114, 11709–11714
14. John, L.C.J. *et al.* (1995) A pathway for lateral root formation in *Arabidopsis thaliana*. *Genes Dev.* 9, 2131–2142
15. Ovečka, M. *et al.* (2018) Multiscale imaging of plant development by light-sheet fluorescence microscopy. *Nat. Plants* 4, 639–650
16. Mairhofer, S. *et al.* (2015) Extracting multiple interacting root systems using X-ray microcomputed tomography. *Plant J.* 84, 1034–1043
17. Morris, E.C. *et al.* (2017) Shaping 3D root system architecture. *Curr. Biol.* 27, R919–R930
18. Goh, T. (2019) Long-term live-cell imaging approaches to study lateral root formation in *Arabidopsis thaliana*. *Microscopy* 68, 4–12
19. Rellán-Álvarez, R. *et al.* (2015) GLO-Roots: an imaging platform enabling multidimensional characterization of soil-grown root systems. *eLife* 4, e07597
20. von Wangenheim, D. *et al.* (2017) Live tracking of moving samples in confocal microscopy for vertically grown roots. *eLife* 6, e26792
21. Lucas, M. *et al.* (2013) Lateral root morphogenesis is dependent on the mechanical properties of the overlaying tissues. *Proc. Natl. Acad. Sci. U. S. A.* 110, 5229–5234
22. Swarup, K. *et al.* (2008) The auxin influx carrier LAX3 promotes lateral root emergence. *Nat. Cell Biol.* 10, 946–954
23. Péret, B. *et al.* (2012) Auxin regulates aquaporin function to facilitate lateral root emergence. *Nat. Cell Biol.* 14, 991–998
24. Kumpf, R.P. *et al.* (2013) Floral organ abscission peptide IDA and its HAE/HSL2 receptors control cell separation during lateral root emergence. *Proc. Natl. Acad. Sci. U. S. A.* 110, 5235–5240
25. Vermeer, J.E.M. *et al.* (2014) A spatial accommodation by neighboring cells is required for organ initiation in *Arabidopsis*. *Science* 343, 178–183
26. Benitez-Alfonso, Y. *et al.* (2013) Symplastic intercellular connectivity regulates lateral root patterning. *Dev. Cell* 26, 136–147
27. Marhavý, P. *et al.* (2016) Targeted cell elimination reveals an auxin-guided biphasic mode of lateral root initiation. *Genes Dev.* 30, 471–483
28. Ramakrishna, P. *et al.* (2019) EXPANSIN A1-mediated radial swelling of pericycle cells positions anticlinal cell divisions during lateral root initiation. *Proc. Natl. Acad. Sci. U. S. A.* 116, 8597–8602
29. Sarkar, A.K. *et al.* (2007) Conserved factors regulate signalling in *Arabidopsis thaliana* shoot and root stem cell organizers. *Nature* 446, 811–814
30. Nacry, P. *et al.* (2005) A role for auxin redistribution in the responses of the root system architecture to phosphate starvation in *Arabidopsis*. *Plant Physiol.* 138, 2061–2074
31. Roycewicz, P.S. and Malamy, J.E. (2014) Cell wall properties play an important role in the emergence of lateral root primordia from the parent root. *J. Exp. Bot.* 65, 2057–2069
32. Vermeer, J.E.M. and Geldner, N. (2015) Lateral root initiation in *Arabidopsis thaliana*: a force awakens. *F1000Prime Rep.* 7, 32
33. Reinhardt, H. *et al.* (2016) Tonoplast aquaporins facilitate lateral root emergence. *Plant Physiol.* 170, 1640–1654
34. Péret, B. *et al.* (2014) Sequential induction of auxin efflux and influx carriers regulates lateral root emergence. *Mol. Syst. Biol.* 9 699–699
35. Orman-Ligeza, B. *et al.* (2016) RBOH-mediated ROS production facilitates lateral root emergence in *Arabidopsis*. *Development* 143, 3328–3339
36. Manzano, C. *et al.* (2014) The emerging role of reactive oxygen species signaling during lateral root development. *Plant Physiol.* 165, 1105–1119
37. Fernández-Marcos, M. *et al.* (2017) Control of *Arabidopsis* lateral root primordium boundaries by MYB36. *New Phytol.* 213, 105–112
38. Scheres, B. and Krizek, B.A. (2018) Coordination of growth in root and shoot apices by AIL/PLT transcription factors. *Curr. Opin. Plant Biol.* 41, 95–101
39. Hofhuis, H. *et al.* (2013) Phyllotaxis and rhizotaxis in *Arabidopsis* are modified by three plethora transcription factors. *Curr. Biol.* 23, 956–962
40. Drapek, C. *et al.* (2017) Uncovering gene regulatory networks controlling plant cell differentiation. *Trends Genet.* 33, 529–539
41. Shimotohno, A. *et al.* (2018) Root stem cell niche organizer specification by molecular convergence of PLETHORA and SCARECROW transcription factor modules. *Genes Dev.* 32, 1085–1100
42. Birnbaum, K. *et al.* (2003) A gene expression map of the *Arabidopsis* root. *Science* 302, 1956–1960
43. Himanen, K. *et al.* (2004) Transcript profiling of early lateral root initiation. *Proc. Natl. Acad. Sci. U. S. A.* 101, 5146–5151
44. Brady, S.M. *et al.* (2007) A high-resolution root spatiotemporal map reveals dominant expression patterns. *Science* 318, 801–806
45. De Smet, I. *et al.* (2008) Receptor-like kinase ACR4 restricts formative cell divisions in the *Arabidopsis* root. *Science* 322, 594–597
46. Voß, U. *et al.* (2015) The circadian clock rephases during lateral root organ initiation in *Arabidopsis thaliana*. *Nat. Commun.* 6, 7641
47. Lucas, M. *et al.* (2011) Plant systems biology: network matters. *Plant Cell Environ.* 34, 535–553
48. Haque, S. *et al.* (2019) Computational prediction of gene regulatory networks in plant growth and development. *Curr. Opin. Plant Biol.* 47, 96–105
49. Lucas, M. *et al.* (2008) Auxin fluxes in the root apex co-regulate gravitropism and lateral root initiation. *J. Exp. Bot.* 59, 55–66
50. Lavenus, J. *et al.* (2015) Inference of the *Arabidopsis* lateral root gene regulatory network suggests a bifurcation mechanism that defines primordia flanking and central zones. *Plant Cell* 27, 1368–1388
51. Gardner, T.S. *et al.* (2000) Construction of a genetic toggle switch in *Escherichia coli*. *Nature* 403, 339–342
52. Shoval, O. and Alon, U. (2010) SnapShot: network motifs. *Cell* 143 326–326
53. Tyson, J.J. *et al.* (2003) Sniffers, buzzers, toggles and blinkers: dynamics of regulatory and signaling pathways in the cell. *Curr. Opin. Cell Biol.* 15, 221–231

54. Trinh, D.C. *et al.* (2019) PUCHI regulates very long chain fatty acid biosynthesis during lateral root and callus formation. *Proc. Natl. Acad. Sci. U. S. A.* 116, 14325–14330
55. Ghorbani, S. *et al.* (2015) Expanding the repertoire of secretory peptides controlling root development with comparative genome analysis and functional assays. *J. Exp. Bot.* 66, 5257–5269
56. Oh, E. *et al.* (2018) Signaling peptides and receptors coordinating plant root development. *Trends Plant Sci.* 23, 337–351
57. Fernandez, A. *et al.* (2015) The GLV6/RGF8/CLEL2 peptide regulates early pericycle divisions during lateral root initiation. *J. Exp. Bot.* 66, 5245–5256
58. Murphy, E. *et al.* (2016) RALFL34 regulates formative cell divisions in *Arabidopsis* pericycle during lateral root initiation. *J. Exp. Bot.* 67, 4863–4875
59. Roberts, I. *et al.* (2016) CEP5 and XIP1/CEPR1 regulate lateral root initiation in *Arabidopsis*. *J. Exp. Bot.* 67, 4889–4899
60. Gonneau, M. *et al.* (2018) Receptor kinase THESEUS1 is a rapid alkalinization factor 34 receptor in *Arabidopsis*. *Curr. Biol.* 28, 2452–2458
61. Toyokura, K. *et al.* (2019) Lateral inhibition by a peptide hormone-receptor cascade during *Arabidopsis* lateral root founder cell formation. *Dev. Cell* 48, 64–75
62. Laskowski, M. and Tusscher, K.H. ten (2017) Periodic lateral root priming: what makes it tick? *Plant Cell* 29, 432–444
63. Du, Y. and Scheres, B. (2018) Lateral root formation and the multiple roles of auxin. *J. Exp. Bot.* 69, 155–167
64. Deak, K.I. and Malamy, J. (2005) Osmotic regulation of root system architecture. *Plant J.* 43, 17–28
65. Babé, A. *et al.* (2012) Repression of early lateral root initiation events by transient water deficit in barley and maize. *Philos. Trans. R. Soc. B Biol. Sci.* 367, 1534–1541
66. Orman-Ligeza, B. *et al.* (2018) The xerobranching response represses lateral root formation when roots are not in contact with water. *Curr. Biol.* 28, 3165–3173
67. Bao, Y. *et al.* (2014) Plant roots use a patterning mechanism to position lateral root branches toward available water. *Proc. Natl. Acad. Sci. U. S. A.* 111, 9319–9324
68. Orosa-Puente, B. *et al.* (2018) Root branching toward water involves posttranslational modification of transcription factor ARF7. *Science* 362, 1407–1410
69. Sun, C-H. *et al.* (2017) Nitrate: a crucial signal during lateral roots development. *Front. Plant Sci.* 8, 485
70. Shahzad, Z. and Amtmann, A. (2017) Food for thought: how nutrients regulate root system architecture. *Curr. Opin. Plant Biol.* 39, 80–87
71. Fredes, I. *et al.* (2019) Nitrate signaling and the control of *Arabidopsis* growth and development. *Curr. Opin. Plant Biol.* 47, 112–118
72. Tabata, R. *et al.* (2014) Perception of root-derived peptides by shoot LRR-RKs mediates systemic N-demand signaling. *Science* 346, 343–346
73. Ohkubo, Y. *et al.* (2017) Shoot-to-root mobile polypeptides involved in systemic regulation of nitrogen acquisition. *Nat. Plants* 3, 17029
74. Little, D.Y. *et al.* (2005) The putative high-affinity nitrate transporter NRT2.1 represses lateral root initiation in response to nutritional cues. *Proc. Natl. Acad. Sci. U. S. A.* 102, 13693–13698
75. Alvarez, J.M. *et al.* (2014) Systems approach identifies TGA1 and TGA4 transcription factors as important regulatory components of the nitrate response of *Arabidopsis thaliana* roots. *Plant J.* 80, 1–13
76. Ho, C.H. *et al.* (2009) CHL1 functions as a nitrate sensor in plants. *Cell* 138, 1184–1194
77. Bouguyon, E. *et al.* (2015) Multiple mechanisms of nitrate sensing by *Arabidopsis* nitrate transceptor NRT1.1. *Nat. Plants* 1, 15015
78. Bouguyon, E. *et al.* (2016) Nitrate controls root development through post-transcriptional regulation of the NRT1.1/NPF6.3 transporter/sensor. *Plant Physiol.* 172, 1237–1248
79. Chen, X. *et al.* (2016) Shoot-to-root mobile transcription factor HY5 coordinates plant carbon and nitrogen acquisition. *Curr. Biol.* 26, 640–646
80. Ang, L.H. *et al.* (1998) Molecular Interaction between COP1 and HY5 defines a regulatory switch for light control of *Arabidopsis* development. *Mol. Cell* 1, 213–222
81. van Gelderen, K. *et al.* (2018) Far-red light detection in the shoot regulates lateral root development through the HY5 transcription factor. *Plant Cell* 30, 101–116
82. Huang, L. *et al.* (2015) HY5 regulates nitrite reductase 1 (NIR1) and ammonium transporter1;2 (AMT1;2) in *Arabidopsis* seedlings. *Plant Sci.* 238, 330–339
83. Passot, S. *et al.* (2018) A new phenotyping pipeline reveals three types of lateral roots and a random branching pattern in two cereals. *Plant Physiol.* 177, 896–910
84. Hochholdinger, F. *et al.* (2018) Genetic control of root system development in maize. *Trends Plant Sci.* 23, 79–88
85. Meng, F. *et al.* (2019) Molecular mechanisms of root development in rice. *Rice* 12, 1
86. Brunet, T. *et al.* (2013) Evolutionary conservation of early mesoderm specification by mechanotransduction in Bilateria. *Nat. Commun.* 4, 2821
87. Zhang, H. *et al.* (2013) Quantitative phosphoproteomics after auxin-stimulated lateral root induction identifies an SNX1 protein phosphorylation site required for growth. *Mol. Cell. Proteomics* 12, 1158–1169
88. Pandey, S.K. *et al.* (2018) LBD18 uses a dual mode of a positive feedback loop to regulate ARF expression and transcriptional activity in *Arabidopsis*. *Plant J.* 95, 233–251
89. Tang, L.P. *et al.* (2017) FUSCA3 interacting with LEAFY COTYLEDON2 controls lateral root formation through regulating YUCCA4 gene expression in *Arabidopsis thaliana*. *New Phytol.* 213, 1740–1754
90. Hirota, A. *et al.* (2007) The auxin-regulated AP2/EREBP gene PUCHI is required for morphogenesis in the early lateral root primordium of *Arabidopsis*. *Plant Cell* 19, 2156–2168
91. Marchant, A. *et al.* (2002) AUX1 promotes lateral root formation by facilitating indole-3-acetic acid distribution between sink and source tissues in the *Arabidopsis* seedling. *Plant Cell* 14, 589–597
92. Porco, S. *et al.* (2016) Dioxygenase-encoding AtDAO1 gene controls IAA oxidation and homeostasis in *Arabidopsis*. *Proc. Natl. Acad. Sci. U. S. A.* 113, 11016–11021
93. Chen, Q. *et al.* (2015) A coherent transcriptional feed-forward motif model for mediating auxin-sensitive PIN3 expression during lateral root development. *Nat. Commun.* 6, 8821
94. Bergonci, T. *et al.* (2014) *Arabidopsis thaliana* RALF1 opposes brassinosteroid effects on root cell elongation and lateral root formation. *J. Exp. Bot.* 65, 2219–2230
95. Fernandez, A. *et al.* (2013) Transcriptional and functional classification of the GOLVEN/ROOT GROWTH FACTOR/CLE-like signaling peptides reveals their role in lateral root and hair formation. *Plant Physiol.* 161, 954–970
96. Van Damme, D. *et al.* (2011) *Arabidopsis* α aurora kinases function in formative cell division plane orientation. *Plant Cell* 23, 4013–4024
97. Zhu, Q. *et al.* (2019) A MAPK cascade downstream of IDA–HAE/HSL2 ligand–receptor pair in lateral root emergence. *Nat. Plants* 5, 414–423
98. Berhin, A. *et al.* (2019) The root cap cuticle: a cell wall structure for seedling establishment and lateral root formation. *Cell* 176, 1367–1378
99. Shukla, V. *et al.* (2019) Endogenous hypoxia in lateral root primordia controls root architecture by antagonizing auxin signaling in *Arabidopsis*. *Mol. Plant* 12, 538–551
100. Castro, P.H. *et al.* (2015) SIZ1-dependent post-translational modification by SUMO modulates sugar signaling and metabolism in *Arabidopsis thaliana*. *Plant Cell Physiol.* 56, 2297–2311

nature plants

BRIEF COMMUNICATION

https://doi.org/10.1038/s41477-019-0580-z

Early developmental plasticity of lateral roots in response to asymmetric water availability

Daniel von Wangenheim[1,2*], Jason Banda[1], Alexander Schmitz[2], Jens Boland[3], Anthony Bishopp[1], Alexis Maizel[3], Ernst H. K. Stelzer[2] and Malcolm Bennett[1*]

Root branching is influenced by the soil environment and exhibits a high level of plasticity. We report that the radial positioning of emerging lateral roots is influenced by their hydrological environment during early developmental stages. New lateral root primordia have both a high degree of flexibility in terms of initiation and development angle towards the available water. Our observations reveal how the external hydrological environment regulates lateral root morphogenesis.

The soil environment contains a variety of niches for a growing root to explore. This complex environment consists of nutrient-rich areas, air pockets and stones, among other matter, and strongly varies in its moisture distribution, to which we refer as the hydrological landscape. The ability of a root system to efficiently absorb water and nutrients from a heterogeneous medium depends on its architecture and its ability to adapt to the available potential resources[1]. For example, plants generate lateral roots in nutrient-rich patches and reduce branching in dry areas[2,3]. Similarly, roots emerge on the side of the primary root that is in contact with moisture, a mechanism called hydropatterning[4,5]. Here, we show that lateral root morphogenesis is steered by the available moisture during lateral root primordia initiation, while outgrowth stages and plasticity in organogenesis are probably directed by lateral root-flanking cells.

Lateral roots originate primarily from the pericycle cell layer in both angiosperms and gymnosperms. The radial distribution of lateral roots is partly determined by the geometry of the root with respect to underlying phloem and xylem tissues[6]. *Arabidopsis* has a diarch root with two xylem poles and lateral roots initiate in the pericycle cells overlaying one xylem pole[7,8] (Fig. 1a,b; Supplementary Fig. 1). To investigate how the vascular geometry of *Arabidopsis* affects the positioning of lateral root primordia in response to different moisture levels, we grew plants on an agar surface to expose roots to two distinct water environments: one side in contact with the agar (termed contact-side) versus humidity from the air (termed airside). We then captured three-dimensional (3D) image stacks of roots grown on the agar surface using light sheet fluorescence microscopy (LSFM) (Fig. 1c; Supplementary Figs. 2 and 3; Supplementary Video 1). We observed that both the orientation of the xylem pole axis and the lateral root primordium initiation site relative to the agar surface are uniformly distributed across the radius of the root. In the case of lateral root primordium (LRP) initiation sites, 54% orient towards the gel versus 46% towards the airside (Fig. 1d,e). This suggests that in our set-up, the choice of the initiation site is not influenced by a moisture gradient. However, 80% of the lateral root emergence angles were <90° and pointed towards the agar (Fig. 1c–e). When does this apparent asymmetry of the emergence angle of the organ arise?

To investigate the angle of the lateral root outgrowth relative to the xylem pole, we defined a line from the xylem pole to the tip of the primordium (Fig. 1c). The angle on top of the xylem pole is defined as 0°. Our experiments revealed that this angle varied by more than 70° (Fig. 1f,h). The primordia emerging on the airside oriented mainly towards the gel surface. In contrast, primordia initiating on the contact-side oriented mainly parallel to the gel surface. These results indicate that the lateral root outgrowth angle is highly plastic and steers organ development preferentially towards externally available water sources.

We tested whether external water availability is the stimulus for the orientation of the lateral root outgrowth when it grows along the agar surface. Hence, we quantified lateral root angles when grown embedded in gel or immersed in water to provide uniform mechanical or aqueous environments, respectively. In both cases, we observed that the angles of the orientations of the lateral roots were significantly smaller relative to the angles of roots grown on agar (Fig. 1g,h). Hence, when moisture is uniformly available, the lateral root outgrowth angles tend to distribute evenly and deviate less from the axis of xylem poles.

Next, we investigated at which developmental stage (or stages) the bias in lateral root emergence angle arises. Lateral root primordia originate from dividing cells located in five to eight adjacent pericycle cell files, which undergo a series of anticlinal, periclinal and then radial divisions[9–12]. Earlier studies have reported the importance of the cell file that directly overlies the xylem pole during lateral root morphogenesis in *Arabidopsis*[8,10,13]. This 'central' cell file forms the tip of the primordium and contributes most of the cell mass at the time of emergence[12]. However, the role of flanking cell files could be more important than previously reported. To uncover the contribution of each cell file, we manually tracked cell contours in a transversal cross-section post emergence in two independent experiments (Fig. 2a). This analysis revealed that all cell files contribute to the final lateral root primordium, but flanking cell files continue to contribute to the volume of a primordium, whereas the central cell file provides only a thin cell file (Fig. 2a). This highlights that all contributing pericycle cell files play an important role through different stages of lateral root morphogenesis.

The contribution of individual cell files is highly variable[12]. This could be due to differences in radial division rates between cell files, which increases the width of the primordium (Fig. 2b). To address this possibility, we re-analysed five published datasets[12] and observed that the occurrence of radial divisions varied (Fig. 2c).

[1]Plant and Crop Sciences, School of Biosciences, University of Nottingham, Nottingham, UK. [2]Buchmann Institute for Molecular Life Sciences, Goethe-Universität Frankfurt am Main, Frankfurt am Main, Germany. [3]Centre for Organismal Studies, Heidelberg University, Heidelberg, Germany. *e-mail: daniel.vonwangenheim@nottingham.ac.uk; malcolm.bennett@nottingham.ac.uk

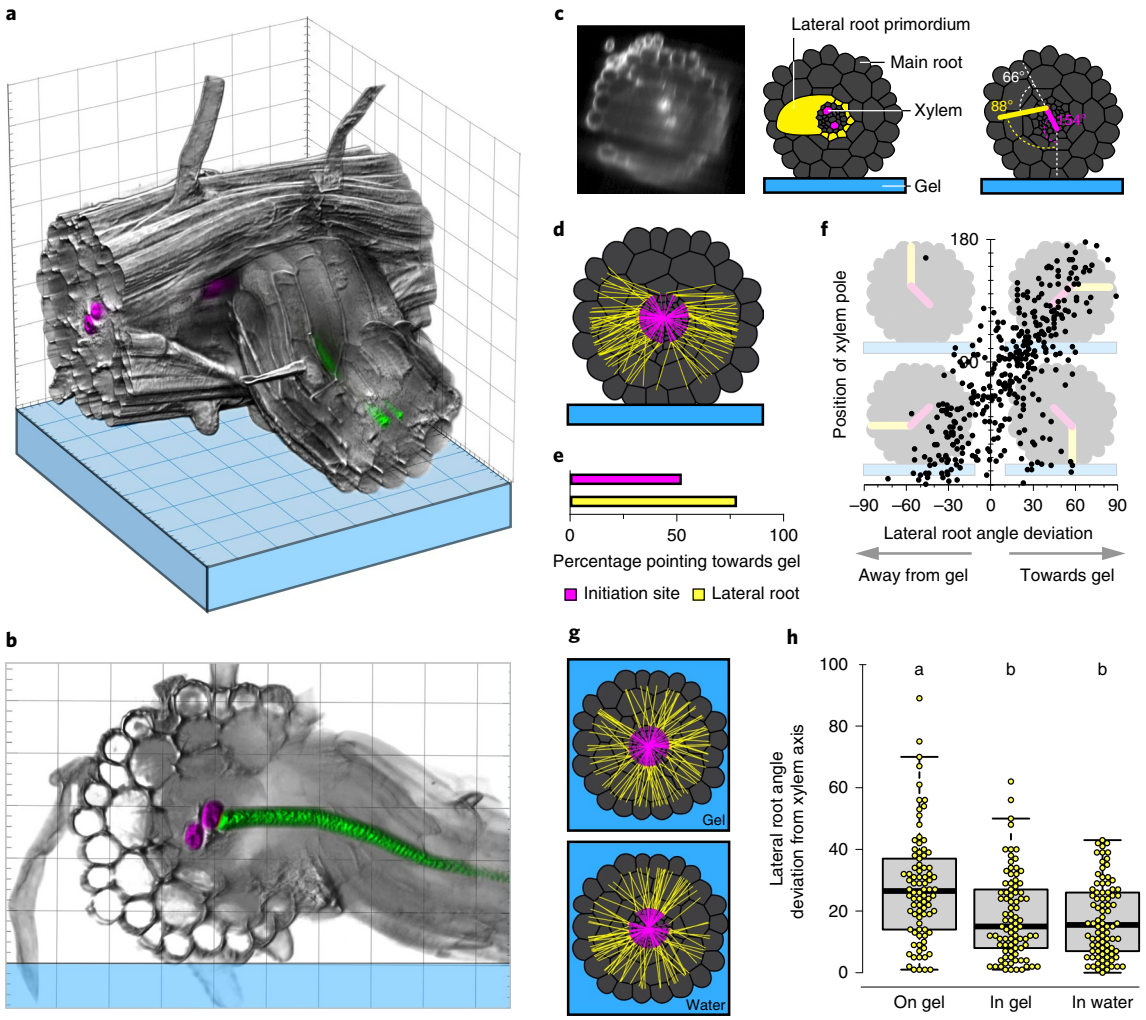

Fig. 1 | *Arabidopsis* branching is influenced by the position of the root in the agar. a, A 3D rendering of the autofluorescence signal of a lateral root grown out of the main root captured by multiview LSFM. **b**, The two xylem strands of the lateral root (green) are connected to one of the two xylem strands of the main root (magenta). Scaling boxes are 25 µm in size, while tick marks are 5 µm. **c**, Autofluorescence 3D light sheet imaging of a young primordium (left), a schematic (middle) and the corresponding angles (right) of the xylem axis (magenta) and the lateral root (yellow) relative to the gel surface. The white angle represents the orientation of the lateral root relative to the xylem axis. **d**, The complete overlaid set of $n = 87$ angle measurements based on $n = 10$ biologically independent samples (dataset 180912). **e**, Percentage of lateral roots oriented towards the gel; that is, <90° with respect to the agar surface (dataset 180912, $n = 87$). **f**, Lateral root angle deviation relative to the xylem axis plotted against the position of the xylem relative to the gel surface. Lateral roots orient towards the agar when initiation occurs on the airside (upper right) and away from the gel when initiation faces the contact side (lower left). No lateral root is oriented towards the air when initiation occurs on the airside (upper left). The data are derived from five independent experiments. In total, 352 primordia from 42 plants were analysed (Supplementary Fig. 3). Bivariate Pearson correlation was used to test the linear relationship between the position of the xylem pole and the lateral root outgrowth angle. A strong positive correlation was found, with $r = 0.726$ ($P = 7.8545 \times 10^{-59}$; two-tailed test). **g**,**h**, Lateral roots grown in gel or water have a smaller deviation angle relative to the xylem pole axis than those grown on gel. Overlaid set (**g**) and plot (**h**) of angle measurements are shown. Data were derived from one experiment, and 87 images were analysed per condition. Centre lines show the medians. Box limits indicate the 25th and 75th percentiles as determined by R software (https://www.r-project.org/); whiskers extend 1.5 times the interquartile range from the 25th and 75th percentiles, data points are plotted as yellow circles. Statistical differences were analysed using one-way analysis of variance and Tukey's honest significant difference test ($P < 0.0001$; 95% confidence interval). Statistically similar groups are indicated by the same letters.

In datasets 121211 and 130607, radial divisions occurred preferentially on one side of the primordium, which resulted in an asymmetric increase in width (Fig. 2c). Hence, although these images were acquired from samples submerged in a specimen chamber of the light sheet microscope, they reveal plasticity in the direction of radial growth. Even in these datasets, radial divisions promote growth along a particular direction and provide a basis for influencing the angle of the lateral root outgrowth.

The direction of lateral root outgrowth is determined by the radial cell divisions in flanking cell files. However, there are earlier events that influence the angle of outgrowth. Recently, we reported the expression of the early lateral root marker *pLBD16::LBD16:GFP*[14] preferentially in pericycle cells facing the agar (contact-side)[5]. To investigate the radial position of early events during lateral root initiation relative to the xylem pole axis, we captured the expression of LBD16:GFP (a fusion protein of LBD16 and green fluorescent protein (GFP)) with respect to the xylem pole. In 39 lateral root primordia datasets, we observed 13 cases in which LBD16 expression was not strictly above the xylem pole (Supplementary Fig. 4). In Fig. 2d–f (and Supplementary Video 2), we show the most

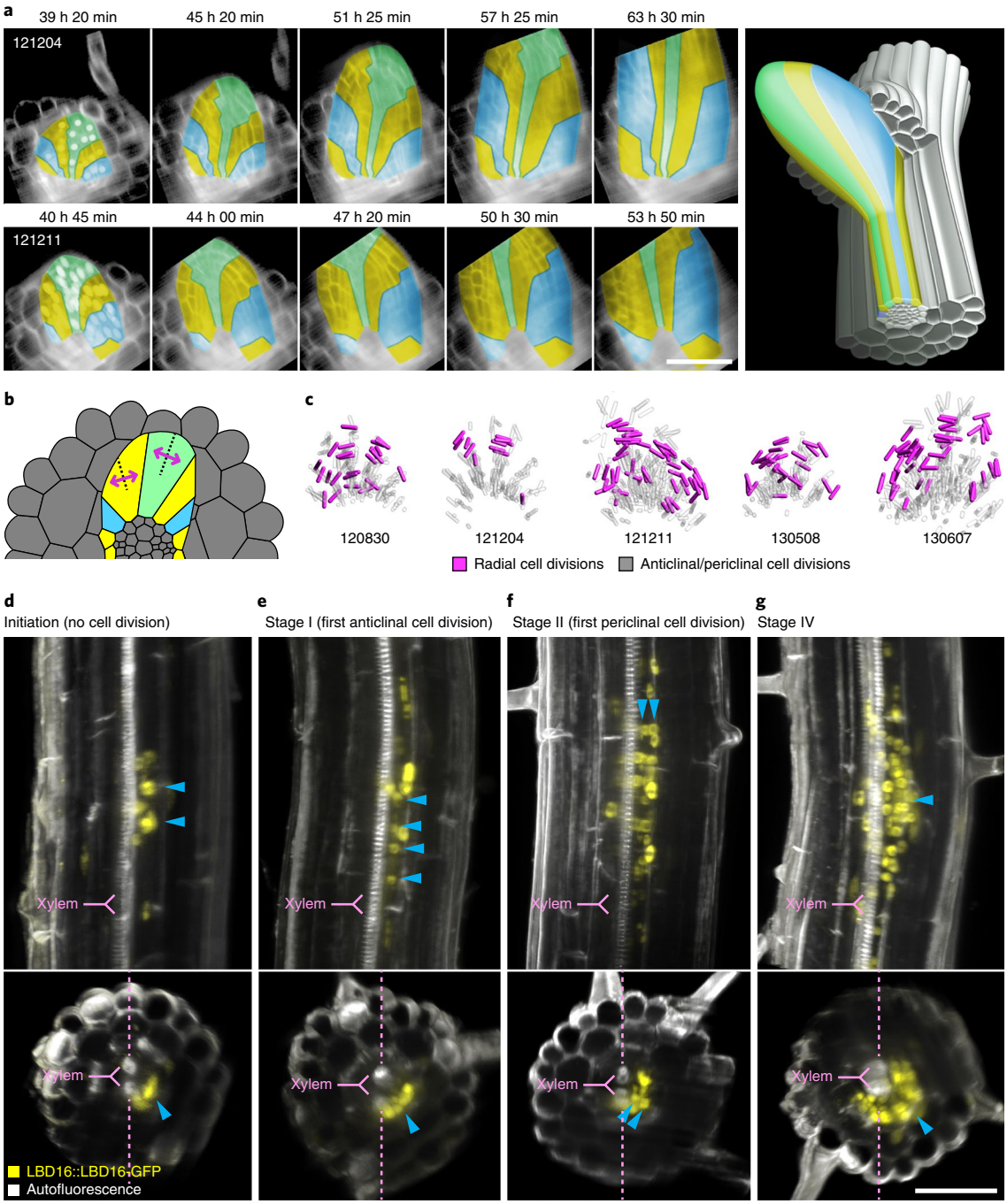

Fig. 2 | Lateral root development is flexible during all developmental stages. a, Cell file tracking from 3D LSFM time-course datasets (121204 and 121211)[12] of two biologically independent experiments. The colour of the cell file indicates which group of cells are derived from the same mother cell. Here, the green cells represent the central cell file. They derive from the cell that undergoes the first periclinal division on its way to becoming a lateral root primordium. This figure illustrates that the contribution of flanking cell files (yellow and blue cell files) increases over time and pushes the central cell file out of the main root. **b**, Schematic of radial divisions in some cell files, which increases the width of the primordium. **c**, Cell division pattern analyses from five biologically independent time-course data (120830, 121204, 121211, 130508 and 130607) reveal that radial divisions occur preferentially on one side. Thus, the lateral root bends along one direction. **d**–**g**, Four individual roots show the expression pattern of LBD16 during the first stages of lateral root development. That is, indicated by blue arrowheads, the migration of nuclei before the first cell division (**d**), the first anticlinal cell division (**e**), the first periclinal division (**f**) and a stage IV primordium (**g**). The central file is not strictly above the xylem pole. The dashed pink lines indicate the xylem pole axis. The upper panels show a longitudinal section of a 50-µm thick central section of the root (maximum intensity projection); the lower panels show a transversal cross section spanning a 100-µm long segment of the root (maximum intensity projection). A total of 39 primordia were scanned in three independent experiments. For these experiments, the number of times that the central file was not in line with the xylem pole axis was 14 (Supplementary Fig. 4). Scale bars, 50 µm.

extreme examples of deviations in central cell file location relative to the xylem pole axis. The migration of nuclei before the first cell division (Fig. 2d), the first anticlinal cell division (Fig. 2e) and the first periclinal division (Fig. 2f) were independently observed in different plants. Hence, the selection of pericycle cell files that contribute to a new lateral root primordium takes place at a very early

developmental stage; that is, before the first cell division. We had previously shown that developmental plasticity drives the selection of cells along the longitudinal axis of the root[12]. Our new findings reveal that developmental plasticity also exists in the radial axis.

We conclude that external water availability profoundly influences lateral root formation during organ emergence. Lateral roots are critical for exploring large volumes of soil for nutrients and moisture. To efficiently acquire water, plants have developed mechanisms that drive lateral root outgrowth towards external water availability[4,5]. In contrast to these earlier studies, which focused on the underlying molecular mechanisms that control this behaviour, this study focused on cell-to-organ-scale mechanisms that contribute to the outgrowth of the LRP in response to water availability. Our study reveals that unlike the xylem pole axis, the selection of pericycle cell files that initiate a new lateral root primordium is linked to the external hydrological landscape. Our results also reveal that radial divisions steer outgrowth of the LRP. These two mechanisms potentially steer lateral roots towards external water. The strong impact of the hydrological landscape explains the non-stereotypical patterns of division reported for the morphogenesis of lateral root primordia[11,12]. Collectively, our observations suggest that the external hydrological environment regulates lateral root organogenesis from initiation to outgrowth and represents a potential adaptive advantage when foraging under heterogeneous soil conditions.

Methods

Plant material and growth conditions. The *Arabidopsis thaliana* ecotype Columbia (Col-0) was used as the wild type. The reporter line *pLBD16::LBD16-GFP* was previously published[14]. *A. thaliana* seed lines were surface sterilized for 3 min using 10% (v/v) bleach containing 0.001% Triton X-100. This was followed by five washes with sterile water and then stratified at 4 °C for 48 h in the dark. Seeds were germinated on media containing half-strength Murashige and Skoog (MS) media (2.15 g per litre) (Sigma), MES buffer (0.97 g per litre), 1% sucrose and 1% Bacto agar at pH 5.7. Seedlings were grown vertically for 10 days under a continuous temperature of 22 °C with a 16-h photoperiod (150 µmol m^{-2} s^{-1}). The same medium plates were used to let plants grow in the gel. Plants for the hydroponic experiments were grown in 96-well plates with roots immersed in Hoagland's medium.

LSFM using the Zeiss Lightsheet Z.1 for outgrowth angle measurements. For LSFM[15], *A. thaliana* seedlings were carefully (without moving them) glued on the media plate using 1% agarose. Root segments (3 cm in length from the root tip) were cut out (including the gel) and transferred to a sample holder as previously described[16] (Supplementary Fig. 1). The entire volume of the root was captured, including the gel substrate, using a 405-nm laser (laser intensity in ZEN set to 35%). Autofluorescence was filtered between 505 and 545 nm. The angles of the xylem pole axis and of the lateral root relative to the surface of the medium were measured in a cross-section using ImageJ/Fiji (ImageJ v.1.52n)[17]. The line tool was used to draw a line parallel to the surface of the gel. Angles of xylem were measured by drawing a line from one xylem pole (the xylem without the primordium) to the other xylem pole (the xylem adjacent to the primordium). The angle of the lateral root primordium was measured by drawing a line from the xylem (adjacent to the primordium) to the tip of the primordium. Angles were exported from Fiji and normalized to the angle of the surface of gel. Since the angles measured in Fiji cover the range between −180° and +180°, the angles used in this paper were transformed to become all positive between 0° and 360° and rotated so that the angle 0° is perpendicular to the gel surface and 180° is pointing to the air. The angles of the lateral roots are presented as follows: orientations towards the gel have positive values and those away from the gel have negative values. When xylem angles are smaller than 180° (on the right side of the radius), the angle becomes the difference of the xylem angle minus the lateral root angle otherwise the lateral root angle minus the xylem angle.

Data visualization. Angle measurements were visualized using Adobe After Effects (v.16.1.2) (Fig. 1d,g; Supplementary Fig. 3; Supplementary Video 1). The 3D data visualization was performed using the software Arivis Vision 4D (v.3.1.2.) (Figs. 1a,b and 2c,d–g; Supplementary Fig. 4; Supplementary Video 2). Figures were assembled in Adobe Photoshop (v.20.0.5) and Adobe Illustrator (v.23.0.3).

Multiview LSFM. *A. thaliana* seedlings were grown on the surface of media plates (half-strength MS media plus 1.0% Bacto agar). Roots were covered with 1% agarose containing fluorescent beads (PS-Speck, fluorescent beads, ThermoFisher, catalogue number P7220) and further processed according to the protocol depicted in Supplementary Fig. 2. Roots were imaged using a Zeiss Lightsheet Z1 microscope. Images (Fig. 1a,b) were captured using a W Plan-Apochromat ×20/1.0 objective and the PCO.edge camera module (CMOS; 1,920 × 1,920 pixels). The excitation wavelength was 405 nm for autofluorescence of yellow fluorescent protein. The emission filters were bandpass 505–545 nm for GFP and bandpass 525–545 nm for yellow fluorescent protein. Multiview images were set-up using the Quick-Setup option in the software ZEN. Single views were fused using bead-based registration via the Fiji plugin Multiview Reconstruction[18,19].

Statistical methods. All statistics were run in IBM SPSS statistics 24. All assumptions for one-way analysis of variance were tested and met (verified using distribution plots and Levene's test). Different letters indicate a significant difference between treatments ($P < 0.05$).

Reporting Summary. Further information on research design is available in the Nature Research Reporting Summary linked to this article.

Data availability

The data for Fig. 1f is shown in Supplementary Video 1. Other datasets can be shared upon reasonable request.

Received: 26 March 2019; Accepted: 11 December 2019;
Published online: 03 February 2020

References

1. Morris, E. C. et al. Shaping 3D root system architecture. *Curr. Biol.* **27**, R919–R930 (2017).
2. Drew, M. C. Comparison of the effects of a localized supply of phosphate, nitrate, ammonium and potassium on the growth of the seminal root system, and the shoot, in barley. *N. Phytol.* **75**, 479–490 (1975).
3. Orman-Ligeza, B. et al. The xerobranching response represses lateral root formation when roots are not in contact with water. *Curr. Biol.* **28**, 3165–3173 (2018).
4. Bao, Y. et al. Plant roots use a patterning mechanism to position lateral root branches toward available water. *Proc. Natl Acad. Sci. USA* **111**, 9319–9324 (2014).
5. Orosa-Puente, B. et al. Root branching toward water involves posttranslational modification of transcription factor ARF7. *Science* **362**, 1407–1410 (2018).
6. von Guttenberg, H. in *Handbuch der Pflanzenanatomie* (ed. Linsbauer, K.) Band 8 (Gebrüder Bornträger, 1940).
7. Casero, P. J., Casimiro, I. & Lloret, P. G. Lateral root initiation by asymmetrical transverse divisions of pericycle cells in four plant species: *Raphanus sativus*, *Helianthus annuus*, *Zea mays*, and *Daucus carota*. *Protoplasma* **188**, 49–58 (1995).
8. Laskowski, M. J., Williams, M. E., Nusbaum, H. C. & Sussex, I. M. Formation of lateral root meristems is a two-stage process. *Development* **121**, 3303–3310 (1995).
9. Casimiro, I. et al. Auxin transport promotes *Arabidopsis* lateral root initiation. *Plant Cell* **13**, 843–852 (2001).
10. Dubrovsky, J. G., Rost, T. L., Colón-Carmona, A. & Doerner, P. Early primordium morphogenesis during lateral root initiation in *Arabidopsis thaliana*. *Planta* **214**, 30–36 (2001).
11. Lucas, M. et al. Lateral root morphogenesis is dependent on the mechanical properties of the overlaying tissues. *Proc. Natl Acad. Sci. USA* **110**, 5229–5234 (2013).
12. von Wangenheim, D. et al. Rules and self-organizing properties of post-embryonic plant organ cell division patterns. *Curr. Biol.* **26**, 439–449 (2016).
13. Casimiro, I. et al. Dissecting *Arabidopsis* lateral root development. *Trends Plant Sci.* **8**, 165–171 (2003).
14. Goh, T., Joi, S., Mimura, T. & Fukaki, H. The establishment of asymmetry in *Arabidopsis* lateral root founder cells is regulated by LBD16/ASL18 and related LBD/ASL proteins. *Development* **139**, 883–893 (2012).
15. Stelzer, E. H. K. Light-sheet fluorescence microscopy for quantitative biology. *Nat. Methods* **12**, 23–26 (2015).
16. von Wangenheim, D., Hauschild, R. & Friml, J. Light sheet fluorescence microscopy of plant roots growing on the surface of a gel. *J. Vis. Exp.* **2017**, e55044 (2017).
17. Schindelin, J. et al. Fiji: an open-source platform for biological-image analysis. *Nat. Methods* **9**, 676–682 (2012).
18. Preibisch, S., Saalfeld, S., Schindelin, J. & Tomancak, P. Software for bead-based registration of selective plane illumination microscopy Data. *Nat. Methods* **7**, 418–419 (2010).
19. Preibisch, S. et al. Efficient Bayesian-based multiview deconvolution. *Nat. Methods* **11**, 645–648 (2014).

Acknowledgements

This work was supported by awards from the Biotechnology and Biological Sciences Research Council (grant nos. BB/M012212, BB/G023972/1, BB/R013748/1,

BB/L026848/1, BB/M018431/1, BB/PO16855/1 and BB/M001806/1), the European Research Council FUTUREROOTS Advanced Investigator (grant no. 294729) and the Leverhulme Trust (grant no. RPG-2016-409). E.H.K.S. is funded by the Deutsche Forschungsgemeinschaft (CEF-MC I/II, DFG Exc 115). Research at the Maizel Lab is supported by the DFG FOR2581, the Land Baden-Württemberg, the Chica und Heinz Schaller Stiftung, the CellNetworks cluster of excellence and the Boehringer Ingelheim Foundation.

Author contributions

D.v.W., J. Banda, A.B., A.M., E.H.K.S. and M.B. designed the experiments. D.v.W. and J. Banda performed the experiments, and D.v.W., J. Banda, A.S., J. Boland, A.B., A.M., E.H.K.S. and M.B. analysed the data. D.v.W., J. Banda and M.B. wrote the manuscript with contributions from all the other authors.

Competing interests

The authors declare no competing interests.

Additional information

Supplementary information is available for this paper at https://doi.org/10.1038/s41477-019-0580-z.

Correspondence and requests for materials should be addressed to D.v.W. or M.B.

Reprints and permissions information is available at www.nature.com/reprints.

Publisher's note Springer Nature remains neutral with regard to jurisdictional claims in published maps and institutional affiliations.

nature research

Corresponding author(s): Malcolm Bennett and Daniel von Wangenheim

Last updated by author(s): Nov 2, 2019

Reporting Summary

Nature Research wishes to improve the reproducibility of the work that we publish. This form provides structure for consistency and transparency in reporting. For further information on Nature Research policies, see Authors & Referees and the Editorial Policy Checklist.

Statistics

For all statistical analyses, confirm that the following items are present in the figure legend, table legend, main text, or Methods section.

n/a	Confirmed	
☐	☒	The exact sample size (*n*) for each experimental group/condition, given as a discrete number and unit of measurement
☐	☒	A statement on whether measurements were taken from distinct samples or whether the same sample was measured repeatedly
☐	☒	The statistical test(s) used AND whether they are one- or two-sided *Only common tests should be described solely by name; describe more complex techniques in the Methods section.*
☒	☐	A description of all covariates tested
☐	☒	A description of any assumptions or corrections, such as tests of normality and adjustment for multiple comparisons
☐	☒	A full description of the statistical parameters including central tendency (e.g. means) or other basic estimates (e.g. regression coefficient) AND variation (e.g. standard deviation) or associated estimates of uncertainty (e.g. confidence intervals)
☐	☒	For null hypothesis testing, the test statistic (e.g. *F*, *t*, *r*) with confidence intervals, effect sizes, degrees of freedom and *P* value noted *Give P values as exact values whenever suitable.*
☒	☐	For Bayesian analysis, information on the choice of priors and Markov chain Monte Carlo settings
☒	☐	For hierarchical and complex designs, identification of the appropriate level for tests and full reporting of outcomes
☐	☒	Estimates of effect sizes (e.g. Cohen's *d*, Pearson's *r*), indicating how they were calculated

Our web collection on statistics for biologists contains articles on many of the points above.

Software and code

Policy information about availability of computer code

Data collection	ZEN 2014 software for Zeiss Z1 Light Sheet Fluorescent Microscope.
Data analysis	One-way ANOVA and Pearson correlation were run using IBM SPSS statistics 24 software. ImageJ (version 1.52n), MS Excel 2016, Adobe After Effects (version 16.1.2), Arivis Vision 4D (version 3.1.2.) Adobe Photoshop (version 20.0.5), Adobe Illustrator (version 23.0.3)

For manuscripts utilizing custom algorithms or software that are central to the research but not yet described in published literature, software must be made available to editors/reviewers. We strongly encourage code deposition in a community repository (e.g. GitHub). See the Nature Research guidelines for submitting code & software for further information.

Data

Policy information about availability of data

All manuscripts must include a data availability statement. This statement should provide the following information, where applicable:

- Accession codes, unique identifiers, or web links for publicly available datasets
- A list of figures that have associated raw data
- A description of any restrictions on data availability

Fig 1 F data freely available on the following link: https://youtu.be/A3qsY1evmQ0. Other data sets can be shared when requested.

Field-specific reporting

Please select the one below that is the best fit for your research. If you are not sure, read the appropriate sections before making your selection.

☒ Life sciences ☐ Behavioural & social sciences ☐ Ecological, evolutionary & environmental sciences

Life sciences study design

All studies must disclose on these points even when the disclosure is negative.

Sample size	No sample-size calculations were performed. Sample sizes were chosen based on similar previous published peer-reviewed papers.
Data exclusions	No data was excluded from these experiments.
Replication	All datasets comprise of multiple repeats taken within one month from a controlled growth condition. These data confirmed reproducibility.
Randomization	Samples were taken from multiple plates grown in the same growth conditions on the same type of media to account for plate effects. Plates varied in positions to account for positioning effect.
Blinding	Does not apply on our experiment, as we use the same WT control (Col-0) in the first experiments and afterwards only one fluorescent line (LBD16-GFP). Furthermore, due to the sample preparation for Light Sheet imaging blind picking for the different treatments is impossible.

Reporting for specific materials, systems and methods

We require information from authors about some types of materials, experimental systems and methods used in many studies. Here, indicate whether each material, system or method listed is relevant to your study. If you are not sure if a list item applies to your research, read the appropriate section before selecting a response.

Materials & experimental systems

n/a	Involved in the study
☒	☐ Antibodies
☒	☐ Eukaryotic cell lines
☒	☐ Palaeontology
☐	☒ Animals and other organisms
☒	☐ Human research participants
☒	☐ Clinical data

Methods

n/a	Involved in the study
☒	☐ ChIP-seq
☒	☐ Flow cytometry
☒	☐ MRI-based neuroimaging

Animals and other organisms

Policy information about studies involving animals; ARRIVE guidelines recommended for reporting animal research

Laboratory animals	10 day old Arabidopsis thaliana ecotype Col-0 (WT) and LBD16::LBD16:GFP in Col-0 background were used in these experiments.
Wild animals	Did not involve wild animals.
Field-collected samples	Does not involve field collected material.
Ethics oversight	Approval to work with transgenic organisms in this study was approved by the School of Bioscience, Nottingham.

Note that full information on the approval of the study protocol must also be provided in the manuscript.